EFFECT OF CONFINEMENT ON SHEAR DOMINATED REINFORCED CONCRETE ELEMENTS

A Dissertation

by

SURAPHONG POWANUSORN

Submitted to the Office of Graduate Studies of
Texas A&M University
in partial fulfillment of the requirements for the degree of

DOCTOR OF PHILOSOPHY

December 2003

Major Subject: Civil Engineering

EFFECT OF CONFINEMENT ON SHEAR DOMINATED REINFORCED CONCRETE ELEMENTS

A Dissertation

by

SURAPHONG POWANUSORN

Submitted to Texas A&M University
in partial fulfillment of the requirements
for the degree of

DOCTOR OF PHILOSOPHY

Approved as to style and content by:

Joseph M. Bracci (Co-Chair of Committee)	Peter B. Keating (Co-Chair of Committee)
Jose M. Roesset (Member)	Mary Beth D. Hueste (Member)
Terry L. Kohutek (Member)	Paul N. Roschke (Interim Head of Department)

December 2003

Major Subject: Civil Engineering

ABSTRACT

Effect of Confinement on Shear Dominated Reinforced Concrete Elements.
(December 2003)

Suraphong Powanusorn, B.Eng., Chulalongkorn University, Bangkok;

M.Eng.Sc., University of New South Wales, Sydney

Co-Chairs of Advisory Committee: Dr. Joseph M. Bracci
Dr. Peter B. Keating

It has been demonstrated that transverse reinforcement not only provides the strength and stiffness for reinforced concrete (RC) members through direct resistance to external force demands, but also helps confine the inner core concrete. The confinement effect can lead to improved overall structural performance by delaying the onset of concrete fracture and allowing more inelastic energy dissipation through an increase in both strength and deformability of RC members.

The objective of this research was to evaluate the effect of confinement due to the transverse reinforcement on enhancing the shear performance of RC members. A new constitutive model of RC members was proposed by extending the Modified Compression Field Theory (MCFT) to incorporate the effect of confinement due to transverse reinforcement by adjusting the peak stress and peak strain of confined concrete in compression. The peak stress of confined concrete was determined from the five-parameter failure surface for concrete developed by Willam and Warnke (1974). The peak strain adjustment was carried out using a relationship proposed by Mander et al. (1988).

The proposed analytical model was compared with results from an experimental program on sixteen RC bent caps with varied longitudinal and transverse reinforcement details. Two-dimensional Finite Element Modeling (FEM) using the proposed constitutive model was conducted to numerically simulate the RC bent cap response.

Results showed that the proposed analytical model yielded good results on the prediction of the strength but significantly overestimated the post-cracking stiffness of the RC bent cap specimens. The results also indicated that the confinement effect led to enhanced overall performance by increasing both the strength and deformability of the RC bent caps.

Two potential causes of the discrepancy in the underestimation of the RC bent cap deformations, namely the effects of concrete shrinkage and interfacial bond-slip between the concrete and main flexural reinforcement in the bent caps, were discussed. Parametric studies showed that the tension-stiffening in the proposed constitutive models to implicitly take into account the bond-slip between the concrete and main flexural reinforcement was the major cause of the overestimation of the post-cracking stiffness of RC bent caps. The explicit use of bond-link elements with modified local bond stress-slip laws to simulate the slip between the concrete and main flexural reinforcement led to good predictions of both strength and deformation.

This dissertation is dedicated to my family.

My Father Wirat, for his belief in my potential and his unconditional love and support.
My Mother Lee Kiew, for her love and caring that brought me up in this world.
My Step-Mom Pittaya, for her love and support as if you were my surrogate mother.
My cousin Kanchana and her deceased husband Prasert, for all their love and best wishes and bringing me up in my childhood.

With all my Love.

ACKNOWLEDGEMENTS

I would like to express my sincere gratitude to my advisor, Dr. Joseph M. Bracci, not only for introducing me to the intriguing field of the mechanics of confined RC members, but also for his efforts to cultivate my English and for his advice on several aspects of becoming an insightful structural engineer. Without his warm, dedicated, and energetic support and his belief in my potential, this work would never have been completed.

I am also deeply indebted to Dr. Peter B. Keating for his generosity in serving as the co-chair of the dissertation committee and for fruitful discussions on several occasions while I had a directed studies class under his supervision. His magnanimity is also remembered.

Thanks are also due to Prof. Jose M. Roesset, Dr. Mary Beth D. Hueste, and Dr. Terry L. Kohutek for serving on my dissertation committee. It was always such a joyful experience being educated by Prof. Roesset with his celebrated lectures, entertainment packages, a few neuro-diagnostic social engagements and farewell parties. I was also lucky enough to have an opportunity to work with Dr. Hueste and Dr. Kohutek while I was serving as a teaching assistant in the 111 and 112 classes. This unique experience will definitely be beneficial as I pursue an academic career.

Special thanks are also paid to Prof. Frank J. Vecchio of the University of Toronto for his generosity in providing clarifications on certain aspects of the MCFT. Efforts by Dr. Evan Bentz, also of the University of Toronto, to promote the use of the non-commercial software Response-2000 to help understand the realm of the MCFT are also appreciated.

I would also like to thank my fellow graduate students. Thanks to Bradley Young for allowing me to have full access to the experimental results on RC bent caps, to John Steele for a wonderful friendship and for his hard work in building our test samples on composite RCS systems, and to Dr. Adam Rinehart for being such a wonderful officemate. Our discussions beyond academic matters were well mixed and helped me to understand various aspects of American life.

The members of the technical staff of the Texas Engineering Experiment Station (TEES) Testing, Machining, and Repair Facility, namely Mr. Andrew Fawcett, Mr. Gerry Harrison and Mr. Jeff Perry deserve special thanks for their time, effort and commitment to experimental research.

Thanks are also noted to my truest friends: in-coming Dr. Chalongrath Pholsiri, Dr. Phansak Sattayhatewa, Mr. Witoon Worasetakarnkij, Mr. Thosaphol Katejanekarn, Mr. Pracha Vora and his wife for our long-lasting friendship and for helping me settle in the US. I must also thank my special friend, Varissara Wan La-Iad, for talking me through both the rough times and happy times, despite being half the world away.

Thanks are also paid to the interlibrary loan service officers of Texas A&M University.

Finally, the funding for this research was provided by the Texas Department of Transportation (Project 0-1851), the National Science Foundation under Grant No. CMS-9733959, and the Department of Civil Engineering. This support is gratefully acknowledged.

The content of this dissertation reflects the views of the author, who is responsible for the facts and accuracy of the data presented herein. The contents do not necessarily reflect the official view or policies of the sponsoring agencies. This

dissertation does not constitute a standard, specification, or regulation, nor is it intended for construction bidding, or permit purposes. Trade names are used solely for information and not for product endorsement.

TABLE OF CONTENTS

CHAPTER Page

CHAPTER Page

LIST OF TABLES

LIST OF FIGURES

Page

Page

CHAPTER I

INTRODUCTION

1.1 BACKGROUND

The design of reinforced concrete (RC) elements prone to shear deformations has long been a topic of extensive research investigations. Design procedures have changed over the years to include several factors previously disregarded to improve the shear performance of structural concrete components. Due to an increasing demand of large member sizes and high strength materials in modern concrete construction, rational models that take into account equilibrium, compatibility, and material constitutive relationships for shear design are preferable to empirical equations currently used in design practice because of the following reasons:

(1) Rational models provide insight into the response and failure mechanism of the structural members, which could give engineers a platform for better structural design in complicated loading situations; and

(2) Empirical equations are normally based on extensive experiments on a wide variety of member sizes. Code equations are normally derived from a curve fitting procedure of the test results along with the concept of structural reliability. However, it is debatable whether the use of empirical design equations is justified for members whose sizes are beyond the range of the experimental tests, particularly for RC structures in which strength is affected by size (Bazant and Planas, 1998).

As described previously, rational models should encompass all three essential elements of mechanics: (1) Equilibrium; (2) Compatibility; and (3) Material Constitutive

---

This dissertation follows the style and format of the *Journal of Structural Engineering*, ASCE

Models. Under the framework of continuum mechanics under normal circumstances, the equilibrium and compatibility conditions remain unchanged for all situations. Therefore, it could be stated that the material constitutive model is the most crucial factor for formulating the mathematical model for structural members.

There are several models under the framework of mechanics that are specifically designed for the characterization of material behavior. For reinforced concrete, extensive research has been attempted to formulate the constitutive model for concrete and reinforced concrete. However, normal frameworks usually fail to capture all salient features of the mechanical behavior of concrete or RC members. One of the most fundamental behaviors of concrete that poses a major obstacle to engineers and mechanicians in an attempt to construct a mathematical constitutive model is cracking. Physically, the presence of cracks signifies the formation of new stress-free surfaces in a given body. Cracks also cause redistribution of stress and changes of stiffness within the members, whether reinforced or unreinforced. The prediction of the initiation and the evolution of cracking under loading and unloading is vital to the modeling of structural concrete.

There are two fundamentally different methods to model cracks in structural concrete: (1) discrete crack model; and (2) smeared crack model. Both models are generally implemented for the analysis of RC member response under the context of the Finite Element Method (FEM). The discrete crack model is apparently a more reasonable way to model cracks both logically and physically. In this model, cracks are modeled as two adjacent stress-free surfaces totally separated from each other. In order to apply the discrete crack model to an initially uncracked member, the change in the topology of FEM mesh is required as the criterion for crack initiation is fulfilled at a certain point within a member. For members where cracks are diffused, the change in FEM mesh may prove too cumbersome. The smeared crack model was then proposed to overcome this difficulty (Rashid, 1968). In the smeared crack model, cracks are

modeled by modifying the principal tensile stress at the integration point once the crack has assumed to occur (Rashid, 1968).

Early researchers adopted the linear elastic-fracture model where cracks are modeled using discrete or smeared crack models. Uncracked concrete between cracks carrying compressive and small tensile stresses is assumed to behave linear elastically. Under service load levels, the model may yield good analytical predictions of RC member responses. However, the range of capability of the linear elastic-fracture model is limited because concrete also exhibits non-linearity under higher levels of compressive stress.

There are several mathematical models available to characterize non-linearity in compression. The simplest possible models are the non-linear elastic models obtained by calibrating model parameters with triaxial test data. By definition, the loading-reloading paths for non-linear elastic model are the same, which is not true for concrete. To overcome this difficulty, the non-linear elastic models must be enhanced by loading and unloading criterion to distinguish the direction of loading. However, the loading and unloading criteria are normally well defined for uniaxial loading conditions. An extension to multiaxial stress conditions is rather ambiguous.

Early attempts to avoid the ambiguity between loading and unloading criteria were implemented by extending the theory of plasticity, which is usually adopted for modeling metallic materials, to concrete. Through the use of the yield and potential functions, the loading and unloading criteria are well defined. However, additional problems arise due to the fact that the stiffness of unloading and reloading remains unchanged throughout the entire load history under the context of plasticity theory. Recent studies by Lee (1996) adopted the plastic-damage model for characterizing the multiaxial loading condition. By introducing additional damage variables, the evolution of stiffness degradation under increasing stress and strain can be taken into account,

although additional hysteresis upon reloading is ignored. Fig. 1.1 shows all fundamental aspect of loading, unloading, and reloading of the theory of plasticity, damage mechanics, plastic-damage model, and true concrete behavior under compressive cyclic load reversal.

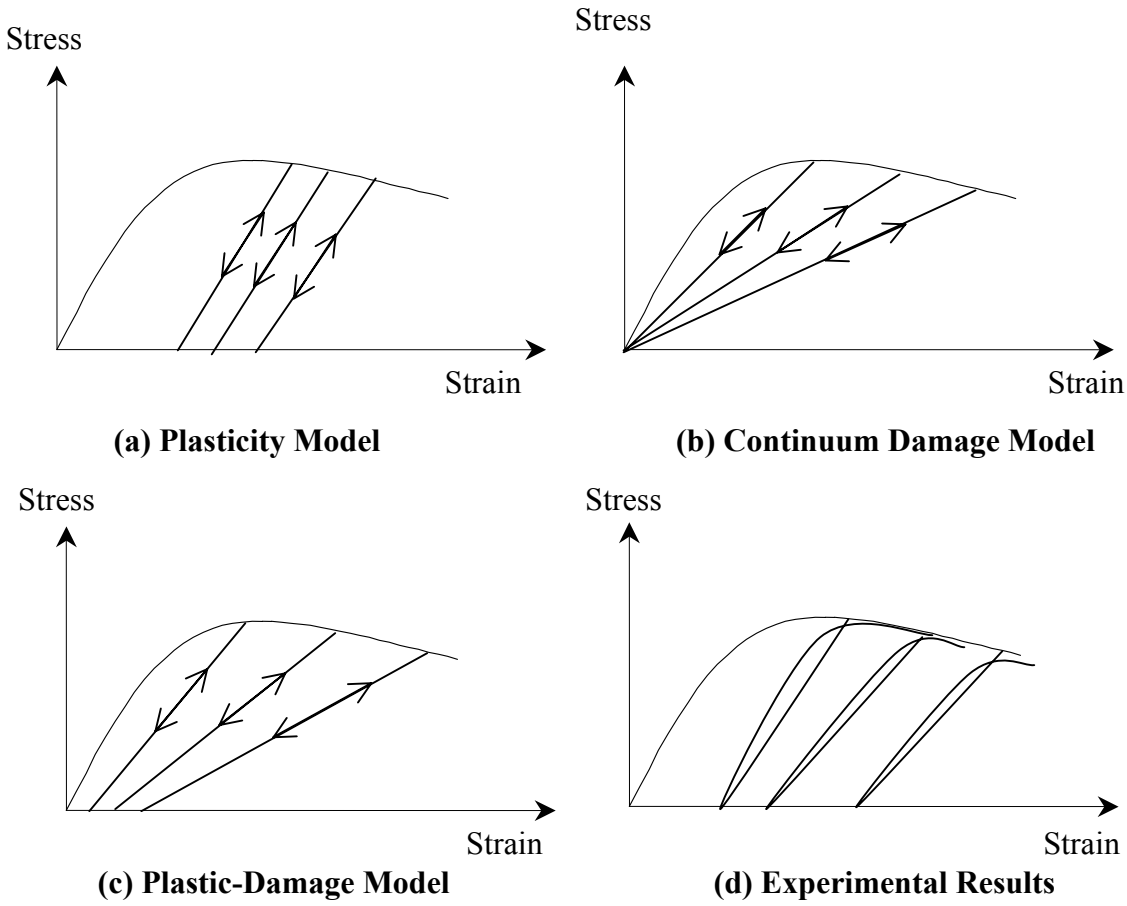

Figure 1.1 Stress-Strain Curves of Concrete under Uniaxial Compression

Although several mathematical frameworks are available for constructing the constitutive behavior of concrete, all proposed models are rarely accessible for practical purposes because of the following reasons:

(1) The models are generally calibrated from multiaxial data of unreinforced concrete specimens. An immediate extension to reinforced concrete remains dubitable; and

(2) The models are normally too complicated to be used by practitioners as sophisticated numerical algorithms are generally required to integrate the inelastic strain at each load increment.

In order to compromise between rationality and practical purposes, Vecchio and Collins (1982) developed the Modified Compression Field Theory (MCFT) for modeling reinforced concrete membrane type elements. Based on an extensive experimental program on RC panels predominantly subjected to shear stress, an explicit form of a constitutive model, which does not require numerical integration of the inelastic strain, was developed. In essence, MCFT may be viewed as the non-linear elasticity model where the constitutive relationships of concrete are expressed in terms of principal stresses and strains. The constitutive equations proposed in MCFT show a strong coupling effect between the concrete principal compressive and principal tensile stress and strain directions. The presence of a principal tensile strain in the direction transverse to the axis of applied compression generally reduces the concrete compressive strength, i.e. softening effect.

Concrete strength, either in uniaxial or multiaxial, is also strongly dependent on the hydrostatic pressure. Generally, the compressive strength and deformability of concrete increases as the applied hydrostatic pressure increases. In seismically active zones, use of seismic hoop reinforcement in structural joint regions, columns and beams are required in modern building codes. The primary purpose of the seismic hoop reinforcement is to confine the core concrete and thereby creates increased hydrostatic pressures that allows for significant energy dissipation by longitudinal reinforcement yielding. Numerous research studies have been done on the use of passive and active

measures to provide confinement to RC members for enhancing the axial and flexural performance of RC elements, either for rehabilitation or retrofit of existing structures. Relative little has been done on the effect of confinement on the shear performance of RC members.

An experimental program was conducted at Texas A&M University to evaluate the effect of reinforcement details on the structural performance of RC bent caps where shear was considered to be the dominant action in the load transfer mechanism (Bracci et al., 2000). It was observed that under typical reinforcement details, the main flexural reinforcement (top steel) was loaded beyond the yield limit at failure. Therefore, the typical mode of failure of the RC bent caps was considered to be a combination of flexure and shear failures. However, it was observed that by increasing the amount of shear stirrup reinforcement, the failure load and deformation of the RC bent cap increased, given the same flexural reinforcement details. This result somewhat contradicted the conclusions made by Ferguson (1964) on similar specimens that shear reinforcement has very little or no effect on the strength of similar RC bent caps. It was then hypothesized that the amount of stirrups had no direct influence on the failure mechanism of RC bent caps. However, an observable increase in strength and deformation of the members was attributed to the effect of confinement due to the out-of-plane horizontal leg of stirrups as shown in Fig. 1.2 (Bracci et al., 2000). The effect of confinement helps increase the strength and deformability of concrete in compression, which helps delay the compressive fracture of concrete on the compression face. Given the same amount of main reinforcement, confined specimens are able to sustain larger deformations which, in turn, ensure a level of overstrength of members due to an increase in strength of the concrete from the confinement and main reinforcing steel due to strain hardening.

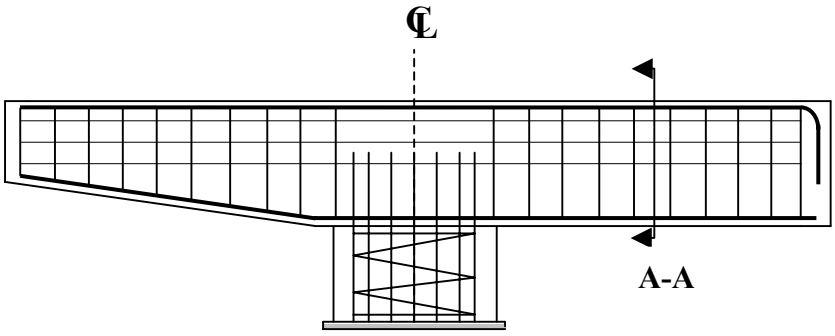

(a) Typical RC Bent Cap Details

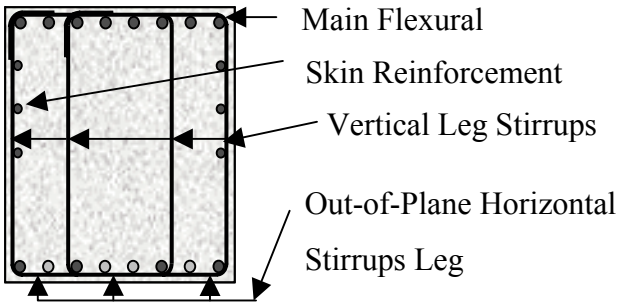

b) Section A-A

Figure 1.2 Schematic Figure Showing Bent Cap Reinforcing Details (after Bracci et al., 2000)

Experiments on unreinforced concrete elements subjected to tensile loading under displacement-control loading show that concrete has limited capacity in carrying tensile stress after cracking. This capacity of concrete to carry limited stress after cracking is generally termed tension-softening. Under the context of the MCFT, the effect of cracking of reinforced concrete in the principal tensile direction is handled by decreasing the tensile stress according to the constitutive relationship of concrete in tension. However, it was experimentally found that the post-peak tensile stress-strain relationship of concrete in RC members is generally much higher than that of

unreinforced concrete. This effect is called tension-stiffening, which is generally acknowledged to be attributed to the interfacial bond stress between the concrete and reinforcing steel. For RC members with well-distributed reinforcement, the average stress-strain of concrete in tension can be modeled with sufficient accuracy with the proposed tension stiffening. However, for unconventional RC members such as RC bent caps where reinforcement is not well-distributed, the effect of local bond-slip can pose difficulties such that the average approach used by tension-stiffening may cause large errors in numerical simulations.

1.2 RESEARCH OBJECTIVE

The main objective of this dissertation is to evaluate the effect of confinement due to the out-of-plane horizontal legs of stirrups on enhancing the shear performance of RC members through the development of an appropriate finite element model. Analytical studies are limited to two-dimensional RC elements subjected to monotonic and quasi-static loading conditions. Emphasis in this research is placed on:

(1) Extending the constitutive relationship under the framework of the MCFT to incorporate the effect of confinement. Because the constitutive relationships in MCFT were established based on experimental results of RC panel elements without out-of-plane stirrups, the constitutive relationships of the MCFT require modifications. The confining stress due to out-of-plane reinforcing steel is caused by the lateral expansion strain of concrete subjected to compression. Consequently, the constitutive relationships of concrete in compression are modified through the adjustment of peak stresses and strains;

(2) Perform sensitivity studies on the effect of bond-slip between the concrete and main reinforcing steel on the overall structural performance of RC bent caps. Comparisons are made between the approaches handled by tension-stiffening and

through explicit bond-slip models between the concrete and the main reinforcing steel; and

(3) Compare results from numerical simulations with the experimental studies on RC bent caps conducted at Texas A&M University (Bracci et al., 2000). This is one of the possible alternatives to verify the validity of the proposed modified constitutive relationship of the MCFT by incorporating confinement.

1.3 SCOPE OF WORK

The following is an overview of this dissertation. Chapter II reviews the current literature on the constitutive modeling of concrete and reinforced concrete members. The new constitutive relationships of concrete considering the effect of confinement are formulated in Chapter III. Chapter IV summarizes the experimental program conducted as a part of a research program at Texas A&M University on RC bent caps. A comparison between the experimental and analytical results using the new constitutive relationship presented in Chapter III is presented in Chapter V, where the confinement effect and parametric studies on the effect of shrinkage and bond-slip between the concrete and reinforcing steels are highlighted. Chapter VI summarizes the major findings of this research and presents conclusions that are drawn from these findings. Suggestions for future research are also made, which may further help validate the analytical model that includes the effect of confinement and bond-slip on the performance of RC members under both service and failure load levels.

CHAPTER II

REVIEW OF LITERATURE

2.1 INTRODUCTION

In this chapter, past research on the constitutive modeling of reinforced concrete members, including the effects of confinement due to transverse reinforcement, is summarized. Because reinforced concrete comprises two distinct components, namely, concrete and reinforcing steel, available constitutive modeling techniques for each component shall be explained separately. Relative merits of each technique are also discussed. As for any composite cross-section, the interaction between the concrete and reinforcing steel, namely the bond between the reinforcing bars embedded in concrete, requires further justification. A simplified technique to model the interaction between concrete and reinforcing steel is also described.

Two constitutive models based on the framework of non-linear elasticity, namely, the Modified Compression Field Theory (MCFT) of the University of Toronto Research Group and the Softened Truss Model (STM) of the University of Houston Research Group are discussed. Because the constitutive model proposed in this dissertation is based on these two models, a comprehensive description and discussion on the MCFT and STM is made in this chapter.

2.2 REVIEW OF CONSTITUTIVE MODELING OF CONCRETE

The focus of this section is to describe the fundamental behavior of concrete required for constitutive modeling. Five important aspects attributed to the unique mechanical behavior of concrete are described: (1) Heterogeneity; (2) Non-linearity; (3) Pressure dependency; (4) Softening and (5) Size effect. Influence of each aspect on the overall behavior of concrete is briefly discussed.

(1) Heterogeneity

Concrete, being a composition of water, cement, aggregates, and admixtures, of itself is a heterogeneous material consisting of several phases of material. Each constituent plays a major part in the overall mechanical behavior of concrete under the applied load and environment. In general, hardened concrete is relatively weak in tension and strong in compression. The typical stress-strain curves for normal strength concrete for both uniaxial tension and compression are shown in Fig. 2.1.

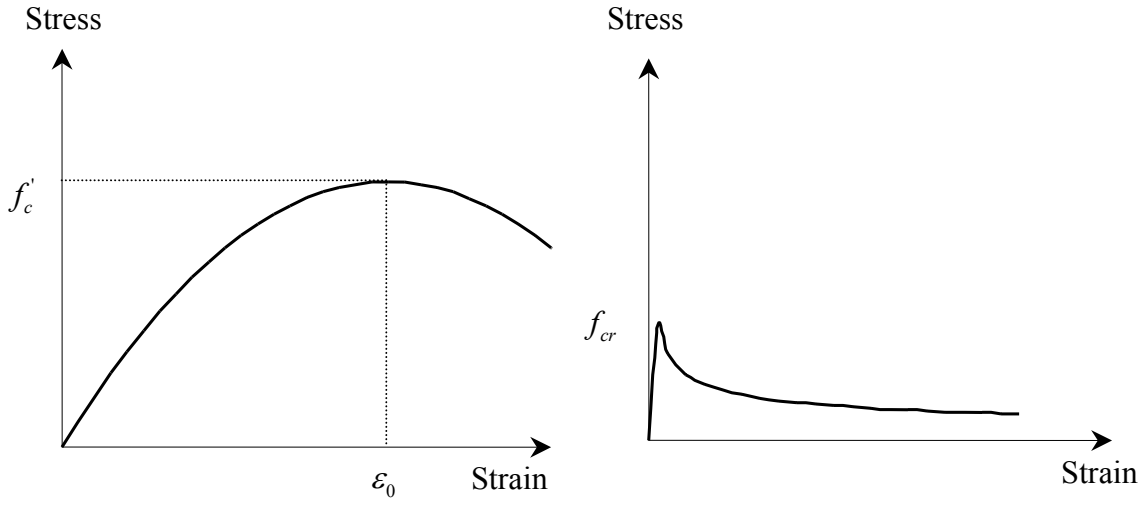

(a) Compression **(b) Tension**

Figure 2.1 Uniaxial Stress-Strain Curves of Concrete

(2) Non-linearity

Fig. 2.1 shows that the stress-strain relationship of concrete has a limited range of linearity. After a certain threshold, the linear-elastic assumption becomes inapplicable. The non-linearity in stress-strain relationship is attributed to several mechanisms such as the presence of micro-cracks, non-linearity of the constituents, and interfacial friction between the constituents. This mechanism is generally irreversible and evolves as the applied stress changes.

(3) Pressure Dependency

The dependence of strength and deformation under the direction of the applied load makes the constitutive modeling of concrete a very difficult task. The problem becomes further complicated under multiaxial loading where confinement also has a significant influence on the strength, deformability, and failure mode of concrete. Willam et al. (1986) reported a different failure mode from triaxial compressive tests of normal strength concrete under confining stress ranging from 100 psi to 2000 psi as shown in Fig. 2.2. Under low confining stress, concrete cylinders fail by crushing of the concrete along with splitting tension cracks parallel to the direction of the applied load. A single major shear crack is formed at failure for an intermediate level of confinement. Under high confining stress, no major cracks form and inelastic deformation is distributed within the concrete specimen. In any event, strength and deformability of a concrete cylinder increases as confining stress increases.

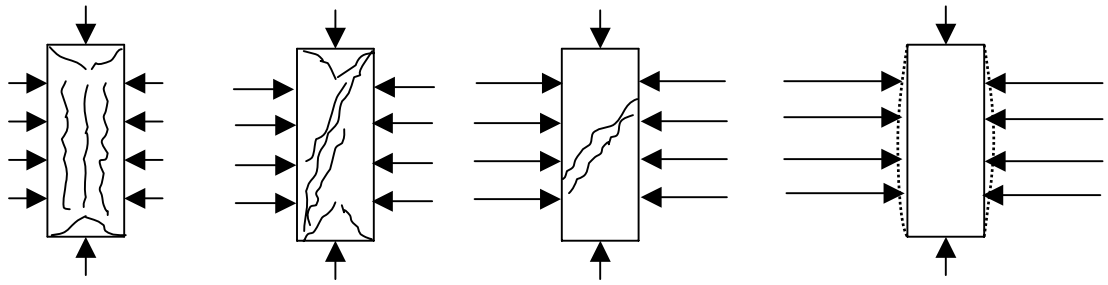

(a) 100 psi **(b) 500 psi** **(c) 1000 psi** **(d) 2000 psi**

Figure 2.2 Failure Modes of Concrete Cylinders under Various Confining Stresses

(4) Softening

Another important aspect that must be taken into account is the post-peak stiffness and strength, or softening. As shown in Fig. 2.1, concrete exhibits softening in both uniaxial tension and compression tests, though the mechanisms behind them are rather different. Fig. 2.3 shows the fracture process zone of concrete under uniaxial tension and compression tests.

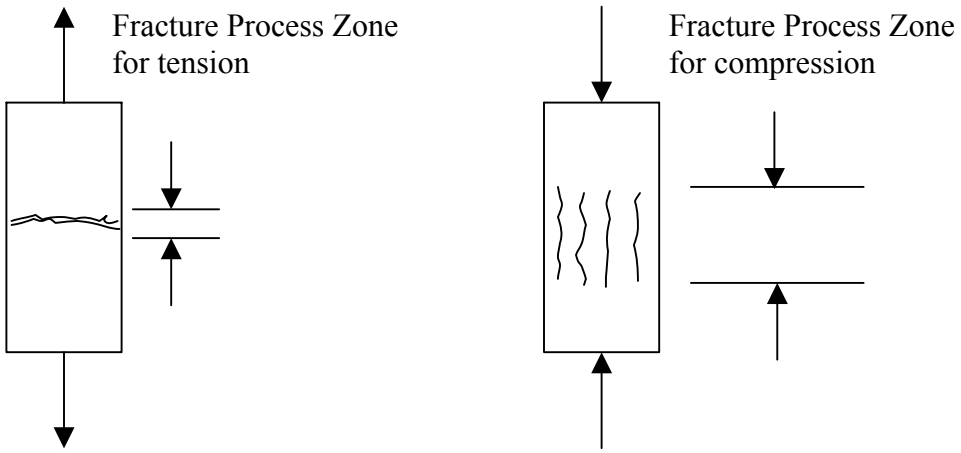

Figure 2.3 Fracture Process Zone of Concrete

At peak concrete stress in a uniaxial tension test, a single crack perpendicular to the direction of applied tension forces generally dominates. Under a displacement control experiment, a sudden drop of stress after initial cracking is generally reported. The crack becomes wider under increasing strain and gradually decreasing stress until the fracture strain is reached as the tension specimen is separated into two parts.

The post-peak stress and strain of concrete under uniaxial compressive stress is governed by a different mechanism. At peak stress, the formation of several distributed cracks in the form of micro-cracking parallel to the direction of the applied stress is generally observed. These parallel and distributed cracks begin to coalesce to form a few dominant cracks under increasing strains and gradually decreasing stresses. At peak strain, crushing of concrete along with the widening of splitting parallel cracks is generally observed.

(5) Size Effect

The concrete stress-strain relationship exhibits strong size dependence. Van Mier (1986) conducted an experimental study on the influence of the specimen size on the uniaxial compressive stress-strain relationship of concrete. Typical results are given in Fig. 2.4, which shows the post-peak stress-strain curve for specimens with heights varying from 50-200 mm. However, if the stress-post-peak displacement curves are plotted instead of stress-strain relationship, the effect of specimen size diminishes as shown in Fig. 2.5. Based on the strain gauge reading at several locations along the length of specimens during uniaxial compression test, Van Mier (1986) showed that only strain measurements near the fracture process zone exhibited post-peak deformation while strains outside the cracking zone unloaded. The phenomenon is a fracture-related process and often termed strain-localization. Concrete stress-strain relationship in uniaxial tension also exhibits strong size-dependence in the post-peak region (Van Mier, 1986).

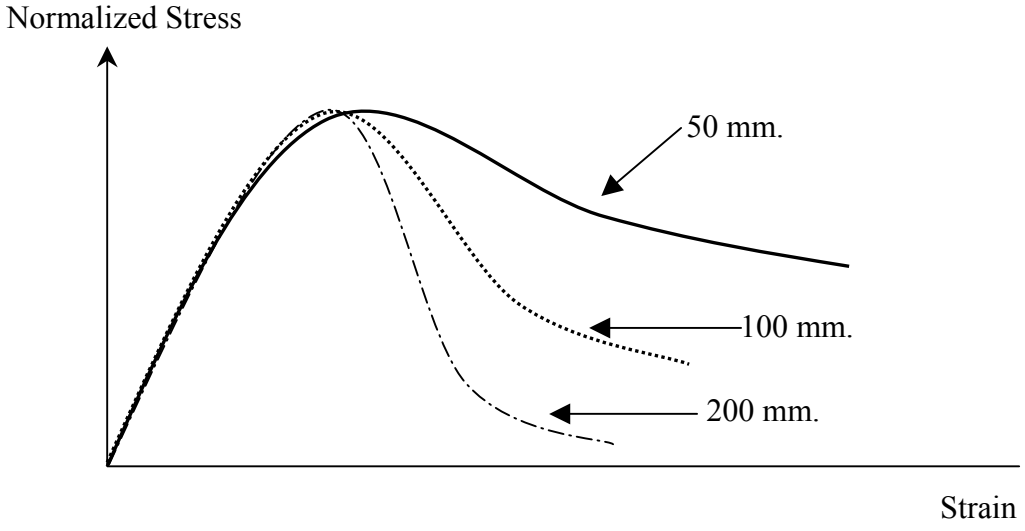

Figure 2.4 Size Effect on Uniaxial Compressive Stress-Strain

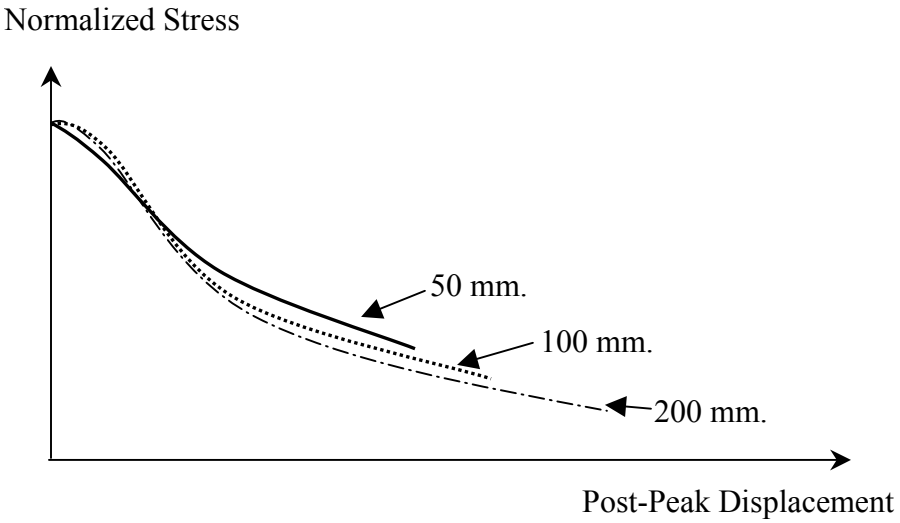

Figure 2.5 Stress-Deformation Plot Independent of Size Effect

There are several frameworks of mechanics that can characterize concrete behavior. The level of complicacy of the model is directly related to the ability of the model to capture important features of mechanical behavior of concrete previously explained and to match the number of available test data that the model is used for calibration. The next section summarizes four distinguished frameworks for material characterization: (1) Non-Linear Elasticity Model; (2) Plasticity Model; (3) Microplane Model and (4) Non-Local Model. The abilities and deficiencies of each individual model are also discussed.

2.2.1 Non-Linear Elasticity Model

The non-linear elasticity model is probably the simplest model available to make a reasonable analytical prediction for all engineering materials. According to Chen and Saleeb. (1982), there are two schemes to characterize the material response using elastic material models: (1) Hyperelastic model and (2) Hypoelastic model. In the hyperelastic model, the material stiffness matrix is expressed in terms of the total stress-strain. In order to satisfy the thermodynamic constraint, the stiffness matrix must be symmetric. By definition, the constitutive relationship for hyperelastic model is independent of path.

Therefore, the loading and unloading curves are always the same. This characteristic is essentially not true for concrete.

The hypoelastic model was proposed by Truesdell (1955). In this model, the material is assumed to be incrementally linear. In other words, the constitutive relationships are expressed in terms of the incremental stress-strain. The material stiffness matrix depends on the current state of stresses as well as the path taken to the current state. Therefore, the total loading-unloading paths are generally different.

Chen and Saleeb (1982) summarizes a systematic way to characterize the material response using the theory of tensorial invariants for both hyperelastic and hypoelastic models. However, the method becomes mathematically more involved with several material constants required to be determined from experiments. In practice, a simplified method based on experimental observations is normally adopted, even though this method of material characterization is mathematically less rigorous.

Kupfer and Gerstle (1973) performed an experiment on unreinforced concrete panels under biaxial stresses. The test setup was such that the applied stress ratio in two orthogonal directions was constant. Concrete constitutive relationships for 2D plane stress analyses were proposed in terms of decoupled secant shear and bulk moduli of concrete, which were empirically obtained from tests as a function of octahedral shear stress (τ_{oct}) and strain (γ_{oct}). The secant form of this 2D total stress-strain relationship is given by:

$$\begin{pmatrix} \sigma_x \\ \sigma_y \\ \tau_{xy} \end{pmatrix} = 4G_s \frac{3K_s + G_s}{3K_s + 4G_s} \begin{bmatrix} 1 & \frac{3K_s - 2G_s}{2(3K_s + G_s)} & 0 \\ \frac{3K_s - 2G_s}{2(3K_s + G_s)} & 1 & 0 \\ 0 & 0 & \frac{3K_s + 4G_s}{4(3K_s + G_s)} \end{bmatrix} \begin{pmatrix} \varepsilon_x \\ \varepsilon_y \\ \gamma_{xy} \end{pmatrix} \quad (2.1)$$

where G_s and K_s is the secant shear and bulk moduli of elasticity, respectively

Cedolin et al. (1977) reviewed various experimental results on concrete subjected to triaxial stress state and proposed a 3D stress-strain relationship, also in terms of decoupled secant shear and bulk moduli. However, different expressions from Kupfer and Gerstle (1973) were presented. Cedolin et al. (1977) claimed that the secant bulk modulus of elasticity of concrete should be expressed as a function of octahedral normal strain (ε_{oct}), while the secant shear modulus should be represented by a function of octahedral shear strain (γ_{oct}). This form of constitutive relationship by Cedolin et al. (1977) satisfies the thermodynamic requirement on the existence of elastic strain energy and may be regarded as a truly hyperelastic model (Chen and Saleeb, 1982). The constitutive relationship proposed by Cedolin et al. (1977) is given by:

$$\begin{pmatrix} \sigma_x \\ \sigma_y \\ \sigma_z \\ \tau_{xy} \\ \tau_{xz} \\ \tau_{yz} \end{pmatrix} = \begin{bmatrix} K_s + \frac{4}{3}G_s & K_s - \frac{2}{3}G_s & K_s - \frac{2}{3}G_s & 0 & 0 & 0 \\ K_s - \frac{2}{3}G_s & K_s + \frac{4}{3}G_s & K_s - \frac{2}{3}G_s & 0 & 0 & 0 \\ K_s - \frac{2}{3}G_s & K_s - \frac{2}{3}G_s & K_s + \frac{4}{3}G_s & 0 & 0 & 0 \\ 0 & 0 & 0 & G_s & 0 & 0 \\ 0 & 0 & 0 & 0 & G_s & 0 \\ 0 & 0 & 0 & 0 & 0 & G_s \end{bmatrix} \begin{pmatrix} \varepsilon_x \\ \varepsilon_y \\ \varepsilon_z \\ \gamma_{xy} \\ \gamma_{xz} \\ \gamma_{yz} \end{pmatrix} \tag{2.2}$$

Chen and Saleeb (1982) indicated several drawbacks of models proposed by Kupfer and Gerstle (1973) and Cedolin et al. (1977). Firstly, the inherent assumption on isotropy of concrete is used by both models throughout the entire load history. This assumption contradicts observed test results in which cracking occurs. Because both models were calibrated on a number of test results which were predominantly under biaxial or triaxial compression, with only a limited numbers of tests with tensile loading in one of the directions, the effect of cracking and crack-induced anisotropy cannot be

modeled accurately. A separate scheme is required to extrapolate the models into the cracked region. Secondly, both models employed the decoupled secant bulk and shear moduli assumption which neglect the effect of dilatancy, the occurrence of volumetric strain under purely deviatoric stress, at high stress levels. Kotsovos and Newman (1978) attempted to correct this drawback by using coupled secant bulk and shear moduli, which takes into account the dilatancy effect. But the constitutive relationship still assumes the isotropy of concrete. A special crack handling procedure was still required.

In contrast to the secant stiffness formulation presented above, a different formulation based on incremental (hypoelastic) stress-strain formulation can also be conducted. In this form, both the loading and unloading path are, in general, different. Therefore, it could be used to model the cases where the applied load is non-proportional. The general form of this hypoelastic model is given by:

$$d\sigma_{ij} = C^{\tan}_{ijkl} d\varepsilon_{kl} \tag{2.3}$$

where, $d\sigma_{ij}$ = increment of stress tensors

$C^{\tan}_{ijkl}$ = tangent stiffness of material

$d\varepsilon_{kl}$ = increment of strain tensors

Chen and Saleeb(1982) showed that the secant stiffness formulations developed by Kupfer and Gerstle (1973), Cedolin et al. (1977) and Kotsovos and Newman (1978) could be entirely formulated in incremental (hypoelastic) form by simply differentiating Eqs. 2.1 and 2.2 with respect to the strain components for 2D and 3D problems, respectively. Chen et al. (1982) pointed out that a caution must be taken into consideration in order to use the hypoelastic model in FEM. Because nonlinear FEM applications employed an iterative procedure to solve the system of equations, a system of unbalanced forces within an increment is calculated on the basis of the current stress. Using hypoelastic models, the integration of stress under a finite strain increment may

lead to cumulative errors that may grow uncontrollably. This error accumulation due to the application of a finite strain increment is explained in Fig. 2.6 below. One way to avoid these numerical difficulties is to use a very small strain increment. Another method to reduce this numerical error is by using the secant total stress-strain to calculate stress used in the residual force calculation when the structure is on the loading path as in Fig. 2.6. The tangent stiffness of the material written in hypoelastic form is only used in the stiffness matrix of the system. Generally, unloading is assumed to occur elastically. Therefore, no special treatment is required under these circumstances. However, a condition to examine whether the structure is on the loading and unloading path within the increment is not easy. Generally, the introduction of yield functions from the theory of plasticity is additionally required. Note that if the hypoelastic stress-strain relationships are obtained from differentiating the secant total stress-strain relationship, the total form of stress-strain relationship to be use in the residual force calculation can be obtained automatically. In general hypoelastic formulation, this closed form total stress-strain relationship may not be derivable. Therefore, extreme caution must be exercised when using this particular constitutive relationship.

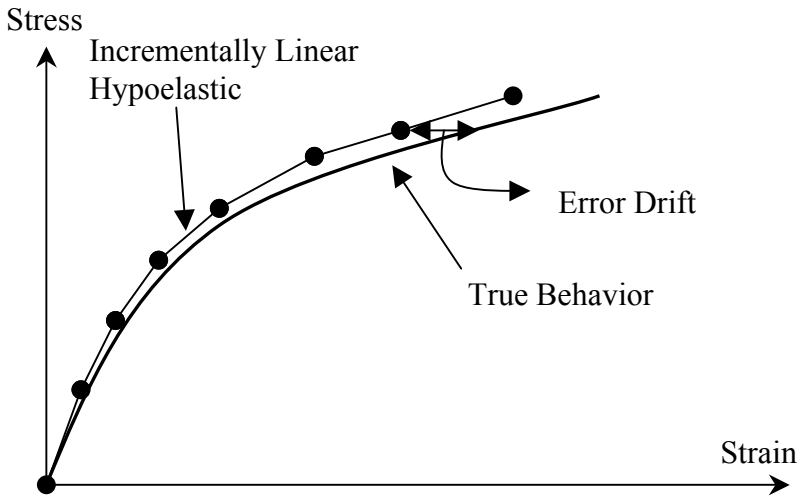

Figure 2.6 Error Drift due to the Use of Explicit Integration Scheme for Hypoelastic Model

Darwin and Pecknold (1977) developed an orthotropic hypoelastic model for 2D plane stress analysis using the principal direction as the axis of orthotropy. The stress-strain behavior along the principal direction is defined by using an equivalent uniaxial strain in that principal direction. The equivalent uniaxial strain is introduced merely to capture the Poisson expansion strain in other directions. The general equivalent uniaxial stress-strain relation involves a parameter to take into account the effect of increase in the peak stress and strain due to the biaxial stress condition. Therefore, the effect of strength and ductility enhancement can be incorporated. A crack is assumed to develop when the principal tensile stress in one of the directions exceeds the tensile strength of concrete. Concrete between cracks remains capable of resisting additional compressive or tensile strength provided that its magnitude does not violate the assumed failure criterion. Bathe and Sundberg (1986) extended the model developed by Darwin and Pecknold (1977) to three dimensions. The residual capability of concrete to carry additional tensile stress across cracking is also incorporated Bathe and Sundberg (1986). It was reported that this type of model yielded good results for proportional loading path and further investigation was required for non-proportional loading paths (Bathe and Sundberg, 1986).

2.2.2 Plasticity Model

The theory of plasticity is typically used to describe the inelastic behavior of engineering materials. The theory was initially developed to model metallic and geological materials. The central idea of the theory of plasticity is the decomposition of the total strain increment ($d\varepsilon_{ij}$) into two components, an elastic reversible strain ($d\varepsilon_{ij}^{e}$) and inelastic irreversible strain ($d\varepsilon_{ij}^{p}$) increments as shown below:

$$d\varepsilon_{ij} = d\varepsilon_{ij}^{e} + d\varepsilon_{ij}^{p} \tag{2.4}$$

The stress change ($d\sigma_{ij}$) is only attributed to the elastic strain increment given by the following relationship:

$$d\sigma_{ij} = C_{ijkl} d\varepsilon^{e}_{kl} \tag{2.5}$$

where C_{ijkl} is the elastic material stiffness matrix.

Two additional concepts are introduced in the classical theory of perfect plasticity, the existences of yield surface (F) and the plastic potential surface (G). The yield surface is a scalar function, usually expressed in terms of six components of 3D stresses ($F(\sigma_{ij}) = 0$), used to define the threshold where inelasticity is assumed to initiate. The plastic potential surface is also a scalar function of 3D stresses ($G(\sigma_{ij}) = 0$) and is used to define the plastic strain increment ($d\varepsilon^{p}_{ij}$) with the relationship given by:

$$d\varepsilon^{p}_{ij} = d\lambda \frac{\partial G}{\partial \sigma_{ij}} \tag{2.6}$$

where $d\lambda$ is a constant which can be determined by imposing the consistency condition on the yield surface given by:

$$\frac{\partial F}{\partial \sigma_{ij}} d\sigma_{ij} = 0 \tag{2.7}$$

By substituting Eqs. 2.4-2.6 into 2.7, the following relationship can be obtained:

$$d\sigma_{ij} = \left[C_{ijkl} - \frac{C_{ijmn} \dfrac{\partial F}{\partial \sigma_{mn}} \dfrac{\partial G}{\partial \sigma_{pq}} C_{pqkl}}{\dfrac{\partial F}{\partial \sigma_{rs}} C_{rstu} \dfrac{\partial G}{\partial \sigma_{tu}}} \right] d\varepsilon_{kl} \tag{2.8}$$

The classical theory of plasticity was subsequently enriched by the introduction of hardening and softening parameters that essentially defines the change in size of the yield surface according to the hardening rules.

Because the theory of plasticity is founded on the existence of yield and plastic potential functions and its hardening rules, the level success of the application of the theory of plasticity to concrete lies on the construction of realistic yield and plastic potential surfaces and their evolution based on limited experimental evidences. For concrete applications, the growth of the yield surface initiates at a certain stress threshold (initial yield surface) until a particular point has been reached where no further evolution can occur (Failure Surface). Chen and Chen (1975) employed three-parameters obtained from three sets of experimental testing on biaxial stress state, namely, uniaxial tensile strength, compressive strength, and equal biaxial compressive strength to construct the three-parameter failure surface. The initial and subsequent yield surfaces are assumed to have a similar shape to the failure surface but of a smaller size. Originally, Chen and Chen (1975) assumed that concrete is capable of carrying stress once the final failure surface is reached (when cracking or crushing occurs). This assumption is essentially not true for unconfined or moderately confined concrete. Chen and Suzuki (1980) proposed a zoning technique to correct this drawback by differentiating between cracking and crushing failure. In the cracking zone, cracks are assumed to occur in the direction perpendicular to the principal tensile stress, which will be completely released after cracking. Concrete between cracks remains capable of transferring additional forces until subsequently cracking or crushing occurs. Note that the method proposed by Chen and Suzuki (1980) employed the fixed crack assumption. In other words, additional stresses carried by concrete between cracks is expressed in terms of stiffness in the fixed crack coordinate throughout the subsequent loading. For the crushing zone, all components of stresses are released and concrete is assumed to entirely lose its strength and stiffness.

Hseih et al. (1982) extended the Chen and Chen (1975) work from biaxial to triaxial stress condition. The four-parameter failure surface was proposed as it better represented concrete under a triaxial stress state. However, a similar procedure proposed by Chen and Chen (1975) is still used. The initial and subsequent yield surfaces are assumed to have the same shape as the final failure surface but with a smaller size. The zoning technique developed by Chen and Suzuki (1980) is also employed for stress release.

Models proposed by Chen and Chen (1975) and Hseih et al. (1982) completely release tensile stress as the failure surface is reached in the cracking zone. In strain-controlled uniaxial tensile experiments (Van Mier, 1986), strain softening is generally observed. Therefore, the concept of completely releasing the stress may underestimate the contribution of tensile stress across the crack. Han and Chen (1985) employed the Willam and Warnke's five-parameter failure surface with non-uniform hardening rule to model the triaxial behavior of concrete. Non-uniform hardening means that the initial and subsequent yield surfaces do not have a geometrically similar shape as of the failure surface, since the plot of failure surface in three principal stress axes are generally open at one end. However, the initial yield surface proposed by Han and Chen (1985) is closed. Subsequent yield surfaces gradually open up until it asymptotically reaches the failure surface as stress increases. In summary, three major changes by Han and Chen (1985) are made from the previous two models: (1) the non-associative flow rules are employed; (2) tensile stress across the crack is gradually released by softening; and (3) non-uniform hardening is assumed.

Several improvements have been proposed to the models above using the theory of plasticity. The Han and Chen model (1985) only takes into account the tensile softening, yet assumes the sudden drop of stress in crushing zone. Experimental evidences show that softening also exists in compression. The slope of the softening curve also shows size dependent phenomenon. The fixed crack assumption is also

dubitable as experimental results show that the crack direction can rotate, particularly, in the test under non-proportional loading path. Pramono and Willam (1987) proposed the fracture-energy based plasticity model using Leon failure criteria (Romano, 1969), which encapsulates the Mohr-Coulomb failure criteria with Rankine tension cut-off into a single function. In this model, the rotating crack is assumed. In other words, no specific crack direction is registered and the crack condition depends only on the current stresses, which is controlled only by the failure surface. The initial and subsequent yield surfaces are related to the Leon failure surface by using a hardening parameter. However, once the failure surface is reached, softening is assumed to occur. This softening results in a shrinking of the failure surface from the initial failure surface to the current failure surface. The derivation of softening parameters is based on the fracture energy of concrete in Mode I (tensile) and II (shear) fracture. In general, this softening modulus is size dependent. Therefore, the application of this model to FEM requires the adjustment of these softening parameters according to the mesh size. The resulting model is in good agreement with the experiments performed by Klisinski (1985) on triaxial tests of concrete with a wide range of confining stresses. The failure modes are also correctly predicted.

Feenstra (1993) developed a similar model to the fracture energy-based plasticity proposed above. However, two separate failure surfaces in the form of Von Mises and Rankine failure surface were employed. The model was therefore named the composite plasticity model. However, the softening moduli were derived on the basis of tensile and compressive fracture energy. The model was applied in the FEM code to analyze panels subjected to predominantly tensile and shear stress. A uniform 20 percent decrease in uniaxial compressive strength was assumed under such condition. Good agreement with the experimental results was also observed.

2.2.3 Microplane Model

Most non-linear elasticity-based and plasticity-based constitutive relationships proposed so far were intended for capturing the non-linearity in triaxial compression states. In fact, only a limited number of experiments cover the multiaxial tension-compression state (Kupfer and Gerstle, 1973). Special treatment is required to extrapolate the model into the cracking state. Most models necessitate the calculation of principal stresses for manipulating the crack direction. As explained in the previous sections, two different models are generally accepted to take into account the effect of cracking: (1) rotating crack model and (2) fixed crack model. Regardless of the assumption made on the coincidence between the principal stresses and strain, additional assumptions must be made on the stress-strain relationship of concrete between cracks, which may not be consistent with models used for uncracked states. Bazant (1983) showed that in the orthotropic hypoelastic model of Darwin and Pecknold (1977) using the fixed crack assumption the proposed constitutive relationship may violate the principle of material frame-indifference. In addition, he objected to the rotating crack model, which assumes the coincidence of principal stresses and strain directions based on the physical and thermodynamics theories.

In order to construct a consistent model capable of handling both pre- and post-crack regions and also satisfying the laws of thermodynamic, Bazant and Oh (1985) developed a microplane model for concrete. In essence, the model assumes that stresses at a point can be determined on the basis of volume averaging of the stress vector over a unit sphere as shown in Fig. 2.7. Bazant and Oh (1985) proposed that the surface of the unit sphere consists of an infinite number of planes called microplanes on which a traction vector acts. By using the principal of virtual work, the stress at a point is expressed as volume average of traction vectors on all microplanes. The volume averaging is calculated by numerical integration on an appropriate number of directions, which are fixed throughout the entire load-history.

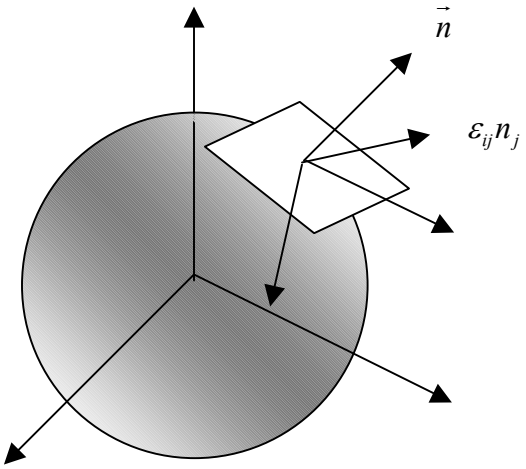

FIGURE 2.7 Microplane Model

The most important aspect for the microplane model is the definition of a traction vector under a given state of strain. Bazant and Oh (1985) proposed that these traction vectors on a given microplane should be defined in terms of the normal and tangential strains obtained from the decomposition of the applied strain. In the original model, only the traction normal to the microplane is taken into account. The resulting model applied well for concrete subjected to predominantly tension. Subsequent refinements (Bazant and Bhat, 1988, Carol et al. 1992) were carried out to extend the applicability of the model to multiaxial stress states where the effect of confinement, damage, and cyclic loading can be consistently incorporated.

2.2.4 Non-Local Model

Classical theories of the constitutive modeling of the so-called "simple materials" are formulated in local format. Essentially, this formulation assumes that a state of stress at a point depends only on the strain and/or strain history of that point. However, in heterogeneous materials like concrete, the definition of the state of stress or strain at a point is irrelevant because the state of stress and strain at a point is not uniform due to the existence of defects and heterogeneities. The same argument is probably correct for

all engineering materials. However, most materials, such as metals, have a microstructure whose scale is infinitesimal compared to the level of observation in practical engineering application. Under this circumstance, the notion that the state of stress and strain is uniform at a point could be well applied within the scale of engineering interests. However, the microstructure of concrete is relatively large. Therefore, the effect of non-uniformity of stress and strain within the range of engineering application can be significant. This was also confirmed by experimental results, such as the strain-controlled uniaxial tension or compression tests where a zone of strain localization in the softening range is observed within the specimen (Van Mier, 1986). Within the zone of localized deformation, the material remains loaded while the rest of the specimen unloads as shown schematically in Fig. 2.8. The stress-strain curve in softened range also shows strong size effect as previously discussed.

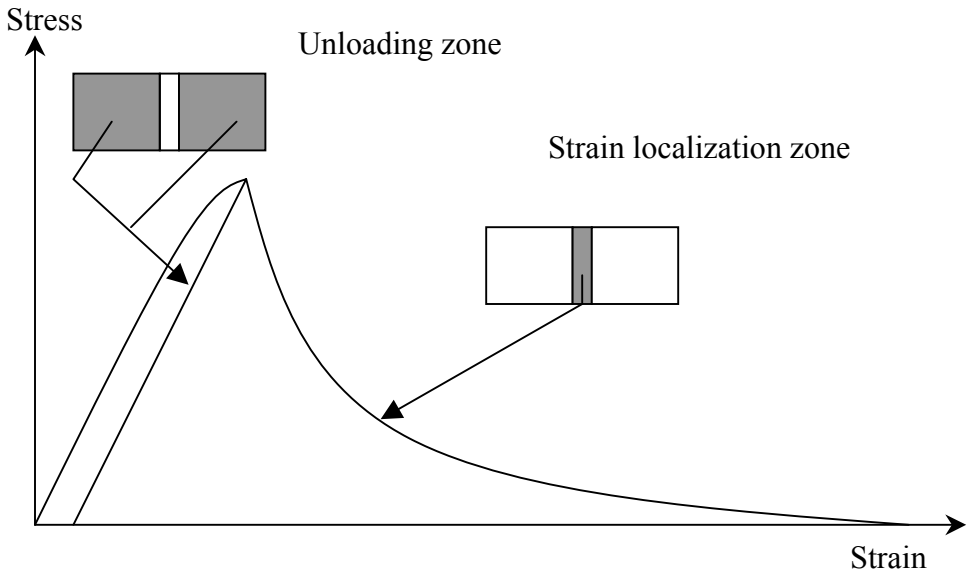

Figure 2.8 Strain Localization in Softening Materials

In order to numerically simulate the effect of non-uniformity of stress and strain due to the inhomogeneity of the materials, Prevost and Hughes (1981) proposed a zone of imperfection where the material properties within this zone are slightly reduced.

Using this approach, Bazant and Cedolin (1980) showed that the application of a local continuum to numerical implementation, particularly, FEM for softening materials like concrete could lead to the results which are mesh-size dependent in the softened range.

In spite of the fact that the softened stress-strain curve for concrete is size-dependent, the softened stress-displacement relationship is virtually independent of the specimen size (Van Mier, 1986). The area under the stress-displacement curve represents the amount of energy release for crack propagation (fracture energy) (Bazant and Planas, 1998). Bazant and Oh (1985) postulated that the size of this strain-localized zone is a material property, which does not depend upon the member size. This assumption also implicates the existence of the constant fracture energy. For concrete in tension, the size of this strain localization zone is approximately 3-4 times the maximum size of aggregate (Bazant and Cedolin, 1980).

Several methods have been proposed to circumvent the numerical difficulties associated with the objectivity with regards to the mesh size dependency. De Borst et al. (1993) categorized three general methods to account for strain-localization issues. The method proposed by Pramono and Willam (1987) and Feenstra and De Borst (1995) using the theory of plasticity complemented with fracture mechanics concepts represents one of the three methods summarized by De Borst et al. (1993). Essentially, the fracture energy-based plasticity model proposed by Pramono and Willam(1987) and Feenstra and De Borst (1993) adjusted the softening parameter to depend on the mesh size. Cabot and Bazant (1987) adapted the classical theory of non-local continuum (Eringen and Edelen 1972) to develop a constitutive relationship of concrete using the continuum damage mechanics. Essentially, the model assumes that the state of stress at a point depends not only on the strain at that point but also its neighboring points within a certain length scale. The third method was called the gradient-plasticity model (Pamin, 1994) where the strain gradients, along with the characteristic size, are incorporated directly into the yield function.

2.3 CONSTITUTIVE MODELING OF REINFORCING STEEL

For general engineering applications, the elastoplastic constitutive relationship, either with or without strain hardening, is normally assumed for ductile reinforcing steel, as shown in Fig. 2.9. Because quasi-static loading conditions are only considered in this report, the complicated phenomena, like the general curved hysteretic stress-strain relationship under dynamic loading, will be completely neglected.

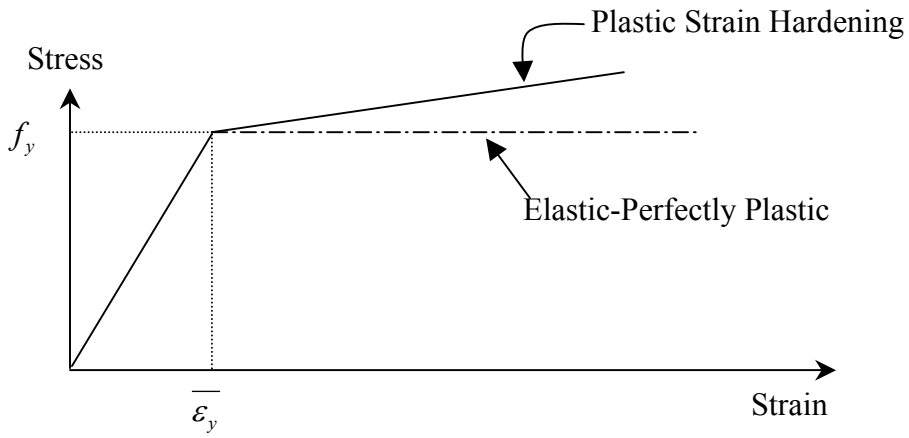

Figure 2.9 Idealized Stress-Strain Curve for Reinforcing Steel

2.4 TENSION-STIFFENING

Tension-stiffening refers to the ability of cracked RC members to carry additional average stresses in the direction perpendicular to the crack and offers post-cracking stiffness to the member. It is crucial to note the difference between the terminologies used between the tension-softening and tension-stiffening effects. In this dissertation, tension-softening refers to the softened part of the tensile stress-strain relationship of bare concrete and is controlled by the appearance of a single crack. Tension stiffening, on the other hand, refers to the softened tensile stress-strain curve of concrete in RC members and is controlled by the occurrence of multiple cracks. Tension stiffening is, therefore, obtained by averaging strain over all cracks within the members.

The concept of tension stiffening was originally proposed by Scanlon and Murray (1974) in the study of deflections in RC slabs. Scanlon and Murray (1974) found that slab deflections were overestimated when the post-cracking stress of concrete was ignored and proposed that additional concrete tensile stress should be included. Fig. 2.10 shows the stress-strain relationship for concrete in tension used by Scanlon and Murray (1974).

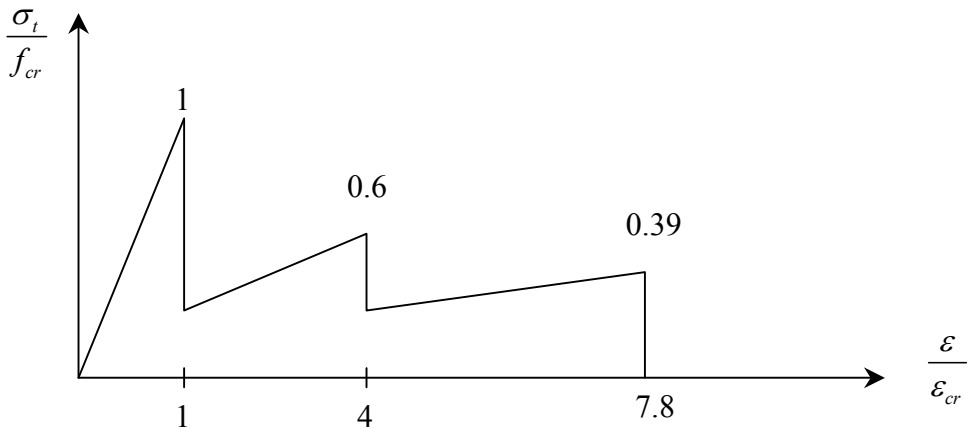

Figure 2.10 Tension-Stiffening Model by Scanlon and Murray (1974)

A simple model to explain the effect of tension stiffening in RC members was proposed by Tamai et al. (1987). In this model, a RC member is subjected to uniaxial tension as shown in Fig. 2.11. As soon as multiple cracks form with certain crack spacing, concrete stress at the crack location suddenly drops and reinforcing steel is the major load carrying mechanism at the crack location. Considering a free body diagram as shown in Fig. 2.12. It can be concluded that concrete between cracks should help carry a certain amount of stress and the stress in reinforcing steel between cracks should be less than that at the crack location. Therefore, a load transfer mechanism between concrete and steel should exist through the concrete-reinforcing steel interface between cracks as shown in Fig 2.12

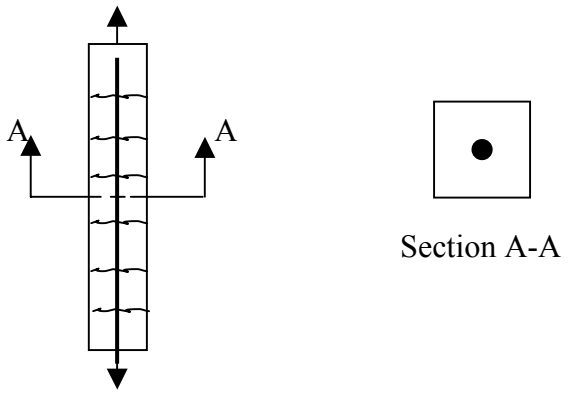

Figure 2.11 RC Members Subjected to Uniaxial Tension

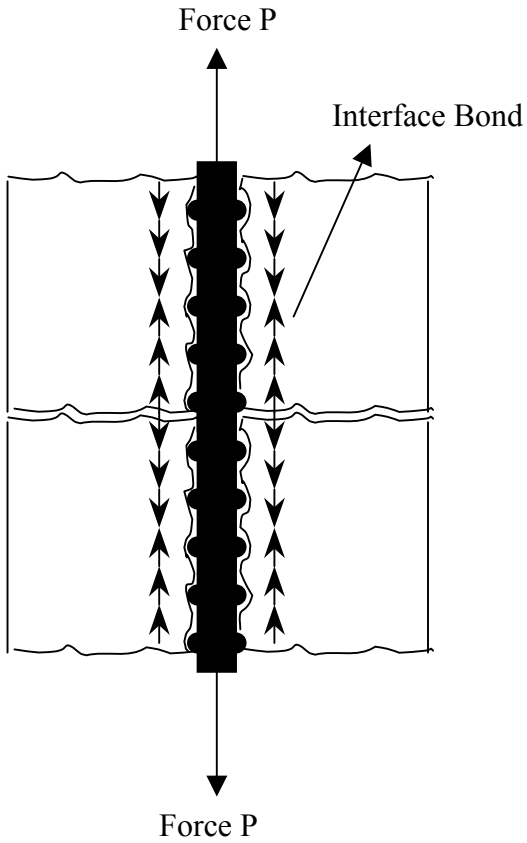

Figure 2.12 Free Body Diagram for Cracked RC Members

Recent studies by Ahn (1996) showed that this post-cracking stress in concrete can be attributed to two sources: (1) Tension-softening of bare concrete; and (2) Bond mechanism between concrete and reinforcing steel. Ahn (1996) describes a typical average stress-strain curve of RC members subjected to uniaxial tension and divides the curve into three regions as shown in Fig. 2.13. The first region represents the uncracked state where concrete remains elastic and fully participates in carrying tension. The tension-softening effect is the major load transfer mechanism in the second region. In the third region, tension in concrete is provided by interfacial bond stress between the concrete and reinforcing steel.

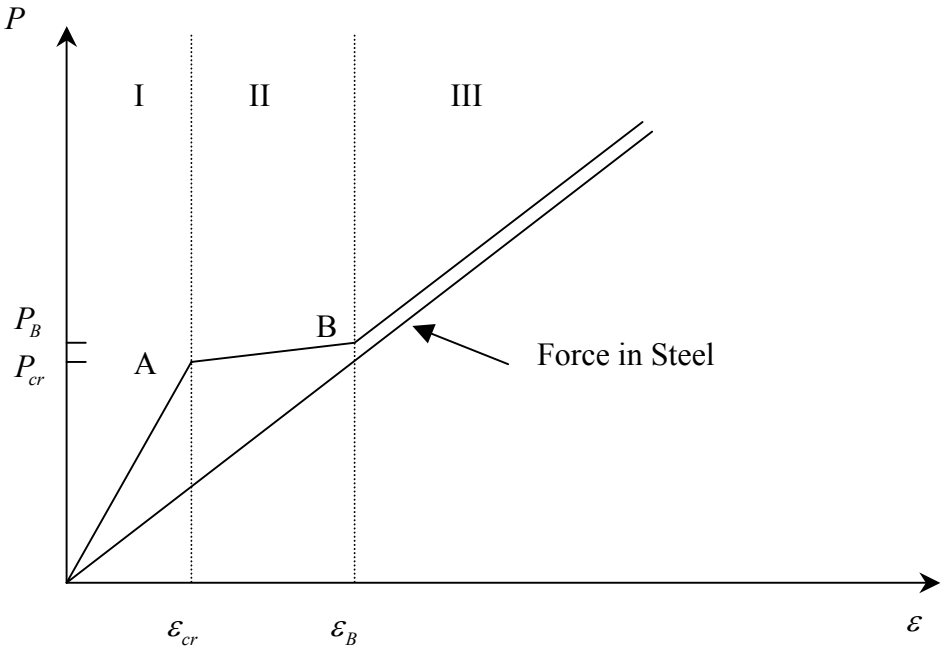

Figure 2.13 Load-Deformation Curve for RC Members Subjected to Uniaxial Tension

2.5 SUMMARY OF AVAILABLE CONSTITUTIVE MODELS OF RC MEMBERS

There are an abundant number of constitutive models available in the literature as summarized above. However, most models are concentrated on the behavior of concrete alone. In fact, the calibration and verification of each model are normally carried out on the uniaxial, biaxial and triaxial tests of unreinforced concrete. Many models are calibrated on the basis of predominantly triaxial compression tests with only limited test data including tensile stress in one of these multiaxial directions. In FEM analyses, a special technique is normally introduced to handle the situation when cracks occur. These additional crack handling schemes are merely an extrapolation of the multiaxial model using a limited knowledge on behavior of concrete in tension obtained from uniaxial tests. In addition, the presence of reinforcing steel in RC members may significantly alter the behavior of concrete. The situation becomes more complicated when the interaction between concrete and reinforcing steel, such as interface bond and slip, is taken into account.

In order to balance the complex phenomena in RC members with engineering applications, certain simplifications of the complex constitutive modeling are required. Based on the arguments presented in the previous paragraph, the effect of cracking and interfacial bond-slip in RC members should also be taken into account and verified on the basis of experimental testing. Two prominent research groups, University of Toronto and University of Houston, have conducted both experimental and analytical studies to develop constitutive models for RC members explicitly incorporating the effect of cracking into the models. It should also be noticed that these two research groups concentrated their studies on shear-dominated members in two dimensions. In other words, the models proposed are calibrated from two-dimensional plane stress analyses with one principal compressive strain and another principal tensile strain where cracking occurs.

2.5.1 Toronto Group Research

Pioneering by Collins (1978) on an attempt to provide a simple and rational model for shear design of RC members, three distinctive constitutive models have been continuously developed by Toronto Research Group: (1) Compression Field Theory (CFT); (2) Modified Compression Field Theory (MCFT); and (3) Disturbed Stress Field Model (DSFM). These three models assume that cracked reinforced concrete panels can be homogenized and treated as a new composite material whose mechanical behavior can be rather different from its constituents, namely, concrete and reinforcing steels. An extensive experimental program has been conducted over the years at the University of Toronto (Vecchio and Collins, 1982, and Vecchio and Collins, 1986). The main emphasis of the experimental program was to develop the constitutive relationship for cracked RC panels, cracked directions, and changes of the concrete constitutive relationship due to the composite action with the reinforcing steels.

The CFT and MCFT are based on the postulate that the concrete principal stress and strain directions coincide, while the DSFM relaxes this assumption and allows the deviation of these two principal stresses and strains to occur by the slip of embedded reinforcing bars. Willam et al. (1987) have classified the constitutive model of CFT and MCFT as a sub-category of non-linear elasticity where the constitutive relationship is expressed in terms of stress and strain in the principal direction. Many researchers in the past claimed that this type of model assumes that the crack direction, which is assumed to be the same as the principal stress and strain directions, constantly rotates regardless of the loading history. This implies that a crack has no memory. In reality, cracks do not continuously rotate as assumed in the model and the constitutive relationship based on this assumption may seem unjustified. A better definition of this model may be obtained if the notion of crack rotation is ignored and the constitutive relationship is formed based on a specific type of non-linear elasticity where the current principal stress is expressed as a function of the current principal strain as clarified by Willam et al. (1987). In other words, there is no unique relationship between the direction of current

crack and the current principal tensile direction. However at incipient cracking, the crack direction would coincide with the principal tensile stress direction.

Experimental results by Vecchio and Collins (1982) showed that the deviation between the direction of principal stresses and strains were within 10 degrees for 28 test panels over a wide range of steel reinforcement ratio under biaxial loading. In some loading scenarios, for panels with equal reinforcement ratios in two perpendicular directions, the discrepancies become less and the direction of principal stresses and strains virtually coincide. Therefore, it could be said that this assumption is rather justified for the 28 test panels, and possibly for practical application using uniform reinforcing steel.

2.5.1.1 Compression Field Theory (CFT)

Collins (1978) developed the CFT for analysis of two-dimensional (plane) reinforced concrete elements and structures subjected to shear as the antithesis of Wagner tension field theory used for steel design. The CFT postulates that, after cracking, a compression field is developed in the concrete as the major load transfer mechanism in RC members. Post-cracking tension forces in the concrete perpendicular to the compression field are negligible. Fig. 2.14a shows a typical compression field developed within a RC member and Fig. 2.14b highlights the end region of shear force dominated behavior.

Assumptions Used for the Development of CFT

According to Collins (1978), the following assumptions were made in the development of the two-dimensional CFT:

(1) Within a member, a state of two-dimensional stresses ($\sigma_x, \sigma_y, \tau_{xy}$) and strains ($\varepsilon_x, \varepsilon_y, \gamma_{xy}$) exists. The two-dimensional stress and strain components can be expressed on 2D Mohr's circle of stresses and strains as shown in Fig. 2.15;

(2) Directions of the concrete principal stresses and strains coincide;

(3) Principal tensile stresses in the direction perpendicular to principal compression are negligible;

(4) Stresses ($\sigma_x, \sigma_y, \tau_{xy}$) and strains ($\varepsilon_x, \varepsilon_y, \gamma_{xy}$) represent the average stresses and strain acting upon a material point within a member. This assumption essentially applies the homogenization of the cracked RC membrane. Local effects due to localized cracking are ignored;

(5) Constitutive relationships of concrete in the principal compressive stress direction is known or can be uniquely obtained from experiments, and can also be expressed in terms of the two principal strain components;

(6) Reinforcing steel in longitudinal and transverse directions are perfectly bonded to the concrete. Originally, Collins assumed elastic-perfectly plastic behavior for the reinforcing steel, but modifications can be made rather easily to incorporate post-yield strain hardening of the reinforcing steel.

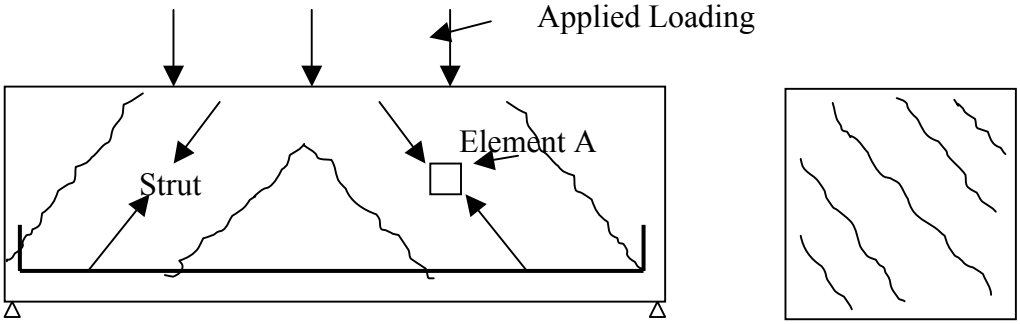

(a) RC Members with Shear Dominated Behavior **(b)Element A**

Figure 2.14 Compression Field in RC Members

The governing equations for CFT are derived from the basic laws of mechanics as follows:

Equilibrium

Consider a two-dimensional Mohr's circle of stress as shown in Fig. 2.15. Given the direction of principal compressive stress of concrete (θ_σ) and principal tensile and compressive stresses (σ_{c1}, σ_{c2}), the equilibrium equations expressed in terms of the X and Y global coordinates are:

$$\begin{aligned} \sigma_x &= \frac{(\sigma_{c1}+\sigma_{c2})}{2} - \frac{(\sigma_{c1}-\sigma_{c2})}{2}\cos(2\theta_\sigma) + \rho_x\sigma_{sx} \\ \sigma_y &= \frac{(\sigma_{c1}+\sigma_{c2})}{2} + \frac{(\sigma_{c1}-\sigma_{c2})}{2}\cos(2\theta_\sigma) + \rho_y\sigma_{sy} \\ \tau_{xy} &= \frac{(\sigma_{c1}-\sigma_{c2})}{2}\sin(2\theta_\sigma) \end{aligned} \tag{2.9}$$

where, σ_x = total applied stress in the global X direction

σ_y = total applied stress in the global Y direction

τ_{xy} = total applied shear stress in the global X-Y direction

σ_{c1} = concrete principal tensile stress

σ_{c2} = concrete principal compressive stress

σ_{sx}, σ_{sy} =steel stress in global X and Y directions, respectively

ρ_x, ρ_y = reinforcement ratio in global X and Y directions, respectively

θ_σ = angle between the global X-direction and direction of minor principal concrete stress.

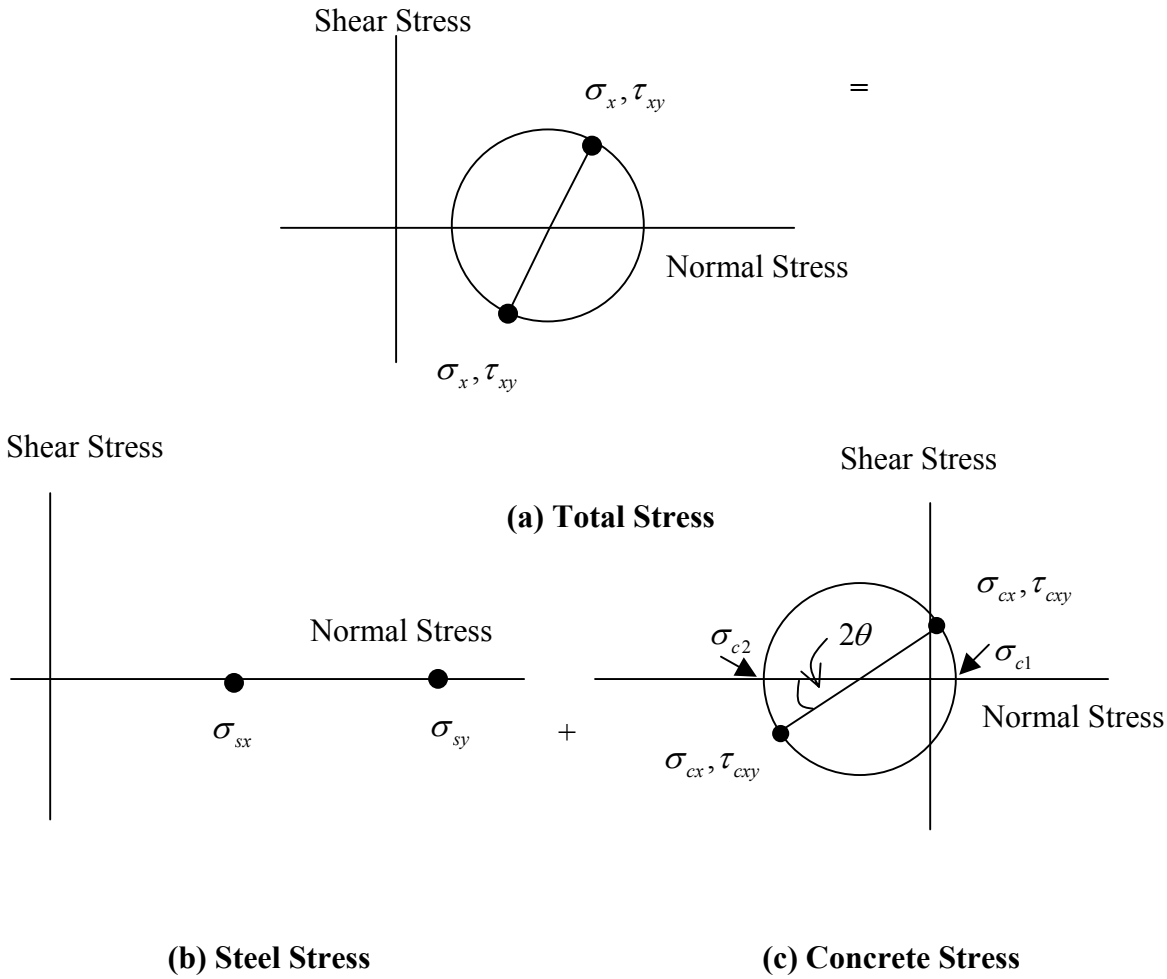

(b) Steel Stress **(c) Concrete Stress**

Figure 2.15 2D Equilibrium Equations by Mohr's Circle of Stress

Compatibility

The compatibility condition in CFT can be derived from the two-dimensional Mohr's circle of strain as shown in Fig. 2.16. Given the direction of principal compressive strain of concrete (θ_ε) and two values of principal strain ($\varepsilon_{c1}, \varepsilon_{c2}$), the following equations can be derived:

$$\varepsilon_{cx} = \frac{(\varepsilon_{c1}+\varepsilon_{c2})}{2} - \frac{(\varepsilon_{c1}-\varepsilon_{c2})}{2}\cos(2\theta_{\varepsilon})$$
$$\varepsilon_{cy} = \frac{(\varepsilon_{c1}+\varepsilon_{c2})}{2} + \frac{(\varepsilon_{c1}-\varepsilon_{c2})}{2}\cos(2\theta_{\varepsilon}) \qquad (2.10)$$
$$\gamma_{cxy} = (\varepsilon_{c1}-\varepsilon_{c2})\sin(2\theta_{\varepsilon})$$

where ε_{cx} = concrete strain in the global X direction

ε_{cy} = concrete strain in the global Y direction

γ_{cxy} = concrete shear strain in the global X-Y direction

ε_{c1} = concrete strain in the major principal direction

ε_{c2} = concrete strain in the minor principal direction

θ_{ε} = angle between the global X-direction and direction of minor principal concrete strain

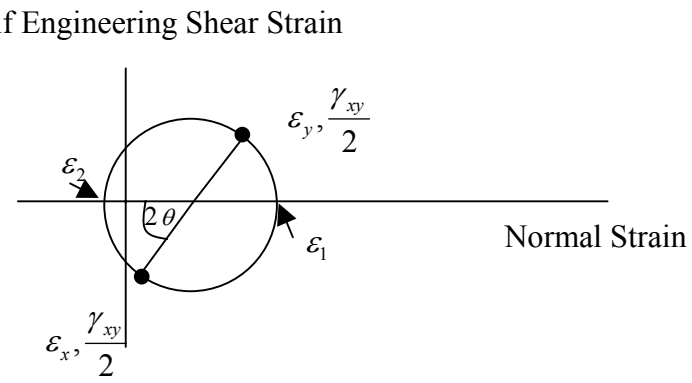

Figure 2.16 2D Mohr's Circle of Strain for Compatibility Condition

Note that based on the initial assumption made for the CFT, the angle θ_{ε} is the same as θ_{σ}. In addition, because perfect bond between concrete and reinforcing steel is assumed, all components of concrete strain are also equal to the steel strains:

$$\varepsilon_{cx} = \varepsilon_{sx} = \varepsilon_x \text{ , and } \varepsilon_{cy} = \varepsilon_{sy} = \varepsilon_y \tag{2.11}$$

Constitutive Relationships

Based on Collins (1978), the constitutive relationship of concrete in the principal directions should be expressed as a function of principal stresses and strains. The mathematical forms of the concrete constitutive relationship are:

$$\sigma_{c1} = f_1(\varepsilon_1, \varepsilon_2) \tag{2.12}$$

$$\sigma_{c2} = f_2(\varepsilon_1, \varepsilon_2) \tag{2.13}$$

From Eqs. 2.12 and 2.13, two cases can be distinguished based on the algebraic sign of the two principal strains:

(1) For tensile (positive) principal strains, Collin (1978) assumed the following:

$$\sigma_{c1} = E_c \varepsilon_1 \text{ , } \varepsilon_1 < \varepsilon_{cr} \text{ and} \tag{2.14}$$

$$\sigma_{c1} = 0 \text{ , } \varepsilon_1 > \varepsilon_{cr}$$

(2) For compressive (negative) principal strain, Collins (1978) adopted the parabolic curve proposed by Hognestad (1951) for concrete in compression.:

$$\sigma_{c2} = f_c^{'} \left(\frac{2\varepsilon_2}{\varepsilon_0} - \left(\frac{\varepsilon_2}{\varepsilon_0} \right)^2 \right) \tag{2.15}$$

where, ε_2 = principal compressive strain

ε_0 = strain corresponding to peak stress in an unconfined compression test, generally taken as 0.002

$f_c^{'}$ = unconfined compressive strength of concrete at 28 days

2.5.1.2 Modified Compression Field Theory (MCFT)

While the application of CFT to strength predictions of RC members yielded reasonably accurate results, the deformation counterpart was generally overestimated. Vecchio and Collins (1982) improved CFT by incorporating some residual post-cracking tensile stress into the model. The resulting model was then named the Modified Compression Field Theory (MCFT). In general, MCFT employs the same sets of governing equations as the CFT, except that the constitutive relationships in the **principal** directions were modified.

An extensive experimental program was conducted at the University of Toronto to verify the assumptions constituting the MCFT, to calibrate the stress-strain relationship of concrete in the principal compressive direction, and to determine the appropriate constitutive relationship for concrete in tension. Tests were performed on 28 panels with varying ratios of biaxial stress components and reinforcement in two perpendicular directions. Fig. 2.17 shows the general test setup by Vecchio and Collins (1982). External loads were applied through a series of shear rigs along the boundary of the test panels, which were built by a series of vertical and horizontal rigid links that were connected to the load control units. The applied biaxial load ratios were controlled by the magnitude of forces applied through the horizontal and vertical rigid links as shown in Fig. 2.17c.

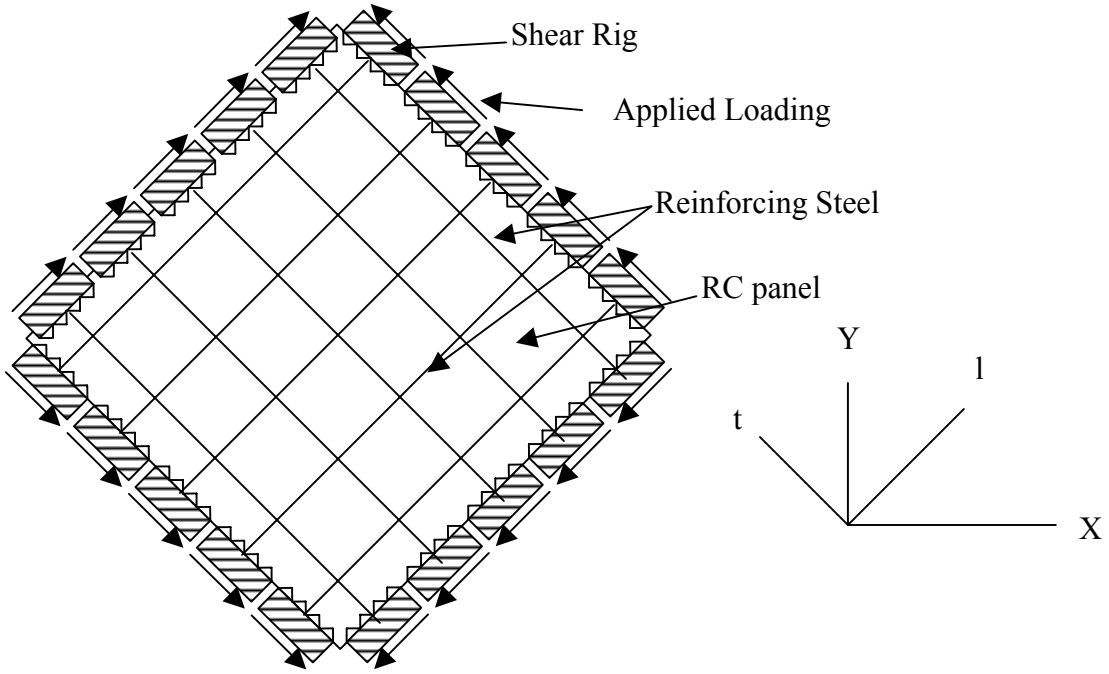

(a) RC Test Panel **(b) Coordinate Systems**

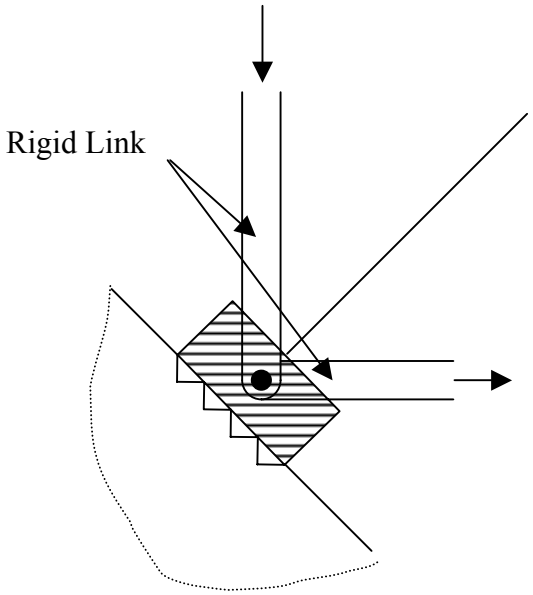

(c) Shear Rig

Figure 2.17 RC Test Panel by Vecchio and Collins (1982)

Model Calibration

At a certain stage, the following data was obtained from strain gauge and loading cell readings: (1) Total stresses applied through the shear rigs ($\sigma_x, \sigma_y, \tau_{xy}$); and (2) Average strains ($\varepsilon_x, \varepsilon_y, \varepsilon_l, \varepsilon_t$) from 28 locations on the RC membrane. From a given strain ($\varepsilon_x, \varepsilon_y$), stress contributions from the steel (σ_{sx}, σ_{sy}) can be calculated from constitutive relationship for reinforcing steel described earlier. Concrete stresses ($\sigma_{cx}, \sigma_{cy}, \tau_{cxy}$) can be determined by using Eq. 2.9. Note that Vecchio and Collins (1982) assumed that the reinforcing steel is an elastic-perfectly plastic material and used this assumption to determine steel and concrete stresses throughout their report.

From the three stress components $\sigma_{cx}, \sigma_{cy}, \tau_{cxy}$, two values of concrete principal stresses can be determined using two-dimensional Mohr's circle of stress (Eq. 2.9). Similarly, two-dimensional Mohr's circle of strain from four values of strain gauge reading $\varepsilon_x, \varepsilon_y, \varepsilon_l, \varepsilon_t$ can also be constructed (Eq. 2.10). Note that there is one redundant strain component and this required a curve fitting procedure to determine the best fit. With this procedure, the two principal strains can be calculated. With this given information, the relationships between principal stresses and strain can be determined (Eqs. 2.12 and 2.13), and the assumption that the principal stresses and principal strains directions coincide can be verified by comparing θ_σ and θ_ε obtained from above. Fig. 2.18 shows typical results obtained from the calibration process proposed by Vecchio (1982).

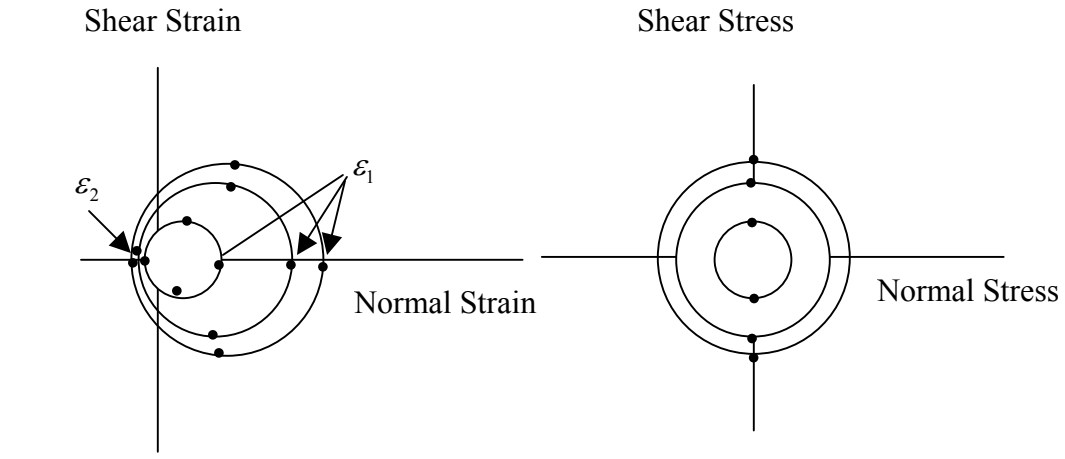

(a) Strain from Strain Gauges **(b) Total Stress from Loading Cell**

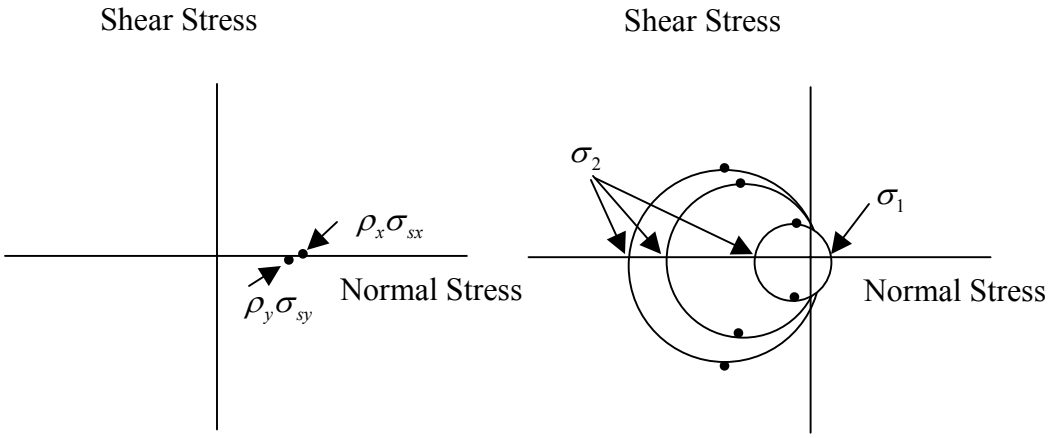

(c) Steel Stress obtained from (a) **(d) Concrete Stress = (b)-(c)**

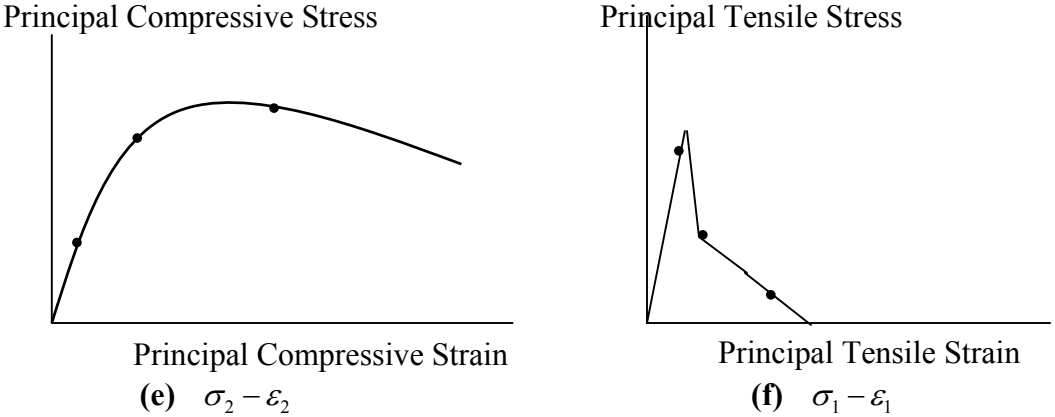

(e) $\sigma_2 - \varepsilon_2$ **(f)** $\sigma_1 - \varepsilon_1$

Figure 2.18 Model Calibration for the MCFT

Constitutive Relationships

The main objective of the MCFT is to incorporate the contributions from the concrete tensile stress into the model. Vecchio and Collins (1982) calibrated the model based on experimental results from 28 test panels and proposed the following constitutive relationship for concrete in principal tensile direction:

$$\sigma_{c1} = E_c \varepsilon_1 \ , \ \varepsilon_1 < \varepsilon_{cr} \text{ and} \tag{2.16}$$

$$\sigma_{c1} = \frac{f_{cr}}{1+\sqrt{200\varepsilon_1}} \ , \ \varepsilon_1 > \varepsilon_{cr}$$

Based on the experiments conducted by Vecchio and Colins (1982), the presence of tensile stress or strain perpendicular to the existing compressive stress somewhat decreased the compressive strength in that direction. The following equation was originally proposed for stress-strain relationship in the principal compressive direction.

$$\sigma_{c2} = \beta f_c^{'} \left(\frac{2\varepsilon_2}{\beta\varepsilon_0} - \left(\frac{\varepsilon_2}{\beta\varepsilon_0} \right)^2 \right) \tag{2.17}$$

$$\beta = \frac{1}{0.85 - 0.27\frac{\varepsilon_1}{\varepsilon_2}} \leq 1.0$$

Note that the β factor represents the decrease in peak stress and strain associated with the peak stress.

Crack Check

Vecchio and Collins (1982) found that the plot of the experimental results of principal tensile stress-strain relationship experienced a wide range of scattering. In order to find the best representation of the curve passing through all those points, Vecchio and Collins (1982) proposed the tensile stress-strain relationship in the form of

Eq. 2.16. However, Vecchio and Collins (1982) explicitly stated that the proposed equation was obtained by best fitting the experimental results where yielding of reinforcement was not dominant. Experimental results showed that, in cases where yielding occurred, the tensile stress in concrete was much lower than that was predicted by Eq. 2.16. Therefore, a scheme to extend the applicability of Eq. 2.16 to the cases where yielding occurs was proposed. This process was termed "crack check". Vecchio and Collins (1982) assumed the following:

$$\sigma_{c1} = \frac{f_{cr}}{1+\sqrt{200\varepsilon_1}} \le \rho_x (f_{yx} - \sigma_{sx}) \sin^2 \phi_x + \rho_y (f_{yy} - \sigma_{sy}) \cos^2 \phi_y \tag{2.18}$$

where ϕ_x, ϕ_y = angles between the crack direction and the reinforcement in global X and Y directions, as shown in Fig. 2.19, respectively.

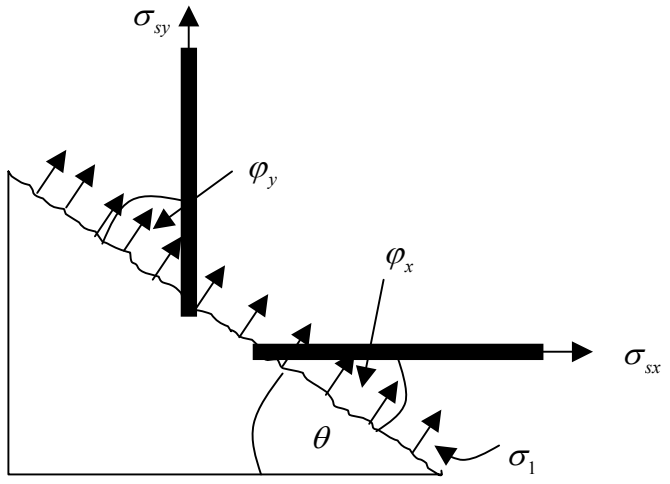

Figure 2.19 Free Body Diagram at Crack Location

Essentially, this equation limits the tensile stress in concrete such that the summation of average concrete and reinforcing steel stress at crack locations, where yielding of reinforcement occurs, does not exceed the yield stress of reinforcing steel.

2.5.1.3 Disturbed Stress Field Model (DSFM)

Vecchio (2000) developed the Disturbed Stress Field Model along the same lines as the MCFT with relaxed assumption on the coincidence of concrete principal stress and strain directions. Because the direction of the principal concrete stress and strain are no longer coincident, additional shear components exist across the crack. Vecchio (2000) attributed the existence of this shear component to the slip between concrete and reinforcement interface. Comprehensive information on the DSFM may be obtained from Vecchio (2000).

2.5.2 Houston Group Research

Parallel to the development of the MCFT, an extensive experimental program was conducted on the behavior of reinforced concrete membrane elements at the University of Houston (Hsu 1988, Belarbi and Hsu, 1994, Belarbi and Hsu, 1995, Pang and Hsu, 1996, Zhang and Hsu, 1997 and Zhu and Hsu, 2002). Hsu (1988) proposed a conceptual model based on the same equilibrium and compatibility equations as the Toronto Research Group and applied his theory to determine the strength for RC members subjected to shear and torsion. This model laid the foundation for his subsequent refinements and was later termed the Softened Truss Model (STM).

2.5.2.1 Rotating Angle Softened Truss Model (RA-STM)

Extensive experimental programs (Belarbi, 1991 and Pang, 1991) were performed in order to determine the appropriate constitutive relationship of concrete in the **principal** direction and of concrete with embedded reinforcing steel as required in the STM proposed by Hsu (1988). The resulting model was later called Rotating Angle Softened Model (RA-STM).

Fig. 2.20 shows the general test setup for the universal panel tester developed by Belarbi (1991) and Pang (1991). There are several differences between the shear-rig panel tester developed by Vecchio and Collins (1982) and the universal panel tester. Firstly, the external loads are applied through a series of hydraulic jacks and rigid links only capable of applying the axial forces lying in the horizontal and vertical axis as shown in the figure above. Consequently, only the condition of normal stress exists on the horizontal and vertical sides of the panel. The vertical and horizontal axes are also the principal direction of the applied stresses. The stress conditions at other planes are obtained by using the stress transformation relationship (Mohr's circle of total stress). Secondly, the sizes of the test panels were different. The test panel size developed by the University of Toronto was 35x35 inches, with the thickness of 2.75 inches. Square panels tested by Belarbi (1991) and Pang (1991) 55 inches wide and 7 inches thick. The thickness of the test panel can be increased up to 16 inches.

The RA-STM employs the same set of assumptions made in the CFT and MCFT as listed in Section 2.5.1.2. Consequently, the governing relations for equilibrium and compatibility are the same (see Eqs. 2.9 and 2.10). The diversion from the MCFT lies in the model calibration. Vecchio and Collins (1982) assumed that the concrete is perfectly bonded to the reinforcing steel and the behavior of embedded reinforcement is elastic-perfectly plastic like that of a bare bar. From the data measurements obtained from the strain gauges, the steel stress is obtained directly from the assumed stress-strain relationship. The concrete tensile constitutive relationship in the principal direction is a derived quantity as explained in Section 2.3.2.

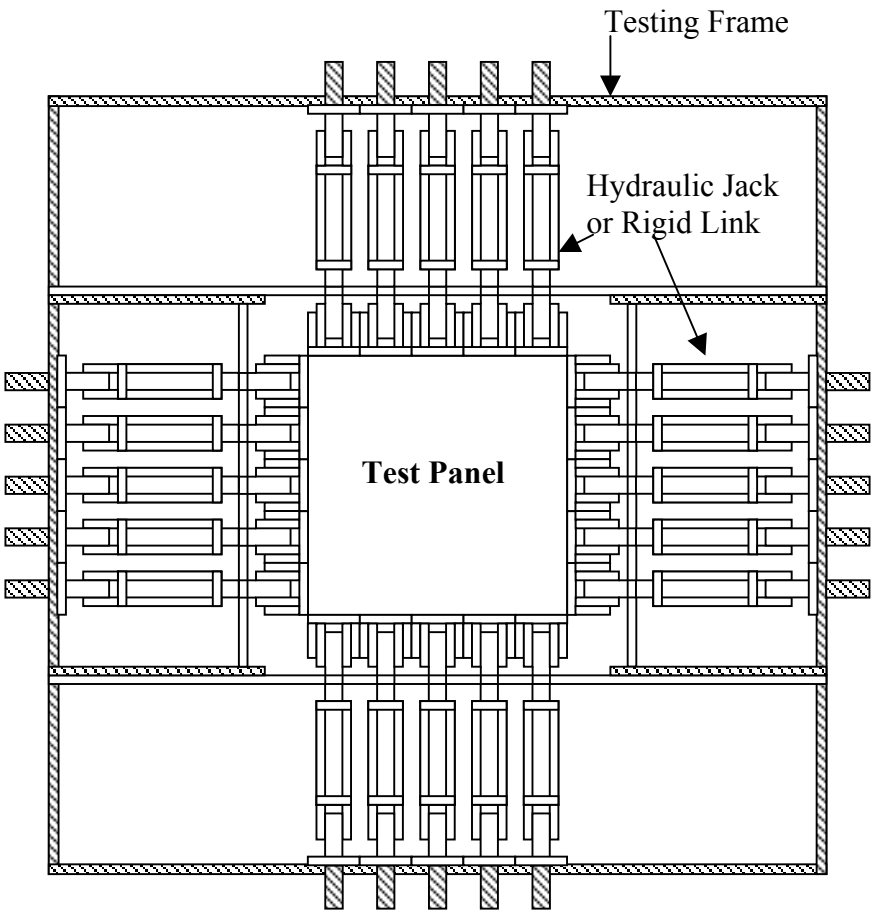

Figure 2.20 Universal Panel Tester Developed at the University of Houston

Although RA-STM assumes a perfect bond between the concrete and reinforcing steel, the constitutive relationship of the embedded reinforcing steel is assumed to be unknown beforehand and is determined from the test results. From a uniaxial tensile test on reinforced concrete prisms by Tamai et al. (1987), it was found that the average stress-strain of reinforcing steel embedded in concrete is different from that of the bare bar. Tamai et al. (1987) reported the absence of the yield plateau and a lower yield strength in the average stress-strain of the embedded bar. This discrepancy was attributed to the effect of tension stiffening and interfacial bond and slip as described in Section 2.2.3.

Model Calibration

Belarbi (1991) and Pang (1991) conducted an experimental program on RC panels using the universal panel tester developed by Hsu et al. (1995). As previously described, the objective of this experimental program was to determine the constitutive model of concrete in the principal compressive direction and of embedded reinforcing steel in tension, assuming that the stress-strain relationship of concrete in principal tensile direction is known. Two fundamentally different test series were performed (Belarbi, 1991, and Pang, 1991). The reinforcement in panels tested by Belarbi (1991) aligned with the vertical and horizontal axis of the panel, while Pang (1991) used orthotropic reinforcement that was oriented 45 degrees angle away from the horizontal-vertical axis as shown in Fig. 2.21.

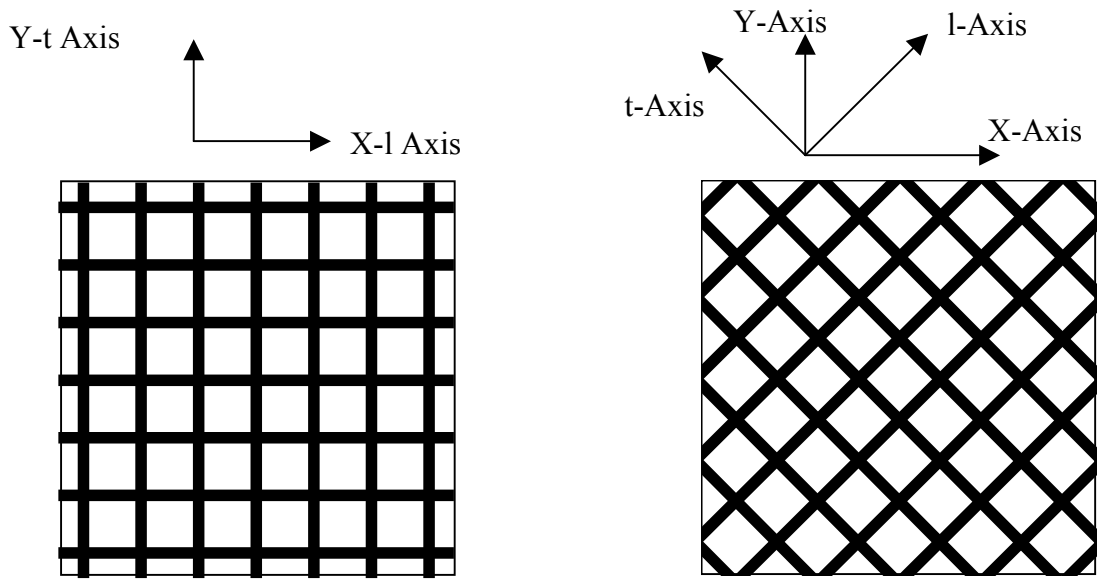

(a) Belarbi's Test Series **(b) Pangs' Test Series**

Figure 2.21 Reinforcement Orientation Used by the University of Houston Research Group

The calibration of the model equations by Belarbi (1991) is rather straightforward. Because the total applied stresses in the vertical and horizontal directions are the applied principal stresses and the reinforcement is also aligned with the principal directions, the vertical and horizontal axes are, therefore, the concrete principal direction. The equilibrium condition in the global X-Y (Horizontal-Vertical) direction is given by Eq. 2.9.

The applied stress and strain in the global X-Y directions can be found from the load cells and the LVDTs installed on the test machine, respectively. Belarbi (1991) assumed that the pre-yield stress-strain relationship of the embedded bar is the same as that of the bare bar. Therefore, given a state of average strain measured from the LVDTs, the steel contribution to the total applied stress can be determined using stress-strain relationship of the bare bar. Consequently, the average stress-strain of concrete in tension can be determined from Eq. 2.9. A simplified equation for average stress-strain relationship of concrete was then proposed by curve fitting from the experimental data:

$$\sigma_{c1} = E_c \varepsilon_1 \ , \ \ \varepsilon_1 < 0.00008 \text{ and} \tag{2.19}$$

$$\sigma_{c1} = f_{cr} \left(\frac{0.00008}{\varepsilon_1}\right)^{0.4} \ , \ \varepsilon_1 > 0.00008$$

where E_c = Modulus elasticity of concrete $= 47,000\sqrt{f_c'}$, in psi.

f_{cr} = Cracking strength of concrete = $3.75\sqrt{f_c'}$, in psi.

However, the post-yield stress-strain relationship of the embedded reinforcing steel was assumed to be unknown. Eq. 2.19 was extrapolated to determine the post-yield constitutive relationship of reinforcing steel. The process became the reverse of the method to determine the average stress-strain of concrete. Essentially, given a state of applied stresses and measured average strain in principal tensile direction, the steel stress

was obtained by subtracting the concrete stress determined from Eq. 2.9 from the total applied stress. The same process was repeated for the various strains to obtain the average stress-strain relationship of embedded steel. Similarly, the stress-strain of concrete in the principal compressive direction can also be determined using the same procedure.

Because the orthogonal reinforcement in the Panel Test Series by Pang (1991) made a 45 degree angle with the global X-Y axis, the model calibration was relatively more complex. In addition to the LVDTs used for measuring the strain in X-Y directions (directions of the applied stresses) as in the Belarbi's test series, an extra set of LVDTs was required to measure strains in the direction of the reinforcing steel.

Pang (1991) divided his thirteen test panels into three groups. The first group contained equal reinforcement ratio. This series of panels was tested under equal magnitudes of monotonic stress in the global X-Y directions, but in opposite direction. Using the Mohr's circle of total stresses, these applied stresses cause pure shear conditions along the reinforcement axes that were 45 degrees from the X-Y axis. The second group of the test series was subjected to the same loading conditions as the first test series except that the reinforcement ratios in the two orthogonal directions were not equal. The last group of specimens was essentially the same as the first group of specimen tested under sequential loading. Essentially, the equal, but opposite, stresses were alternately applied along the X-Y axis.

Because of the complexities involved in the calibration process, Pang (1991) employed two calibration steps. The first step was to determine the stress-strain relationship of embedded reinforcement. Because the second series of the test panels contained unequal reinforcement ratios there were more unknowns than provided equations. Therefore, information on the embedded steel stress could not be deduced from the available test data. By using symmetry of reinforcement in the first and third

test series, that additional unknown was eliminated. Therefore, the stress-strain relationship of embedded bar in tension was determined. It was assumed that the same set of stress-strain relationships of embedded bar calibrated from the first and third test series were also applicable to the second test series. The constitutive relationship of concrete in principal compressive direction was carried out in the second calibration step, which required the use of the stress-strain relationship of embedded reinforcement obtained from the first step.

- First step calibration

Consider a stress condition in the direction of the reinforcement (l-t axis) as shown in Fig. 2.21b. As explained in the previous paragraphs, the applied stress condition for the test series conducted by Pang (1991) imposed the state of pure shear on the l-t axis. In other words, no net normal stress existed in either direction of the reinforcement axis. The stress transformation relationship (Eq. 2.9) may be rewritten in this l-t axis as

$$\begin{aligned} \sigma_l &= \frac{(\sigma_{c1}+\sigma_{c2})}{2} - \frac{(\sigma_{c1}-\sigma_{c2})}{2}\cos(2\theta_\sigma) + \rho_l\sigma_{sl} = 0 \\ \sigma_t &= \frac{(\sigma_{c1}+\sigma_{c2})}{2} + \frac{(\sigma_{c1}-\sigma_{c2})}{2}\cos(2\theta_\sigma) + \rho_t\sigma_{st} = 0 \\ \tau_{lt} &= \frac{(\sigma_{c1}-\sigma_{c2})}{2}\sin(2\theta_\sigma) \end{aligned} \qquad (2.20)$$

Note that the angle θ_σ now becomes the angle between the principal compressive stress direction and the l- axis.

By using symmetry, the angle θ_σ must be equal to 45 degrees for panels with equal reinforcement ratio in l-t axis. This condition also results in equal stresses in the reinforcement in l-t direction. Adding the first and second equations of Eq. 2.20,

substituting θ_σ = 45 degrees, and using the fact that the stresses in steel in l- and t-direction are equal results in:

$$\sigma_{sl} = \sigma_{st} = -\frac{\sigma_{c1} + \sigma_{c2}}{2\rho} \tag{2.21}$$

Substituting θ_σ = 45 degrees into the third equation of Eq. 2.20 results in

$$\tau_{lt} = \frac{(\sigma_{c1} - \sigma_{c2})}{2} \tag{2.22}$$

Subtracting σ_{c1} from the above equation results in

$$\tau_{lt} - \sigma_{c1} = \frac{(\sigma_{c1} - \sigma_{c2})}{2} - \sigma_{c1} = -\frac{\sigma_{c1} + \sigma_{c2}}{2} \tag{2.23}$$

Substituting Eq. 2.23 into Eq. 2.21 gives:

$$\sigma_{sl} = \sigma_{st} = \frac{\tau_{lt} + \sigma_{c1}}{\rho} \tag{2.24}$$

Note that Eqs. 2.21-2.24 are only valid for panels with equal reinforcement ratio in l-t directions subject to pure shear loading. This equation was used to calibrate the stress-strain relationships of embedded reinforcing steel in the first and third test series (Pang, 1991). As can be seen from Eq. 2.24, an additional assumption regarding the tensile stress-strain relationship of concrete must be made to calculate σ_{c1} in order to determine the stress in σ_{sl} or σ_{st} from Eq. 2.24 above. Pang (1991) assumed that the concrete tensile stress-strain relationship proposed by Belarbi (1991) (Eq. 2.19), which is essentially the same as that proposed by Tamai et al. (1987), remained valid. Using this

assumption, the stress-strain relationship of embedded bar can be determined by substituting τ_{lt} and σ_{c1} which can be determined from all measured state of strains ($\varepsilon_x, \varepsilon_y, \varepsilon_l, \varepsilon_t$) readings from LVDTs.

- Second step calibration

The second step calibration involved the determination of the constitutive relationship of concrete in the principal compressive direction. Adding the first and second equations from Eq. 2.20 results in:

$$\sigma_l + \sigma_t = \sigma_{c1} + \sigma_{c2} + \rho_l \sigma_{sl} + \rho_t \sigma_{st} \text{ or} \tag{2.25}$$
$$\sigma_{c2} = \sigma_l + \sigma_t - (\rho_l \sigma_{sl} + \rho_t \sigma_{st} + \sigma_{c1})$$

Because all test panels by Pang (1991) enforced the condition of pure shear, the above equation can be rewritten as:

$$\sigma_{c2} = -(\rho_l \sigma_{sl} + \rho_t \sigma_{st} + \sigma_{c1}) \tag{2.26}$$

Under a given state of strains ($\varepsilon_l, \varepsilon_t$) measured from LVDTs, the stress contribution due to embedded steel (σ_{st}, σ_{sl}) can be determined from the stress-strain relationship obtained from step 1 defined above. In addition, from the measured strains ($\varepsilon_x, \varepsilon_y, \varepsilon_l, \varepsilon_t$), two principal strains ($\varepsilon_1, \varepsilon_2$) can be determined using Mohr's circle of strain. Note that this process is the same as defined by Vecchio and Collins (1982). Recall that there is one redundant strain component. Pang (1991) explicitly employed the least square technique to determine the two principal strains ($\varepsilon_1, \varepsilon_2$). Given the information regarding principal strain (ε_1), the principal tensile stress (σ_{c1}) can be determined using Eq. 2.19. Substituting $\sigma_{st}, \sigma_{sl}, \sigma_{c1}$ into Eq. 2.26 gives the principal compressive stress (σ_{c2}). Pang (1991) employed this process to calibrate the stress-

strain relationship for concrete in principal compressive direction using test data from thirteen test panels.

Constitutive Relationships

Based on the model calibration from experimental results, Belarbi (1991) proposed a stress-strain relationship of embedded steel reinforcement in tension, concrete in tension and compressive as follows:

- Embeded steel reinforcement in tension:

$$\sigma_s = E_s\varepsilon_s, \sigma_s \le (0.93-2B)f_y \qquad (2.27)$$
$$= (0.91-2B)f_y + (0.02+0.25B)E_s\varepsilon_s, \sigma_s > (0.93-2B)f_y$$

where $B = \frac{1}{\rho}\left(\frac{f_{cr}}{f_y}\right)^{1.5}$

- Concrete in tension:

$$\sigma_{c1} = 47,000\sqrt{f_c'}\varepsilon_1, \varepsilon_1 < 0.00008 \qquad (2.28)$$
$$= 3.75\sqrt{f_c'}\left(\frac{0.00008}{\varepsilon_1}\right)^{0.4}, \varepsilon_1 > 0.00008$$

- Concrete in compression:

$$\sigma_{c2} = \varsigma f_c'\left[2\frac{\varepsilon_2}{\varsigma\varepsilon_0} - \left(\frac{\varepsilon_2}{\varsigma\varepsilon_0}\right)^2\right], \varepsilon_2 < \varsigma\varepsilon_0 \qquad (2.29)$$
$$= \varsigma f_c'\left[1 - \left(\frac{\frac{\varepsilon_2}{\varsigma\varepsilon_0} - 1}{\frac{2}{\varsigma} - 1}\right)^2\right], \varepsilon_2 > \varsigma\varepsilon_0$$

where ς = peak stress and strain softening factor $= \dfrac{0.9}{\sqrt{1+400\varepsilon_1}}$

Subsequent work by Pang (1991) showed that Eq. 2.27 remained valid for panels whose reinforcements are not aligned with the principal direction of concrete. However, the stress-strain relationship of embedded reinforcement should be modified. The stress-strain relationship of embedded bar proposed by Pang (1991) was

$$\sigma_s = E_s\varepsilon_s, \sigma_s \le (0.93-2B)(1-\frac{2-\frac{\alpha_2}{45^o}}{1000\rho})f_y \tag{2.30}$$

$$= f_y\left[0.91-2B)+(0.02+0.25B)\frac{\varepsilon_s}{\varepsilon_y}\right]\left[1-\frac{2-\frac{\alpha_2}{45^o}}{1000\rho}\right],$$

$$\sigma_s > (0.93-2B)(1-\frac{2-\frac{\alpha_2}{45^o}}{1000\rho})f_y$$

2.5.2.2 Fixed Angle Softened Truss Model (FA-STM)

Pang and Hsu (1996) argued the inadequacy of the rotating crack assumption and claimed that the concrete contribution to the shear strength of RC members cannot be taken into account using RA-STM. To properly account for shear strength contribution due to concrete, Pang and Hsu (1996) claimed that crack angle should be kept fixed once it is formed. Pang (1991) and Pang and Hsu (1996), based on this conceptual model, proposed that the concrete stress in fixed crack coordinate system should be expressed in terms of strain components in the direction of the crack. Fig. 2.22 shows the Mohr's circle of stress in the FA-STM. Because this fixed crack direction is, in general, not the same as the current principal stress and strain direction, shear stress components along the crack also exist. The identification of three main concrete stress components acting on the crack is required: (1) Direct stress parallel to the crack; (2) Direct stress normal to the crack; and (3) Shear stress on the crack. Experimental programs were conducted to

determine the constitutive relationships of concrete in the fixed crack coordinate (Pang and Hsu, 1996, Hsu and Zhang, 1997). Pang and Hsu (1996) and Hsu and Zhang (1997) postulated that the direction of the fixed crack direction should be the same as the principal tensile direction of the **total** applied stress not the principal **concrete** stress as assumed in RA-STM.

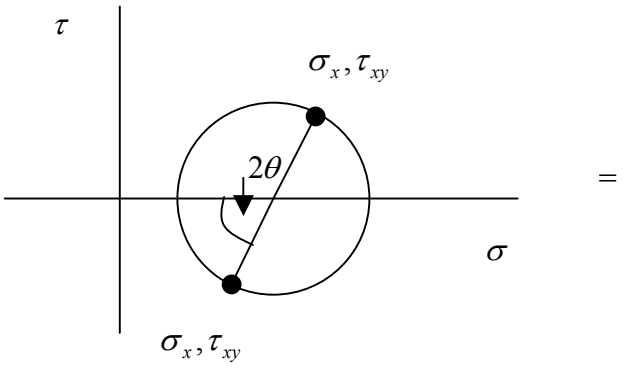

(a) Total Stress

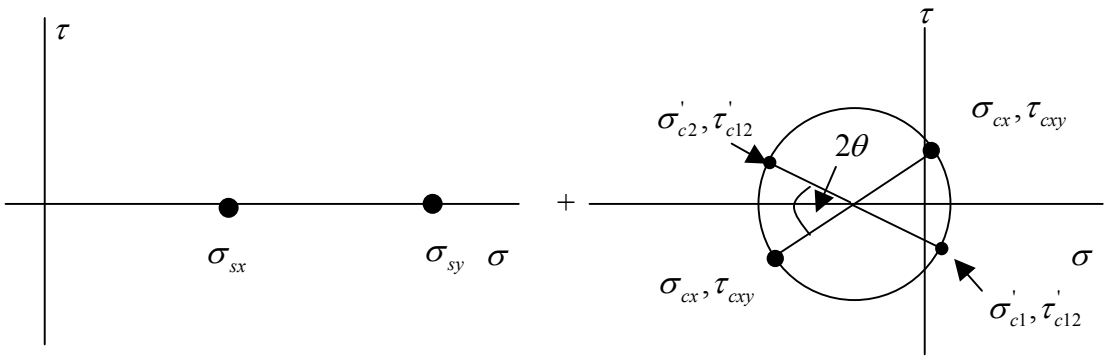

(b) Steel Stress **(c) Concrete Stress**

Figure 2.22 Equilibrium Condition for FA-STM Using 2D Mohr's Circle

It should be noted that all test panels tested by Pang (1991) and Zhang (1995) were tested under monotonically increased stresses. In addition, the majority of the test panels were also subjected to proportional loading conditions. Therefore, the principal

tensile direction of the total applied stresses was fixed throughout the loading history for each panel.

Governing Equations for FA-STM

Given a state of total applied stresses ($\sigma_x, \sigma_y, \tau_{xy}$), the fixed angle θ can be determined from the principal tensile direction of $\sigma_x, \sigma_y, \tau_{xy}$ as:

$$\theta = \frac{1}{2}\tan^{-1}\frac{2\tau_{xy}}{\sigma_y - \sigma_x} \tag{2.31}$$

- Equilibrium

The equilibrium between the total applied stresses ($\sigma_x, \sigma_y, \tau_{xy}$) and stress condition in the fixed angle θ coordinate can be determined from the Mohr's circle of stress shown in Fig. 2.22 and can be written as

$$\begin{aligned}
\sigma_x &= \frac{(\sigma_{c1}^{'} + \sigma_{c2}^{'})}{2} - \frac{(\sigma_{c1}^{'} - \sigma_{c2}^{'})}{2}\cos(2\theta) + \tau_{c12}^{'}\sin(2\theta) + \rho_x\sigma_{sx} \\
\sigma_y &= \frac{(\sigma_{c1}^{'} + \sigma_{c2}^{'})}{2} + \frac{(\sigma_{c1}^{'} - \sigma_{c2}^{'})}{2}\cos(2\theta) - \tau_{c12}^{'}\sin(2\theta) + \rho_y\sigma_{sy} \\
\tau_{xy} &= \frac{(\sigma_{c1}^{'} - \sigma_{c2}^{'})}{2}\sin(2\theta) + \tau_{c12}^{'}\cos(2\theta)
\end{aligned} \tag{2.32}$$

where $\sigma_{c1}^{'}$ = concrete tensile stress perpendicular to the θ direction

$\sigma_{c2}^{'}$ = concrete compressive stress along the θ direction

$\tau_{c12}^{'}$ = concrete shear stress on the crack face along the θ direction

- Compatibility

The compatibility between the strain in the global X-Y coordinate and the angle coordinate defined by the direction of the total applied stress can be derived using the 2D Mohr's circle of strain or the strain transformation relationship as shown in Fig. 2.23.

$$\varepsilon_{cx} = \frac{(\varepsilon_{c1}^{'} + \varepsilon_{c2}^{'})}{2} - \frac{(\varepsilon_{c1}^{'} - \varepsilon_{c2}^{'})}{2}\cos(2\theta) + \frac{\gamma_{c12}^{'}}{2}\sin(2\theta)$$

$$\varepsilon_{cy} = \frac{(\varepsilon_{c1}^{'} + \varepsilon_{c2}^{'})}{2} + \frac{(\varepsilon_{c1}^{'} - \varepsilon_{c2}^{'})}{2}\cos(2\theta) - \frac{\gamma_{c12}^{'}}{2}\sin(2\theta) \qquad (2.33)$$

$$\gamma_{cxy} = (\varepsilon_{c1}^{'} - \varepsilon_{c2}^{'})\sin(2\theta) + \frac{\gamma_{c12}^{'}}{2}\cos(2\theta)$$

where $\varepsilon_{c1}^{'}$ = concrete strain perpendicular to the θ direction

$\varepsilon_{c2}^{'}$ = concrete strain along the θ direction

$\gamma_{c12}^{'}$ = concrete shear strain in the θ direction

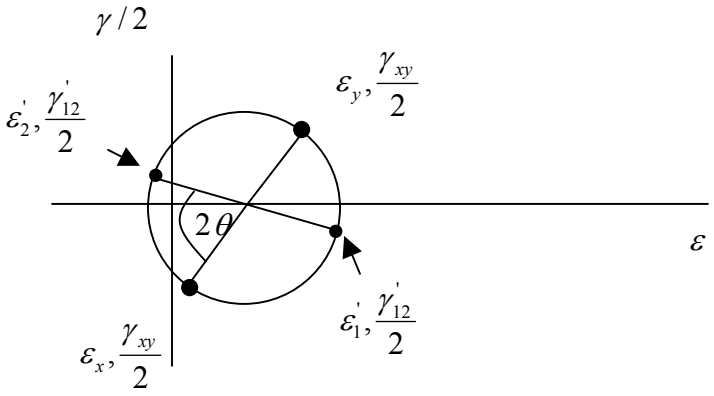

Figure 2.23 2D Mohr's Circle of Strain for FA-STM

Model Calibration

Pang (1991) used the same set of experimental results as previously used in the calibration of RA-STM to develop the constitutive relationship for FA-STM. The

calibration process was similar to that of RA-STM. However, the component $\tau_{c12}^{'}$ must also be identified. Because the constitutive relationships of concrete are now written in terms of **stresses-strains in fixed crack coordinates**, not the principal stress-strain as in the RA-STM, a slight modification from the two step procedure proposed by Pang (1991) was carried out.

Pang (1991) established the two step procedure similar to the scheme used to calibrate the RA-STM for constructing the stress-strain relationship for FA-STM. The first step involved the determination of the stress-strain relationship of embedded bar from the first and third series of the test as described previously. It was shown that for the first and third test series, the angles θ_{σ} and θ coincide. Therefore, the stress-strain relationship of embedded bars derived for RA-STM was also applicable to FA-STM. No further discussion would be made here. The second step calibration involves the development of the stress-strain relationship, written in terms of fixed crack coordinate, for compressive stress in the direction parallel to the fixed crack angle and the shear stress existing along the crack surface.

Pang (1991) employed the third equation of Eq. 2.32 to determine the compressive stress $\sigma_{c2}^{'}$ parallel to the fixed crack direction. Note that the X-Y coordinates were changed to the l-t coordinates for convenience. Recall that all panels in the test series conducted by Pang (1991) enforced the absence of σ_l and σ_t. This corresponds to the angle θ equals to 45 degrees. In other words, the crack angle makes an angle 45 degree with the l-t coordinate. This corresponds to the direction of the applied tensile stress along the X-axis. Substituting θ=45 degrees into the third equation of Eq. 2.32 gives:

$$\sigma_{c2}^{'} = \sigma_{c1}^{'} - 2\tau_{lt} \tag{2.34}$$

Note that under the test condition imposed by Pang (1991), the strains along the X-axis and Y-axis become the tensile strain perpendicular to the fixed angle and the compressive strains along the fixed angle, respectively. Given the information regarding $\sigma_{c2}^{'}$ obtained from Eq. 2.34, the relationship between $\sigma_{c2}^{'}$ and $\varepsilon_1^{'}$ and $\varepsilon_2^{'}$ can be established. Note that the tensile stress-strain relationship between $\sigma_{c1}^{'}$ and $\varepsilon_1^{'}$ must also be assumed. Pang (1991) assumed that Eq. 2.19 as proposed by Tamai et al. (1987) and Belarbi (1991) were also applicable here.

The shear stress along the fixed-crack coordinate can be obtained by subtracting the second equation from the first equation of Eq. 2.32. Substituting θ=45 degrees for the test series resulted in:

$$\tau_{c12}^{'} = \frac{1}{2}(\rho_l \sigma_{sl} - \rho_t \sigma_{st}) \tag{2.35}$$

Similarly, Eq. 2.35 was used to develop the relationship between shear stress $\tau_{c12}^{'}$ and strain measure from LVDTs ($\varepsilon_l, \varepsilon_t, \varepsilon_x, \varepsilon_y$).

Zhang (1995) adopted a similar procedure to that proposed by Pang (1991) to extend the applicability of the FA-STM to high strength concrete. Zhang (1995) showed that the strength of concrete has an effect on the stress-strain relationship of concrete developed under the framework of FA-STM.

Constitutive Relationships

Pang (1991) and Zhang (1995) proposed that Eq. 2.30 be used to determine the stress-strain relationship for embedded reinforcement. For concrete stress-strain in the fixed angle direction, Pang (1991) and Zhang (1995) proposed that the same form as Eq. (2.28) and (2.29), except that the parameter ε_1 and ε_2 were changed to $\varepsilon_1^{'}$ and $\varepsilon_2^{'}$. In

other words, the strain in fixed angle coordinate was defined entirely by the total applied stress instead of the rotating principal strain.

An additional constitutive relationship for shear stress across the fixed angle was also proposed by Pang (1991) and Zhang (1995):

$$\tau'_{c12} = \tau'_{c12m}\left[1-(1-\frac{\gamma'_{c12}}{\gamma'_{c12o}})^6\right] \tag{2.36}$$

where τ'_{c12m} = maximum shear stress in fixed crack angle

γ'_{c12o} = shear strain corresponding to the τ'_{c12m}

Because Eq. 2.36 is too complicated to be used in FEM analysis, recent studies by Zhu and Hsu (2002) simplified Eq. 2.36 by using the shear tangent stiffness proposed by Willam et al. (1987). The resulting relationship has the form

$$\tau'_{c12} = \frac{\sigma'_{c1}-\sigma'_{c2}}{2(\varepsilon'_{c1}-\varepsilon'_{c2})}\gamma'_{c12} \tag{2.37}$$

2.5.2.3 Softened Membrane Model (SMM)

Zhu and Hsu (2002) employed the FA-STM to perform experimental and analytical studies on RC panels. The universal panel tester developed at the University of Houston was upgraded such that both stress and strain control experiments can be performed. Two major modifications were made to the FA-STM. Firstly, the concrete shear stress-strain relationship was simplified as explained in the previous section. Additional information on the Poisson's effect was also incorporated into the original FA-STM. Comprehensive information on the development and model calibration of the SMM can be found in Zhu and Hsu (2002).

CHAPTER III

CONSTITUTIVE MODEL FORMULATION

3.1 INTRODUCTION

A constitutive model for confined reinforced concrete members prone to shear mechanisms, within the framework of the MCFT and RA-STM, is proposed in this chapter. Certain features from both MCFT and RA-STM are selectively incorporated into the proposed model based on the structural performance and numerical efficiency points of view. The derivation of a new constitutive relationship of concrete in compression, including the effects of confinement from the transverse reinforcement, is presented. In essence, the new concrete constitutive relationship involves the modification of the peak stress and strain of the Popovic (1973) or Mander (1988) constitutive relationships for concrete through the use of the five-parameter concrete failure surface of Willam and Warnke (1974). The confining stresses used for determining this peak stress are obtained from the stresses in the principal direction. The advantage of this method is the effect of transverse reinforcing steel acting as a confining agent to the core concrete can be taken into account rather easily. In the next chapter, the constitutive relationship derived in this chapter will be used to perform an analytical study on the effect of confinement from transverse reinforcement in RC members and will be compared to the results of RC bent cap experimental tests (Bracci et al., 2000).

3.2 PROPOSED CONSTITUTIVE RELATIONSHIPS

The constitutive model at the continuum level is derived in this section with the main emphasis on its use in FEM analyses. Within this setting, the problem invariably involves the evaluation of stress and tangent or secant stiffness corresponding to a given state of strain. The fundamental background for the derivation of the element stiffness matrix will be summarized. However, the secant stiffness matrix used in this model is, in general, non-symmetric. Because the current computer program developed by the

author cannot handle this non-symmetry of the stiffness matrix, a commercial FEM analysis program ABAQUS© (Hibbitt, Karlsson & Sorensen, Inc. 2002.), with the ability to incorporate a user-defined material subroutine, is used to perform this analytical study. The numerical implementation of this derived material secant stiffness matrix through ABAQUS will be explained.

3.2.1 Basic Assumptions

The proposed constitutive model follows the fundamental assumptions used in the MCFT (Vecchio and Collins, 1982) and RA-STM (Belarbi and Hsu, 1995). The fundamental assumptions used for this type of constitutive relationship are summarized as follows:

- Directions between principal stresses and strains coincide;
- Principal stresses can be expressed as a function of principal strains; and
- Reinforcing steel is perfectly bonded to the adjacent concrete.

The first two assumptions imply that the material axis of orthotropy is essentially the principal stress and strain directions as shown in Fig. 3.1. The third assumption allows the average stress of reinforced concrete to be written in terms of the sum of two components, that of the concrete and reinforcing steel. The detailed formulation of the proposed model is given in the next sections.

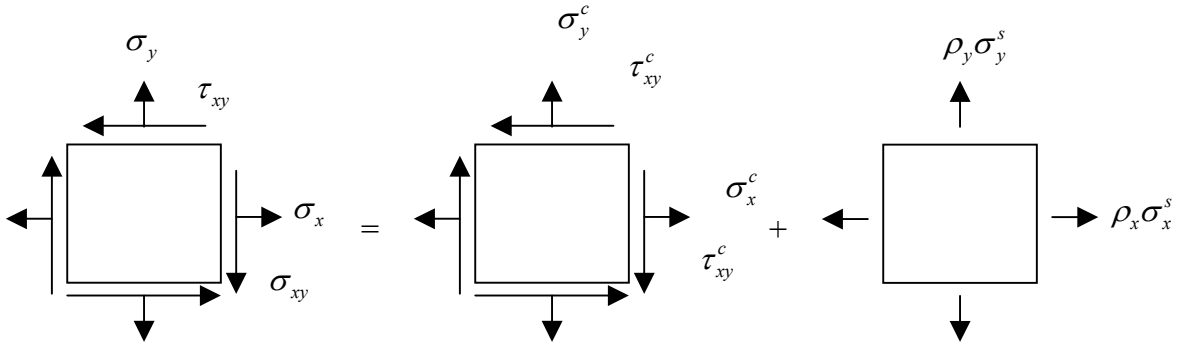

Figure 3.1 Total Stress Decomposition into Concrete and Steel Stress

3.2.2 Principal Stress and Strain Transformation

Equilibrium and compatibility between the principal directions and the global X-Y directions can be expressed by using the stress-strain transformation relationships as shown in Chapter II. The equation will be repeated here for the sake of completeness. The Mohr's circle of stress and strain transformation is shown in Fig. 3.2.

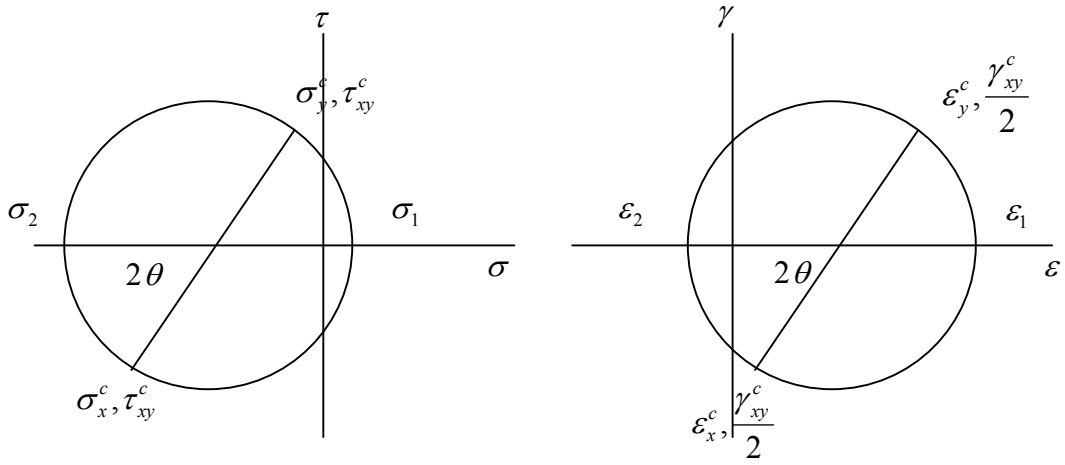

(a) Stress **(b) Strain**

Figure 3.2 Two-Dimensional Stress and Strain Transformation

The equation of equilibrium for the states of stresses are defined below:

$$\sigma_x = \frac{(\sigma_{c1}+\sigma_{c2})}{2} - \frac{(\sigma_{c1}-\sigma_{c2})}{2}\cos(2\theta_\sigma) + \rho_x\sigma_{sx}$$

$$\sigma_y = \frac{(\sigma_{c1}+\sigma_{c2})}{2} + \frac{(\sigma_{c1}-\sigma_{c2})}{2}\cos(2\theta_\sigma) + \rho_y\sigma_{sy} \qquad (3.1)$$

$$\tau_{xy} = \frac{(\sigma_{c1}-\sigma_{c2})}{2}\sin(2\theta_\sigma)$$

where σ_x = total applied stress in the X direction

σ_y = total applied stress in the Y direction

τ_{xy} = total applied shear stress in the X-Y direction

σ_{c1} = principal concrete stress in the major direction

σ_{c2} = principal concrete stress in the minor direction

θ_{σ} = angle between the global X-direction and direction of minor principal concrete stress

The compatibility equation for the states of strains are:

$$\begin{aligned} \varepsilon_{cx} &= \frac{(\varepsilon_{c1}+\varepsilon_{c2})}{2} - \frac{(\varepsilon_{c1}-\varepsilon_{c2})}{2}\cos(2\theta_{\varepsilon}) \\ \varepsilon_{cy} &= \frac{(\varepsilon_{c1}+\varepsilon_{c2})}{2} + \frac{(\varepsilon_{c1}-\varepsilon_{c2})}{2}\cos(2\theta_{\varepsilon}) \\ \gamma_{cxy} &= (\varepsilon_{c1}-\varepsilon_{c2})\sin(2\theta_{\varepsilon}) \end{aligned} \tag{3.2}$$

where ε_{cx} = concrete strain in the X direction

ε_{cy} = concrete strain in the Y direction

γ_{cxy} = concrete shear strain in the X-Y direction

ε_{c1} = principal concrete strain in the major direction

ε_{c2} = principal concrete strain in the minor direction

θ_{ε} = angle between the Global X-direction and direction of minor principal concrete strain

Note that due to the three main assumptions made above, $\theta_{\varepsilon} = \theta_{\sigma}$, $\varepsilon_{cx} = \varepsilon_{sx} = \varepsilon_{x}$, and $\varepsilon_{cy} = \varepsilon_{sy} = \varepsilon_{y}$

3.2.3 Concrete Constitutive Relationship

In the MCFT, the constitutive relationships of concrete are expressed in terms of principal stresses and strains. Two types of stress-strain relationships based on the algebraic sign of principal strains are required.

3.2.3.1 Concrete in Compression

There are several constitutive relationships for unconfined concrete in compression utilized in the literature. The original MCFT (Vecchio and Collins, 1982) proposed the use of the Hognestad parabola for the compression curve for unconfined concrete:

$$\sigma_c = f_c^{'}\left(\frac{2\varepsilon_c}{\varepsilon_0} - \left(\frac{\varepsilon_c}{\varepsilon_0}\right)^2\right) \tag{3.3}$$

where σ_c = concrete stress in compression

$f_c^{'}$ = unconfined 28 day compressive strength

ε_c = concrete strain

ε_0 = concrete strain corresponding to peak strength

However, it was found that this equation has a relatively steep post-peak response for confined concrete, which may not represent a true behavior near the peak strength of the confined members. Vecchio (1992) adopted two separate equations for pre-peak region and post-peak region in confined concrete. The same Hognestad parabola is used for pre-peak while the modified Kent-Park model is employed for post-peak. The relationships used were:

$$\sigma_c = f_{cc}^{'}\left(\frac{2\varepsilon_c}{\varepsilon_{cc}} - \left(\frac{\varepsilon_c}{\varepsilon_{cc}}\right)^2\right), \quad 0 < \varepsilon_c < \varepsilon_{cc}$$

$$\sigma_c = f_{cc}^{'}\left(1 + Z_m(\varepsilon_c - \varepsilon_{cc})\right) \geq 0.2 f_{cc}, \quad \varepsilon_c > \varepsilon_{cc} \tag{3.4}$$

$$Z_m = \frac{0.5}{\frac{3 + 0.002 f_c^{'}}{f_c^{'} - 1000} + \frac{2 f_{cb} + f_{cn}}{65250} - \varepsilon_{cc}}$$

where $f_{cc}^{'}$ = concrete confined compressive strength (psi)

ε_c = concrete strain

ε_{cc} = concrete strain corresponding to peak strength

f_{cb} = the smaller confined stress (psi)

f_{cn} = the difference between two confining stresses (psi)

Note that the above equations are used to determine the confined concrete stress with two predefined confining stresses in the direction perpendicular to the direction where stress is to be determined. Fig. 3.3 shows the schematic description of the situation in which Eq. 3.4 is applied.

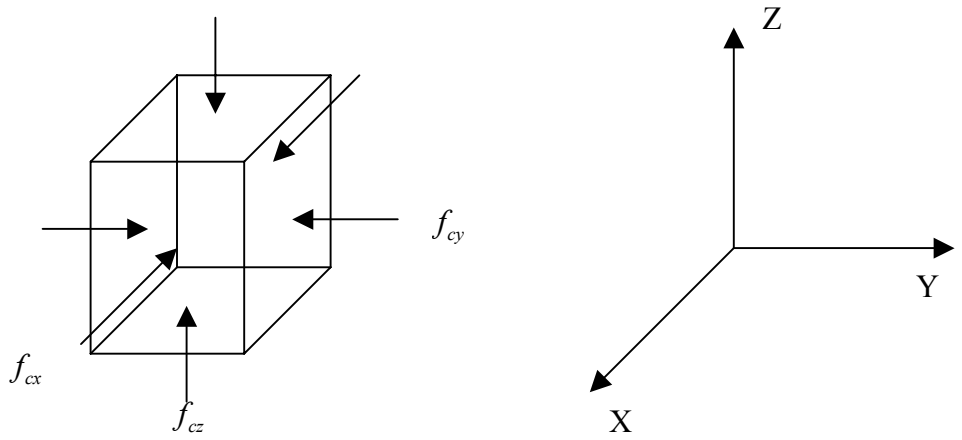

Figure 3.3 Triaxial State of Stresses with Unequal Confining Stresses

Mander et al. (1988) adopted a stress-strain curve proposed by Popovic (1973) for both confined and unconfined concrete based on extensive testing of confined RC members. The constitutive relationship for concrete compressive stress (σ_c) has the form

$$\sigma_c = \frac{f_{cc}^{'} xr}{r - 1 + x^r} \tag{3.5}$$

where $x = \frac{\varepsilon_c}{\varepsilon_{cc}}$

$$r = \frac{E_c}{E_c - E_{\sec}}$$

E_c = Initial Modulus of Elasticity

$E_{\sec}$ = Secant Modulus of Elasticity determined at the peak stress $= \frac{f_{cc}^{'}}{\varepsilon_{cc}}$

Fig. 3.4 shows the difference between the constitutive relationship for a sample specimen from Mander's equation and two equations proposed by Vecchio (1992). In the pre-peak region, the differences between the two approaches are insignificant. However, the Mander model has a more gradual descending curve in the post-peak region. Since the effects of confinement of heavily detailed RC members are to be incorporated in this study, Mander's model for adjusting the constitutive relationships for concrete is more effective and will be used in this analytical study. In terms of numerical simulation, Mander's model would also be less susceptible to numerical instability.

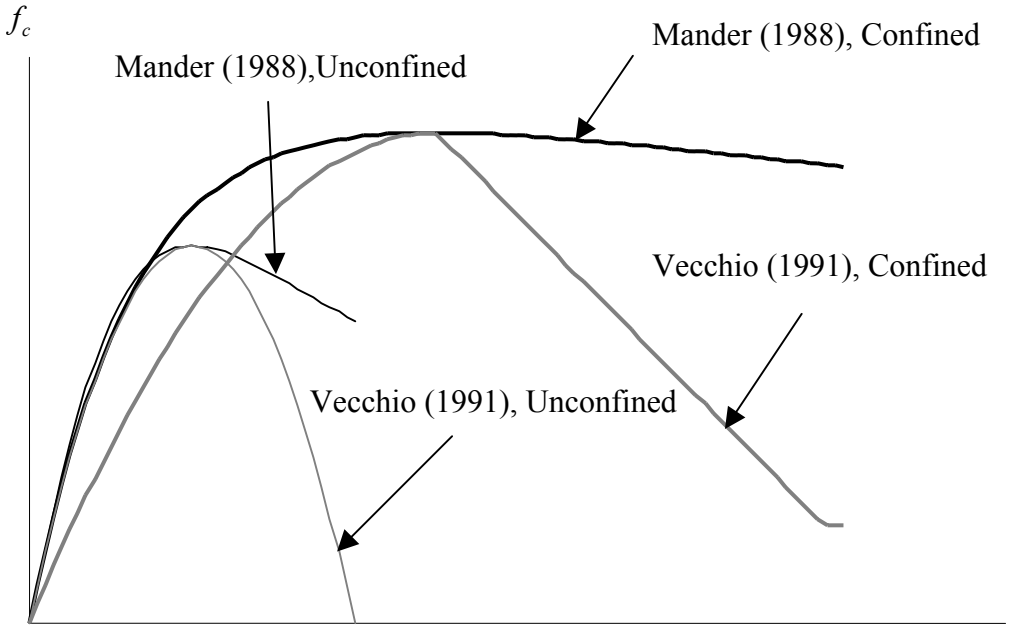

Figure 3.4 Comparison of Different Concrete Compressive Stress-Strain Based Curves

Compression Softening

Experimental evidence by Vecchio and Collins (1982, 1986, and 1993) and Belarbi and Hsu (1995) show a decrease in compressive strength of concrete subjected to biaxial tension-compression (those prone to shear mechanisms). Vecchio and Collins (1982) introduced a softening factor as a function of principal tensile and compressive strain to decrease this peak compressive stress and strain of unconfined concrete. This factor has the following form:

$$\beta = \frac{1}{0.85 - 0.27\frac{\varepsilon_1}{\varepsilon_2}} \leq 1.0 \qquad (3.6)$$

where β = peak stress and strain softening factor

ε_1 = principal tensile strain in concrete

ε_2 =principal compressive strain in concrete acting simultaneously as ε_1

Several refinements have been carried out as the number of experimental data increased since the first expression was proposed in 1982. The best-known model was proposed by Vecchio and Collins (1986) for a simplified procedure for shear design. This model was also adopted in the current AASHTO Code (1999). Unlike the previous model, this factor is only applied to decrease the peak stress, but not the peak strain. This post-peak stress-softening factor (Vecchio and Collins, 1986) is given by:

$$\beta = \frac{1}{0.8 + 0.34\dfrac{\varepsilon_1}{\varepsilon_0}} \leq 1.0 \tag{3.7}$$

Based on numerous tests of sample RC panels at the University of Houston, a similar model for compressive strain softening was proposed by Belarbi and Hsu (1995). Different softening factors are applied to peak stress and strain of unconfined concrete. The generic form of the peak stress (ζ_σ) and peak strain (ζ_ε) softening is given by:

$$\varsigma_\sigma = \frac{0.9}{\sqrt{1 + k_\sigma \varepsilon_1}} \tag{3.8a}$$

$$\varsigma_\varepsilon = \frac{0.9}{\sqrt{1 + k_\varepsilon \varepsilon_1}} \tag{3.8b}$$

The factors k_σ and k_ε take into account the effect of the loading condition, whether it is proportional or sequential loading. However, without a significant loss of accuracy, Belarbi and Hsu (1995) proposed a single softening factor for peak stress and strain:

$$\varsigma = \frac{0.9}{\sqrt{1 + 400\varepsilon_1}} \tag{3.9}$$

Fig. 3.5 shows the comparison between the stress-strain relationships of unconfined concrete using different compression softening factors. The figure shows that, in general, the softening factor proposed by Belarbi and Hsu (1995) leads to reduced compression strength in the post-peak regions. In general the effect of passive confinement due to transverse stirrups would be activated through the Poisson effect due to transverse expansion of compressed concrete. The confining stresses depend on the amount of this transverse expansion, which increases as concrete stress or strain increases. Therefore, the effect of confinement would only be activated at high levels of stress and strain. In this study, Eq. 3.7 based on Vecchio and Collins (1986) will be used.

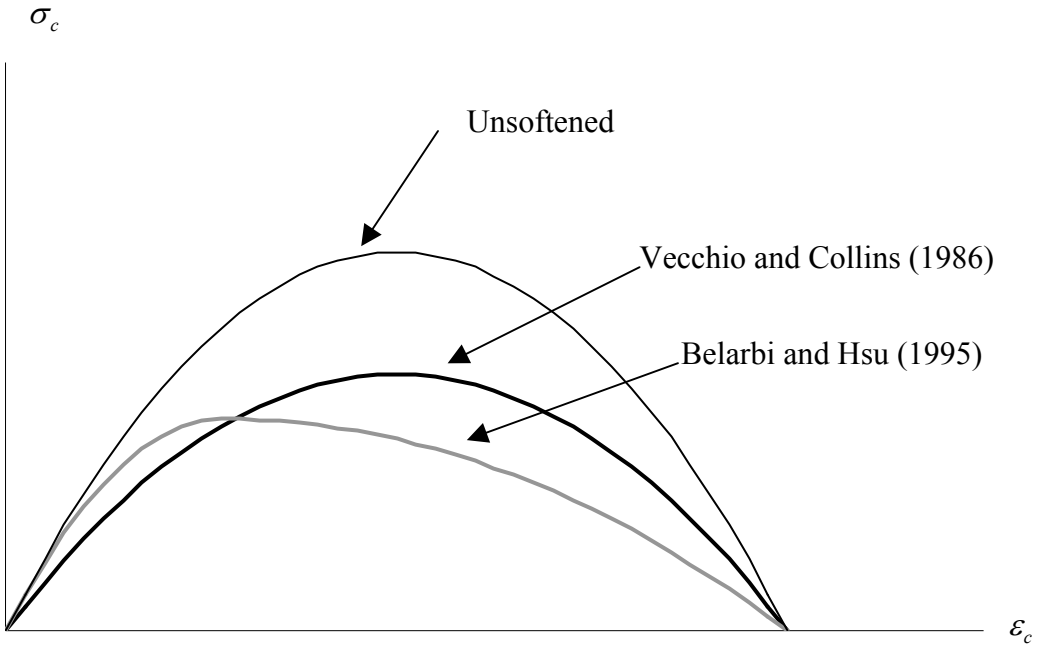

Figure 3.5 Effect of Softening Factor on Compressive Stress-Strain Curve of Concrete

Strength Enhancement Factor due to Confinement

Based on bi-axial tests by Kupfer et al. (1969) and Kotsovos and Newman (1978), and triaxial tests by Gerstle et al. (1980), concrete strength increases as the confining stress increases. Kupfer et al. (1969) conducted an experimental program on bi-axial compression-compression test of normal strength concrete with uni-axial strength varied from 2.7-8.3 ksi and with the varied ratio of compression stress in two directions. It was found that with a ratio of 1 to 1 (true Biaxial-Strength), an average increase of 16 % over the uni-axial strength was observed. Based on the experimental results, a two-dimension failure envelope, as shown in Fig. 3.6, of biaxial strength of concrete was also developed (Kupfer et al., 1969).

As the number of experimental results increased, several researchers have attempted to construct three-dimensional stress failure surfaces for concrete. Because the process involved is similar to the construction of the yield or potential surface of the theory of plasticity, many attempts have been made along this line. The accuracy of the model depends upon the number of test parameters taken into consideration. Vecchio (1992), in early attempts to account for confinement in the MCFT, proposed a model equation based an extrapolation of Kupfer et al. test data. The empirical equation for strength enhancement factor (Vecchio, 1992) is given by

$$K_c = 4.1\left(\frac{f_{cb}}{f_c'}\right) + \left(1 + 0.92\left(\frac{f_{cb}}{f_c'}\right) - 0.76\left(\frac{f_{cn}}{f_c'}\right)^2\right) \tag{3.10}$$

where, K_c = Strength enhancement factor

f_{cb} = the smaller of the two confining stress

f_{cn} = the difference between two confining stress

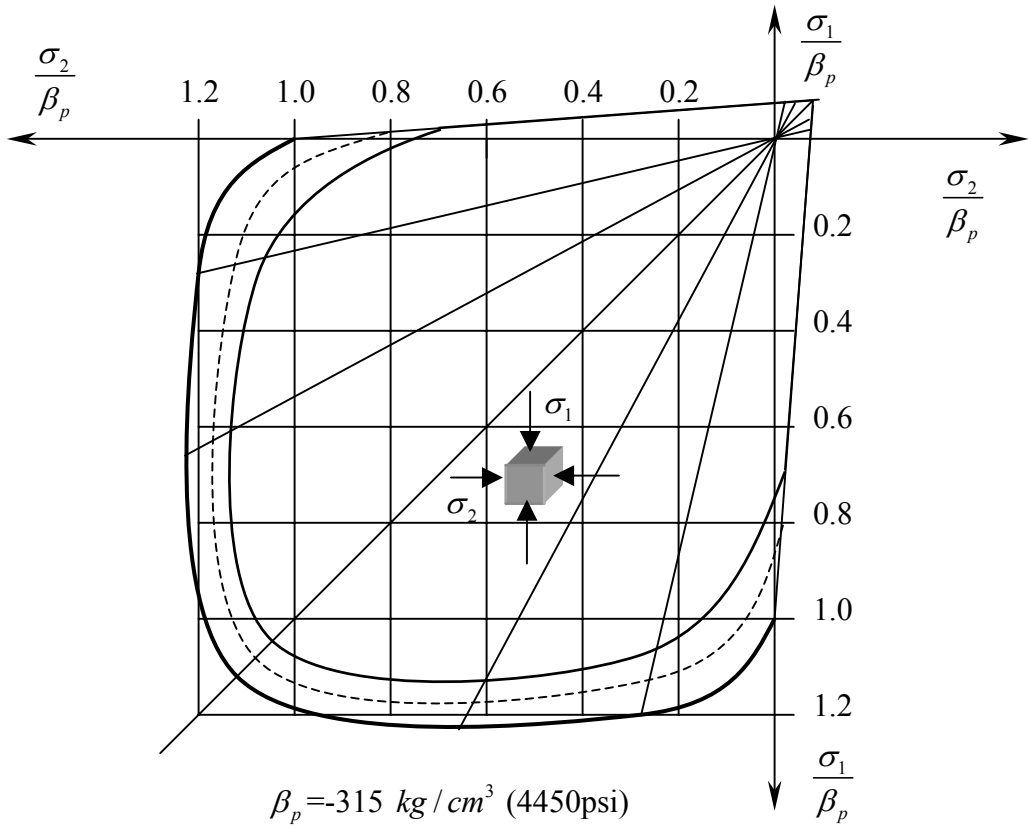

Figure 3.6 Biaxial Failure Envelope for Concrete
(adapted from Kupfer et al., 1969)

Derivation of Strength Enhancement Factor Based on Five-Parameter Failure Surface

The basic idea of the construction of the five-parameters failure surface (Willam and Warnke, 1974) is explained in this section. The formulation, in general, follows the same treatment as Chen (1982) with minor modifications. Because the process of construction of a failure surface in three-dimension principal stress space in the context of theory of plasticity involves the uses of stress-invariant, a brief summary of this concept and notation will be described. Fig. 3.7 shows a general geometric description of the failure surface plotted in three-dimensional principal stress space.

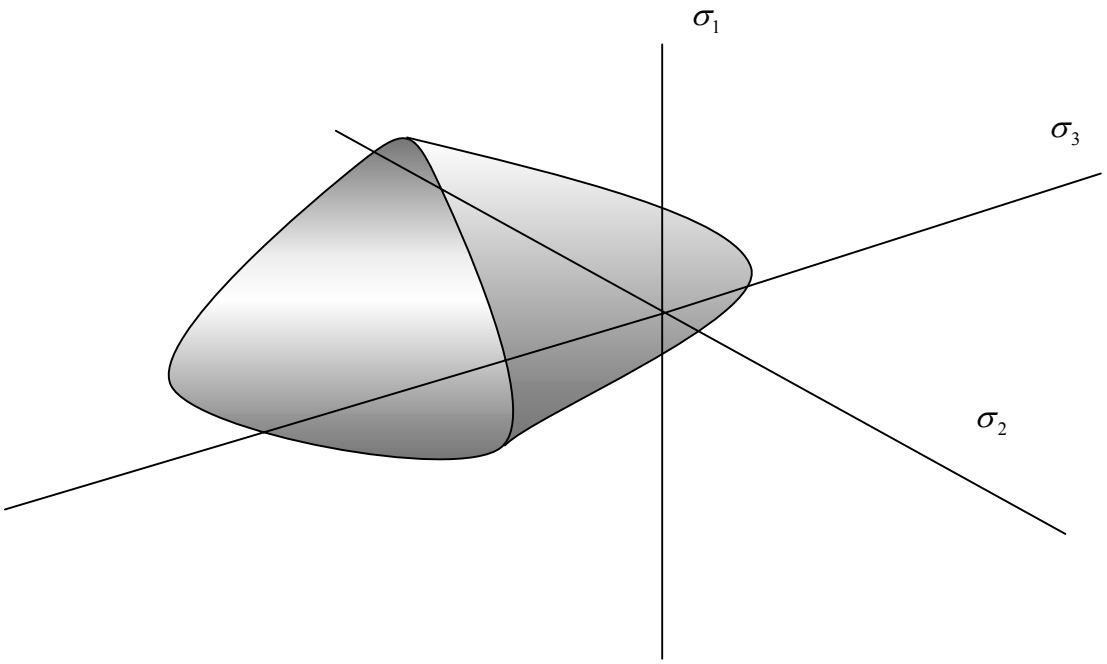

Figure 3.7 Failure Surface in Three Principal Stresses Space

A function representing a surface in three-dimensional principal stress space can be written as:

$$F(\sigma_1, \sigma_2, \sigma_3) = 0 \tag{3.11}$$

Chen (1982) showed that the same surface of the form $F(\sigma_1,\sigma_2,\sigma_3)=0$ can be written as a function of variable (ξ,ρ,θ) in Haigh-Westergaard stress space as shown in Fig. 3.8. The transformation relationships between $(\sigma_1,\sigma_2,\sigma_3)$ and (ξ,ρ,θ) coordinates is given by the following identities:

$$\xi=\frac{1}{\sqrt{3}}I_1=\sqrt{3}\sigma_m$$

$$\rho=\sqrt{2J_2}$$

$$\cos 3\theta=\frac{3\sqrt{3}J_3}{J_2^{3/2}} \tag{3.12}$$

$$\begin{Bmatrix}\sigma_1\\ \sigma_2\\ \sigma_3\end{Bmatrix}=\frac{\xi}{\sqrt{3}}\begin{Bmatrix}1\\ 1\\ 1\end{Bmatrix}+\sqrt{\frac{2}{3}}\rho\begin{Bmatrix}\cos\theta\\ \cos(\theta-\frac{2}{3}\pi)\\ \cos(\theta+\frac{2}{3}\pi)\end{Bmatrix}$$

where I_1 = the first stress invariants = $\sigma_1+\sigma_2+\sigma_3$

σ_m =average or hydrostatic stress = $\frac{I_1}{3}$

J_2 = the second invariant of the deviatoric stess

$$=\frac{1}{6}\left[(\sigma_1-\sigma_2)^2+(\sigma_2-\sigma_3)^2+(\sigma_3-\sigma_1)^2\right]$$

J_3 = the third invariant of the deviatoric stress

$$=\frac{1}{3}(\frac{2\sigma_1-\sigma_2-\sigma_3}{3})(\frac{2\sigma_2-\sigma_1-\sigma_3}{3})(\frac{2\sigma_2-\sigma_1-\sigma_2}{3})$$

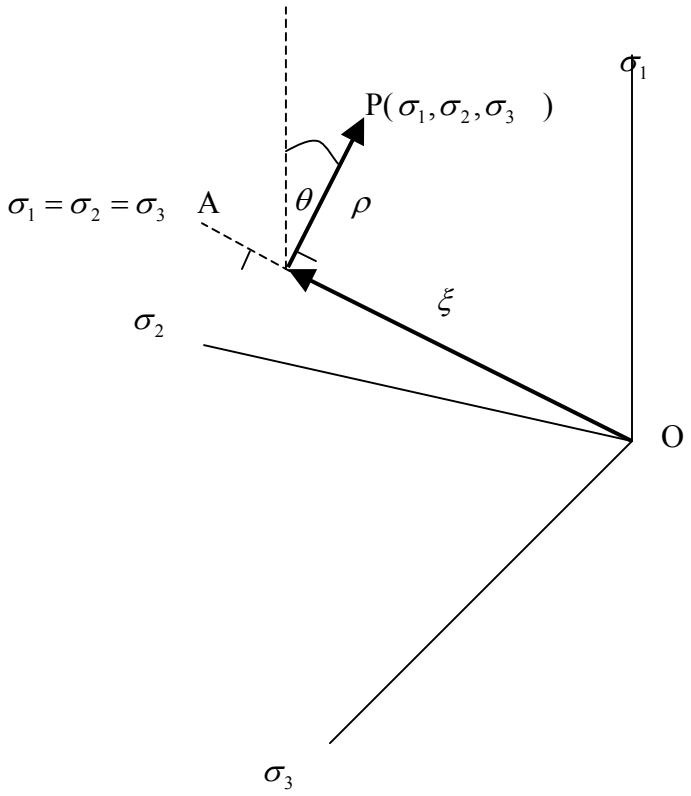

Figure 3.8 Transformation of $(\sigma_1, \sigma_2, \sigma_3)$ to (ξ, ρ, θ) Coordinate

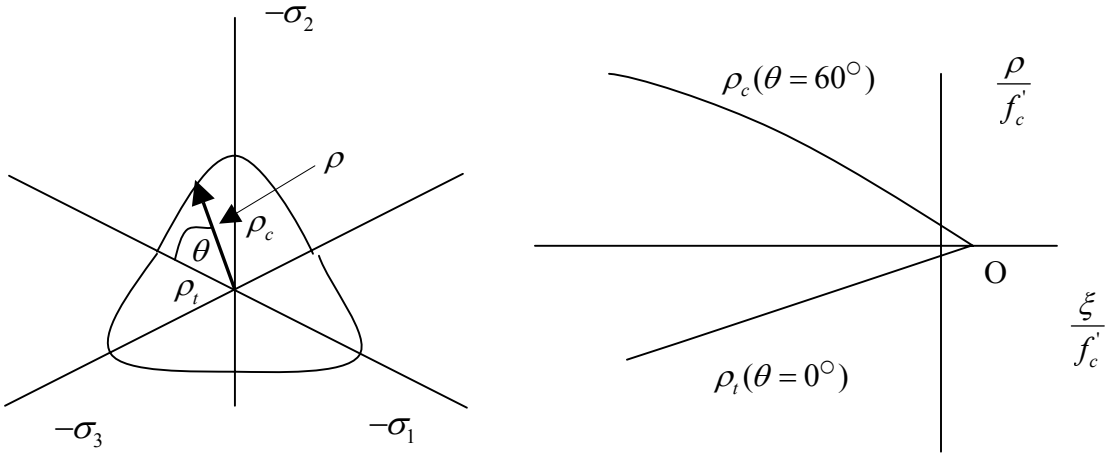

(a) Deviatoric Section **(b) Meridian Curve**

Figure 3.9 Meridian and Deviatoric Cross-Section

The line OA with a unit vector $(\frac{1}{\sqrt{3}},\frac{1}{\sqrt{3}},\frac{1}{\sqrt{3}})$ represents the hydrostatic axis. A plane whose unit normal vector is parallel to the hydrostatic axis is termed the deviatoric plane. At a certain distance ξ, along the hydrostatic axis, a cross-section in the direction parallel to the deviatoric plane can be described mathematically. The general cross-section of the five-parameters failure surface is shown in Fig. 3.9(a) with a threefold symmetry. The meridians of the failure surface are defined as the intersection curves between the failure surface and a plane called the meridian plane, which passes through the hydrostatic axis with the angle θ=constant, as shown in Fig. 3.9 (b)

Willam and Warnke (1974) proposed the use of two parabolas to approximate the meridian curve and a part of an ellipse to best fit the cross section in the deviatoric plane. Through the use of a part of an ellipse to approximate the deviatoric cross-section, Chen (1982) showed that the distance at a certain angle θ between the hydrostatic axes to the surface in the deviatoric plane as shown in Fig. 3.9(a) can be given by:

$$\rho(\theta)=\frac{2\rho_c(\rho_c^2-\rho_t^2)\cos\theta+\rho_c(2\rho_t-\rho_c)\left[4(\rho_c^2-\rho_t^2)\cos^2\theta+5\rho_t^2-4\rho_t\rho_c\right]^{0.5}}{4(\rho_c^2-\rho_t^2)\cos^2\theta+(\rho_c-2\rho_t)^2} \tag{3.13}$$

The distance ρ_c and ρ_t can be approximated by the best fit of two parabola along the tensile (θ=0) and compressive (θ=60) meridians. The equation of the two parabolas can be expressed as

$$\frac{\rho_t}{\sqrt{5}f_c^{'}}=(a_0+a_1(\frac{\sigma_m}{f_c^{'}})+a_2(\frac{\sigma_m}{f_c^{'}})^2) \text{ at } \theta=0 \tag{3.14a}$$

$$\frac{\rho_c}{\sqrt{5}f_c^{'}}=(b_0+b_1(\frac{\sigma_m}{f_c^{'}})+b_2(\frac{\sigma_m}{f_c^{'}})^2) \text{ at } \theta=60 \tag{3.14b}$$

Note that Eq. 3.14a and 3.14b involves 6 parameters. By enforcing that these two meridians intersect the hydrostatic axis at the same point (point O in Fig.3.9), the number of parameters is reduced to five.

The determination of the model parameters required five sets of experimental test data along the compression and tensile meridian as shown in Eq. 3.14. Mander et al. (1988) employed the triaxial test results from Schickert and Winkler (1977) to construct the five-parameters failure surface:

(1) Uniaxial compressive strength ($f_c^{'}, \theta$=60, $\sigma_m = -\frac{f_c^{'}}{3}, \rho = \sqrt{\frac{2}{3}} f_c^{'}$);

(2) Uniaxial tensile strength (f_{cr}, θ=0, $\sigma_m = \frac{f_t}{3}, \rho = \sqrt{\frac{2}{3}} f_{cr}$);

(3) Equal biaxial compressive strength ($f_{bc}^{'}$, θ=0, $\sigma_m = -\frac{2}{3} f_{bc}^{'}, \rho = \sqrt{\frac{2}{3}} f_{bc}^{'}$);

(4) A high compressive stress point (σ_{m1}, ρ_1), obtained from a triaxial test with a constant confining stress in one direction and impose equal biaxial stress in the other two directions up until failure; and

(5) A high compression stress point (σ_{m2}, ρ_2), obtained from a triaxial test with two equal and constant confining stresses in two directions and increase the stress in the third direction until failure.

Chen (1982) showed that from these five triaxial test parameters the constants $a_0, a_1, a_2, b_1, b_2, b_3$ can be expressed as:

$$a_2 = \frac{\sqrt{\frac{6}{5}}\overline{\xi_1}(\overline{f_t^{'}} - \overline{f_{bc}^{'}}) - \sqrt{\frac{6}{5}}\overline{f_t^{'}}\,\overline{f_{bc}^{'}} + \overline{\rho_1}(2\overline{f_{bc}^{'}} + \overline{f_t^{'}})}{(2\overline{f_{bc}^{'}} + \overline{f_t^{'}})(\overline{\xi_1}^2 - \frac{2}{3}\overline{f_{bc}^{'}}\,\overline{\xi_1} + \frac{1}{3}\overline{f_t^{'}}\,\overline{\xi_1} - \frac{2}{9}\overline{f_t^{'}}\,\overline{f_{bc}^{'}})}$$

$$a_1 = \frac{1}{3}(2\overline{f_{bc}^{'}} - \overline{f_t^{'}})a_2 + \frac{6}{5}\frac{\overline{f_t^{'}} - \overline{f_{bc}^{'}}}{2\overline{f_{bc}^{'}} + \overline{f_t^{'}}} \qquad (3.15a)$$

$$a_0 = \frac{2}{3}\overline{f_{bc}^{'}}a_1 - \frac{4}{9}\overline{f_{bc}^{'}}a_2 + \sqrt{\frac{2}{15}}\overline{f_{bc}^{'}}$$

$$b_2 = \frac{\overline{\rho_2}(\overline{\xi_0} + \frac{1}{3}) - \sqrt{\frac{2}{15}}(\overline{\xi_0} + \overline{\xi_2})}{(\overline{\xi_0} + \overline{\xi_2})(\overline{\xi_2} - \frac{1}{3})(\overline{\xi_0} + \frac{1}{3})}$$

$$b_1 = (\overline{\xi_2} + \frac{1}{3})b_2 + \frac{\sqrt{\frac{6}{5}} - 3\overline{\rho_2}}{2\overline{\xi_2} - 1} \qquad (3.15b)$$

$$b_0 = -\overline{\xi_0}b_1 - \overline{\xi_0}^2 b_2$$

where, $\overline{\xi_0} = \dfrac{-a_1 - \sqrt{a_1^2 - 4a_0a_1}}{2a_2}$

$\overline{f_t^{'}}$ = ratio between uniaxial tensile and compressive strength of concrete($\dfrac{f_{cr}}{f_c^{'}}$)

$\overline{f_{bc}^{'}}$ = ratio between biaxial and uniaxial compressive strength ($\dfrac{f_{bc}^{'}}{f_c^{'}}$)

$\overline{\xi_1} = \dfrac{-\sigma_{m1}}{f_c^{'}}$

$\overline{\xi_2} = \dfrac{-\sigma_{m2}}{f_c^{'}}$

$\overline{\rho_1} = \dfrac{\rho_1}{\sqrt{5}f_c^{'}}$

$$\overline{\rho_2} = \frac{\rho_2}{\sqrt{5} f_c^{'}}$$

Because the lack of sufficient triaxial test data, the non-dimensionalized parameters $\overline{f_{bc}^{'}}$, $\overline{\xi_1}$, $\overline{\xi_2}$, $\overline{\rho_1}$, and $\overline{\rho_2}$ will be approximated from the Schickert and Winkler (1977) test data. Note that the same parameters were also used by Mander et al. (1988). The strength parameters from the tests are: $\overline{f_{bc}^{'}}$=1.21, $\overline{\xi_1}$=3.0, $\overline{\rho_1}$=1.24583, $\overline{\xi_2}$=3.0, and $\overline{\rho_2}$=0.568993. The ratio between the uniaxial tensile and compressive strength varies from test to test. However, the uniaxial tensile strength of concrete is estimated by:

$$f_{cr} = 3.75\sqrt{f_c^{'}}\text{, units in psi} \tag{3.16}$$

For certain levels of confining stresses in the two principal directions, the strength envelope may be approximated by the five-parameter failure surface proposed above. Mander et al. (1988) derived a closed form solution for determining the peak strength ($f_{cc}^{'}$) under equal confining stresses ($f_l^{'}$) in the other two directions. The strength enhancement factor (K_c) has the following form:

$$\frac{f_{cc}^{'}}{f_c^{'}} = -1.254 + 2.254\sqrt{1 + 7.94\frac{f_l^{'}}{f_c^{'}}} - 2\frac{f_l^{'}}{f_c^{'}} \tag{3.17}$$

Because the confining stresses in the two directions are, in general, not equal, the determination for strength enhancement factor becomes more involved. Mander et al. (1988) also proposed the use of a graphical method in the form of an alignment chart to find this strength enhancement factor. However, the process becomes too cumbersome to be applied at the micro-level application.

Consider Fig. 3.10, assuming that two values of confining stresses (σ_1, σ_2) are given, a trial peak strength (σ_3^{trial}) will be assumed to have a certain value. Based on this trial stress, the distance ρ^{trial} corresponding to the trial stress (σ_3^{trial}) can be obtained by Eq. 3.12b. The trial mean stress σ_{mt} can be obtained by $\sigma_{mt} = \sigma_3^{trial} + \sigma_1 + \sigma_2$. The angle θ corresponding this trial peak strength can be obtained by Eq. 3.12c.

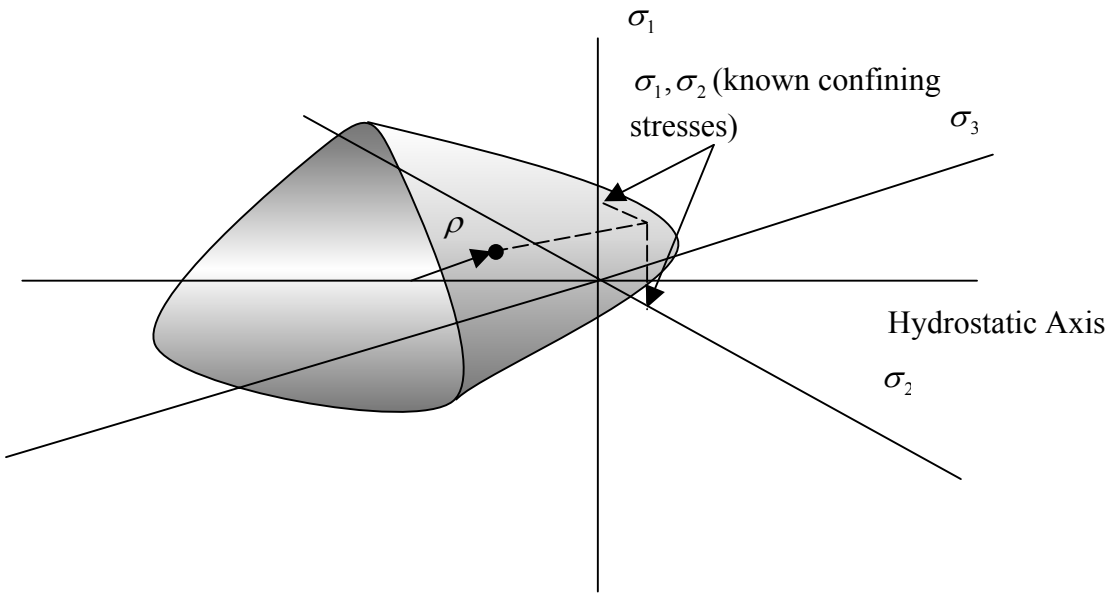

Figure 3.10 Determination of Strength Enhancement Factor

Based on Eqs. 3.13, 3.14, and 3.15, the distance ρ to the failure surface can be obtained. However, the trial point ($\sigma_{mt}, \rho^{trial}, \theta^{trial}$) must also lie on the failure surface. That means ρ must be equal to ρ^{trial}, if σ_3^{trial} is the correct value of the peak strength. Based on this algorithm, the trial and error process on σ_3^{trial} is repeated until the convergence between ρ and ρ^{trial} is achieved.

The flowchart for determining the strength enhancement factor can be presented as in Fig. 3.11.

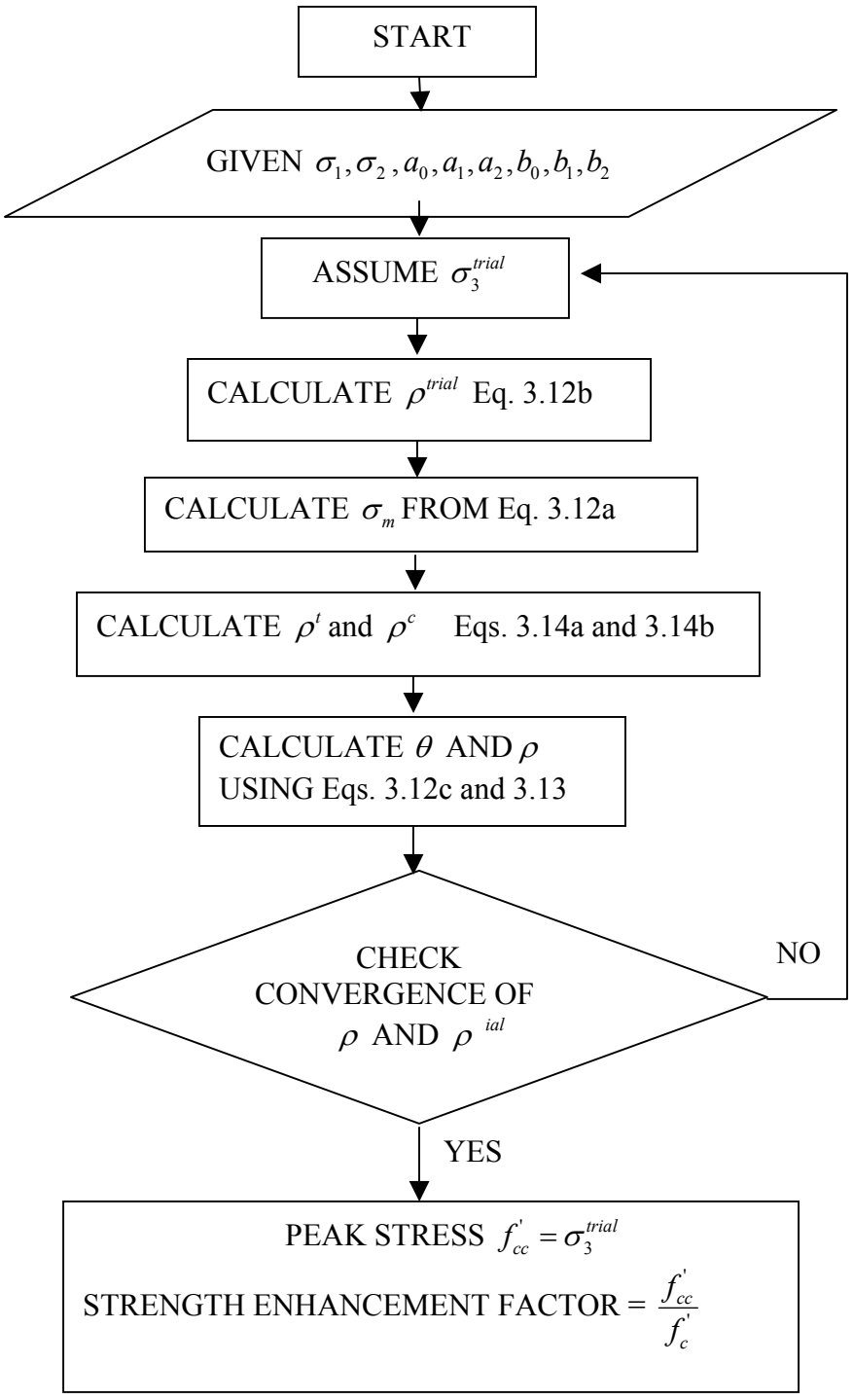

Figure 3.11 Flowchart for Determining the Strength Enhancement Factor

Strain Enhancement Factor due to Confinement

Kupfer et al. (1969) showed that under bi-axial compression-compression tests, peak strain in the concrete also increases as shown in Fig. 3.12.

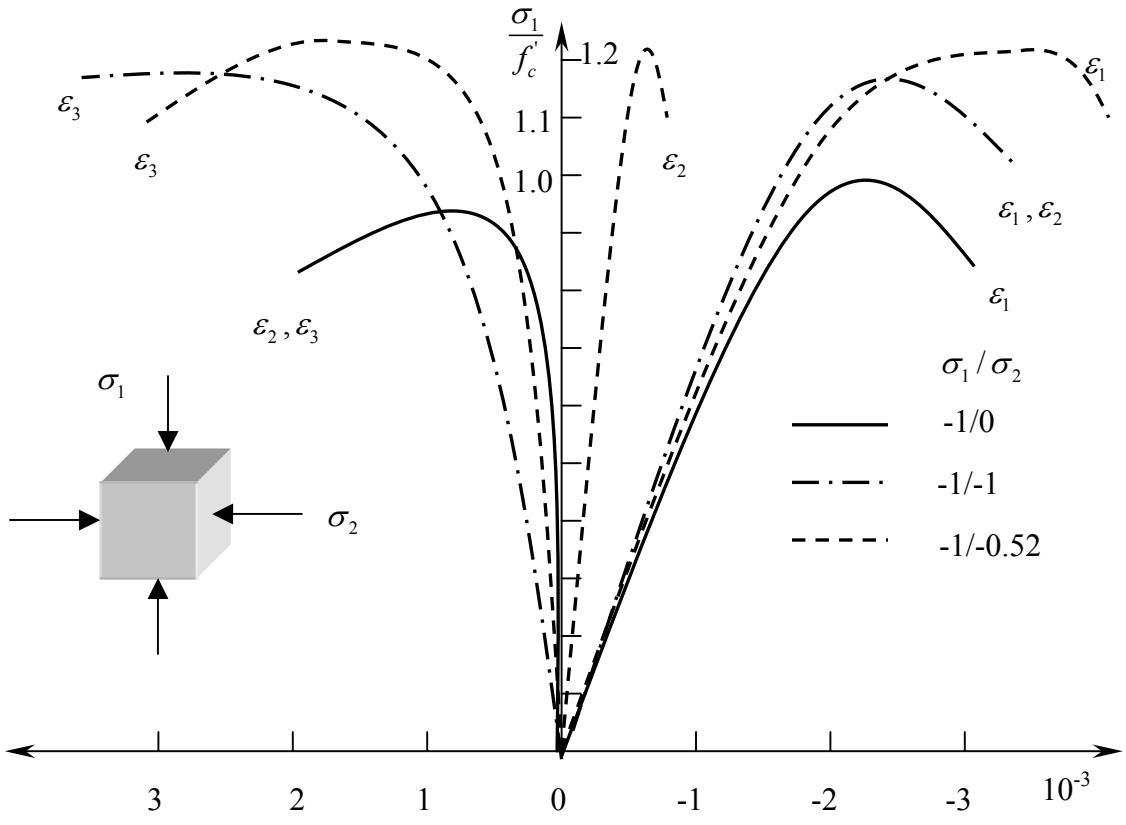

Figure 3.12 Stress-Strain Curve for Concrete Subjected to Biaxial Stress (adapted from Chen and Saleeb, 1982)

Currently, however, there is not sufficient test data to uniquely quantify this peak strain enhancement factor. Vecchio (1992) applied the same stress enhancement factor to modify the peak strain for incorporating the confinement effect into the MCFT. Nonetheless, many experiments show that, in general, the peak strain enhancement factor is larger than the stress enhancement factor (Kupfer et al., 1969). Based on this

evidence, Mander et al. (1988) adopted an equation of the following form to calculate the strain enhancement factor:

$$\frac{\varepsilon_{cc}}{\varepsilon_o} = 1 + 5\left(\frac{f_{cc}^{'}}{f_c^{'}} - 1\right) \tag{3.18}$$

This form of equation will also be used in the model proposed in this dissertation.

3.2.3.2 Concrete in Tension

The stress-strain relationship for reinforced concrete in tension is different from that of the concrete alone. As described in Chapter II, the mode of failure of unreinforced concrete subject to uniaxial tension is governed by a single crack separating the specimen into two parts. This phenomenon involves a strain-localization near the crack while the remainder of the specimen unloads. Van Mier (1986) has shown that the stress-strain curve of unreinforced concrete in tension cannot be treated as a material property, but a member property, that shows a strong size-effect.

Hordjik (1991) conducted an experimental program on unreinforced concrete subjected to uniaxial tension and proposed a post-cracking concrete tensile stress-crack width relationship of unreinforced concrete as:

$$\frac{\sigma_t}{f_{cr}} = \{1 + (c_1 \frac{w}{w_c})^3\} \exp(-c_2 \frac{w}{w_c}) - \frac{w}{w_c}(1 + c_1^{\,3}) \exp(-c_2) \tag{3.19}$$

where, σ_t = concrete stress in tension

w_c = crack opening at the complete release of stress=0.0063 inches

w = crack opening where the stress is determined

c_1, c_2 =material constants =3.0 and 6.93, respectively

Crack opening displacement (w) is a product between the cracking strain and the length of the localized zone. Cracking strain is obtained from the concept of decomposition of the total strain into the concrete elastic strain and cracking strain as shown in Fig. 3.13.

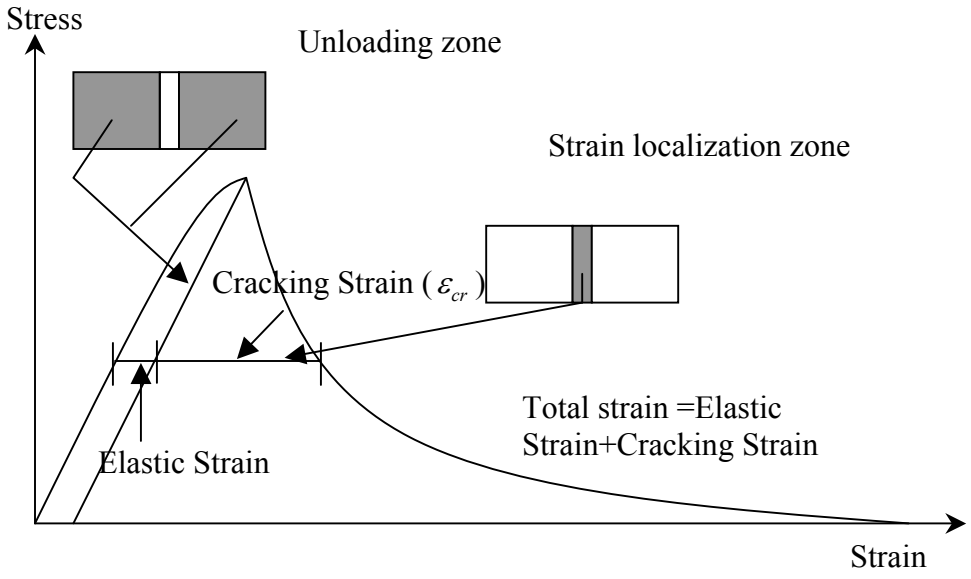

Figure 3.13 Strain Decomposition of Total Strain

On the other hand, multiple cracks always form in reinforced concrete subjected to uniaxial tension as long as the reinforcement ratio at the crack location is sufficiently large to carry the load released from the cracked concrete. A complicated load transfer mechanism results, which involves the bond stresses existing between the concrete and reinforcing steel. In average, concrete between two cracks can resist a certain amount of stress, which is often called tension stiffening. Fig 3.14 shows the average stress-strain of reinforced concrete subjected to uniaxial tension. By subtracting the average steel stress from the total stress, the average concrete stress can be obtained, as shown in Fig. 3.14. Note that if the specimen used in the tension-stiffening experiment contained

several cracks along the length, the tension stiffening may be considered a material property, based on the homogenization principle.

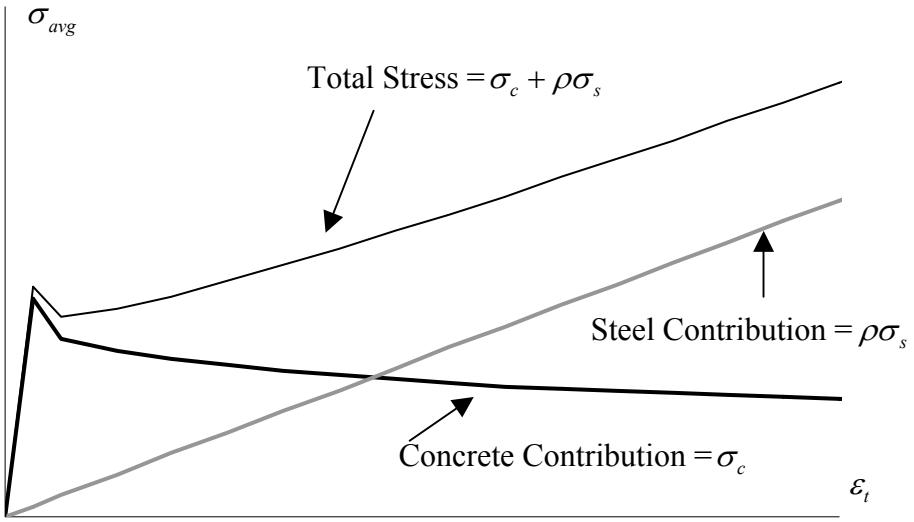

Figure 3.14 Tension-Stiffening Stress in Concrete

There are several factors influencing the concrete tension-stiffening curve. Maekawa and Okamura (1991) concluded that the post-peak tension-stiffening curve depends mainly on the reinforcement ratio and the type of reinforcing steel used, while the pre-peak is essentially the same for all specimen test data. Vecchio (2000) also commented on the effect of reinforcing bar and the crack angle on tension-stiffening.

Maekawa and Okamura (1991) proposed an equation for the average tensile stress-strain curve of reinforced concrete in the following form:

$$\sigma_t = E_c \varepsilon_t, \varepsilon_t < \varepsilon_{cr} \text{ and} \tag{3.20}$$

$$\sigma_t = f_{cr}\left(\frac{\varepsilon_{cr}}{\varepsilon_t}\right)^n \quad , \ \varepsilon_t > \varepsilon_{cr}$$

where, E_c = Modulus of Elasticity of concrete

ε_{cr} = concrete cracking strain

f_{cr} = concrete cracking stress

n = 0.2 and 0.4 for wire mesh reinforcing steel and deformed bar, respectively.

Note that the same relationship was also used by the Tamai et al. (1987) and the University of Houston Research Group (Belarbi and Hsu, 1995, Pang and Hsu, 1996, and Hsu and Zhang, 1997).

Based on the experimental results obtained from RC panel tests with reinforcing wire mesh, Vecchio and Collins (1982) also proposed an average concrete tensile stress-strain relationship:

$$\sigma_t = E_c \varepsilon_t, \varepsilon_t < \varepsilon_{cr} \text{ and} \tag{3.21}$$

$$\sigma_t = \frac{f_{cr}}{1+\sqrt{200\varepsilon_t}} \quad , \ \varepsilon_t > \varepsilon_{cr}$$

However, as the number of experimental data increased, Collins and Mitchell (1987) proposed that the equation be changed in the post-peak by replacing the factor 200 by 500 in the denominator:

$$\sigma_t = E_c \varepsilon_t, \varepsilon_t < \varepsilon_{cr} \text{ and} \tag{3.22}$$

$$\sigma_t = \frac{f_{cr}}{1+\sqrt{500\varepsilon_t}} \quad , \ \varepsilon_t > \varepsilon_{cr}$$

Fig. 3.15 shows the differences of tensile stress-strain curve obtained from Eqs. 3.20, 3.21, and 3.22.

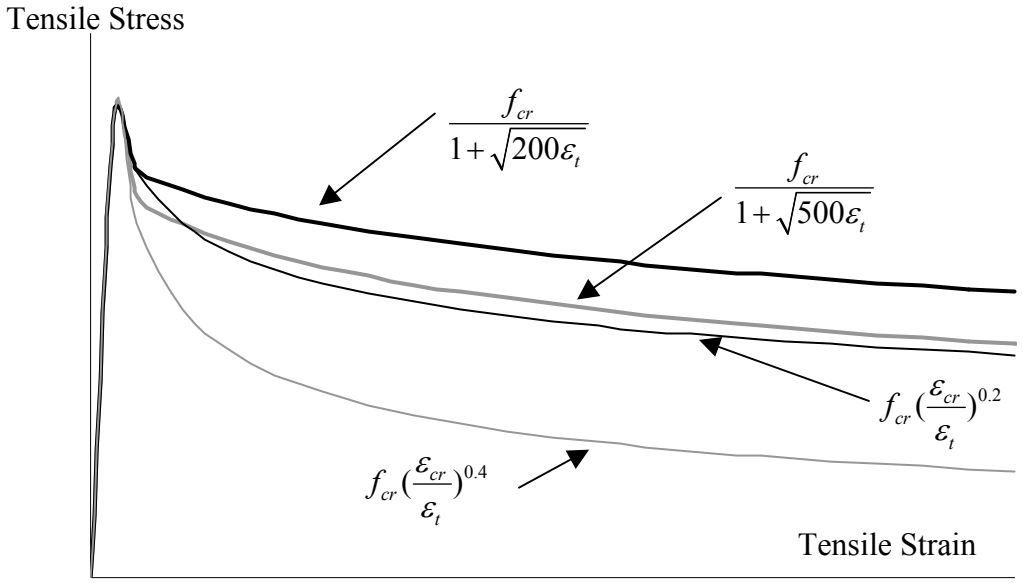

Figure 3.15 Tensile Stress-Strain Curves Including Tension-Stiffening

Recent research by Bentz et al. (2000) incorporated the effect of reinforcing ratio, bar size, and the principal stress and strain directions into the model. Vecchio (2000) also proposed the following equations for the average tensile stress-strain in concrete:

$$\sigma_t = E_c \varepsilon_t, \varepsilon_t < \varepsilon_{cr} \text{ and}$$

$$\sigma_t = \frac{f_{cr}}{1+\sqrt{c_t \varepsilon_t}} \quad , \ \varepsilon_t > \varepsilon_{cr} \tag{3.23}$$

where $c_t = 2.2m$

$$m = \frac{1}{\sum_{i-1}^{n} 4 \frac{\rho_i}{d_{bi}} |\cos\theta_i|}$$

ρ_i = steel reinforcement ratio of the i^{th} direction

d_b^i = bar diameter

θ_i = the direction between the i^{th} reinforcement direction and the principal direction.

For simplicity, this dissertation adopts the Collins and Mitchell Model (1986), with a factor of 500 in the denominator for tension-stiffening zone, while Eq. 3.19 is used for unreinforced concrete regions.

3.2.4 Steel Constitutive Relationship

An average stress-strain relationship for reinforcing steel used in this model development is summarized in this section. Because the constitutive relationship of bare reinforcing steel bars subjected to monotonic uniaxial stress condition is rather well defined, and can be represented by the elastic and isotropic or kinematics hardening assumption, a brief discussion shall be presented. However, the average stress-strain of reinforcing steel bar embedded in concrete may be rather different from those of the bare bar. A detailed discussion on this phenomenon will be explained.

3.2.4.1 Stress-Strain Relationship for Bare Bar

The stress-strain relationships of a reinforcing bar subjected to uniform uniaxial tension or compression are shown in Fig. 3.16. An elastic-perfectly plastic assumption generally yields acceptable results for the response prediction of RC members before yielding. Because of the high deformability of confined concrete members, reinforcing steels may reach the yield point and continue into the post-yielding range well before crushing occurs in concrete. Therefore, the post-yield stiffness of reinforcing steel should also be taken into account.

An elastic plastic strain-hardening assumption will be used for reinforcing steel. As the experimental results used for a model comparison involve only monotonic loading condition, isotropic and kinematics hardening makes no difference. Therefore,

isotropic hardening will be used. The post-yield tangent modulus of reinforcing steel is assumed as 3.0 percent of the initial elastic modulus based on curve fitting.

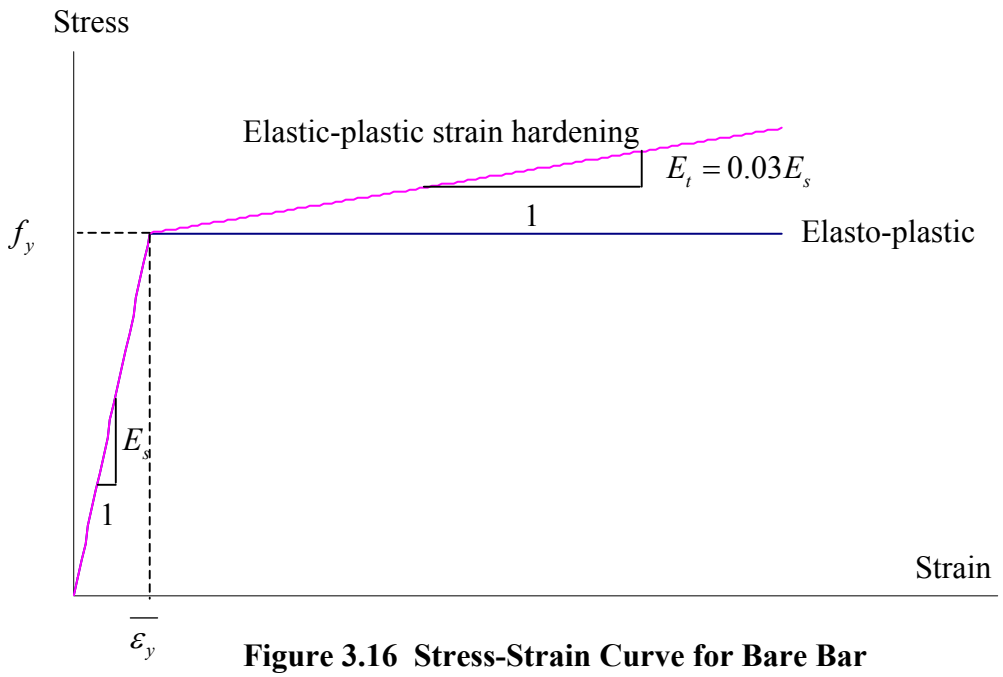

Figure 3.16 Stress-Strain Curve for Bare Bar

3.2.4.2 Adjustment of Tensile Yield Stress of Reinforcing Steel in Concrete

Consider a RC membrane subjected to uniaxial tension as shown in Fig. 3.17a and the free body diagram shown in Fig. 3.17b. At the crack location (section A), ignoring the tensile softening of concrete, only reinforcing steel is responsible for the total stiffness and strength. However, at section B, both the concrete and steel contribute to the stiffness and strength. Because the force balance between sections A and B must always be satisfied, stress in reinforcing steel at section B must be smaller than that at section A. Fig. 3.18a and 3.18b show the variation of the concrete and steel stress between two cracks. The concrete stress is maximum at approximately the mid-section between the cracks, while the maximum steel stress occurs at the crack location. The non-uniformity of stresses in the concrete and reinforcing steel is attributed to the force

transfer between the concrete and reinforcement at the interface. This transfer stress also causes the interface slip between the concrete and reinforcing steel. Therefore the assumption of perfect bond used in the MCFT may not be correct in reality.

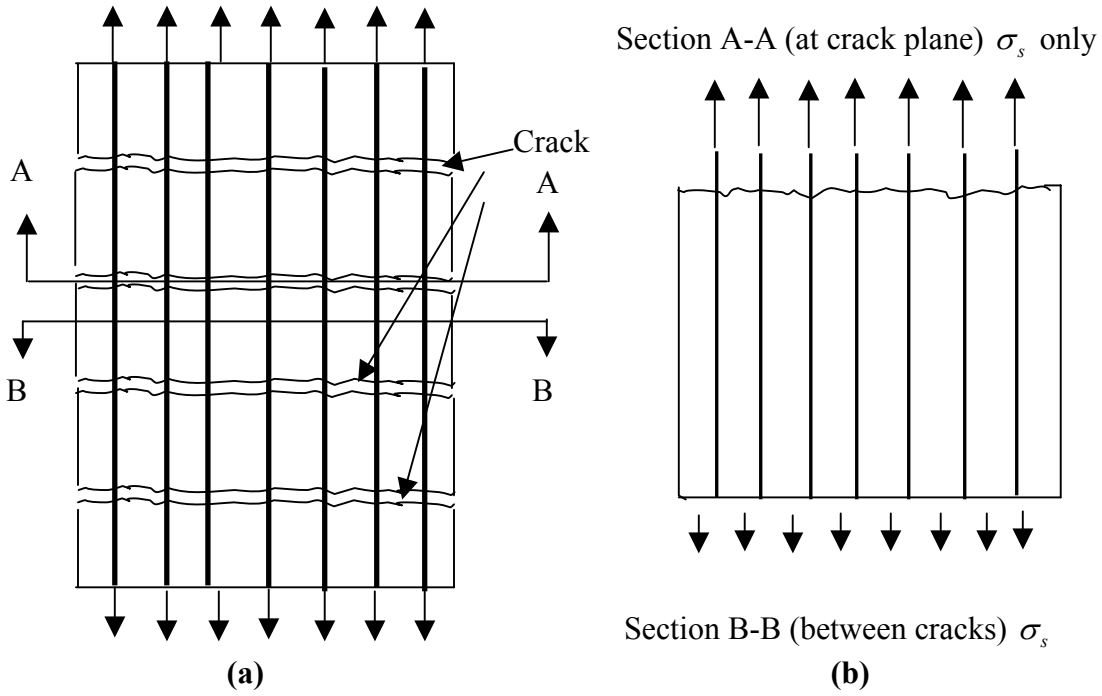

Figure 3.17 Free Body Diagram of Cracked Concrete Subjected to Uniaxial Tension

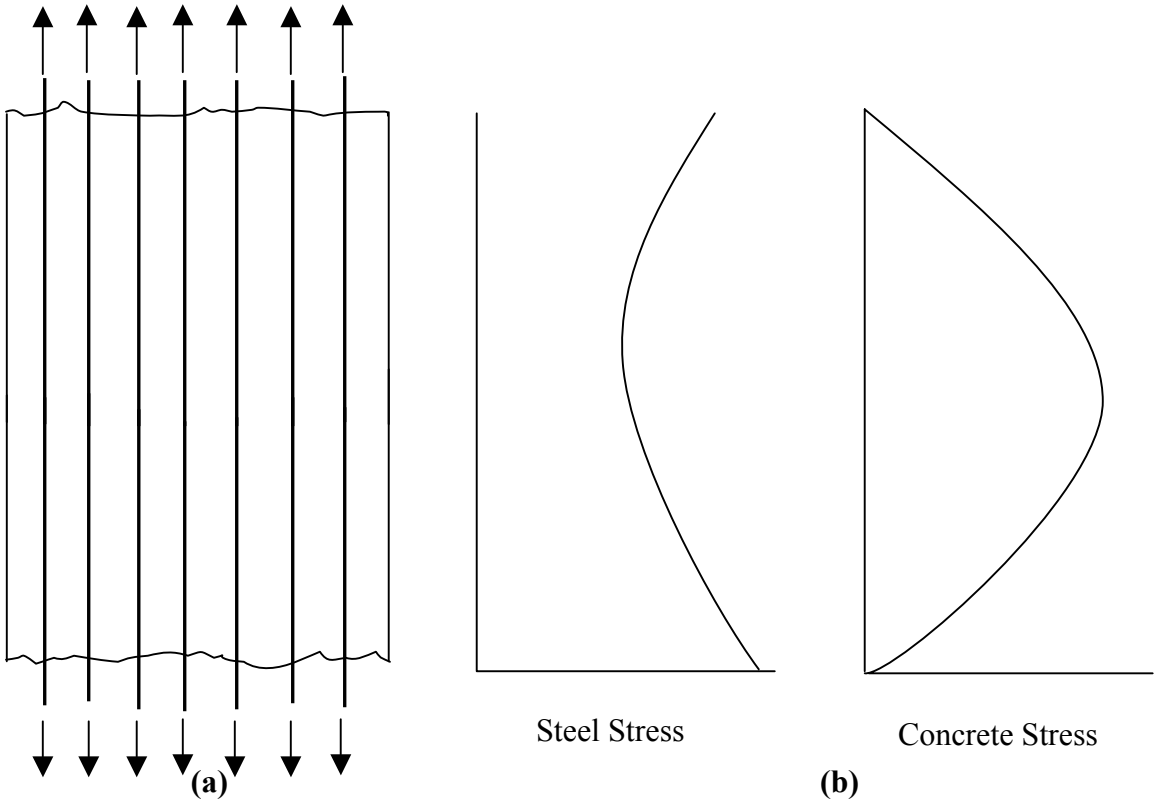

Figure 3.18 Stress Distribution for Concrete and Reinforcement in Cracked RC

Consider Fig. 3.19a, where the total stress, average concrete stress, and steel stress are plotted as a function of average strain. Because the unrealistic perfect bond assumption is employed, the total stress may exceed the yield stress of reinforcing steel at the crack location. Certain measures to correct this deficiency such that the errors due to the model assumption can be controlled must be implemented. Vecchio and Collins (1986) proposed the crack check process by reducing the concrete stresses such that, for a given average strain beyond the yielding strain of reinforcing steel, the total stress cannot exceed the reinforcing steel stress itself. This process is explained in one-dimensional setting as shown in Fig. 3.19b, and Eq 3.24.

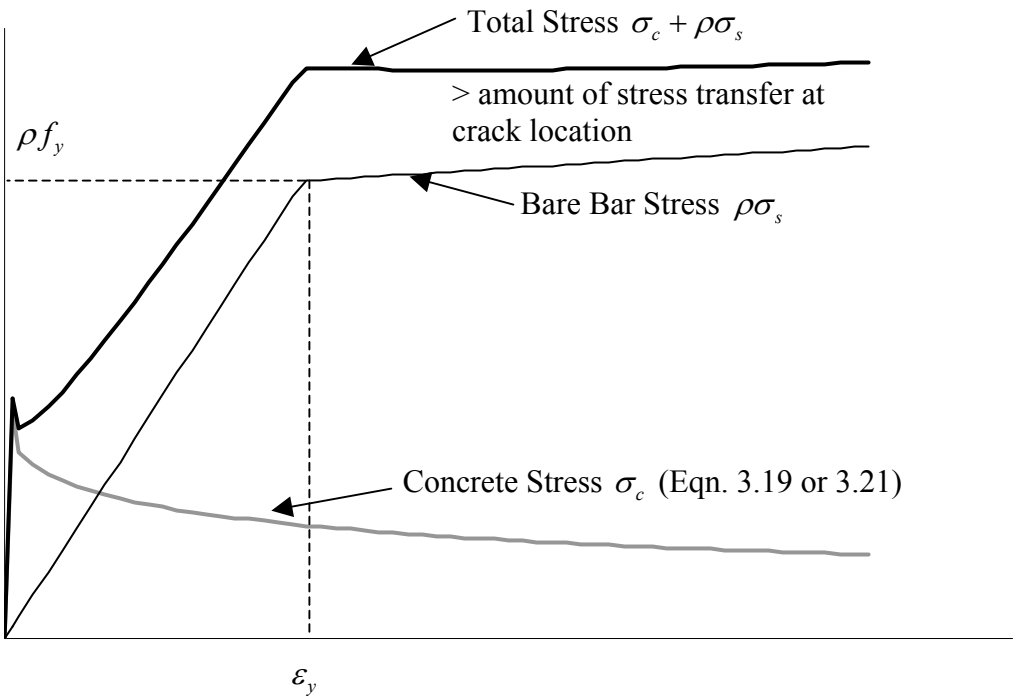

(a) Effect of Overestimation of Total Stress at Crack Location

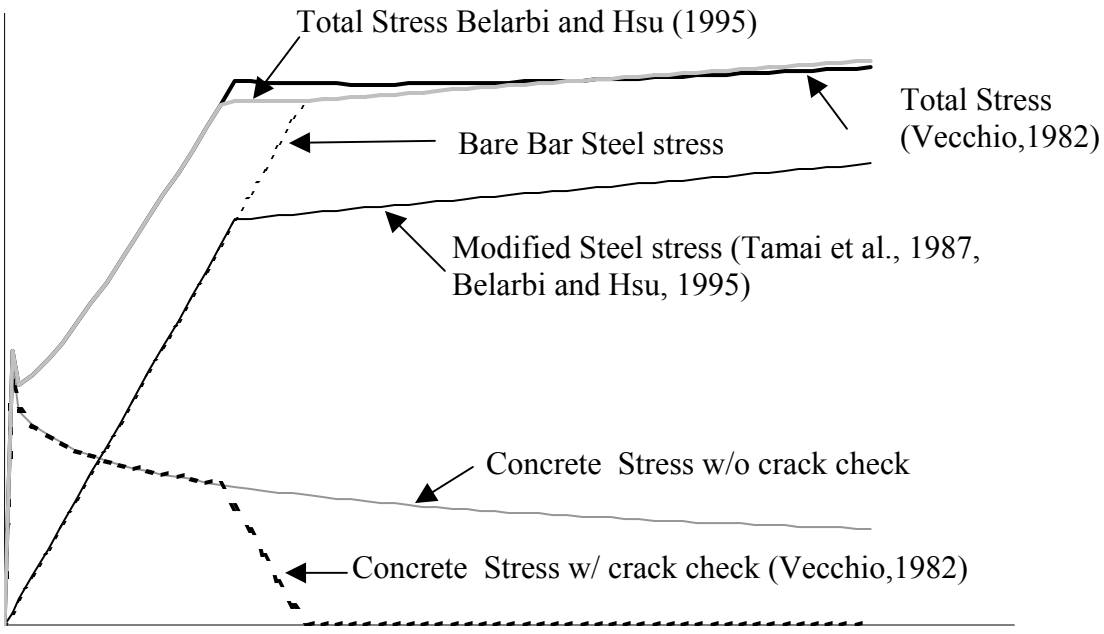

(b) Corrective Approach to Control Total Stress at Crack Locations

Figure 3.19 Crack-Check Process

$$\sigma_t = \frac{f_{cr}}{1+\sqrt{500\varepsilon_1}} \le f_y - \sigma_s \tag{3.24}$$

where f_{cr} = concrete cracking strength

ε_1 = average tensile strain

f_y = yield stress of reinforcing steel

σ_s = steel stress corresponding to the average strain ε_1

For biaxial stress state involving reinforcing steel in both X- and Y- directions, the equation of the following form is proposed (Vecchio and Collins, 1986).

$$\sigma_t = \frac{f_{cr}}{1+\sqrt{500\varepsilon_1}} \le \rho_x (f_{yx} - \sigma_{sx}) \sin^2\theta + \rho_y (f_{yy} - \sigma_{sy}) \cos^2\theta \tag{3.25}$$

On the contrary, Belarbi and Hsu (1994), following the method presented by Tamai et al. (1987), proposed that the decrease of steel stresses be used for the crack check while maintaining the concrete constitutive relationship in the form of Eq. 3.20. The procedure involves modifying the yield stress and post-yield stiffness of bare bar to an apparent yield strength of embedded bar. The one-dimensional crack check process proposed by Belarbi and Hsu (1994) and Tamai et al. (1987) is shown in Fig. 3.19. The mathematical form of the apparent yield stress of the embedded bar is shown below:

$$f_y' = (0.93 - 2B) f_y$$

$$B = \frac{1}{\rho}\left(\frac{f_{cr}}{f_y}\right)^{1.5} \tag{3.26}$$

where f_y' = Apparent yield stress of embedded bar

f_y = Yield Stress of bare bar

f_{cr} = Concrete cracking tensile stress

ρ = steel reinforcement ratio

Belarbi and Hsu (1994) used the value of 2% of the initial elastic modulus of reinforcing steel for the post-yield stiffness for bare bar. This post-yield stiffness is also affected by the tension stiffening of concrete. The complete constitutive relationship of reinforcing steel, including the pre-and post-yield range is given by (Belarbi and Hsu, 1994):

$$\sigma_s = E_s \varepsilon_s, \ \varepsilon_s < \varepsilon_y' = \frac{f_y'}{E_s}$$

$$= (0.91 - 2B) f_y + (0.02 + 0.25B) E_s \varepsilon_s, \varepsilon_s > \varepsilon_y' \qquad (3.27)$$

where σ_s = average stresses in embedded bars

ε_s = average strains in embedded bars

The parameters f_y' and B are the same as previously defined. Note that Eq. 3.27 is presented in a generic form of ε_s and ρ. The average stresses of the embedded bar in X- and Y- directions can be obtained by substituting ε_s and ρ by ε_x, ρ_x or ε_y, ρ_y into 3.27. However, Eq. 3.27 is derived by using the tension stiffening of Eq. 3.20 and the post-peak stiffness of 2 percent of initial stiffness for the reinforcement. Therefore, a manual adjustment must be made if other tension stiffening models are used.

Vecchio (1992) employed the crack check process as summarized in Eq. 3.25 into the Finite Element program. The method employed the convergence check of the secant-stiffness matrix instead of the residual force vector, or displacement vector as implemented in normal commercial packages. Experiences with ABAQUS, through the use of user-defined material subroutines, show that this method may lead to some

numerical difficulties when using a residual force and displacement convergence check. Therefore, the method proposed by Belarbi and Hsu (1994) shall be implemented in this dissertation. Because the constitutive relationships for concrete in tension used in this dissertation is different from that used by Belarbi and Hsu (1994), Eqs. 3.26 and 3.27 require modification.

3.2.5 Numerical Implementation in FEM

3.2.5.1 Fundamentals

The numerical implementation of non-linear finite element analysis is presented in this section. The derivation in this section follows the procedure derived by Chen and Han (1988) with minor modifications. For an incremental analysis, the process invariably involves the determination of the tangent or secant stiffness matrix and a residual force vector. The secant or tangent stiffness matrix of the material can be determined directly. However, the residual force vector, which is the difference between the external applied load at that particular load increment and the internal force vector, requires the stress update algorithm to calculate the internal force vector.

Consider the three dimensional principle of virtual displacement:

$$\int_V \sigma_{ij}\delta\varepsilon_{ij}dV = \int_S T_i\delta u_i + \int_V q_i\delta u_i \tag{3.28}$$

where σ_{ij} = general three dimensional stress tensors

ε_{ij} = general three dimensional strain tensors

T_i = vector of applied surface traction

u_i = three components of displacement vector

q_i = body force vector

Since the scope of this study is limited to two dimensions, small strain assumption. Therefore, there are only three components of stresses and strains in X-Y coordination. For geometrically linear analysis the strain-displacement assumption is given by:

$$\begin{Bmatrix} \varepsilon_{xx} \\ \varepsilon_{yy} \\ \gamma_{xy} \end{Bmatrix} = \begin{Bmatrix} \dfrac{\partial u}{\partial x} \\ \dfrac{\partial v}{\partial y} \\ \dfrac{\partial u}{\partial y} + \dfrac{\partial v}{\partial x} \end{Bmatrix} \tag{3.29}$$

or in the context of finite element analysis

$$\{\varepsilon\} = [B]\{U\}, \{\delta\varepsilon\} = [B]\{\delta U\} \tag{3.30}$$

where $[B]$=strain-displacement matrix

$\{U\}$=displacement vector of the nodal points, related to the displacement vector u_i by

$$\{u_i\} = [N]\{U\} \tag{3.31}$$

$[N]$ is the displacement interpolation function

Substitute Eqs. 3.29, 3.30, and 3.31 into 3.28, neglecting the body force and converting Eq. 3.28 into matrix form gives

$$\int_V [B]^T \{\sigma\} dV = \int_A [N]^T \{T\} dA \tag{3.32}$$

The left hand side of Eq. 3.32 represents the internal force vector $\{F\}$ calculated from the internal stress vector $\{\sigma\}$ (also called return stress), while the right hand side is the total applied force vector $\{P\}$. In general, the internal stress vector is unknown at the beginning of the load step. Therefore, the process requires iteration to solve Eq. 3.32

Defining the residual force vector:

$$\{R\} = \{P\} - \{F\} \tag{3.33a}$$

Because the return stress vector $\{\sigma\}$ can be determined from a given state of displacement vector $\{U\}$ in the strain-driven format, the vector $\{R\}$ and $\{F\}$ should also be a function of the displacement vector $\{U\}$. Assuming after the i^{th} iteration with the displacement vector $\{U\}^i$, Eq. 3.33a can be written as

$$\{R\}^i = \{P\} - \{F\}^i \tag{3.33b}$$

Taking the Taylor series expansion at $\{U\}^i$ and neglecting the higher order terms of Eq. 3.33b yields

$$\{R\}^i + \frac{\partial \{R\}^i}{\partial \{U\}} \Delta\{U\} = 0 \tag{3.34}$$

$$\text{or } \{R\}^i = \frac{\partial \{F\}^i}{\partial \{U\}} \Delta U \tag{3.35}$$

From 3.32,

$$\{F\} = \int_V [B]^T \{\sigma\} dV$$

Defining $\{d\sigma\} = [D_t]\{d\varepsilon\} = [D_t][B]dU$ (3.36)

where $[D_t]$=tangent constitutive matrix

Therefore.

$$\frac{\partial F^i}{\partial U} = \int_V [B]^T [D_t][B] dV = [K_t] \quad (3.37)$$

Substitute Eq. 3.37 into 3.35 gives

$$\{\Delta U\}^i = \left[K_t^i\right]^{-1} \{R\}^i \quad (3.38)$$

Vecchio (1992) proposed that the tangent constitutive matrix be replaced by the secant constitutive matrix $[D_{\text{sec}}]$to avoid possible numerical difficulties due to the fact that softening in concrete may cause the tangent constitutive matrix to be negative. This scheme is also used in this dissertation by simply replacing $[D_t]$by$[D_{\text{sec}}]$ in Eqs. 3.36, 3.37, and 3.38.

The process involved in solving Eq. 3.32 is summarized as follows:

(1) For a given state of displacement $\{u^i, v^i\}$ from the previous iteration, the total strain for the i^{th} step $\{\varepsilon_{xx}, \varepsilon_{yy}, \gamma_{xy}\}^i$ can be determined from the strain-displacement relationships (Eq. 3.29);

(2) Determine the return stress vector $\{\sigma\}$ from a given state of strain $\{\varepsilon_{xx}, \varepsilon_{yy}, \gamma_{xy}\}^i$ and calculate the residual force vector $\{R\}$ from Eqs. 3.32 and 3.33a;

(3) Calculate the secant constitutive matrix $[D_{\text{sec}}]$, substitute into Eq. 3.36 and perform an integration over all elements;

(4) Solve Eq. 3.38 for an incremental displacement vector $\{\Delta U\}$;

(5) Calculate the updated displacements $\{U\}^{i+1} = \{U\}^i + \{\Delta U\}^i$ for the $i+1^{th}$ iteration; and

(6) Repeat (1)-(5) until convergence of the residual force is achieved.

There are two significant steps in the numerical implementation of the process explained above: (1) determination of return stress vector $\{\sigma\}$; and (2) evaluation of secant constitutive matrix $[D_{\text{sec}}]$. These two processes are described in the next sections.

3.2.5.2 Return Stress Vector

Concrete Return Stress

The magnitude as well as the direction of principal strain, where the stress-strain relationship of concrete is defined, corresponding to the i^{th} iteration can be derived from the Mohr Circle of strain and is given by:

$$\varepsilon_1 = \frac{1}{2}(\varepsilon_y + \varepsilon_x) + \sqrt{\frac{1}{2}[(\varepsilon_x - \varepsilon_y)^2 + {\gamma_{xy}}^2]}$$
$$\varepsilon_2 = \frac{1}{2}(\varepsilon_y + \varepsilon_x) - \sqrt{\frac{1}{2}[(\varepsilon_x - \varepsilon_y)^2 + {\gamma_{xy}}^2]} \qquad (3.39)$$
$$\theta = \frac{1}{2}\tan^{-1}[\frac{\gamma_{xy}}{\varepsilon_y - \varepsilon_x}]$$

where ε_1 = major principal strain

ε_2 = minor principal strain

The original MCFT defined the principal stresses σ_{c1} and σ_{c2} in terms of the magnitude of two principal strains obtained using the constitutive relationships presented in Section 3.2.3. However, Belarbi (1991) indicated that for a panel with biaxial tension-compression, an approximation of concrete stress in tension superior to Eq. 3.21 proposed by Vecchio and Collins (1982) may be obtained if the principal compressive strain as well as the principal tensile strain is taken into account. Vecchio (1992) proposed a model that, in effect, decreases the magnitude of parameter ε_1 by taking into account the expansion (Poisson's effect) due to the presence of compression in the perpendicular direction. Fig. 3.20 shows the effect of compression on the magnitude of tensile strain in the perpendicular direction. In essence, the total average strain ε_1 and ε_2 are the superposition of the true applied strain ε_1' and ε_2' and expansion strain $\nu_{12}\varepsilon_2'$ and $\nu_{21}\varepsilon_1'$ as shown in Eq. 3.40:

$$\begin{pmatrix} \varepsilon_1 \\ \varepsilon_2 \end{pmatrix} = \begin{bmatrix} 1 & -\nu_{12} \\ -\nu_{21} & 1 \end{bmatrix} \begin{pmatrix} \varepsilon_1' \\ \varepsilon_2' \end{pmatrix} \tag{3.40}$$

where ν_{12}, ν_{21} = Poisson's ratio giving strain in the 1 direction due to applied strain in the 2 direction, and vice versa

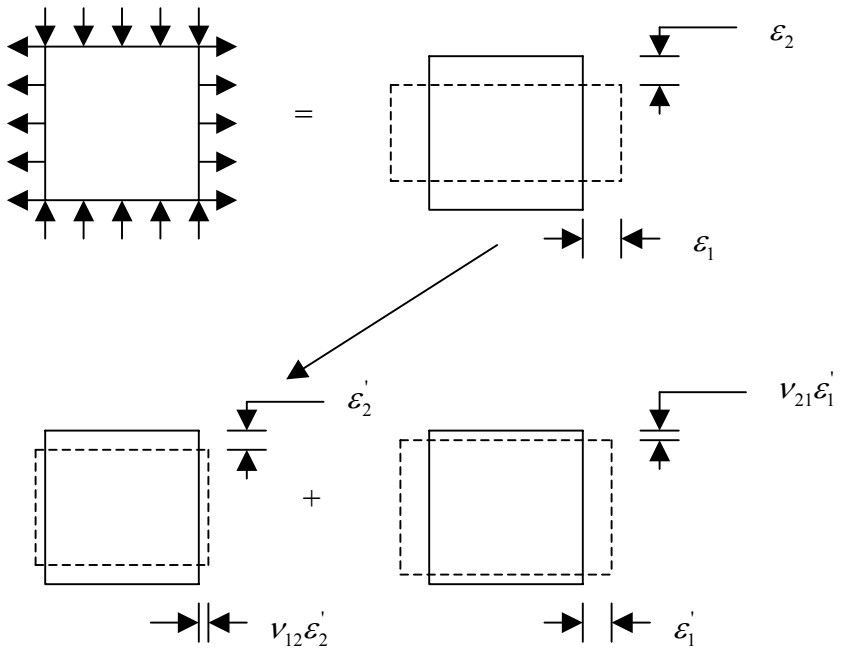

Figure 3.20 Effect of Concrete Expansion on Total Strain

- Concrete Expansion Model

Vecchio (1992) proposed the following models for Poisson ratio (ν) used for calculating the transverse expansion strain due to compression:

$$\nu = \nu_0 \text{ for } 0 < |\varepsilon_c| < \frac{\varepsilon_{cc}}{2}, \text{ and}$$

$$= \nu_0 \left(1 + 1.5\left(\frac{2|\varepsilon_c|}{\varepsilon_{cc}} - 1\right)^2 \right) \leq 0.5, \text{ for } |\varepsilon_c| > \frac{\varepsilon_{cc}}{2} \qquad (3.41)$$

where ν_0 = initial Poisson's ratio of uncracked concrete, taken as 0.2

Similarly, the effect of tensile strain also results in contraction in the transverse direction. For uncracked concrete, the magnitude of contraction can be determined by

the value ν_0 as defined above. However, experimental results (Van Mier, 1986) show that the Poisson's ratio decreases as soon as cracking occurs, and the value asymptotically reaches zero at sufficiently high tension. For simplicity, the Poisson's ratio due to tensile strain of cracked concrete is assumed to be zero in this study. Therefore, for panels with biaxial tension-compression, the parameter ε_2 used in the constitutive relationships in compression (Eqs. 3.3, 3.4, and 3.5), in general, does not require any modification.

However, for the state of biaxial compression-compression stress, Poisson's effect contributes to the overall average strain in the transverse direction. Therefore, the variable ε_2 in Eqs. 3.3, 3.4, and 3.5 should also be modified by taking into account the transverse expansion due to compression. Eq. 3.40 is used to decrease the magnitude of ε_1 and ε_2 (both in compression for this case).

- Out-of-Plane Confinement due to Transverse Hoops

Consider a RC column subjected to uniaxial compression as shown in Fig. 3.21. Poisson's effect causes transverse strain perpendicular to the direction of the axial load. For members without hoops or cross–tie reinforcements, this transverse expansion occurs with stress-free condition in the direction of this transverse strain. However, the presence of the transverse reinforcement would prevent this free expansion because this transverse expansion would cause tension in the transverse reinforcement. This causes a self-equilibrated stress condition in the transverse direction because the sum of concrete and reinforcing steel stress must be zero as shown in Fig. 3.21. Therefore, compressive stress occurs in concrete to balance out the tensile stress in the transverse. In other words, the presence of transverse reinforcement causes confining stress to the inner core concrete when the member is subjected to an axial load. Mander et al. (1988) had quantified the effect of this confining stress on the performance of columns with varying reinforcement ratios and configurations and concluded that the overall stress-strain relationships of the inner core concrete is enhanced. Analytical expressions on the effect

of confinement proposed by Mander et al. (1988) are shown in Section 3.2.3.3 and 3.2.3.4. However, the magnitude of the confining stress due to transverse reinforcement is based on the yielding stress transverse reinforcement. For a low level of applied uniaxial stress, this assumption may be violated. Nonetheless, the presence of the confining stress does not have a significant influence on the change in pre-peak stress-strain curve at low level of applied stress. Therefore, the Mander's method generally yields reasonable results for practical applications when the main objective of the study was near or beyond the post peak performance of a RC column.

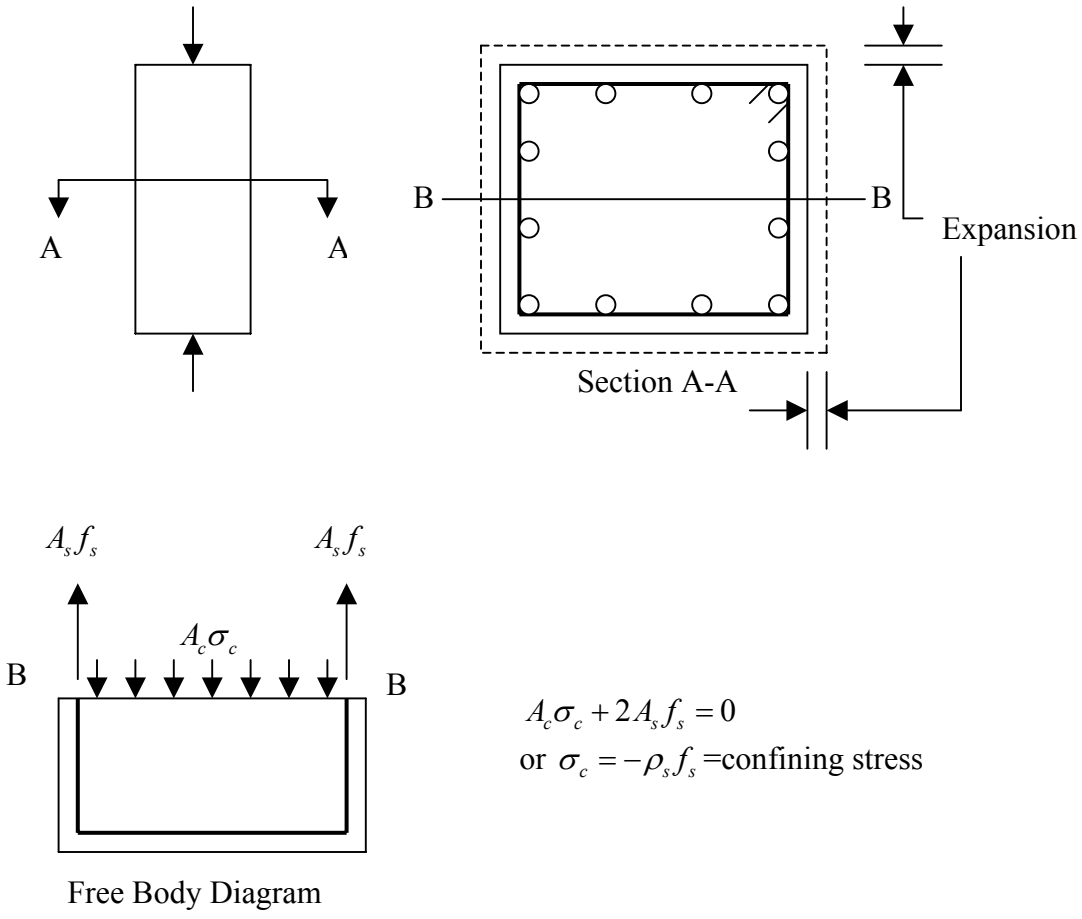

Figure 3.21 Effect of Confinement due to Transverse Reinforcement

The procedure proposed by Mander et al. (1988) is extended to two dimensional stress analysis in this dissertation. However, the confining stress is determined by the amount of Poisson's expansion in this transverse direction. Because the model formulation is based on the two-dimensional stress analysis, the restraining effect due to vertical leg is automatically satisfied as shown in Fig. 1.2. However, the effect of horizontal legs that provide the out-of-plane confinement requires further clarification. Based on magnitude of ε_1 and ε_2 in each iteration, the out-of-plane expansion strain can be approximated by:

$$\varepsilon_3 = \nu_{31}\varepsilon_1' + \nu_{32}\varepsilon_2' \tag{3.42}$$

where ν_1 and ν_2 are the Poisson's ratios due to ε_1 and ε_2 calculated from Eq. 3.40, respectively.

Based on this out-of-plane expansion strain, the confining stress (σ_3) can be approximated by

$$\sigma_{c3} = \rho_3 f_{s3} \tag{3.43}$$

where ρ_3 = out-of-plane reinforcement ratio of the stirrups horizontal legs

f_{s3} = average stress in the stirrups calculated from the out-of-plane expansion strain in Eq. 3.42

Note that Vecchio (1992) also proposed a slightly different expression for the out-of-plane expansion involving the out-of-plane reinforcement ratio. Simplified equations like Eq. 3.43 should also yield reasonable results as, in practice, out-of-plane reinforcement is relatively low (below 2%). Under these circumstances, the out-of-plane

expansion strain predicted by Eq. 3.43 does not significantly deviate from that predicted by Vecchio's (1992) expression.

After taking into account the effect of concrete expansion and confinement, the magnitude of concrete stress in the principal direction can be obtained by substituting the appropriate parameters into Eqs. 3.5, 3.7, 3.19, and 3.22. The final concrete return stress in the global X-Y coordinate is determined by the stress transformation relationship as shown in Eq. 3.1.

In summary, the determination of concrete return stress from a given state of strain $(\varepsilon_x, \varepsilon_y, \gamma_{xy})$ becomes more involved that the originally proposed MCFT. In general, the process is similar to that proposed by Vecchio (1992), taking into consideration the effect of concrete expansion and confinement. Fig. 3.22 shows the flowchart summarizing the steps for calculating the concrete return stress.

Note that in the step for determining σ_{c1}, σ_{c2} from the given $\varepsilon_1', \varepsilon_2', \sigma_{c3}$, three possible scenarios arise:

(1) Both $\varepsilon_1', \varepsilon_2'$ are tensile. In this case, concrete tensile stress in the 1- and 2-direction can be obtained directly by Eq. 3.19 or 3.22;

(2) ε_1' is tensile while ε_2' is compressive. This corresponds to biaxial compressive stress condition and one tension in a triaxial stress state. The concrete tensile stress in the 1-direction is obtained as in the first case. However, the compressive stress in the 2- direction requires the uses of out-of-plane confining stress σ_{c3} to determine the stress and strain enhancement factor as described in Section 3.2.3.3. The unsoftened concrete stress is calculated from Eq. 3.5. The final stress σ_{c2} is obtained by applying the softening factor (Eq. 3.7) to the unsoftened stress determined previously.

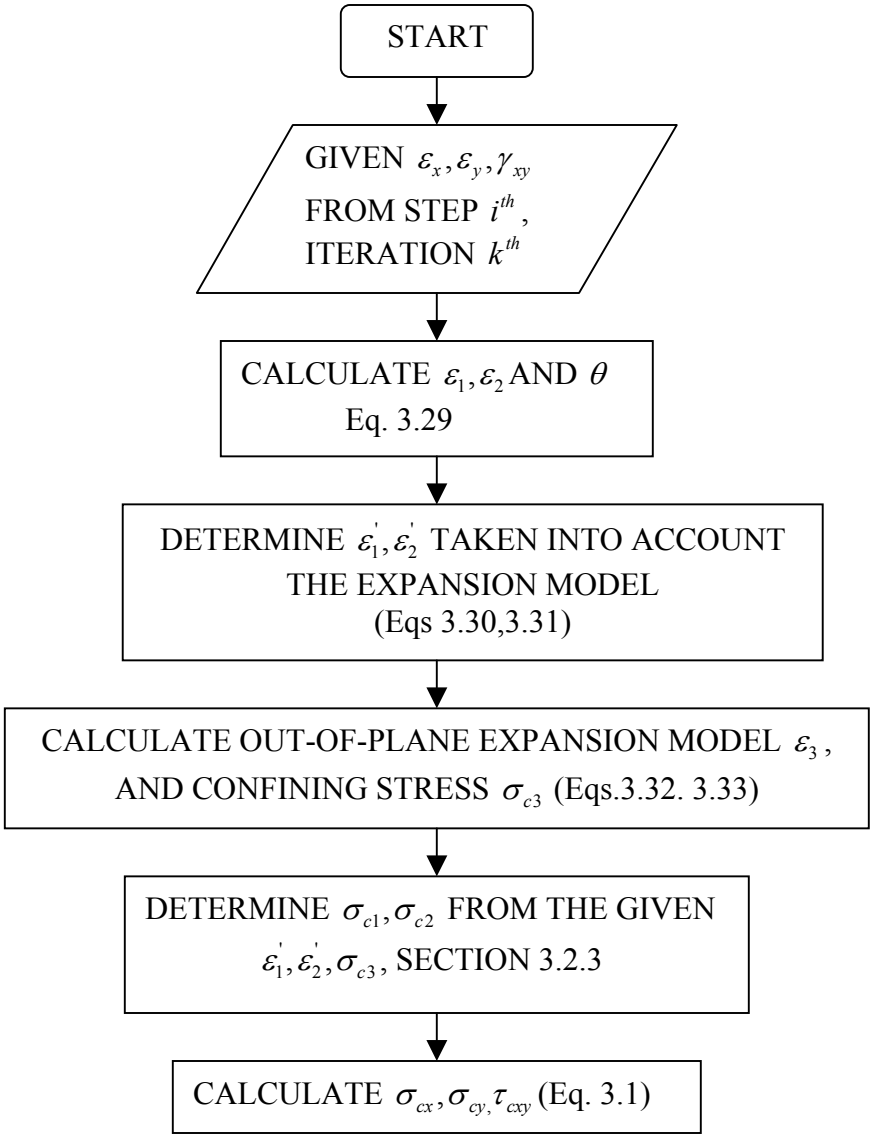

Figure 3.22 Flowchart for Determining the Return Concrete Stress Vector in Non-Linear Solution

(3) Both $\varepsilon_1^{'}, \varepsilon_2^{'}$ are compressive. Because the determination of σ_{c2} from Eq. 3.5 requires a prior knowledge of two confining stress: (a) the known out-of-plane confining stress σ_{c3}; and (b) the unknown stress σ_{c1}, and vice versa. Therefore, the process essentially requires iterations. The simplified procedure is used in this dissertation to avoid possible numerical difficulties. The procedure is as follows:

(i) Use out-of-plane confining stress σ_{c3} to determine the stress and strain enhancement factors in the smaller compressive strain direction $(\varepsilon_1^{'})$ and calculate temporary $\sigma_{c1}^{'}$ from Eq. 3.5 using $\varepsilon_1^{'}$.

(ii) Use $\sigma_{c1}^{'}$ from (i) and σ_{c3} to determine the stress and strain enhancement factors. Use this stress and strain enhancement factor to calculate σ_{c1} and σ_{c2} from Eq. 3.5 using $\varepsilon_1^{'}$ and $\varepsilon_2^{'}$, respectively.

Steel Return Stress

For smeared reinforcements in the definition of MCFT at a given state of strain $\{\varepsilon_x, \varepsilon_y, \gamma_{xy}\}^i$ of the i^{th} iteration, the return stress can be obtained directly using modified from of Eq. 3.27 to take into account the effect of tension stiffening.

Total Return Stress Vector

The total return stress vector $\{\sigma\}$ is essentially the algebraic sum of the concrete return stress and steel return stress as shown in Eq. 3.1

3.2.5.3 Secant Constitutive Matrix

Concrete

In the numerical implementation of FEM, the use of the tangent constitutive matrix generally ensures the quadratic rate of convergence, which is desirable for most applications. Crisfield and Wills (1989) showed that the tangent constitutive matrix of the rotating crack model in terms of the incremental principal stresses and strains for concrete can be written as

$$\begin{bmatrix} d\sigma_1 \\ d\sigma_2 \\ d\tau_{12} \end{bmatrix} = \begin{bmatrix} \frac{\partial \sigma_1}{\partial \varepsilon_1} & \frac{\partial \sigma_1}{\partial \varepsilon_2} & 0 \\ \frac{\partial \sigma_2}{\partial \varepsilon_1} & \frac{\partial \sigma_2}{\partial \varepsilon_2} & 0 \\ 0 & 0 & \frac{\sigma_1 - \sigma_2}{2(\varepsilon_1 - \varepsilon_2)} \end{bmatrix} \begin{bmatrix} d\varepsilon_1 \\ d\varepsilon_2 \\ d\gamma_{12} \end{bmatrix} \quad , \left\{ d\sigma^{12} \right\} = \left[D_c \right]^{12}_{\tan} \left\{ \varepsilon^{12} \right\} \tag{3.44}$$

The superscript 12 shows that this tangent stiffness is written in terms of principal direction. Note that there is an explicit shear stiffness involved even though this elasticity matrix involves only principal stresses and strains. This shear stiffness arises due to the possible crack rotation from the fact that a strain increment may cause principal stress and strain directions to rotate. Therefore, there exists a shear stress and strain with respect to the stress condition before and after crack rotation. For an infinitesimal strain increment, this tangent constitutive matrix ensures the co-rotation of the principal stress and strain direction (Willam et al., 1987).

However, for softening material like concrete, the tangent constitutive matrix may become negative after the peak stress is reached. This negative value of tangent constitutive matrix could cause numerical instability into the model, which leads to bizarre results such as force convergence oscillation or even non-convergent in some cases. Vecchio (1989) proposed the use of secant constitutive matrix for concrete of the form:

$$\left[D_c\right]_{\text{sec}}^{12} = \begin{bmatrix} \overline{E}_{c1} & 0 & 0 \\ 0 & \overline{E}_{c2} & 0 \\ 0 & 0 & \overline{G}_c \end{bmatrix} \tag{3.45}$$

where $\overline{E}_{c1} = \dfrac{\sigma_{c1}}{\varepsilon_1}$, $\overline{E}_{c2} = \dfrac{\sigma_{c2}}{\varepsilon_2}$, and $\overline{G}_c = \dfrac{\overline{E}_{c1}\overline{E}_{c2}}{\overline{E}_{c1} + \overline{E}_{c2}}$

Note that Eq. 3.45 ignores the effect of Poisson's ratio on the constitutive matrix. Vecchio (1992) proposed an alternative formulation for the secant constitutive matrix. The revised model required the decomposition of Poisson's ratio into an elastic component and residual in order to preserve the symmetry of the constitutive matrix. Following the same spirit of Vecchio's (1992) model, a new secant stiffness in terms of the principal can be derived. Because ABAQUS allows the use of non-symmetric stiffness matrix, a more direct approach relaxing the assumption set forward by Vecchio (1992) can be used.

Consider a given state of principal strain ($\varepsilon_1, \varepsilon_2$), the total strain in each direction can be decomposed into two components: (1) the stress-induced part; and (2) the part due to the Poisson's effect as shown in Eq. 3.40.

By defining $E_{c1} = \dfrac{\sigma_{c1}}{\varepsilon_1'}$ and $E_{c2} = \dfrac{\sigma_{c2}}{\varepsilon_2'}$, Eq. 3.40 can be rewritten as:

$$\begin{bmatrix} \varepsilon_1 \\ \varepsilon_2 \end{bmatrix} = \begin{bmatrix} \dfrac{1}{E_{c1}} & \dfrac{-\nu_{12}}{E_{c2}} \\ \dfrac{-\nu_{21}}{E_{c1}} & \dfrac{1}{E_{c2}} \end{bmatrix} \begin{bmatrix} \sigma_{c1} \\ \sigma_{c2} \end{bmatrix} \tag{3.46}$$

By inverting Eq. 3.46, the secant stiffness matrix of concrete in the principal direction is:

$$\begin{bmatrix} \sigma_{c1} \\ \sigma_{c2} \end{bmatrix} = \frac{1}{1-\nu_{12}\nu_{21}} \begin{bmatrix} E_{c1} & \nu_{12}E_{c1} \\ \nu_{21}E_{c2} & E_{c2} \end{bmatrix} \begin{bmatrix} \varepsilon_1 \\ \varepsilon_2 \end{bmatrix} \tag{3.47}$$

As treated by Crisfield and Wills (1989) and Willam et al. (1987), an additional relationship for shear stiffness is required to account for possible crack rotation. Vecchio (1989) proposed the used of $\overline{G}_c = \frac{\overline{E}_{c1}\overline{E}_{c2}}{\overline{E}_{c1}+\overline{E}_{c2}}$ in the early model which neglects the Poisson's effect. Zhu and Hsu (2002) showed that the consistent secant shear-stiffness for FA-STM had the same form as the tangent shear stiffness of the rotating crack angle model as shown in Eq. 3.44. In this dissertation, the tangent shear stiffness will also be used. Preliminary numerical studies show that the use of this tangent shear stiffness results in a more numerically stable solution. The algorithmic secant constitutive matrix becomes

$$\left[D_c\right]^{12}_{\text{sec}} = \frac{1}{1-\nu_{12}\nu_{21}} \begin{bmatrix} E_{c1} & \nu_{12}E_{c1} & 0 \\ \nu_{21}E_{c2} & E_{c2} & 0 \\ 0 & 0 & G_c \end{bmatrix} \tag{3.48}$$

where $E_{c1} = \frac{\sigma_{c1}}{\varepsilon_1'}$, $E_{c2} = \frac{\sigma_{c2}}{\varepsilon_2'}$, and $G_c = \frac{\sigma_{c1}-\sigma_{c2}}{2(\varepsilon_1-\varepsilon_2)}$

Eq. 3.48 represents the secant constitutive matrix in terms of the principal coordinate. The secant constitutive matrix in X-Y coordinate may be obtained through the coordinate transformation:

$$\left[D_c\right]^{XY}_{\text{sec}} = \left[T\right]^T \left[D_c\right]^{12}_{\text{sec}} \left[T\right] \tag{3.49}$$

$$\text{where } [T] = \begin{bmatrix} \sin^2\theta & \cos^2\theta & \cos\theta\sin\theta \\ \cos^2\theta & \sin^2\theta & -\cos\theta\sin\theta \\ -2\cos\theta\sin\theta & 2\cos\theta\sin\theta & \cos^2\theta - \sin^2\theta \end{bmatrix} \tag{3.50}$$

Steel

The secant stiffness matrix for smeared reinforcing steel can be obtained in a straightforward manner. By definition, the secant stiffness (E_s^{sec}) is defined as the ratio between the current stress and strain. Taking into account the reinforcement ratio in each direction, the secant constitutive matrix for smeared steels is

$$[D_s]_{\text{sec}}^{XY} = \begin{bmatrix} \rho_x E_{sx}^{\text{sec}} & 0 & 0 \\ 0 & \rho_y E_{sy}^{\text{sec}} & 0 \\ 0 & 0 & 0 \end{bmatrix} \tag{3.51}$$

Total

The total secant constitutive of RC membrane is obtained by adding Eqs. 3.51 to 3.49 as follows:

$$[D]_{\text{sec}}^{XY} = [D_c]_{\text{sec}}^{XY} + [D_s]_{\text{sec}}^{XY} \tag{3.52}$$

3.3 SUMMARY

The key features of this newly proposed constitutive equation are summarized as follows:

(1) Equilibrium and compatibility conditions are the same as MCFT and RA-STM

(2) Strength enhancement factors are based on the five-parameter failure surface proposed by Willam and Warnke (1974)

(3) Strain enhancement factors are based on the equation proposed by Mander et al. (1988).

(4) Backbone compressive stress curve proposed by Popovic (1973) in both pre- and post-peak ranges.

(5) Softening factors in compression due to the presence of perpendicular tension force are those proposed by Vecchio and Collins (1986).

(6) Constitutive relationship in tension is that proposed by Collins and Mitchell (1987).

(7) Crack check process in MCFT is replaced by modifying the apparent yield stress and post-yield stiffness of reinforcing steel as proposed by Tamai et al. (1987) and Belarbi and Hsu (1994).

CHAPTER IV

EXPERIMENTAL PROGRAM

4.1 PROGRAM OVERVIEW

An experimental program, sponsored by the Texas Department of Transportation (TxDOT), was conducted to determine the cause of excessive cracking in RC bent caps used to support the main bridge superstructures in the State of Texas (Bracci et al., 2000). The study investigated the effect of reinforcement details, both in the form of vertical stirrups used mainly for shear and longitudinal reinforcement for flexure, on the crack patterns and crack width in order to propose an effective reinforcement configuration for crack control. Fig. 4.1 shows the general problematic crack patterns existing near the cantilevered end of RC bent caps under service load conditions.

Figure 4.1 Observed Cracks in RC Bent Caps in the State of Texas

Common practice adopted a crack control procedure by limiting the tensile reinforcement stress to $0.6f_y$ under unfactored service loads as proposed by AASHTO standard specifications. Alternately, ACI 318-95 suggests the use of the so called "z" factors as a parameter for crack control, which is defined as

$$z = f_S \sqrt[3]{d_C A} \tag{4.1}$$

where: f_s = Service stress in the flexural tension reinforcement (ksi)

d_c = Distance from extreme concrete fiber in tension to the centroid of the closest layer of reinforcement (inches).

A = Effective tension area of concrete surrounding the reinforcements, having the same centroid as the reinforcement (in.^{2}/bar).

ACI 318-95 recommended that the calculated "z" factors for a given cross section be limited to 175 kips/inch for interior exposure and 145 kips/inch for exterior exposure.

However, both the z factor and $0.6f_y$ limit proposed by ACI 318-95 and AASHTO were semi-empirically obtained from small-sized members where flexural deformations were dominant. For larger RC members, the main flexural reinforcement is generally located near the tension side of the cross section and skin reinforcement was minimally provided within the section depth. Frantz and Breen (1978) pointed out that, in large RC members with relatively short shear spans, side-face cracks could be wider than the top-face crack and the distribution of skin reinforcement had a significant influence of side-face crack control. In addition, side-face crack orientation in deep beams generally makes an angle with the vertical direction. This implied the existence of shear deformations in the member. These flexural-shear cracks are not taken into account in the code equation. Therefore, the provisions recommended by the current code of practice may not be adequate for crack control in RC bent caps.

In order to perform a parametric study on the effect of reinforcement details on the characteristics of crack width, spacing between cracks and the evolution of cracks under increasing external load, a total of sixteen full-scale RC bent caps were designed, constructed, and tested at Texas A&M University (Bracci et al, 2000, and Young et al., 2002). Fig. 4.2 shows the general test setup for full-scale RC bent caps.

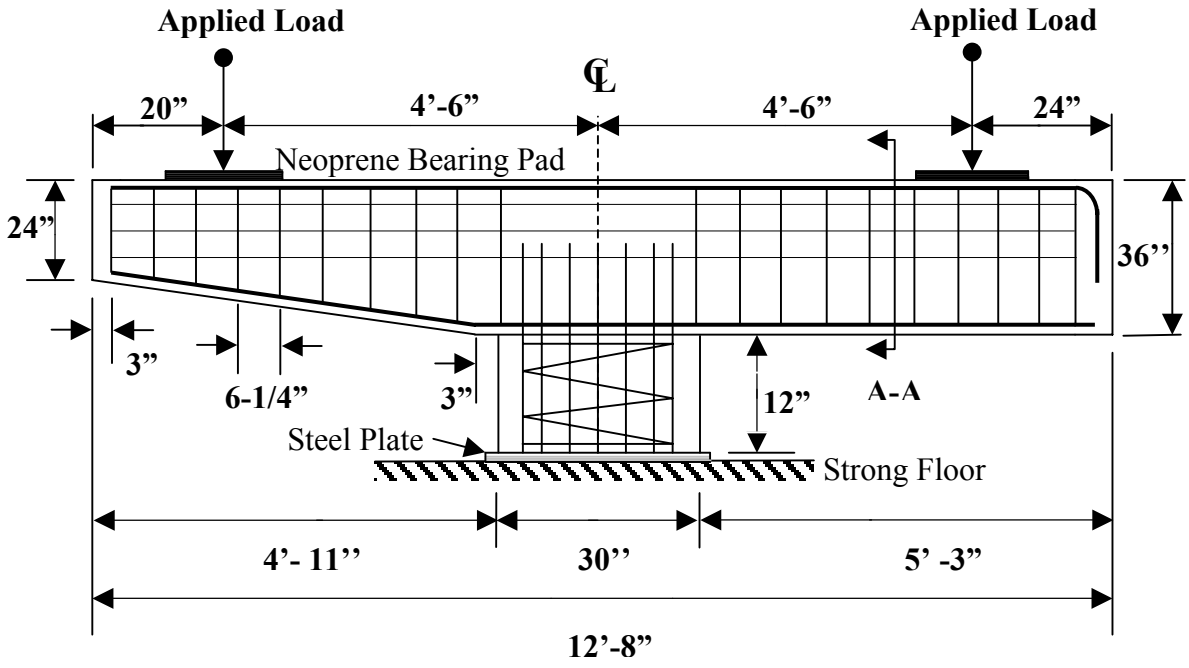

Figure 4.2 RC Bent Caps Test Specimen Details (Bracci et al., 2000)

4.2 SPECIMEN DETAILS

The experimental program was divided into three phases according the amount and configuration of reinforcement details. An alphanumeric system was used to identify the individual specimens, such as 1A, 2A, etc. The number was used to identify the reinforcement configuration and the letter signified the corresponding concrete batch.

4.2.1 First Group of Specimens

The first group of specimens consisted of specimens 1A, 1B, 2A, and 2B. This group of specimens was tested to reproduce the observed cracking pattern in RC bent caps in service and serve as a baseline for the two subsequent groups. Based on actual bent cap reinforcement, specimens in both set 1 and 2 employed 8#8 bars with an equivalent area of 6.32 in^2 in both the tension and compression side of the cross section. The amount of main reinforcement was provided such that the reinforcement stress at the column face was approximately 36 ksi under the applied load of 160 kips at the locations shown in Fig. 4.2. This conforms to the AASHTO requirement for crack control to limit the working stress within $0.6 f_y$ under all combined service loads. Table 4.1 shows design details for the specimens in the first group.

TABLE 4.1 Group #1 Specimen Design Description

Specimen ID	Longitudinal Reinforcement	Skin Reinforcement	'z'[1] (kips/in.)	Design Critical Section	f'c[2] (psi)
1A	8 #8 bars	4 #5 bars	164	Column face	6,217
1B	8 #8 bars	4 #5 bars	164	Column face	5,820
2A	8 #8 bars	6 #4 bars	164	Column face	6,217
2B	8 #8 bars	6 #4 bars	164	Column face	5,820

[1]Calculated at the Column Face, using $f_s = 0.6 f_y$

[2]Determined from standard 28-day compression tests

Four out of the eight reinforcing bars on the compression side (bottom steel) were cut off before entering the column region to avoid joint congestion. Both sets of specimens also adopted #5 bars transverse stirrups with a spacing of 6.25 in. Fig. 4.3 shows the general details of the flexural and shear reinforcement adopted in the first set of specimens.

The difference between the specimens labeled 1 and 2 was the choice of skin reinforcement details. Specimens 1A and 2A adopted skin reinforcement using four #5 bars uniformly distributed into two layers throughout the member depth as shown in Fig. 4.3a. This specific skin reinforcement configuration conforms to the general guidelines recommended by the AASHTO specifications for bridge design prior to 1989.

Ferguson (1964) performed an experimental study on the effect of reinforcement details on the strength and serviceability of RC bent caps whose geometry and the point of application of the load were similar to that were used by Bracci et al. (2000). The conclusion from this work was that the transverse stirrups offered little or no improvement on both the strength and crack control of RC bent caps. However, additional reinforcement in the form horizontal reinforcement (skin reinforcement) provided an enhanced performance of RC bent caps both in terms of strength and crack control. Frantz and Breen (1978) performed an analytical and experimental study on the crack widths in deep inverted-T beams and indicated that the use of skin reinforcement well distributed in the upper tensile zone of the cross section, rather than uniformly distributed throughout the members depth, helped decrease the side-face crack width in deep RC beams. The AASHTO standard subsequent to the 1989 version realized the significance of skin reinforcement detailing on side-face crack control and recommended that the skin reinforcement be distributed in the flexural tension zone of the cross section. Specimens 2A and 2B was designed according to the current AASHTO standard by adopting three layers of 2#4 bars, which gave the same equivalent area of skin reinforcement in Specimen 1A and 1B, distributed in the upper portion of the members as shown in Fig. 4.3b.

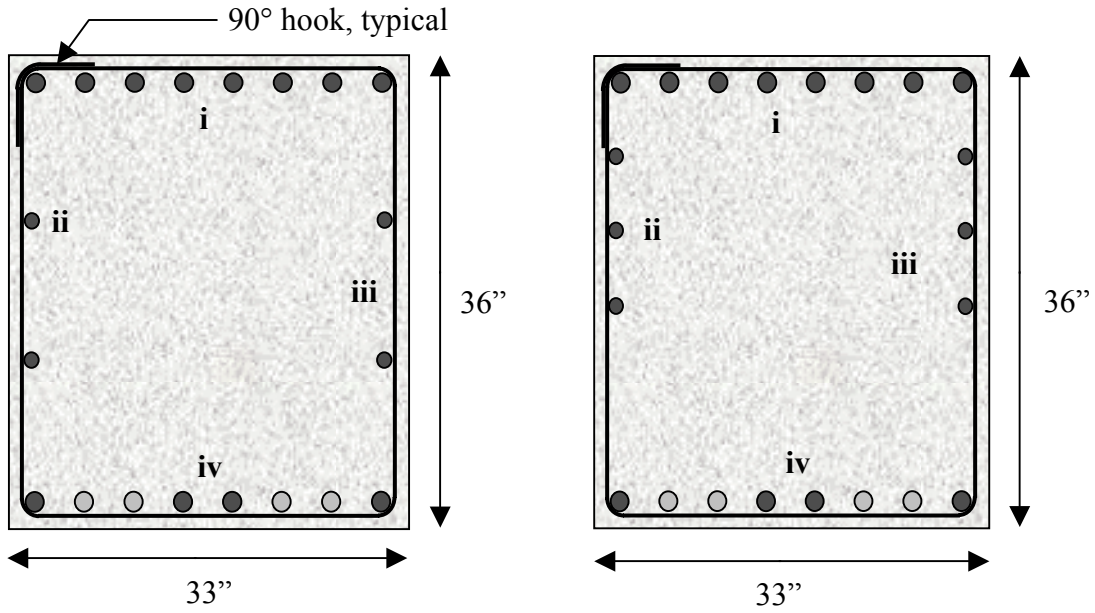

(a) Specimen 1A & 1B Details **(b) Specimen 2A & 2B Details**

i. Main Tension Reinforcement:
8 #8 bars @ 3.75” spacing (A_s = 6.32 in.^{2})

ii. Side-face (skin) Reinforcement:
(a) 2 #5 bars each side @ 9.75” spacing
(b) 3 #4 bars each side @ 5.5” spacing

iii. Transverse Reinforcement:
5 Stirrups @ 6.25” spacing

iv. Compression Reinforcement:
8 #8 bars
4 cut off prior to column support

● Continuous Bars Through Joint
○ Discontinuous Bars at Joint face

Figure 4.3 Group #1 Reinforcement Details, Section A-A (See Fig. 4.2)

4.2.2 Second Group of Specimens

The second group consisted of specimens 3C, 3D, 4C, 4E, 5D, and 5E. The primary purpose of this group of specimens was to perform an experimental parametric study on the influence of the main reinforcing steel on crack patterns in RC bent caps. Specimens 3C and 3D employed 11#7 rebars which had equivalent main tensile reinforcement area to that of the specimens in the first group. However, the use of a smaller bar size with closer spacing between bars was used to reduce the "z" factor. Specimens 4C, 4E, 5D, and 5E employed approximately 20 percent larger reinforcing steel area than group 1 specimens. This corresponded to designing the reinforcing steel area based on the bending moment at the centerline of column rather than at the column face commonly adopted in practice. Table 4.2 and Fig. 4.4 shows the design description and reinforcement details for specimens in the second group.

TABLE 4.2 Group #2 Specimen Design Description

Specimen ID	Longitudinal Reinforcement	Skin Reinforcement	'z'[1] (kips/in.)	Design Critical Section	f'c[2] (psi)
3C	11 #7 bars	6 #4 bars	140	Column face	6,035
3D	11 #7 bars	6 #4 bars	140	Column face	5,508
4C	7 #10 bars	6 #4 bars	125	Column centerline	6,035
4E	7 #10 bars	6 #4 bars	125	Column centerline	7,722
5D	11 #8 bars	6 #4 bars	107	Column centerline	5,508
5E	11 #8 bars	6 #4 bars	107	Column centerline	7,722

[1]Calculated at the Column Face, using $f_s = 0.6 f_y$

[2]Determined from standard 28-day compression tests

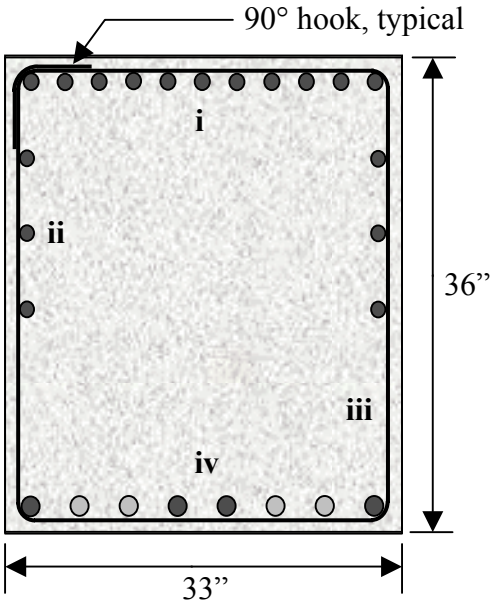

(a) Specimen 3C & 3D Details

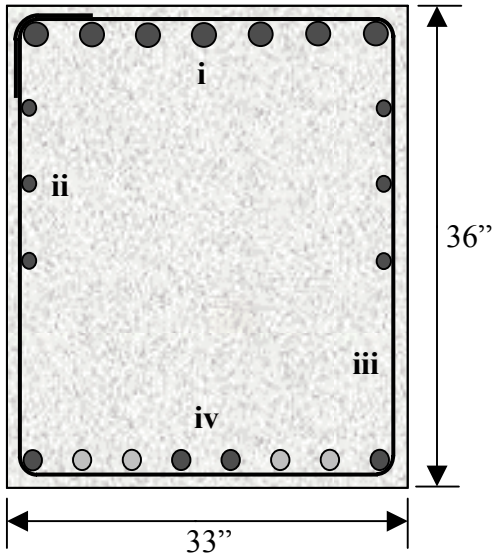

(b) Specimen 4C & 4D Details

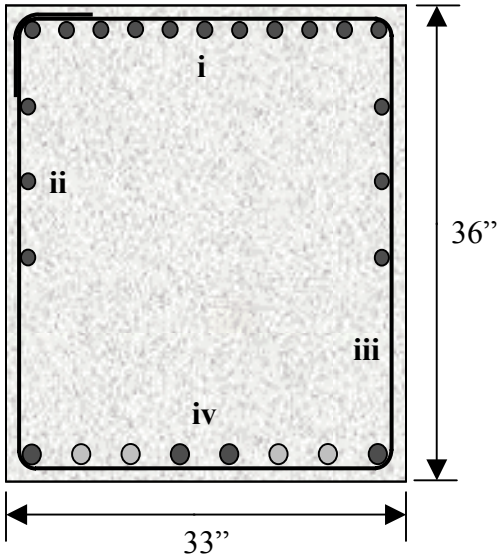

(c) Specimen 5D & 5E Details

i. Main Longitudinal Reinforcement:
   (a) 11 #7 bars @ 2.6” spacing (A_s = 6.60 in.^{2})
   (b) 7 #10 bars @ 4.3” spacing (A_s = 8.89 in.^{2})
   (c) 11 #8 bars @ 2.6” spacing (A_s = 8.69 in.^{2})

ii. Side-face (skin) Reinforcement:
   3 #4 bars each side @ 5.5” vertical spacing

iii. Transverse Reinforcement:
   #5 Stirrups @ 6.25” longitudinal spacing

iv. Compression Reinforcement: 8 #8 bars
   4 cut off prior to column support

Continuous Bars through Joint

Discontinuous Bars at Joint Face

Figure 4.4 Group #2 Reinforcement Details, Section A-A (See Fig. 4.2)

4.2.3 Third Group of Specimens

The third group comprised six specimens (6F, 6G, 7F, 7H, 8G, and 8H) with three reinforcement configurations in three concrete batches. The major difference between this set of specimens and the previous two was the introduction of overlapping stirrups for transverse reinforcement as shown in Fig. 4.5. The use of overlapping stirrups introduced two sources of strengthening for the concrete provided by: (1) confinement; and (2) tension stiffening. Confinement was attributed to the fact that the deformation of the vertical and horizontal legs of stirrups under the presence of load caused confining stresses, which in turn, increased both strength and deformability of concrete in compression. Overlapping stirrups also provide vertical reinforcement in the inner core concrete. When subjected to tension, this transverse reinforcing steel provided tension-stiffening effect through the bond stresses existing between concrete and reinforcing steel interface.

The variation of main reinforcement details was also investigated. Specimens 6F and 6G adopted 5#10 rebars which gave approximately the same reinforcing steel area to the specimens in group 1 but yielded a larger ACI ‘z’ factor. Specimens 7F and 7H adopted 11#8 bars, while specimens 8G and 8H used 8#8 bars. Table 4.3 shows the material properties and design descriptions for specimens in the third group.

Table 4.3 Group #3 Specimen Design Description

Specimen ID	Longitudinal Reinforcement	Skin Reinforcement	'z'[1] (kips/in.)	Design Critical Section	f'c[2] (psi)
6F	5 #10 bars	6 #4 bars	196	Column face	5,460
6G	5 #10 bars	6 #4 bars	196	Column face	5,320
7F	11 #8 bars	6 #4 bars	107	Column centerline	5,460
7H	11 #8 bars	6 #4 bars	107	Column centerline	5,727
8G	8 #8 bars	6 #4 bars	164	Column face	5,320
8H	8 #8 bars	6 #4 bars	164	Column face	5,727

[1]Calculated at the Column Face, using $f_s = 0.6 f_y$

[2]Determined from standard 28-day compression tests

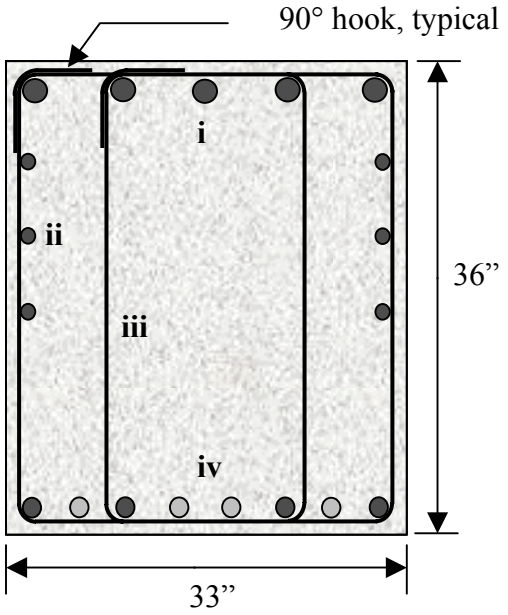

(a) Specimen 6F & 6G Details

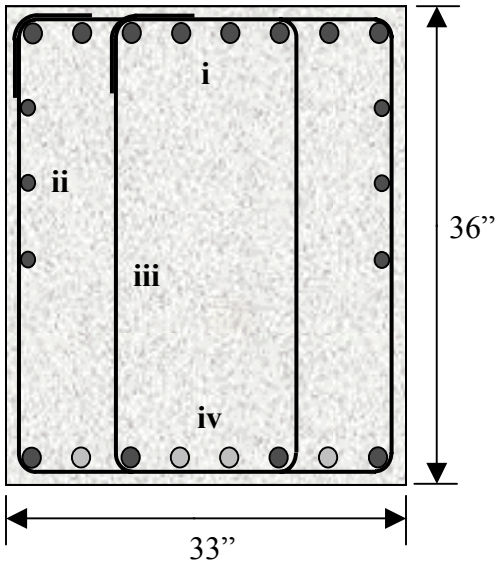

(b) Specimen 8G & 8H Details

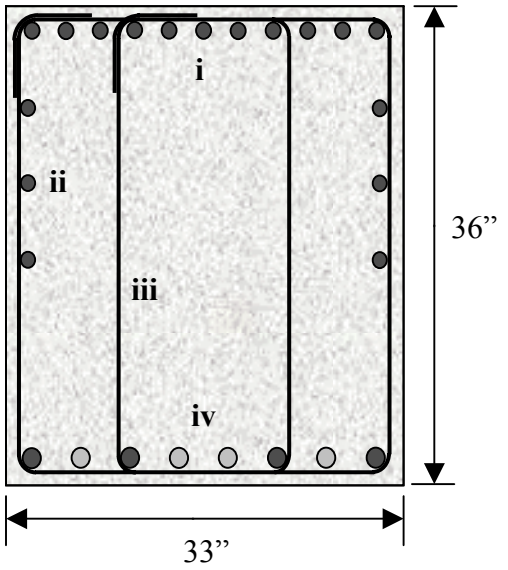

(c) Specimen 7F & 7H Details

i. Main Longitudinal Reinforcement:
   (a) 5 #10 bars @ 6.5” spacing (A_s = 6.35 in.^{2})
   (b) 8 #8 bars @ 3.7” spacing (A_s = 6.32 in.^{2})
   (c) 11 #8 bars @ 2.6” spacing (A_s = 8.69 in.^{2})

ii. Side-face (skin) Reinforcement:
   3 #4 bars each side @ 5.5” spacing

iii. Transverse Reinforcement:
   #5 bars @ 6.25” longitudinal spacing

iv. Compression Reinforcement: 8 #8 bars
   (4 cut off prior to column support)

● Continuous Bars through Joint
○ Discontinuous Bars at Joint Face

Figure 4.5. Group #3 Reinforcement Details, Section A-A (See Fig. 4.2)

4.3 TEST SETUP AND DATA ACQUISITION

The experimental testing was conducted at the Texas Engineering Experiment Station (TEES) at Texas A&M University. Two equal loads were applied in a quasi-static manner using 600 kips capacity actuators to simulate the loads transferred from the main bridge girder near the column region where cracks have been observed. The actuator load was transferred to the specimens via a W14x398 transfer beam sitting on two 8"x16"x1" neoprene bearing pads as shown in Fig. 4.6.

Type CEA-06-250UN-120 Micro-Measurement© strain gauges were used to measure the reinforcement strains at various locations. Because the cantilever part of the bent appeared to experience larger visible cracks in practice, strain gauges were only installed on the cantilever side. Each strain gauge was associated with a number for identification purpose. Figs. 4.7 and 4.8 show the strain gauge locations for groups 1-2, and 3, respectively. Notice that the locations of strain gauges in the third group specimens were slightly different from those in groups 1 and 2 by removing the strain gauges #29 and #31 used for measuring transverse strain in section A in group 1 and 2 specimens to section B for the third group specimens. Particular emphasis was placed on the through-depth strain distribution at sections A and B to determine whether a linear strain distribution commonly used in the engineering beam theory remained valid. Two additional LVDTs (Linear Variable displacement Transformer) were also installed at the location of actuators to measure the deflection at the loading point.

Labview©, a commercially available PC-based data acquisition system, was used for data acquisition on strain gauges, LVDTs, and actuator loads. All data was recorded at every 0.5 seconds from the start until actuator load reached 500 kips or the failure load. At every 40 kips load interval, the data acquisition was paused while keeping the actuator load constant to identify crack patterns and measure crack widths. Crack widths were measured using crack width identification cards at every 40 kips load interval until the actuator loads reached 360 kips when cracks apparently became saturated. After the

crack saturation state, no new crack formed and existing cracks widened beyond the value that is of little practical engineering application. Therefore, no crack information beyond 360 kips actuator load was recorded.

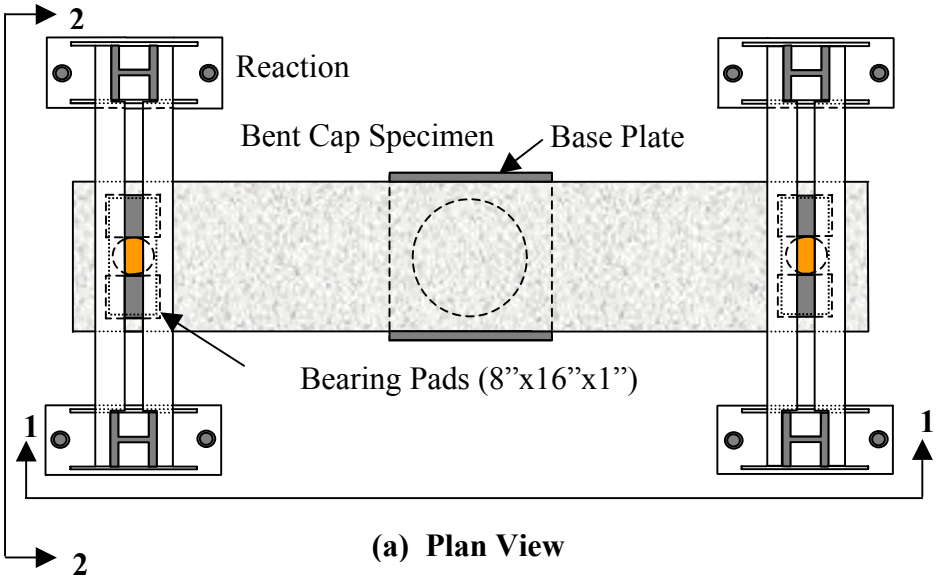

(a) Plan View

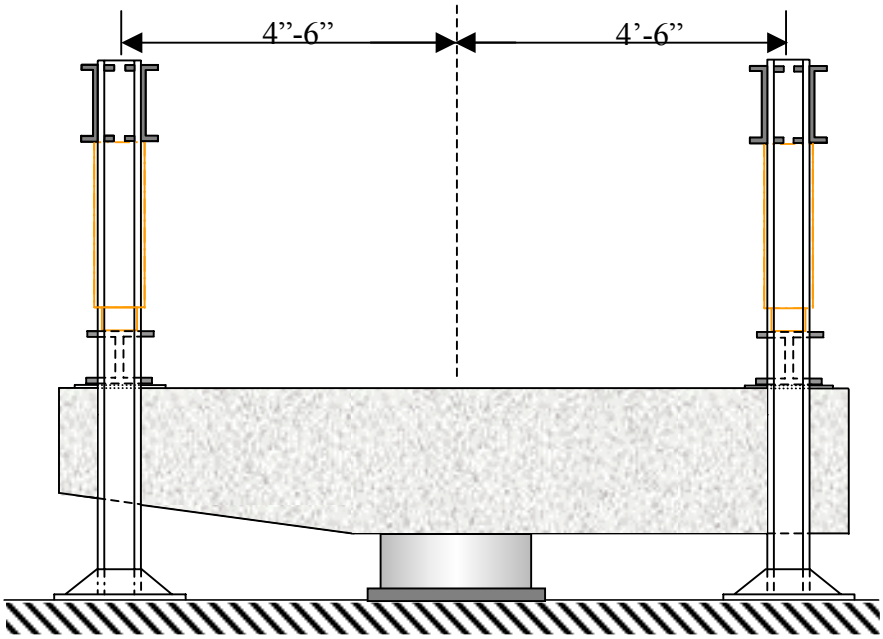

(b) Section 1-1

Figure 4.6. Experimental Test Set-Up

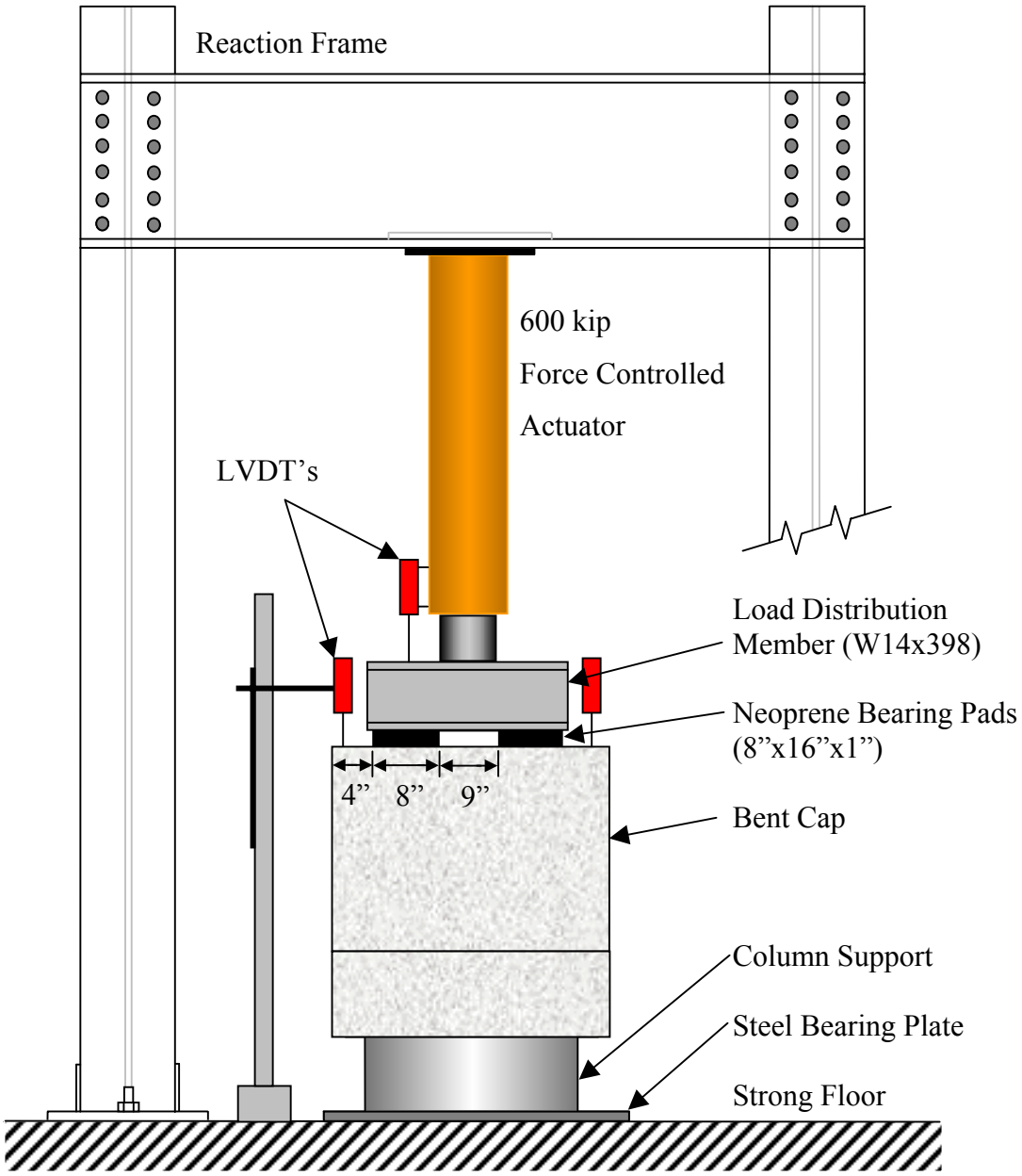

(c) Section 2-2

Figure 4.6. continued

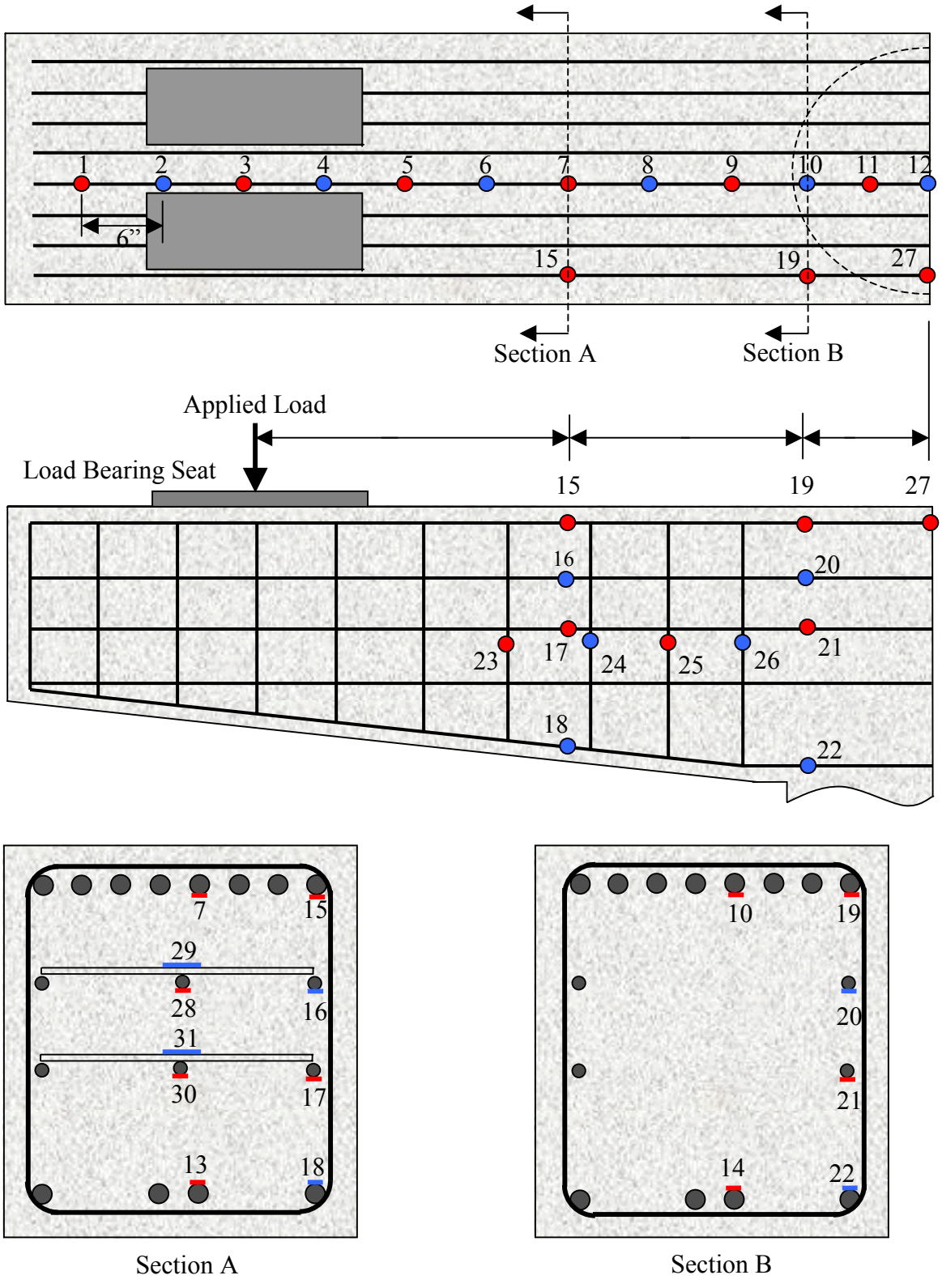

Figure 4.7 Strain Gauge Placement for Group #1 and #2 Specimens

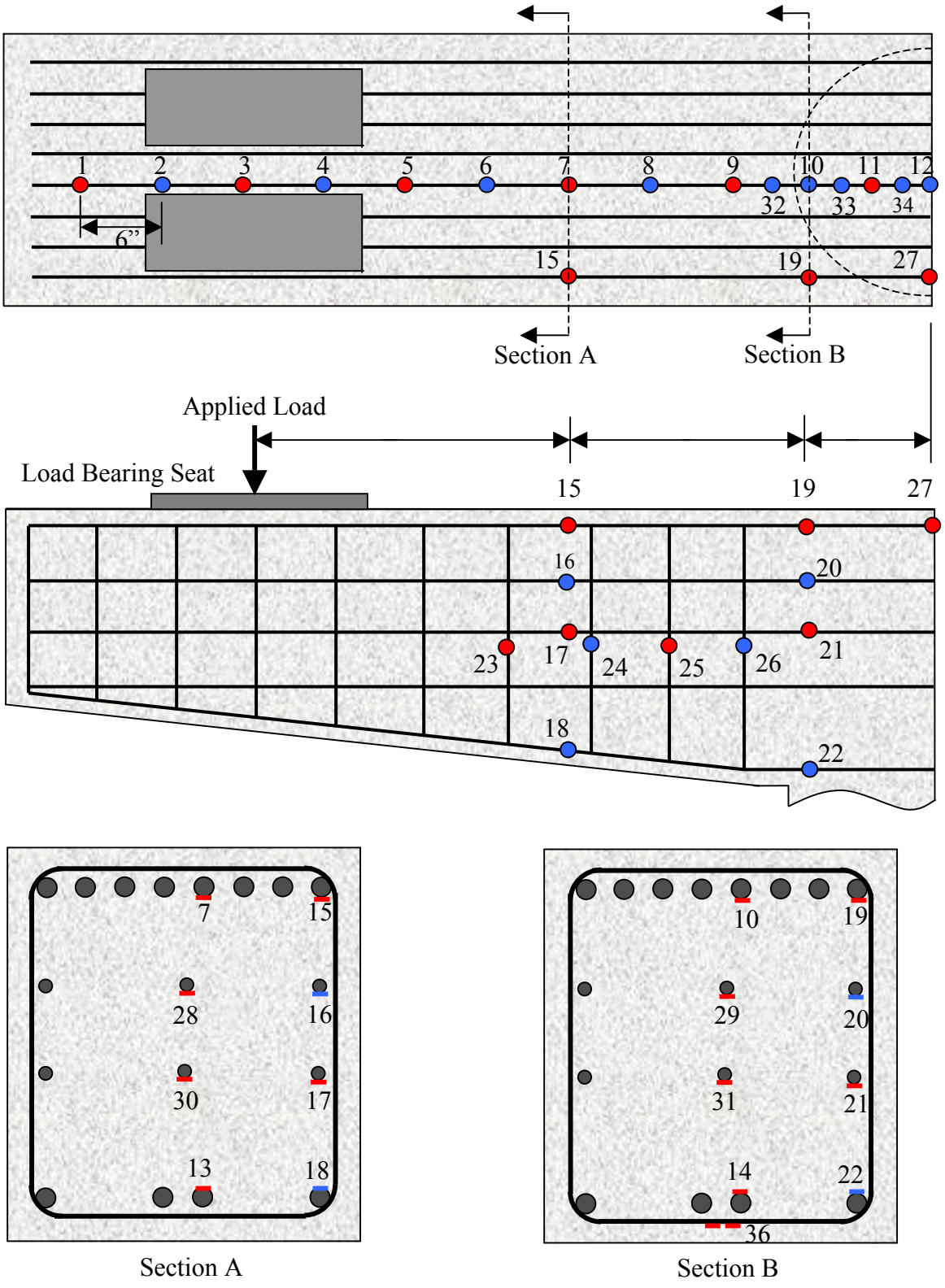

Figure 4.8 Strain Gauge Placement for Group #3 Specimens

CHAPTER V

RESULTS

5.1 INTRODUCTION

Chapter V demonstrates the applicability of the concrete constitutive relationships proposed in Chapter III to simulate the response of reinforced concrete (RC) bent caps as a part of the experimental program as presented in Chapter IV. The newly developed constitutive model for concrete is capable of integrating the effect of confinement, which leads to enhanced performance of RC members, both in terms of strength and deformability. Numerical simulations are conducted with the general purpose finite element analysis program ABAQUS with a user-defined material subroutine derived in Chapter III. Comparisons between the analytical and experimental results are presented.

The objective of Chapter V is twofold. The first part emphasizes the significance of passive confinement effect due to out-of-plane horizontal leg of transverse reinforcement on the overall behavior of RC members. Although preliminary results show that the proposed model is capable of predicting the strength of RC bent caps with good accuracies, the deformation counterpart is somewhat under-predicted. Parametric studies on two possible causes of the discrepancies, e.g. the effect of shrinkage strain and the interfacial bond-slip between concrete and reinforcing steel, are conducted in the second part of this chapter. Results on parametric studies showed that the underestimation of deformation, given the same level of load, is caused by the inaccuracies in incorporating the bond-slip model within the context of tension-stiffening.

5.2 FEM MODEL USING PROPOSED CONSTITUTIVE RELATIONSHIPS

5.2.1 Mesh

Sixteen RC bent caps are modeled using two-dimensional finite element analysis. Three-noded and four-noded plane stress elements are used for the concrete, while the longitudinal reinforcement is modeled by two-noded bar elements. Vertical stirrups and longitudinal skin reinforcements are smeared into the concrete model and their contribution to stiffness and strength are modeled internally by the user-defined material subroutine within the ABAQUS environment. The out-of-plane horizontal legs of transverse reinforcements, as shown in Fig. 1.2, are also modeled by the smearing technique. Note that the out-of-plane stirrups have no direct contribution to the stiffness matrix of the members. However, their presence contributes to the confinement of concrete and, therefore, indirectly provides strength and deformability to RC members.

Fig. 5.1 shows the geometry of the RC bent caps and the idealized finite element mesh used for these analytical studies. Specimens 1A and 1B employed slightly different element material properties from the remaining fourteen specimens because of the different skin reinforcement detailing. Specimens 1A and 1B adopted 4#5 bars distributed evenly throughout the member depth as shown in Fig. 4.3. Therefore, an average value of 0.001 is used for the skin reinforcement ratio embedded in all smeared-reinforcement concrete elements in specimens 1A and 1B. On the other hand, the remaining fourteen specimens used 6#4 bars distributed in the tension zone. In these cases, an average skin reinforcement ratio of 0.0015 is used elements in the upper 21 inches as shown in Fig. 5.2.

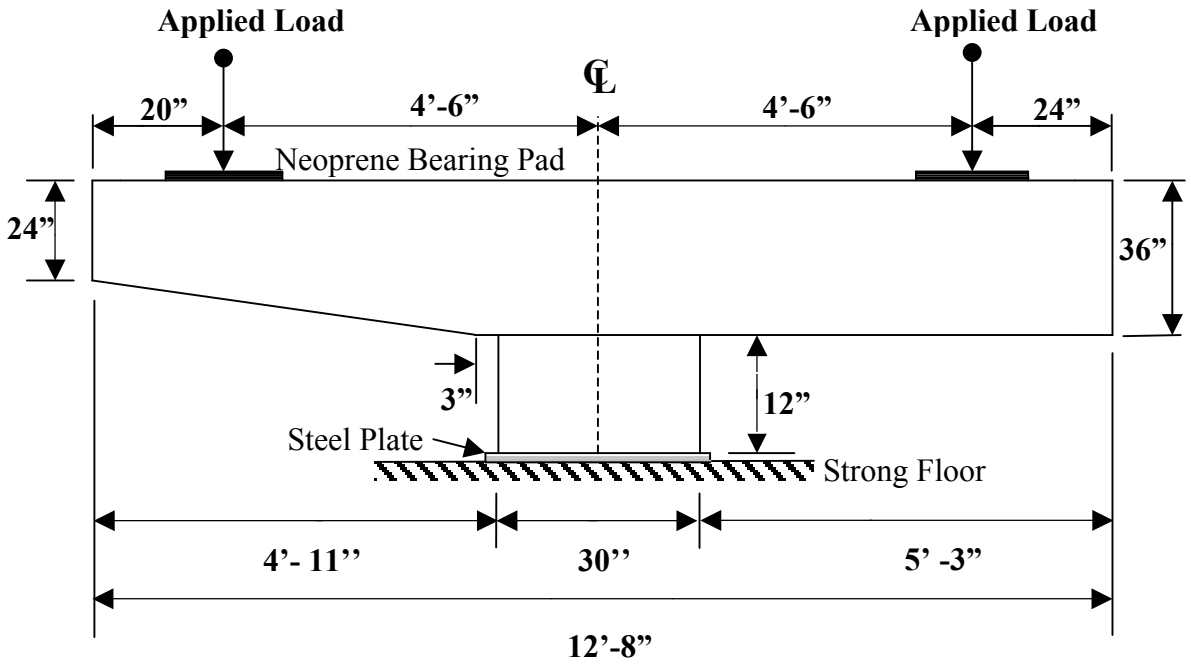

(a) RC Bent Cap Geometry

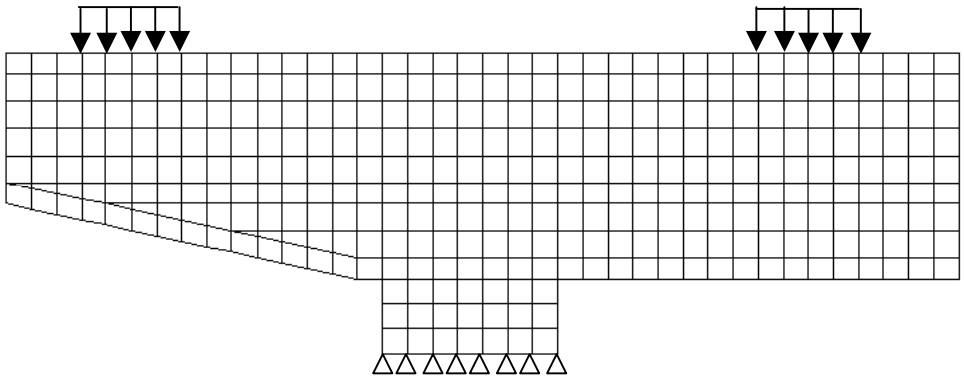

(b) Finite Element Mesh

Figure 5.1 Structural Idealization for RC Bent Caps

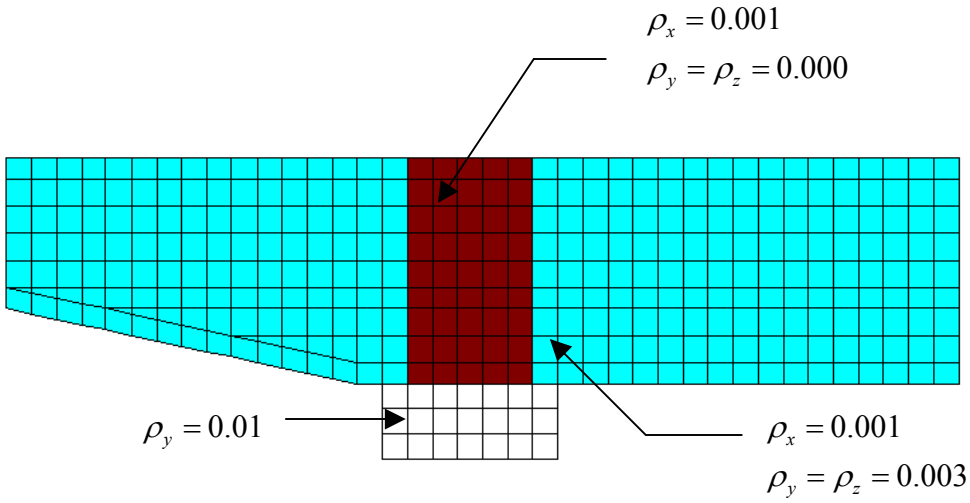

(a) Specimens 1A and 1B

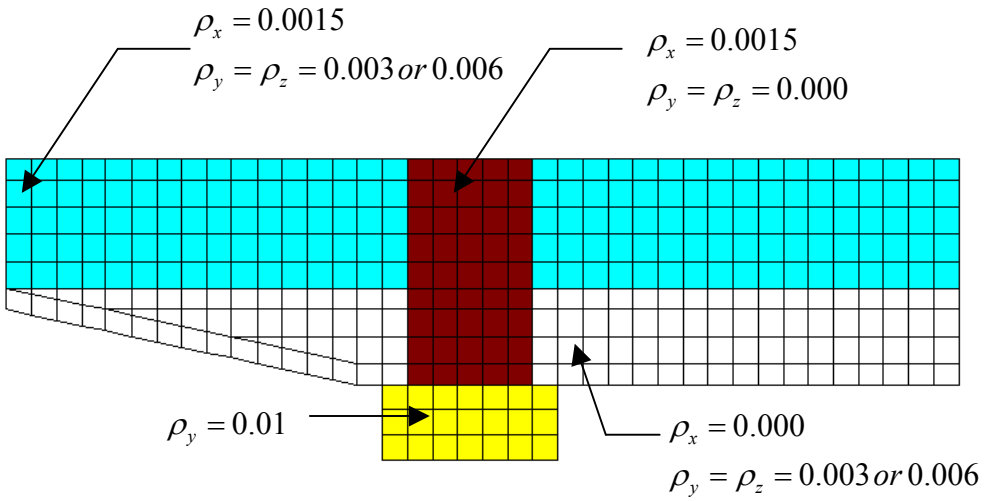

(b) Remaining Fourteen Specimens

Figure 5.2 Smeared Reinforcement Ratios for Different RC Zones

5.2.2 Element Properties

All parameters affecting the stiffness and strength of concrete for a finite element is estimated using the average compressive strength performed on standard cylinder tests. The initial modulus of elasticity and the tensile cracking strength of concrete was estimated from $E_c = 57000\sqrt{f_c'}$ and $f_{cr} = 3.75\sqrt{f_c'}$, respectively. All units are in psi.

The tension-stiffening effect only occurs in adequately reinforced regions and where the bond between the concrete and reinforcing steel is properly mobilized. However, in relatively low reinforcement regions, the proper development of the tension-stiffening field is rather dubitable. Therefore, different tensile characteristics for reinforced concrete should also be taken into consideration based on the above criteria. In these numerical simulations, the tensile constitutive model for concrete elements near the top main reinforcement, as shown in Fig. 5.3, is represented by the stress-strain relationship as proposed in Eq. 3.22. In other regions, the effect of tension-stiffening is ignored and only the tension-softening is considered. Therefore, Eq. 3.19 is adopted for tensile stress-strain relationship in this relatively low reinforcement region as shown in Fig. 5.3.

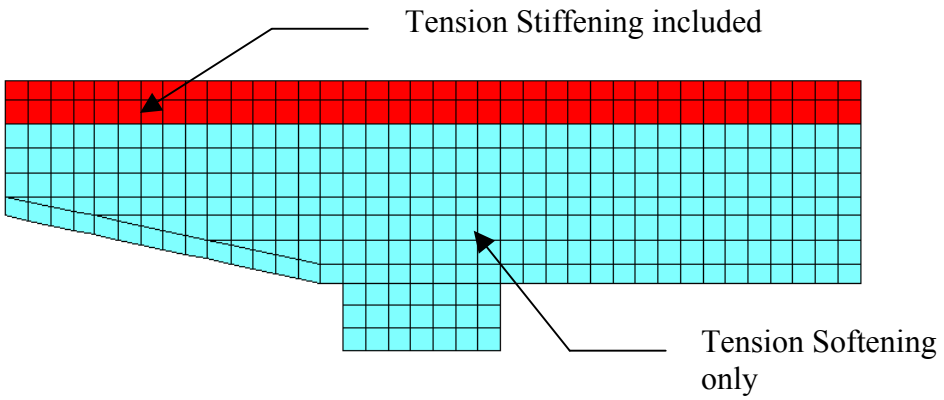

Figure 5.3 Zoning in RC Bent Caps according to Post-Cracking Stress-Strain Curve

The user-defined material subroutine requires a total of eighteen material parameters: (1) Characteristic concrete compressive strength ($f_c^{'}$); (2) Concrete tensile strength (f_{cr}); (3) Strain corresponding to peak compressive stress (ε_0); (4) Initial Poisson's ratio; (5) Modulus of elasticity of reinforcing steel; (6) Post-yield tangent modulus of elasticity of reinforcing steel; (7-9) Yield strength of smeared reinforcing steel in the local horizontal, vertical, and out-of-plane directions, respectively; (10-12) Reinforcement ratio in the local horizontal, vertical, and out-of-plane directions; (13-17) triaxial strength envelope parameters defined as $\overline{f_{bc}^{'}}$, $\overline{\xi_1}$, $\overline{\rho_1}$, $\overline{\xi_2}$, and $\overline{\rho_2}$ in section 3.2.3.3, respectively; and (18) Tension-stiffening option. The tension-stiffening option is set equal to 1 when only tension-softening in considered (Eq. 3.19) and is equal to 2 when full tension-stiffening field is anticipated (Eq. 3.22).

Because of the lack of available triaxial test data, the triaxial strength envelope can only be best estimated on the basis of existing test reports available to date. Numerical simulations in this dissertation adopt the triaxial strength envelope reported by Winkler and Schickert (1977), which was also used by Mander et al. (1988) in their pioneering article on the study of confinement effects of RC columns. Parameters $\overline{f_{bc}^{'}}$, $\overline{\xi_1}$, $\overline{\rho_1}$, $\overline{\xi_2}$, and $\overline{\rho_2}$ are assumed to have the value of 1.21, 3.0, 1.246, 3.0 and 0.569, respectively.

Because of the effect of tension stiffening, the yield strength and post-yield stiffness of the main reinforcing steel should be adjusted to the apparent yield strength, and post-yield stiffness for embedded bars, as described in Section 3.2.4.2. Note that the adjustment of yield strength is only required in the region where tension stiffening is expected, i.e., for the main reinforcing steel and the smeared reinforcement in the top region shown in Fig. 5.3. Because the tensile strength of concrete in the strain-softening zone is practically negligible near the yield strain of the reinforcement, no adjustment for the apparent yield stress and the post-yield stiffness is required. Using Eq. 3.26, the

apparent yield strength for embedded concrete is approximately 54 ksi for all specimens. This value was calculated based on the assumption that the yield strength of reinforcing steel is 60 ksi. The post-yield stiffness of embedded bars slightly increases from 3% of bare bars to 4%.

Table 5.1 shows all parameters that are dependent on the concrete properties and reinforcement details. The concrete compressive strength is averaged from three standard cylinder tests at 28 days for each concrete batch. The ρ_y and ρ_z shown in Table 5.1 are the vertical and out-of-plane reinforcement ratio for concrete in the overhanging part (refer to Fig. 5.2). No stirrup reinforcement was provided in the bent cap over the column region.

TABLE 5.1 Specimen Material and Reinforcing Details

Specimens	$f_c^{'}$ (ksi)	f_{cr} (ksi)	ρ_y (Transverse Reinforcement Ratio)	ρ_z (Out-of-Plane Reinforcement Ratio)
1A	6.2	0.29	0.003	0.003
1B	5.8	0.28	0.003	0.003
2A	6.2	0.29	0.003	0.003
2B	5.8	0.28	0.003	0.003
3C	6.0	0.29	0.003	0.003
3D	5.5	0.27	0.003	0.003
4C	6.0	0.29	0.003	0.003
4E	7.7	0.33	0.003	0.003
5D	5.5	0.27	0.003	0.003
5E	7.7	0.33	0.003	0.003
6F	5.4	0.27	0.006	0.006
6G	5.3	0.27	0.006	0.006
7F	5.4	0.27	0.006	0.006
7H	5.7	0.28	0.006	0.006
8G	5.3	0.27	0.006	0.006
8H	5.7	0.28	0.006	0.006

5.2.3 Boundary Conditions

Bearing pads were assumed to uniformly distribute the actuator load on the top RC bent cap surface. Equivalent nodal forces were calculated from the uniform pressure applied through the element edge. Loads were incremented using 8 kips intervals until numerical instability occurred or convergence could not be achieved within a tolerable limit. Nodes at the columns base supports were assumed to be capable of restraining both x- and y-translation. The applied nodal loads and associated boundary conditions used in this numerical simulation are shown in Fig. 5.1(b).

5.2.4 Convergence Criteria

Two criteria are used to evaluate the convergence of non-linear FEM results within the ABAQUS environment: (1) Incremental displacements; and (2) Residual forces. Incremental displacement criterion assures that the nodal displacement solution converges at a tolerable limit, while the residual force criterion warrants that the equilibrium is adequately satisfied at all nodal points. In general non-linear analysis, ABAQUS recommends the values of 0.01 and 0.005 for incremental displacement and residual forces, respectively. However, in RC applications, these convergence criteria are too strict and larger values should be used. In the present studies, these two numbers were both set at 0.05 for practical purposes. In addition, the maximum number of iterations for incremental solutions was set at 100. In other words, if the number of iterations exceeded 100, the solution is deemed divergent and the entire process stops.

5.3 ANALYTICAL AND EXPERIMENTAL RESULTS

Analytical results from numerical simulations are compared with measured experimental results in this section. Comparisons are then made in terms of load-displacement curves under quasi-static loading conditions and overall strength of the RC bent caps. Recall that two LVDT(s) were installed below the actuators to measure the displacement at the actuator locations. However, typical results reveal that there was a discrepancy between the displacement at the points under the left and right actuators. Initially, the displacement under one actuator was even in the upward direction while another point deflected downward. This phenomenon also occurred randomly, e.g., in one specimen the left actuator may initially have deflected upward while the contrary occurs in others specimen as shown in Fig. 5.4. Therefore, it was concluded that there must be some random occurrences of rocking (rotation) at the base column. To alleviate this error, the average value of the displacement at the left and right actuator is used to compare the experimental and analytical results.

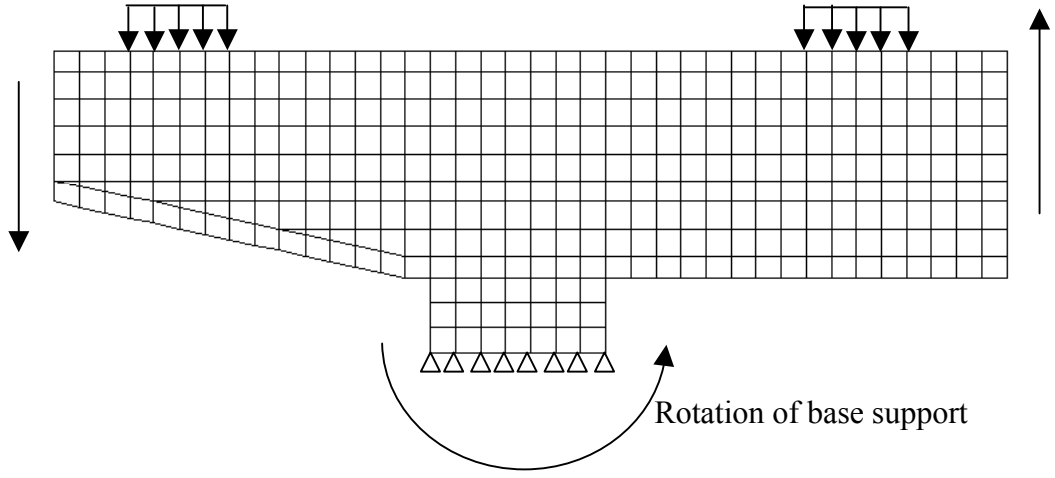

Figure 5.4 Effect of Base Rotation on Displacement of RC Bent Caps

The effect of confinement due to out-of-plane horizontal legs of transverse reinforcement is emphasized. For the sake of comparison, additional numerical simulations are performed, ignoring the effect of out-of-plane horizontal leg of transverse reinforcement by assigning a zero value for out of-plane reinforcement ratio (ρ_z) in each model. Analytical results for both confined and unconfined simulations are compared.

5.3.1 First Group of Specimens

The first group of specimens consisted of specimens 1A, 1B, 2A, and 2B. Reinforcement details for each specimen can be found in Section 4.2. Fig. 5.5(a-d) shows the average actuator force-displacement diagram for specimen 1A, 1B, 2A, and 2B. Recall that the first group of specimens has 8#8 bars as the top main flexural reinforcement. Numerical simulations satisfactorily predicted the load-displacement diagrams for the first group specimen. All specimens in Group 1 exhibited the yield plateau where the main reinforcements reached their yield strength and initiated into the strain hardening range prior to fracture. Analytical results predict the yield strength of approximately 330 kips for all specimens, which agrees well with the experimental results. However, the load-displacement relationship obtained from the experimental results show a more gradual transition between the pre- and post-yielding behavior.

Fig. 5.5 also shows an improvement in strength and deformability of the confined models over the unconfined model. Recall that the model assumes that the out-of-plane horizontal leg of transverse reinforcement stresses depend upon the amount of lateral expansion due to compression. Because the lateral expansive strain is low at lower load regime, the effect of confinement is imperceptible at the lower load regime. As shown in Fig. 5.5, the predicted load-deformation curves for both confined and unconfined models follow essentially the same path at low load levels. At higher load levels, the effect of confinement becomes significant as the confining stress due to out-of-plane

transverse reinforcement increase, which helps the confined models carry additional load while the unconfined model fails prematurely by numerical instability.

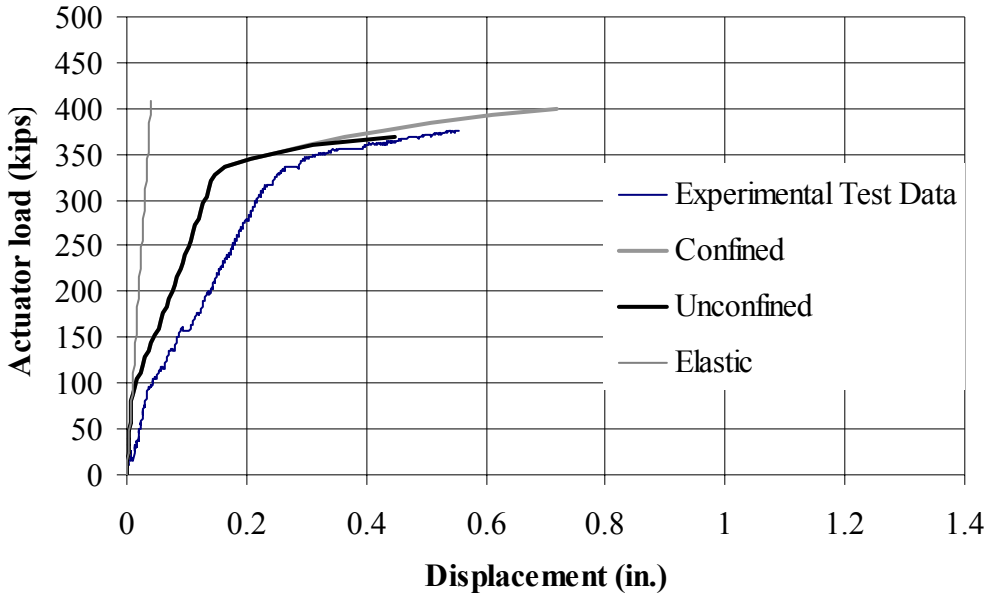

(a) Specimen 1A

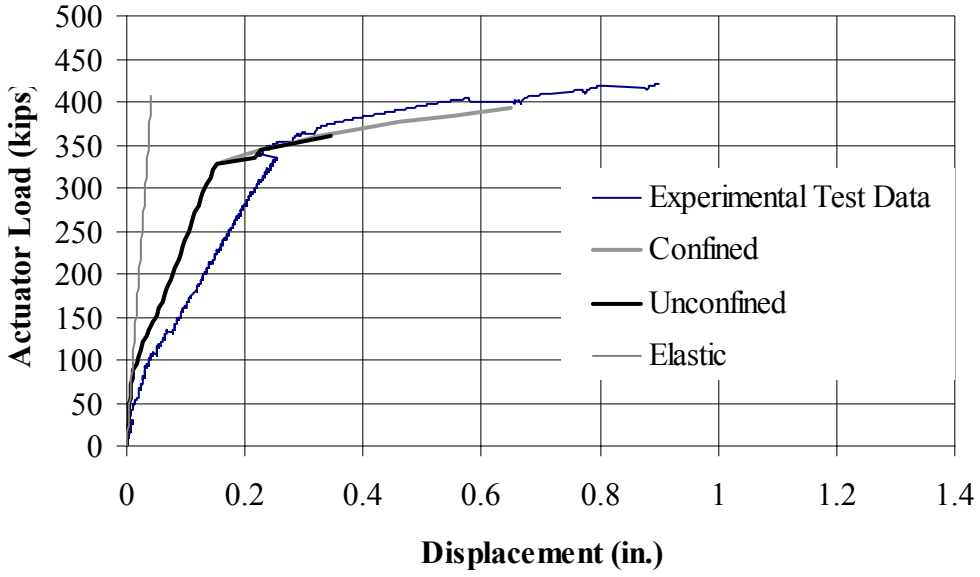

(b) Specimen 1B

Figure 5.5 Load-Deformation Curves for Group 1 Specimens

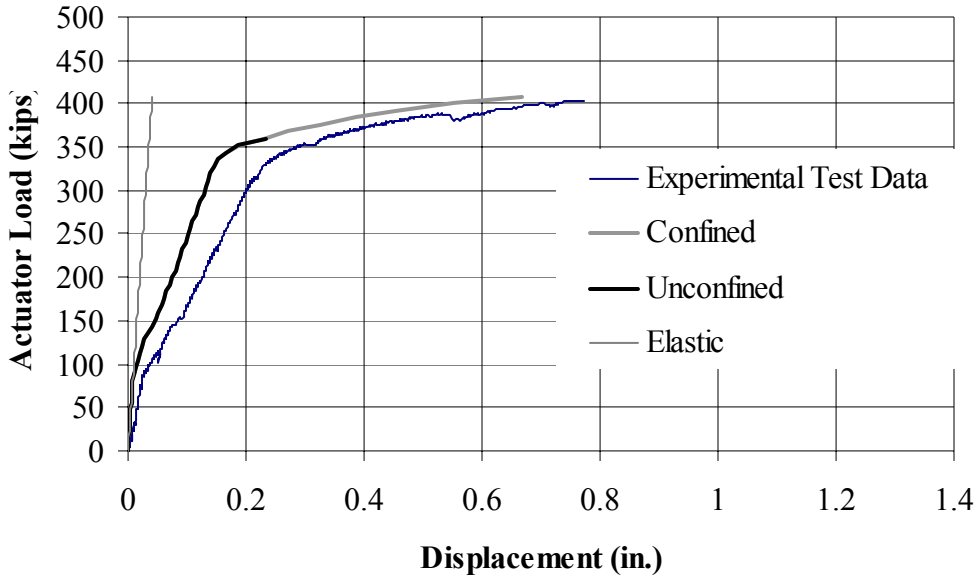

(c) Specimen 2A

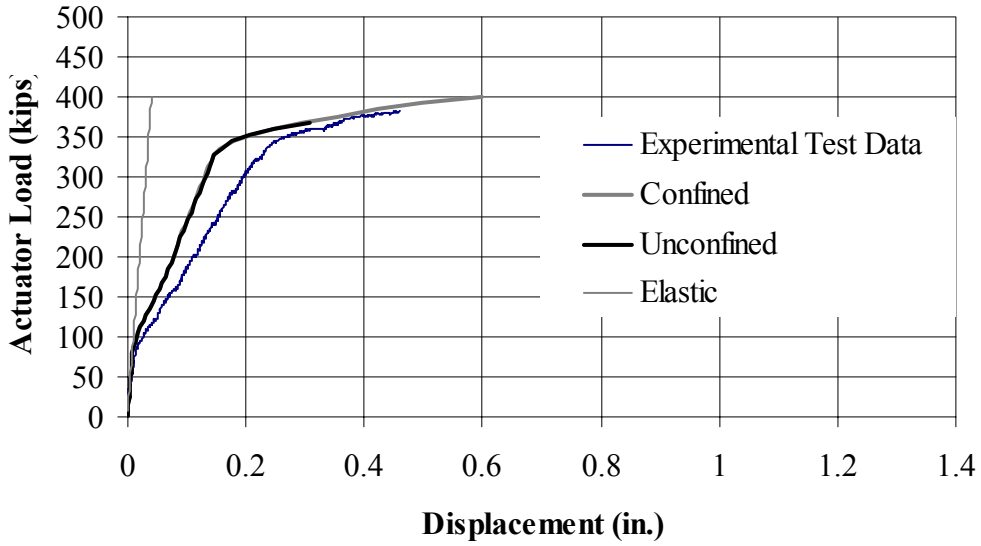

(d) Specimen 2B

Figure 5.5 (Continued)

Table 5.2 compares the strength from numerical simulations and experimental results. The mean normalized strength predictions for the confined and unconfined models for the first group of specimen are 1.01 and 0.92, respectively. Evidently, the confined models perform better than the unconfined model for the first group of specimens.

TABLE 5.2 Strength Comparison for Group #1 Specimens

Model	Experiment (kips)	Confined		Unconfined	
		P_{ult} (kips)	Predicted/Exp.	P_{ult} (kips)	Predicted/Exp.
1A	376	400	1.06	368	0.98
1B	420	392	0.93	360	0.86
2A	404	408	1.01	360	0.89
2B	381	400	1.05	368	0.97
		Mean	1.01		0.92
		Std	0.05		0.05

5.3.2 Second Group of Specimens

The second group of specimens was 3C, 3D, 4C, 4E, 5D, and 5E. Recall that this set of specimens adopted the same skin and transverse reinforcement detailing as specimens 2A and 2B. Skin reinforcement consisting of 6#4 bars that were distributed in the upper tensile zone of the cross section, while a single #5 hoop spaced at 6.25 inches was used as the transverse shear reinforcement.

Fig. 5.6 (a-f) shows the load-displacement diagrams for the second group of specimens. Similarities and differences exist between specimens in first and second groups. Specimens 3C and 3D were reinforced with 11#7 bars, which gave a nominally higher reinforcement ratio than the first group specimens. The experimental load-displacement relationships of specimen 3C and 3D were similar to those of the first group specimens. Yielding in the main flexural reinforcement occurs at the average actuator load of 350 kips which, as expected, is slightly higher than specimens in Group 1.

While specimens 3C and 3D is capable of sustaining a considerable load beyond the reinforcement yielding, specimens 4C, 4E, 5D, and 5E exhibit limited ductility after the main reinforcement yielding. In fact, specimens 4C and 4E failed immediately after the reinforcing steel reached the yield stress while post-yield deformability was virtually negligible in specimens 5D and 5E.

Fig. 5.6 shows that numerical simulations consistently under-predict the deformation, except for specimen 3C. In other words, the proposed constitutive model appears to be too stiff. The causes of the discrepancies are manifolds and will be discussed in Section 5.3.

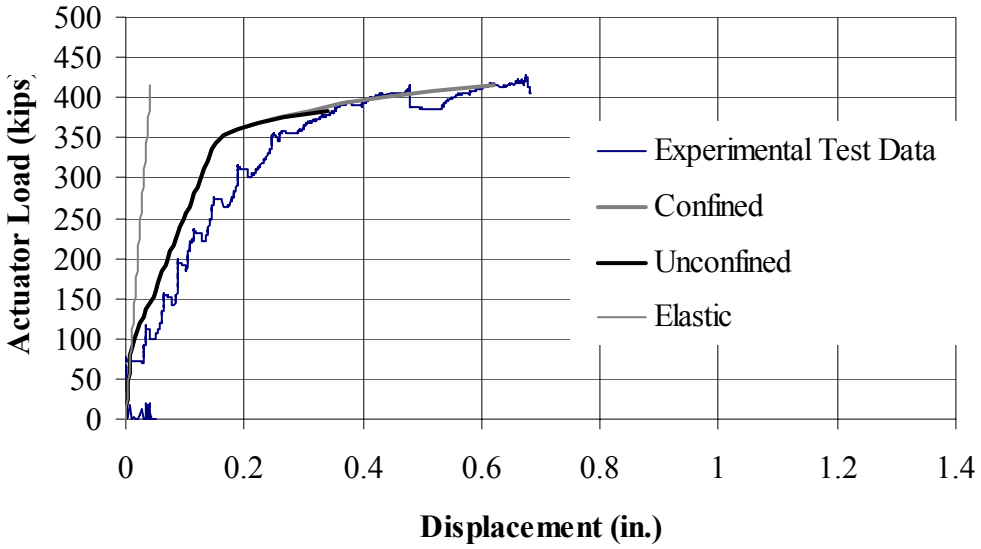

(a) Specimen 3C

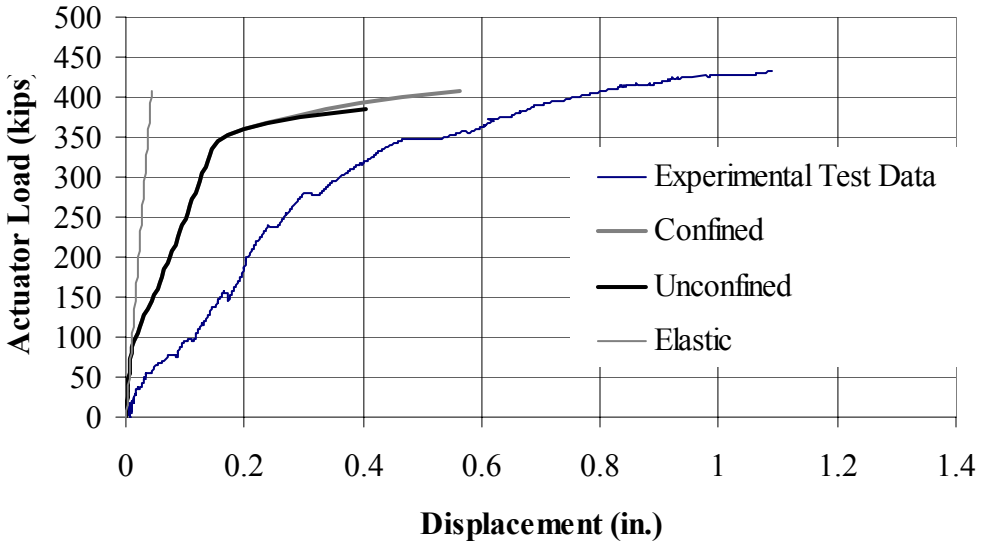

(b) Specimen 3D

Figure 5.6 Load-Deformation Curves for Group 2 Specimens

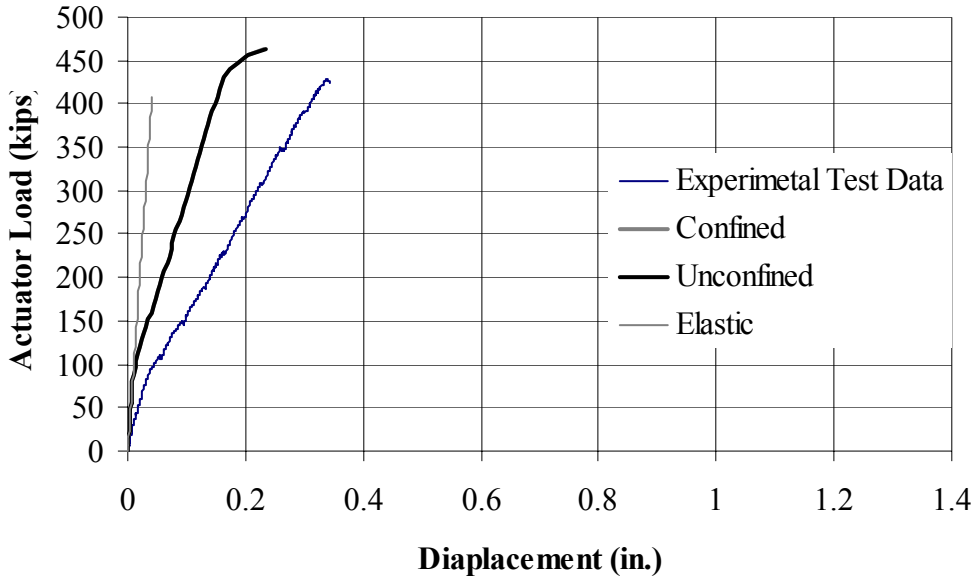

(c) Specimen 4C

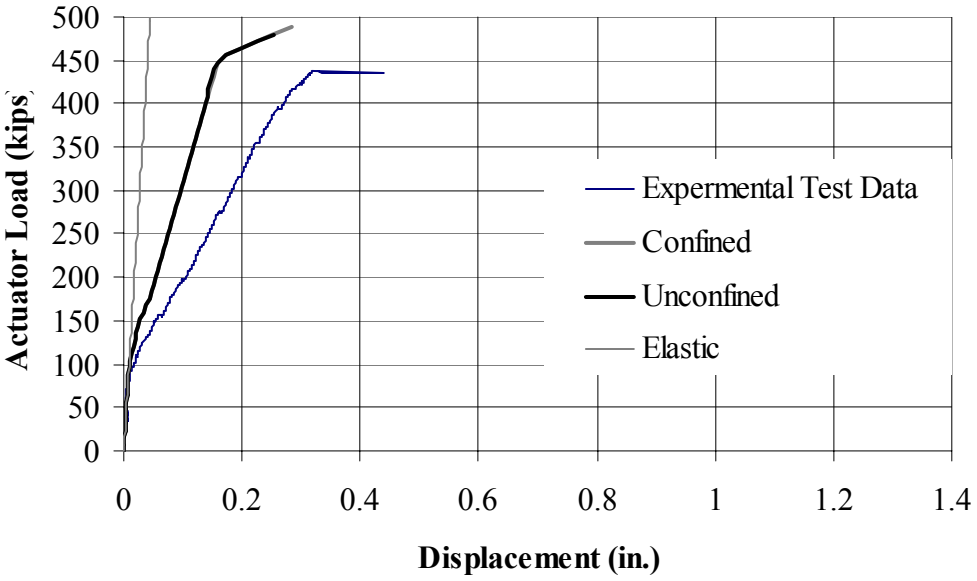

(d) Specimen 4D

Figure 5.6 (Continued)

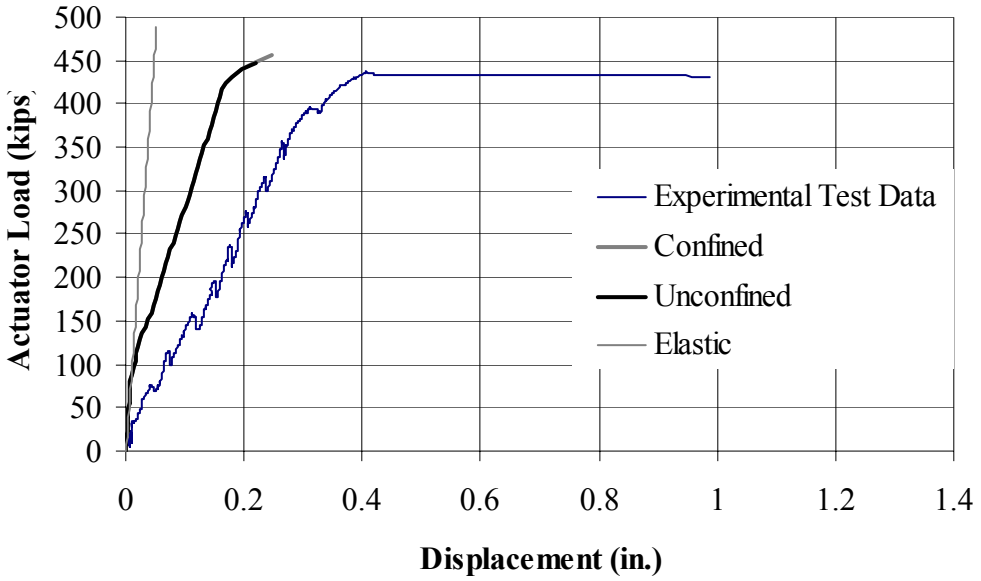

(e) Specimen 5D

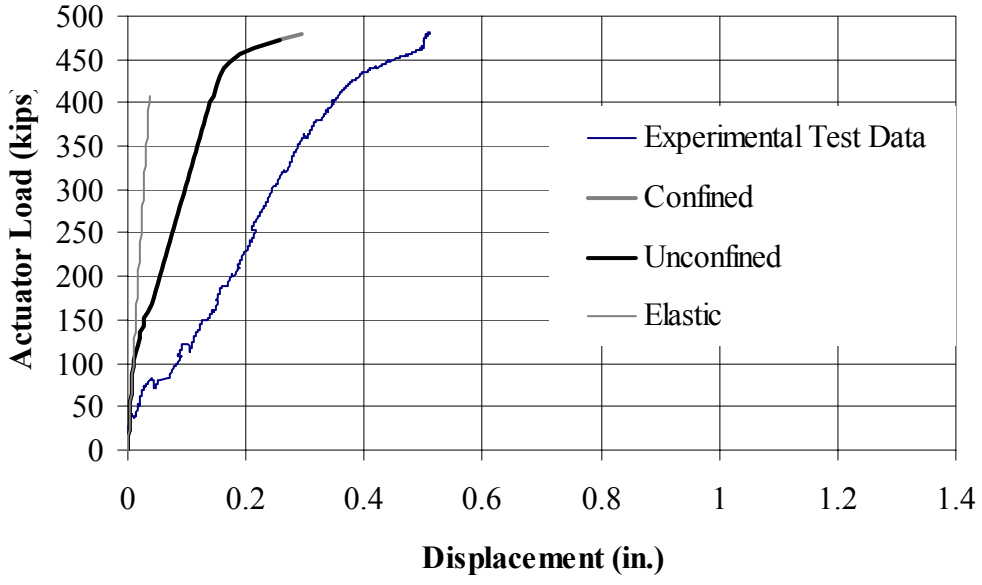

(f) Specimen 5E

Figure 5.6 (Continued)

Table 5.3 shows the comparison between the predicted strength using both the confined and unconfined models and the ultimate actuator forces obtained from experimental studies. Numerical simulations yield sufficiently accurate results of predicted strength for specimens 3C, 3D, 5D, and 5E. However, both confined and unconfined model slightly overestimate the failure load for specimens 4C and 4E. The cause of the overestimation will be subsequently discussed in Section 5.4. Confined models consistently predict higher levels of strength and deformability than the unconfined model. However, the benefit of incorporating confinement into the analytical model is only marginal for the second set of specimens since they physically contain only a single transverse hoop.

TABLE 5.3 Strength Comparison for Group #2 Specimens

Model	Experiment (kips)	Confined		Unconfined	
		P_{ult} (kips)	Predicted/Exp.	P_{ult} (kips)	Predicted/Exp.
3C	428	416	0.97	384	0.90
3D	434	408	0.94	384	0.88
4C	430	464	1.08	464	1.08
4E	453	488	1.08	480	1.06
5D	457	456	1.00	448	0.98
5E	481	480	1.00	472	0.98
		Mean	1.04		1.03
		Std	0.04		0.04

5.3.3 Third Group of Specimens

Fig. 5.7 (a-f) shows the load-displacement diagrams for the third group of specimens. Recall that specimens in this group (7 and 8) adopted the same main reinforcement as specimens 5 and 2, respectively. However, the third group of specimens used overlapping stirrups as the vertical shear reinforcement as shown in Fig. 4.5. Specimens 6F and 6G used 5#10 bars as main reinforcing steel, which yield the equivalent reinforcement ratio as specimen 8 series.

Comparing Figs 5.5 (c) and (d) for the specimen 2 series to Figs. 5.7 (e) and (f) for the specimen 8 series, experimental results show that both the specimen 2 and 8 series give practically the same magnitude of actuator forces at first reinforcement yielding at approximately 330 kips. However, the specimen 8 series were capable of sustaining higher levels of force and ductility. It was clearly evident that the use of overlapping stirrups significantly improves the structural performance as both strength and deformability increased. Similar conclusions can be reached by comparing the load-displacement diagram in Figs. 5.6 (e) and (f) and Fig. 5.7(c) and (d), for specimen 5 and 7 series, respectively. Note that specimen 7F was able to resist an average actuator force of 500 kips without rupture. Although the load cell was able to transmit the maximum load of 600 kips, it was suspected that higher actuator loads might cause some damage to the testing assembly. Therefore, the experiment was terminated at 500 kips as a precaution.

Numerical simulations also yield satisfactory results on the predicted load – displacement diagrams for specimens 6F, 6G, 7F, 7H, and 8G while excellent results are obtained for specimen 8H. However, the analytical results, in average, underestimate the deformation of RC bent caps. The stiff analytical prediction was also obtained for the first and second groups of specimens. The confined models consistently predict higher levels of load and deformation than the unconfined models.

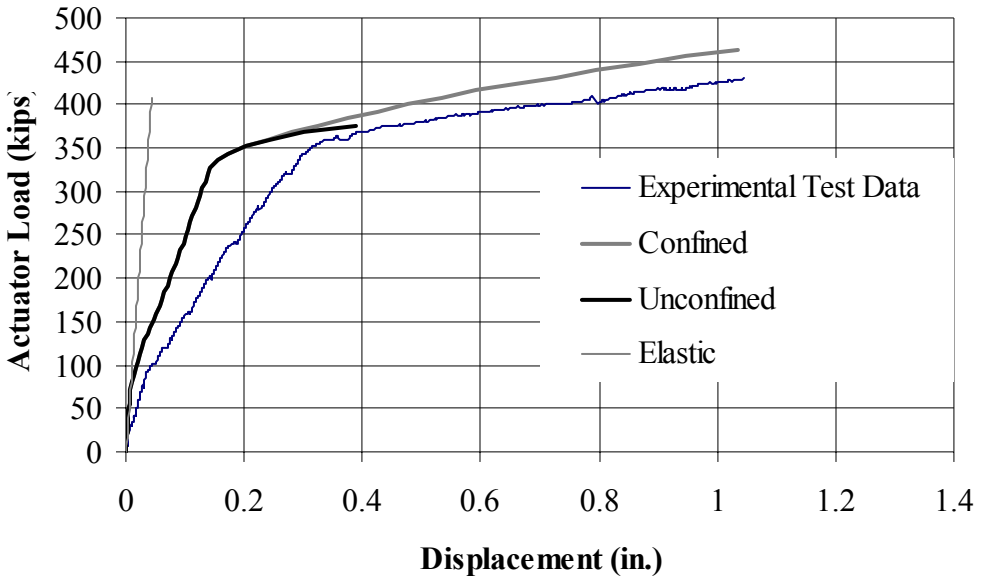

(a) Specimen 6F

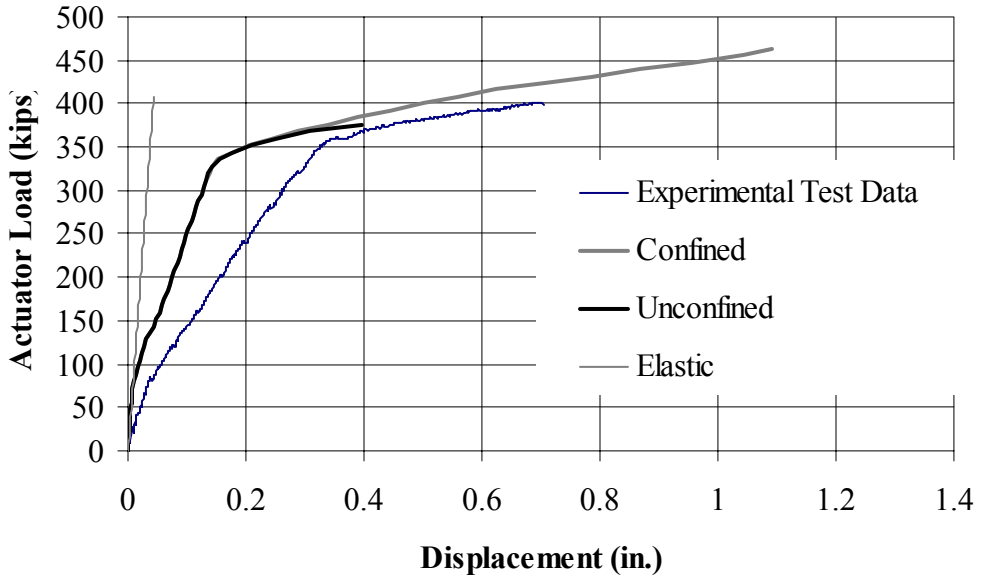

(b) Specimen 6G

Figure 5.7 Load-Deformation Curves for Group 3 Specimens

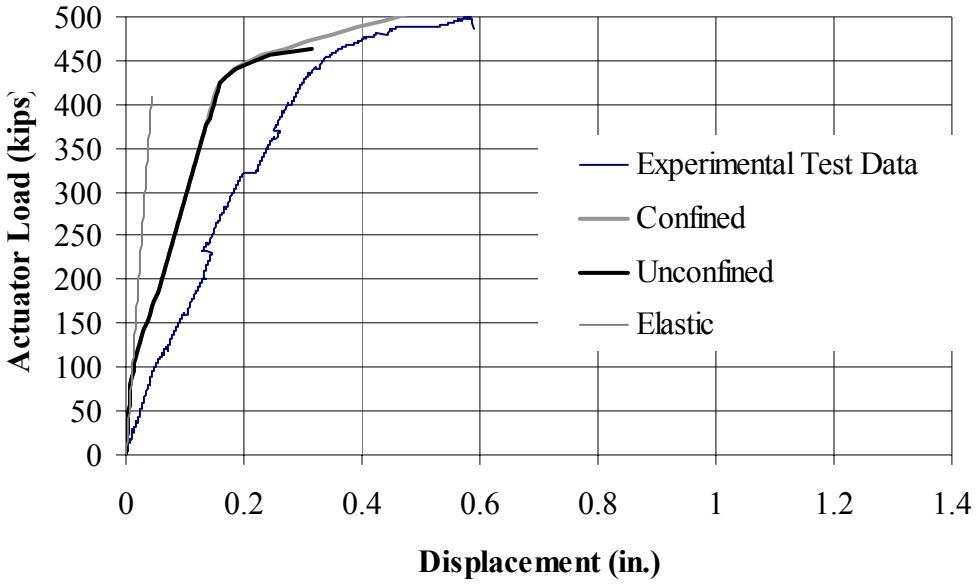

(c) Specimen 7F

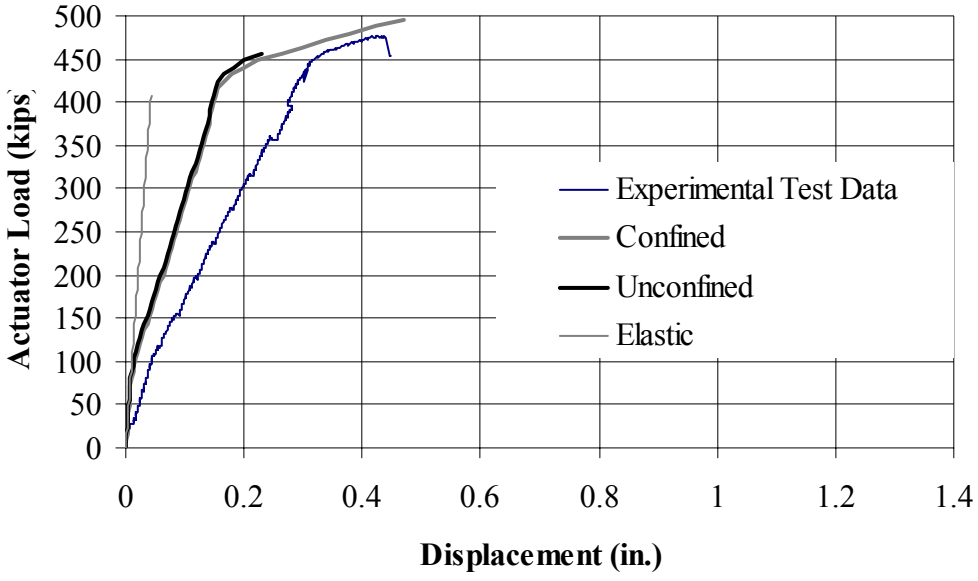

(d) Specimen 7H

Figure 5.7 (Continued)

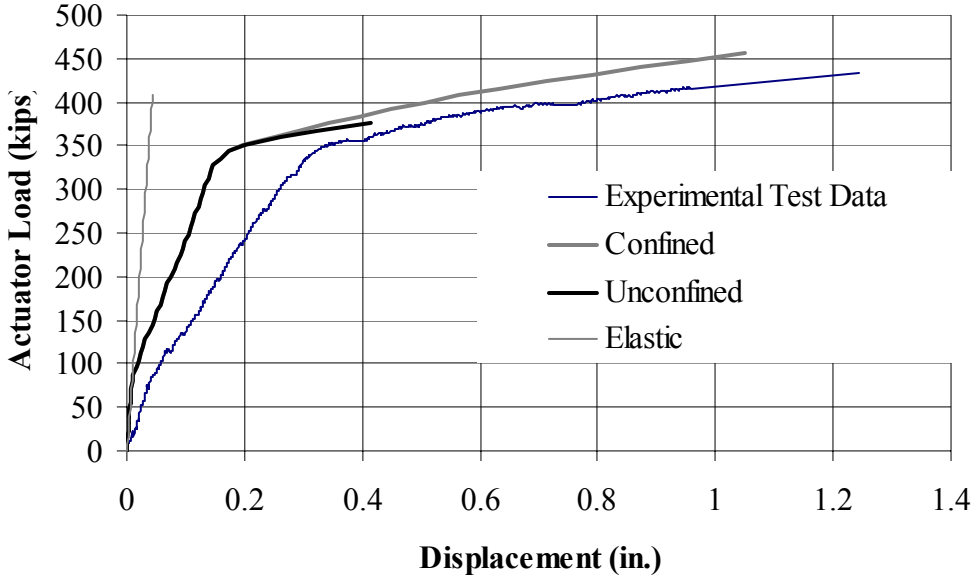

(e) Specimen 8G

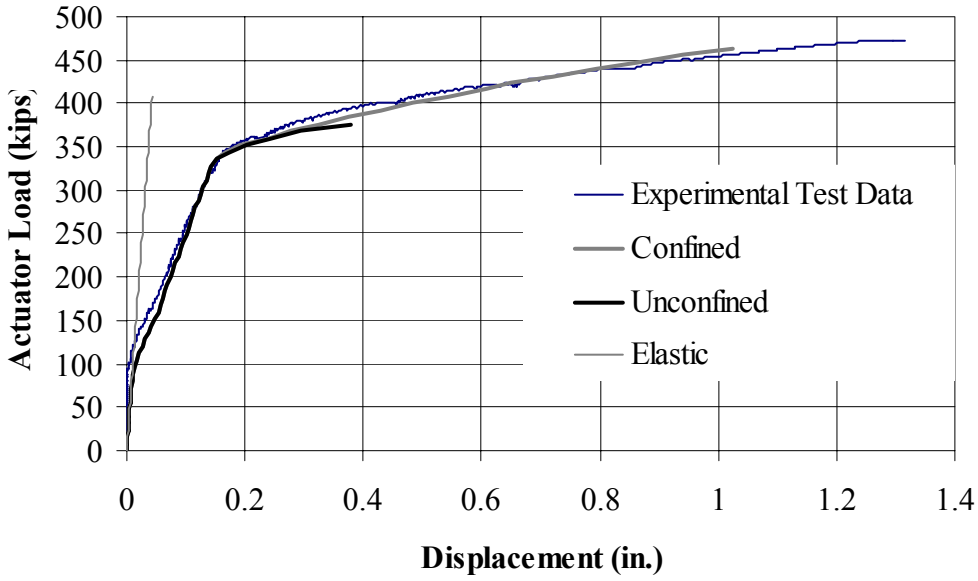

(f) Specimen 8H

Figure 5.7 (Continued)

Table 5.4 compares the experimental and predicted strengths using numerical simulations. The confined models yield consistently higher predicted strength than the unconfined ones. The mean normalized ratio between the predicted and experimental strength was 1.02 and 0.89 for confined and unconfined model, respectively. Evidently, the confined models again yield more accurate results than the unconfined models for the third group of specimens on the strength prediction.

TABLE 5.4 Strength Comparison for Group #3 Specimens

Model	Experiment (kips)	Confined		Unconfined	
		P_{ult} (kips)	Predicted/Exp.	P_{ult} (kips)	Predicted/Exp.
6F	430	464	1.08	376	0.87
6G	402	464	1.15	376	0.94
7F	500	504	1.01	464	0.93
7H	477	504	1.06	456	0.96
8G	433	456	1.05	376	0.87
8H	473	464	0.98	376	0.79
		Mean	1.02		0.89
		Std	0.03		0.06

5.4 DISCUSSION OF RESULTS

5.4.1 General

Results shown in Section 5.3 suggest that the failure mechanism of sixteen RC bent caps designed, built, and tested as a part of the experimental program are of the flexural-shear type. At first cracking load, flexural cracks formed vertically to the member axis with unique crack spacing. After subsequently loading, the existing vertical cracks propagate making an angle with the member axis. This form of cracking is generally associated with shear action. Near the level of load that causes reinforcement yielding, no new cracks formed and existing cracks widened. At failure, the concrete at the compression face at the column started to crush. Crushing of the concrete at the compression face caused unstable cracks propagating from the compression face and merging with the existing inclined cracks to form the failure plane.

Fourteen out of sixteen specimens had some reserve strength beyond the load that caused the first reinforcement yielding. The degree of ductility varies and depends upon the amount of main flexural reinforcement, bar size, and the amount of transverse reinforcement. Only two out of sixteen specimens, i.e. specimen 4C and 4E reinforced with 7#10 bars as the main reinforcement, failed immediately after first reinforcement yielding.

Comparing the experimental results between groups 1, 2, and 3, it was clearly evident that the overlapping stirrups helped improve the performance of RC bent caps. Strain gauge data revealed that only one or two stirrups along the member length actually participate in resisting the load. This result also conforms with the conclusions made by Ferguson (1964) on a similar experimental program on of RC bent caps. Ferguson (1964) showed that with the same amount of main reinforcing steel, vertically-unreinforced bent caps and bent caps with single hoops stirrups had the same level of strength. However, experimental results shown in section 5.3 suggested that the use of overlapping stirrups had a significant effect by enhancing the strength and ductility of

the RC bent cap members. This suggests that the overlapping stirrups help improve the performance of RC bent caps by a mechanism other than participating in resisting load through shear reinforcement. The analytical results showed that one of the possible explanations for this phenomenon is through the effect of confinement caused by the out-of-plane horizontal stirrups leg transverse reinforcement as shown in Fig. 1.2.

5.4.2 Load-Deformation Relationships

Section 5.3 shows that the numerical simulations using implicit bond models yield excellent results on the load-deformation behavior for only two out of sixteen specimens, e.g. on specimens 3C and 8H. Analytical predictions of the remaining fourteen specimens appear to be too stiff after the initial cracking and consistently underestimate the deformation at a certain level of load. Figs. 5.5-5.7 also show the results from linear elastic FEM analysis. The non-linear analysis, as should be anticipated, yields virtually the same results as the linear-elastic model under smaller levels of load. Figs. 5.5 –5.7 shows that, even at a small load level where cracking should not be anticipated and the linear elastic assumption should yield sufficiently accurate results, the analytical models consistently overestimate the initial stiffness of the RC bent caps. Although there are several factors that may contribute to these inaccuracies, given the constraints and testing conditions performed in the experimental program, three fundamental causes of the discrepancies may be identified: (1) inaccuracies in the estimation of material properties; (2) the existence of cracking and microcracking caused by hygrothermal effects; and (3) the inadequacies of the constitutive model to simulate the behavior of RC bent caps.

Inaccuracies in the Estimation of Material Properties

Concrete is a multi-phase material whose constituents are randomly located within the RC members. The parameters used for concrete properties, such as the modulus of elasticity and tensile strength, etc., in the numerical simulations were estimated from the average compressive strength of three standard concrete cylinder

tests for each concrete batch. Table 5.5 shows the test results on compressive strength obtained from each concrete batch. It was clearly indicated that there were uncertainties in the test results on concrete strength performed in the standard cylinder tests. Larger margin of variation of the material properties within a bent cap specimen should be expected because of its enormous size.

TABLE 5.5 Concrete Compressive Strength for Each Batch

Concrete Batch	Strength (psi)			Average	Std
	Cyl. #1	Cyl. #2	Cyl. #3	(psi)	(psi)
A	6135	5835	6680	6217	428
B	5690	6280	5490	5820	411
C	5830	5975	6300	6035	241
D	5545	5400	5580	5508	95
E	7620	7655	7890	7722	147
F	5360	5485	5540	5462	92
G	5230	5510	5220	5320	165
H	5610	5780	5790	5727	101

Existence of Cracking and Microcracking

Hardened concrete contains cracks even without the presence of externally applied load. These forms of cracks are often attributed to shrinkage of the drying cement paste after the initial setting of hardened concrete and the effect of differential temperature due to heat generation due to the hydration reaction during the concrete hardening. These forms of cracks are often small and concentrated on the member surface for normal test specimens and may not have a significant effect on the overall stiffness of RC members. However, Bazant and Raftshol (1982) showed that in thick concrete walls, shrinkage cracks are more widely spaced and have larger crack widths and penetration depths. Because the bent cap specimens are related, the existence of larger and deeper cracks may contribute to the large stiffness degradation of the overall member, which, given the same level of load, results in larger deformations.

Inadequacies of the Constitutive Model

The constitutive relationship in the implicit bond models proposed in this study is based on the MFCT where model calibrations have exclusively been conducted on RC panel members with wall thicknesses relatively small compared to the member size. Although the load transfer mechanism in RC bent caps may contain similar attributes to RC panels, e.g., the shear action plays an important role in resisting the external load, the characteristics of RC panels are different from the RC bent caps used in the current experimental program in several aspects. Two possible differences in member characteristic, which may contribute to the modeling inaccuracies, are discussed here: (1) member width; and (2) reinforcing bar size and distribution.

The rationale behind the effect of member width on the stress-strain relationships is manifold. One such explanation results from the effect of cracking and microcracking as discussed previously. Shrinkage in concrete is often attributed to the moisture migration between the concrete and the surrounding environment. Van Zijl (1999) formulated the mathematical model for shrinkage using the diffusion theory. It could be concluded that the shrinkage strain across the member thickness is non-uniform and its distribution depends upon the moisture exchange rate between material points inside the concrete and air moisture content. The non-uniformity causes residual stress, which may be high enough to cause cracking in concrete members, particularly, for members with larger wall thickness where the degree of non-uniformity is expected to be much larger. Another possible explanation arises from the argument based on fracture mechanics as concrete response often exhibits strong size effect. The effect of size of the constitutive model could be confirmed by comparing the proposed stress-strain relationship of concrete between the RA-STM and MCFT. Recall that both models employ the same sets of equilibrium and compatibility equations. However, the proposed concrete constitutive relationships, which were derived from experiments, show noticeable differences. Although these differences may results from several factors, the effect of size may be one of those sources of discrepancies because the difference in wall

thickness used in the experimental program between the MCFT and RA-STM. Therefore, direct extension of the MCFT to numerical simulation of RC bent caps may cause modeling accuracies.

The size and distribution of the reinforcing steel for typical RC panels used for the calibration of MCFT significantly differs from that adopted in RC bent caps. Reinforcement in the RC panels used in the experimental program by the Toronto Research Group were well distributed and of smaller bar size (#3 and #4 bars, in general). Given the same amount of reinforcing steel ratio, the development of the stress in the reinforcing bars through the concrete-reinforcement interface is more effective when using the smaller bar size. Therefore, use of larger bar sizes may cause interfacial bond-slip problem. Rots (1988) also concluded that the use of smearing techniques for reinforcing steel in regions where reinforcement are, in fact, concentrated could cause errors in the prediction of the crack patterns and overall response of RC members because the effect of bond-slip cannot be taken into account by tension-stiffening approaches. Rots (1988) also proposed that explicit bond-slip models be used for the finite element modeling in regions where the reinforcement is highly concentrated.

5.4.3 Strength Prediction

Although the analytical models overestimate the stiffness of RC bent caps, it is shown that the proposed constitutive is capable of accurately predicting the failure load for RC bent caps. The unconfined model tends to underestimate the RC bent cap strength. In average, the performance of the confined model is superior to the unconfined one regarding the strength prediction as shown in Table 5.6.

TABLE 5.6 Strength Comparison for All Group Specimens

Model	Experiment (kips)	Confined		Unconfined	
		P_{ult} (kips)	Predicted/Exp.	P_{ult} (kips)	Predicted/Exp.
1A	376	400	1.06	368	0.98
1B	420	392	0.93	360	0.86
2A	404	408	1.01	360	0.89
2B	381	400	1.05	368	0.97
3C	428	416	0.97	384	0.90
3D	434	408	0.94	384	0.88
4C	430	464	1.08	464	1.08
4E	453	488	1.08	480	1.06
5D	457	456	1.00	448	0.98
5E	481	480	1.00	472	0.98
6F	430	464	1.08	376	0.87
6G	402	464	1.15	376	0.94
7F	500	504	1.01	464	0.93
7H	477	504	1.06	456	0.96
8G	433	456	1.05	376	0.87
8H	473	464	0.98	376	0.79
		Mean	1.03		0.93
		Std	0.06		0.07

However, both the confined and unconfined models over-predict the ultimate actuator load for specimens 4C and 4D. Recall that specimen 4C and 4D failed immediately after the first reinforcement yielding. The strength prediction on specimens

6 series also indicates larger inaccuracies of the confined model. It should be noticed that both specimen 4 and 6 series adopted #10 bars as the main reinforcing steel. The use of larger bar sizes may cause higher interfacial stresses between concrete and reinforcing steel, given the same reinforcement ratio. Therefore, it was possible that the rupture or slip between concrete and reinforcement interface could contribute to premature failure of specimen 4 and 6 series. Table 5.7(a) and (b) shows the analytical prediction of ultimate actuator forces performed using the confined and unconfined models on RC bent caps based upon the main reinforcement bar size. It is shown that the confined model performs slightly better for specimens reinforced with #7 and #8 bars, but results in an overestimation for specimens reinforced with #10 bars.

TABLE 5.7(a) Strength Comparison for Specimens Reinforced with #7 and #8 Bars

Model	Main Steel	Experiment (kips)	Confined		Unconfined	
			P_{ult} (kips)	Predicted/Exp.	P_{ult} (kips)	Predicted/Exp.
1A	8#8	376	400	1.06	368	0.98
1B	8#8	420	392	0.93	360	0.86
2A	8#8	404	408	1.01	360	0.89
2B	8#8	381	400	1.05	368	0.97
3C	11#7	428	416	0.97	384	0.90
3D	11#7	434	408	0.94	384	0.88
5D	11#8	457	456	1.07	448	1.00
5E	11#8	481	480	1.03	472	0.98
7F	11#8	500	504	1.02	464	0.86
7H	11#8	477	504	1.07	456	0.91
8G	8#8	433	456	1.05	376	0.87
8H	8#8	473	464	1.00	376	0.79
			Mean	1.02		0.91
			Std	0.05		0.06

TABLE 5.7(b) Strength Comparison for Specimens Reinforced with #10 Bars

Model	Main Steel	Experiment	Confined		Unconfined	
			Pult	Predicted/Exp	Pult	Predicted/Exp
4C	7#10	430	464	1.12	464	1.02
4E	7#10	453	488	1.08	480	1.01
6F	5#10	430	464	1.08	376	0.87
6G	5#10	402	464	1.15	376	0.94
			Mean	1.11		0.96
			Std	0.03		0.06

5.5 PARAMETRIC STUDIES

Results in Section 5.3 showed that the constitutive model based on the direct extension of the MCFT to incorporate the confinement effect, as proposed in Chapter III, yielded good results on the strength prediction of RC bent caps. However, the deformation counterpart was underestimated. Several potential causes of the discrepancies were identified and discussed in section 5.4. Despite the large number of parameters affecting the constitutive model of RC structures, two likely sources of discrepancies that could lead to an underestimation of the RC bent cap deformation shall be closely investigated: (1) Shrinkage in the concrete; and (2) Interfacial bond slip between the concrete and main reinforcing steel.

5.5.1 Effect of Shrinkage in Concrete

Shrinkage is known to be a potential cause for excessive cracking in RC members. The real physical cause of shrinkage in concrete is often attributed to the moisture migration between the cement phase and surrounding environments. In microscale, the effect of moisture migration leads to the shrinking of the cement paste surrounded by aggregates, which is the major cause of the microcracks in RC members.

The mechanics behind the shrinkage in concrete is rather complicated. The detailed investigation of the cause and effect of concrete shrinkage is far beyond the scope of this study. The effect of coupling between the mechanical and shrinkage strain will also be disregarded. In addition, the problem will be approached in a macro-level where the cause of shrinkage cracks is attributed to the restraining effect caused by structural configurations or the presence of the reinforcing steel in RC members subjected to uniform shrinkage as shown in Fig. 5.8. With this approach, the effect of microcracking is disregarded.

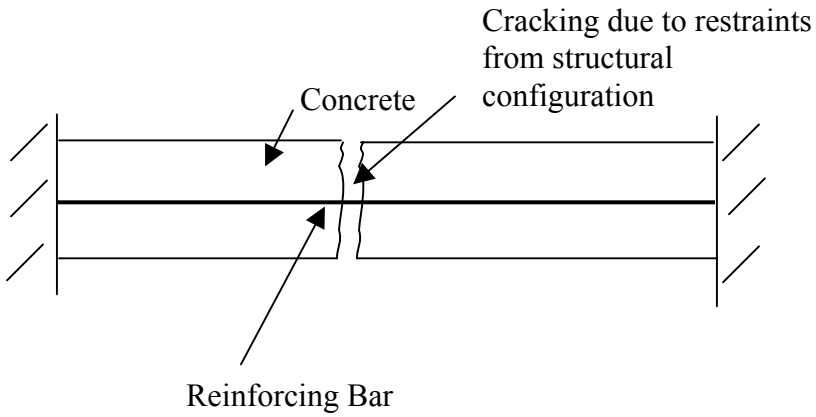

Figure 5.8 Uniform Shrinkage Crack Caused by Member Restraints

5.5.1.1 Modification of the Constitutive Relationships to Incorporate Shrinkage

To incorporate the shrinkage strain, the MCFT-based constitutive relationships for concrete proposed in Chapter III must be modified. The following assumptions are made in the present study:

(1) The total strain in concrete consists of mechanical and shrinkage strain while the total strain in reinforcement is composed of mechanical strain only;

(2) Shrinkage strain in concrete is prescribed and no coupling between mechanical strain and shrinkage strain exists; and

(3) The stress-strain relationship of concrete is expressed in terms of the total strain of concrete and can be described by the constitutive relationships as proposed in Chapter III.

For the purpose of parametric studies, a uniform shrinkage strain of 200 and 400 microstrains is supeimposed to the concrete elements in both global X and Y directions. Given the effect of curing and age of concrete when the bent caps are tested, the number of 400 microstrains may be slightly overestimated for the RC bent caps tested in the experimental program (Bracci et al., 2000). In addition, numerical simulations are performed for the specimens Group 1 only. Therefore, the results only serve as parametric studies.

5.5.1.2 Results

Fig. 5.9 shows the load-displacement diagrams for the first group of specimens using the modified constitutive relationship to incorporate the effect of shrinkage. Data series signified by "Shrinkage 200" and "Shrinkage 400" represent simulated results of RC bent caps incorporating the effect of uniform shrinkage of 200 and 400 microstrains, respectively. Results show that the effect of shrinkage causes a reduction in the first cracking load of RC members in all four simulated bent caps. In cases where the uniform shrinkage strain of 400 microstrains is imposed on the concrete elements, the predictions of first cracking load significantly decreased to a value significantly smaller than those of experimental results. This results in a slight shift of the load-deformation of RC bent caps to the left, which helps the simulated response come closer to the experimental results. The incorporation of shrinkage, as expected, has negligible influence on the ultimate strength as predicted strengths of a RC bent cap member with and without shrinkage are virtually the same. Although the simulated response including uniform shrinkage shifts closer to experimental results, the slope of the predicted post-cracking load-deformation curve remains unchanged, regardless of the magnitude shrinkage strains used in the parametric studies. Therefore, it may be concluded that the effect of shrinkage is not the real physical reason behind the too stiff response of the proposed constitutive relationship as obtained in Section 5.3.

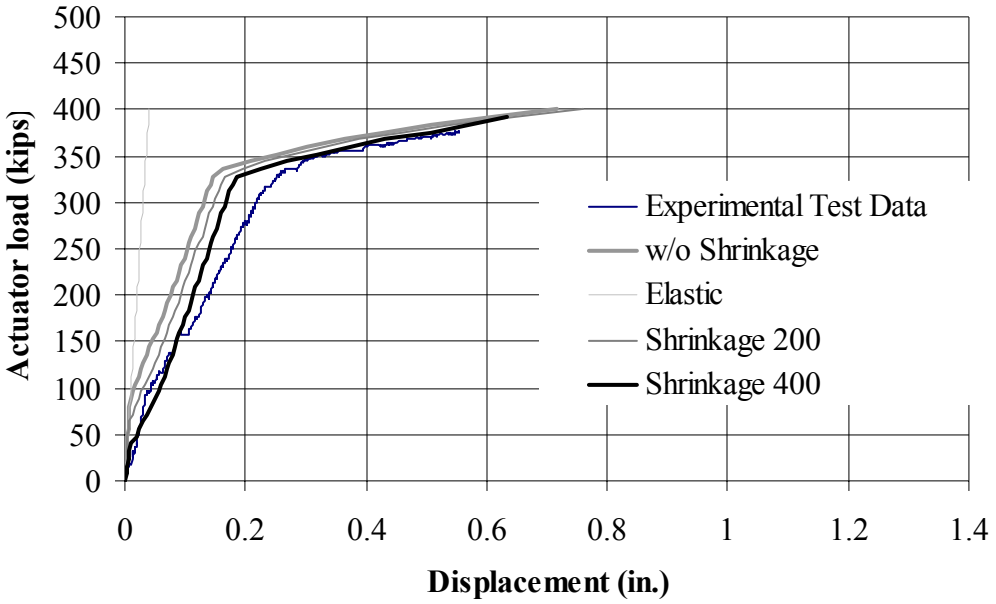

(a) Specimen 1A

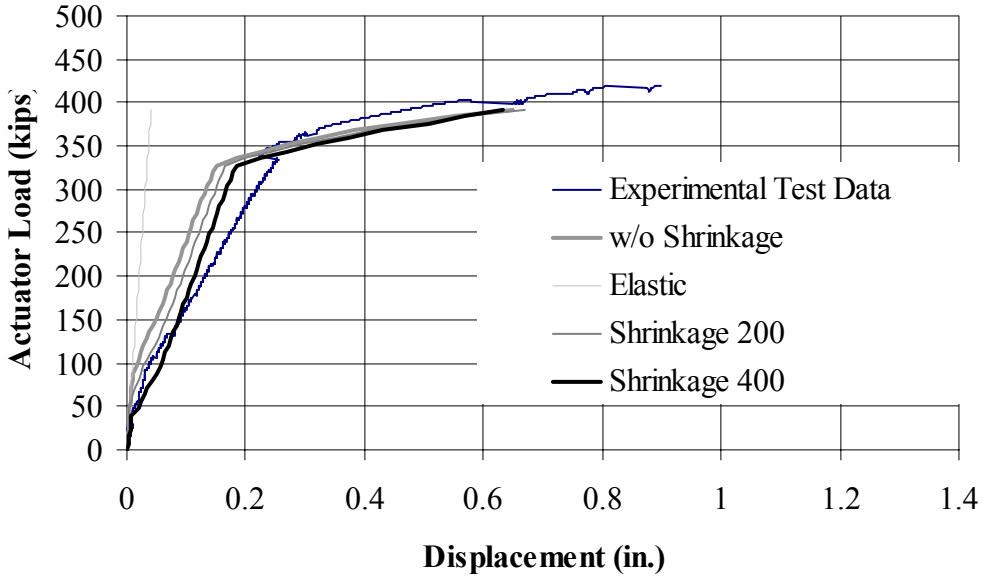

(b) Specimen 1B

Figure 5.9 Parametric Study on the Effect of Shrinkage on Group 1 Specimens

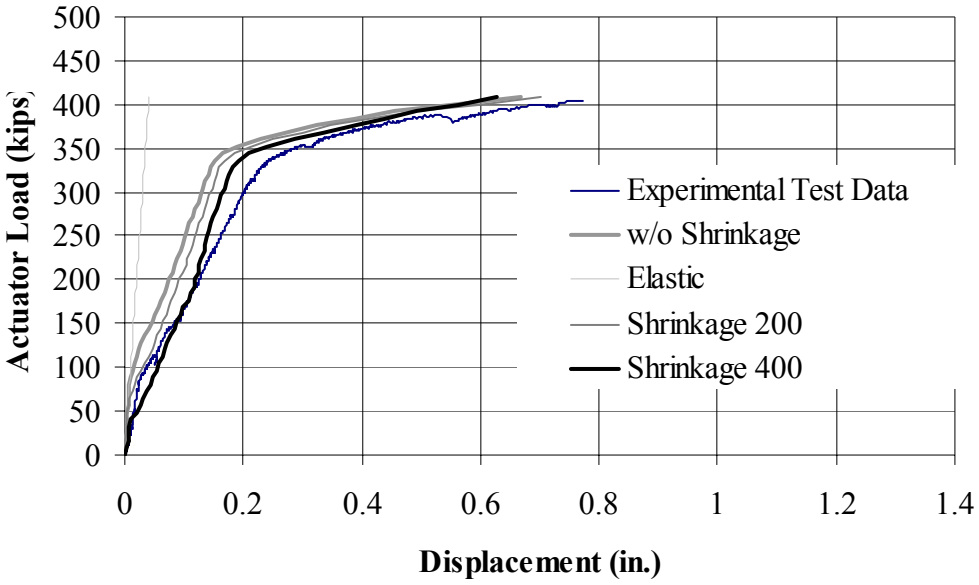

(c) Specimen 2A

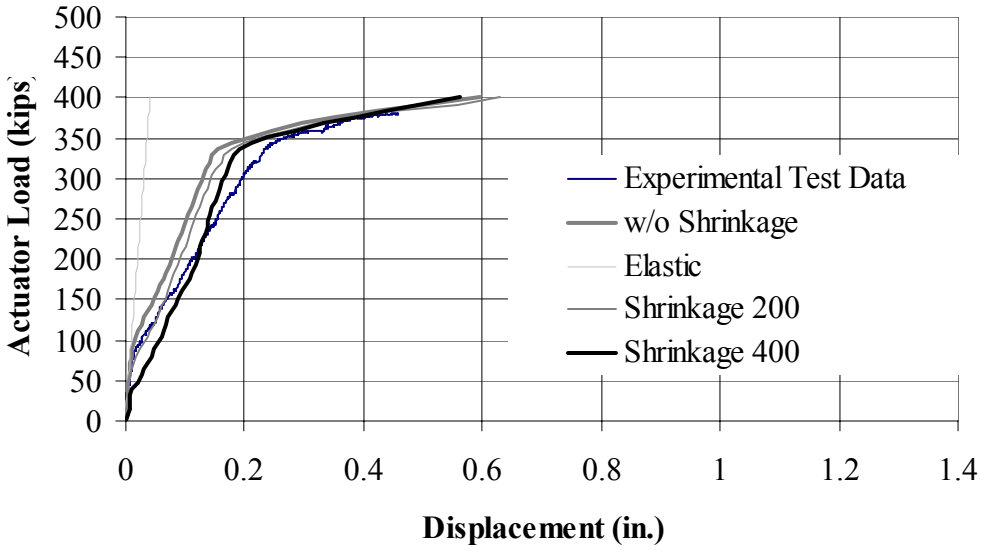

(d) Specimen 2B

Figure 5.9 (Continued)

5.5.2 Effect of Interfacial Bond-Slip

Under the context of the MCFT, the effect of interfacial bond-slip between the concrete and reinforcing steel is taken into account by the tension-stiffening effect by modifying the constitutive relationship of concrete in tension. The tension stiffening effect is essentially a homogenized form of the concrete tensile stress-strain relationship of concrete over several cracks. For RC membrane type elements where reinforcement is uniformly distributed, this approach yields relatively good analytical results as reported by Vecchio and Collins (1982). However, the main flexural reinforcement in RC bent caps is heavily concentrated on the top face of the cross section while only marginal amounts of transverse and skin reinforcement are provided for the remainder of the cross section. The effect of non-uniform reinforcement distribution could lead to the inability of the tension-stiffening concept to model interfacial bond-slip between the concrete and reinforcement (Rots, 1988).

In order to justify the proposition by Rots (1988), parametric studies on the effect of interfacial bond-slip are performed. In this approach, the effect of bond-slip is modeled explicitly through the use of the spring element. Early research on FEM modeling of RC members by Ngo and Scordelis (1967) also adopted the same approach to take into account the effect of slip between concrete and reinforcing steel. In essence, this method separates concrete and reinforcing steel through the use of different nodes numbers even though they may share the same exact geometrical locations at the interfacial zone. Fictitious spring elements are then assigned to simulate the effect of interfacial normal contact and tangential slip as shown in Fig. 5.10. The stiffness normal to the interface is mainly attributed to the dowel action between concrete and reinforcing steel (Rots, 1988), while the stiffness parallel to the interface represents the interfacial slip.

In general both normal and tangential stiffnesses of the spring element should be correctly identified. However, the effect of dowel action between concrete and

reinforcing steel is relatively complicated. Pruijsser (1988) indicated that experimental results on the effect of dowel action is relatively scattered and could be different on several orders of magnitude. Research in the past on FEM modeling of the interfacial bond-slip effect on the overall performance of RC members usually assumed that stiffness in the direction normal to the slip interface is perfectly rigid by assigning very large numbers to this stiffness component. Therefore, this assumption will also be used and only the effect of tangential slip is considered in this dissertation.

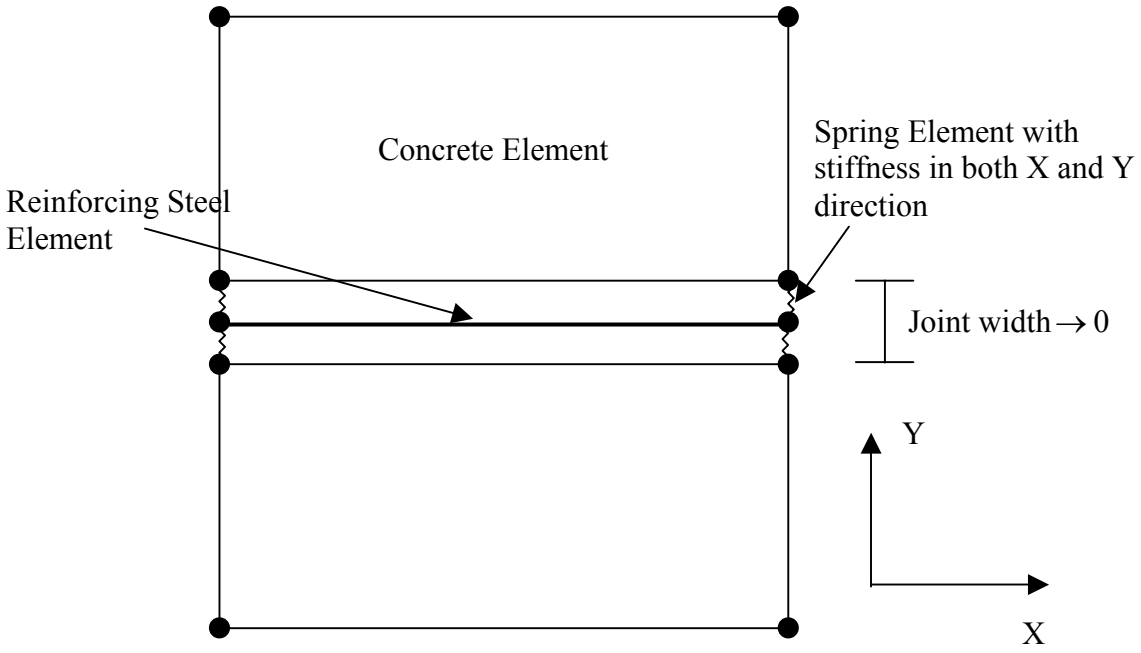

Figure 5.10 Interface Modeling with Spring Element

The mechanical properties of a spring element are crucial for the ability of the model to simulate the slip between concrete and reinforcement interface. Eligehausen et al. (1983) conducted an experimental program to determine the constitutive model for the interfacial slip between the concrete and reinforcement. These results served as the basis for the modeling of the concrete-reinforcement interface and was adopted in the CEB-FIP (1990) model code for bond-slip model, which can be written as:

$$\tau = \tau_{\max}(\frac{s}{s_1})^{0.4},\ s < s_1 \qquad (5.1)$$

$$= \tau_{\max}, s_1 < s < s_2$$

$$= \tau_{\max} - \frac{(\tau_{\max} - \tau_f)}{(s_3 - s_2)}(s - s_2), s_2 < s < s_3$$

$$= \tau_f, s > s_3$$

where, τ = calculated bond stress

s = interfacial slip between the concrete and reinforcement

$\tau_{\max}$ = maximum bond stress = $30.10\sqrt{f_c'}$, unit in psi.

τ_f = bond stress at failure = $0.4\,\tau_{\max}$

s_1, s_2, s_3 = constant =0.004,0.012,0.04 inches, respectively

Solari and Spacone (2001) proposed the CEB-FIP (1990) model to simulate the effect of bond-slip in RC beams model as shown in Fig. 5.11.

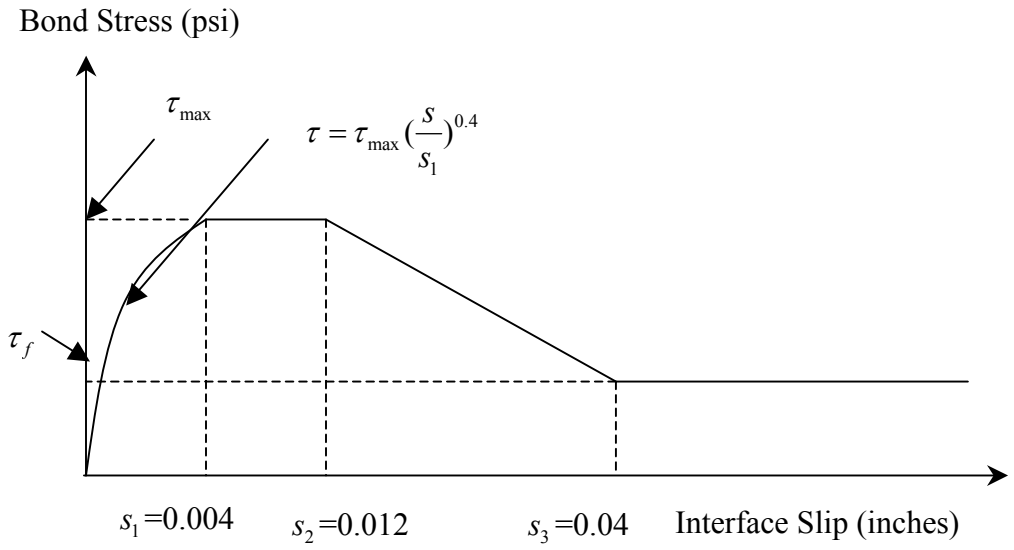

Figure 5.11 CEB-FIP (1990) Interfacial Bond-Slip Model

5.5.2.1 FEM Model for RC Bent Caps Using Explicit Bond-Slip Model

Two-dimensional FEM analyses of RC bent caps similar to those in Section 5.3 are performed. However, the effect of interfacial bond-slip between the concrete and the main reinforcement are explicitly modeled using spring elements. In fact, interfacial slip can also occur between the concrete and skin reinforcement. However, the amount of skin reinforcement is relatively small. Therefore, the negligence of the slip between the concrete and skin reinforcement should not significantly affect the overall load-deformation response, which is the primary goal of this parametric study.

Similar FEM mesh, loading, and boundary condition of the RC bent cap models as those of section 5.3 are used. Three major changes are made: (1) change of the node numbering system along the concrete-reinforcement interface; (2) introduction of spring element; and (3) change of constitutive model of concrete in principal tension directions. Because the effect of interfacial bond-slip is now taken into account by an explicit bond slip model, only tension-softening of concrete after cracking is considered. Therefore, post-cracking stress-strain relationship of concrete is modeled by Eq. 3.19. In addition, only the constitutive model of concrete in compression including confinement is used. As a preliminary investigation, numerical simulations are performed only for Group 1 specimens in this section. As in the previous section, only the simulated response using confined model will be presented.

5.5.2.2 *Results Using CEB-FIP(1990) Bond-Slip Model*

Fig. 5.12 shows the comparison between the predicted load-deformation curves for the first group of RC bent cap specimens using the implicit (tension stiffening) and explicit CEB-FIP (1990) models for the interfacial bond-slip between the concrete and reinforcement. It shows that the use of an explicit bond model yields superior results compared to the implicit bond model as its simulated response of RC bent caps consistently lies closer to the experimental results. The difference in the predicted first cracking load, load at first main reinforcement yielding, and the ultimate strength of RC

bent caps for the implicit and explicit bond model are not significant. However, the predicted post-cracking stiffness of the explicit bond model is smaller and closer to the experimental results.

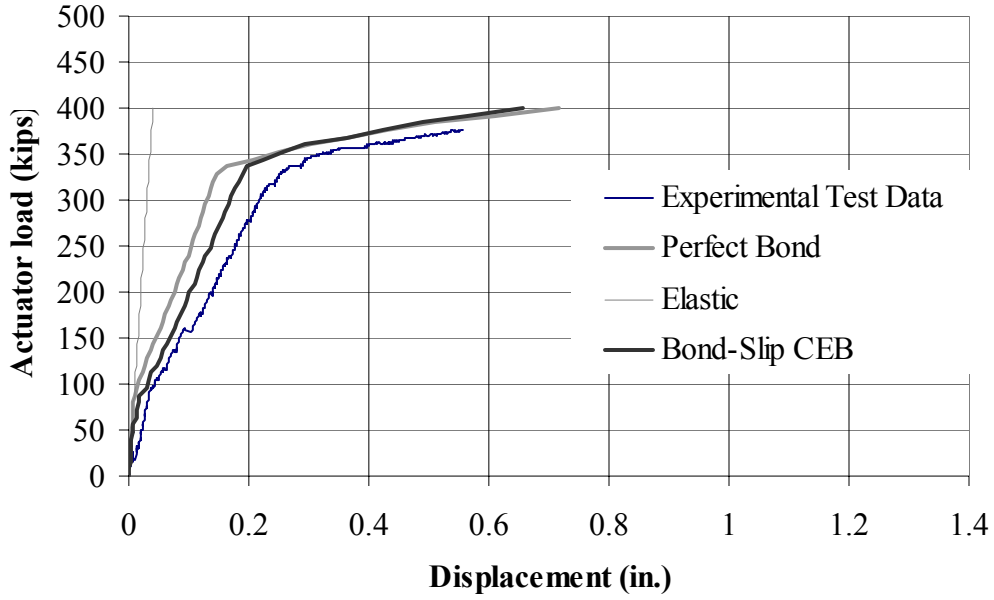

(a) Specimen 1A

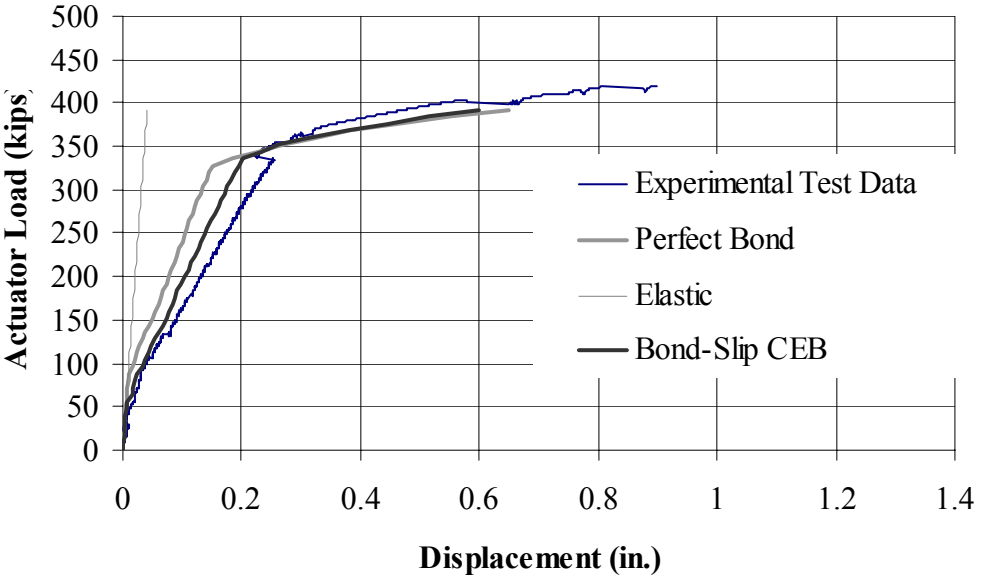

(b) Specimen 1B

Figure 5.12 Simulated Results of Group 1 Specimens Using CEB-FIP (1990) Explicit Bond-Slip Model

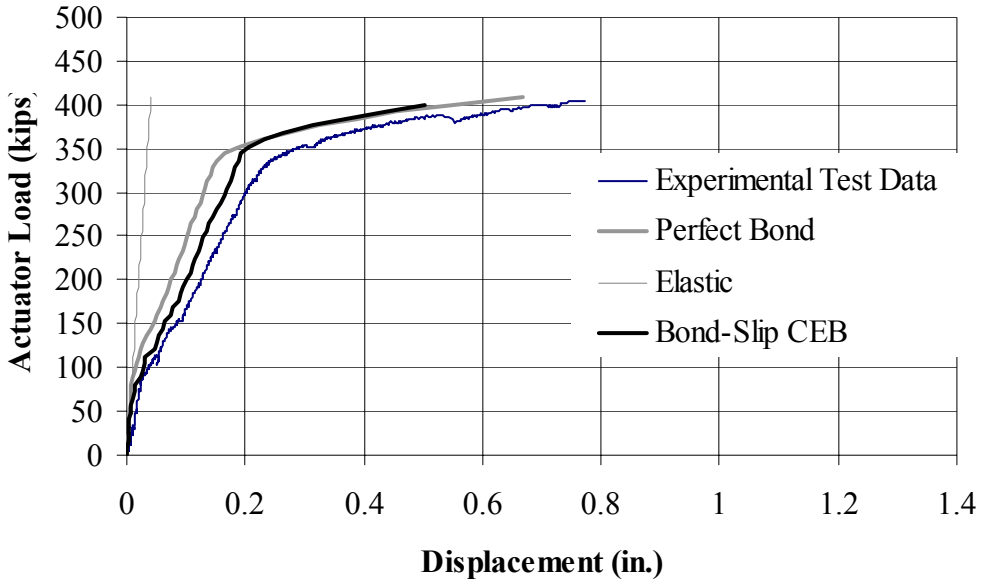

(c) Specimen 2A

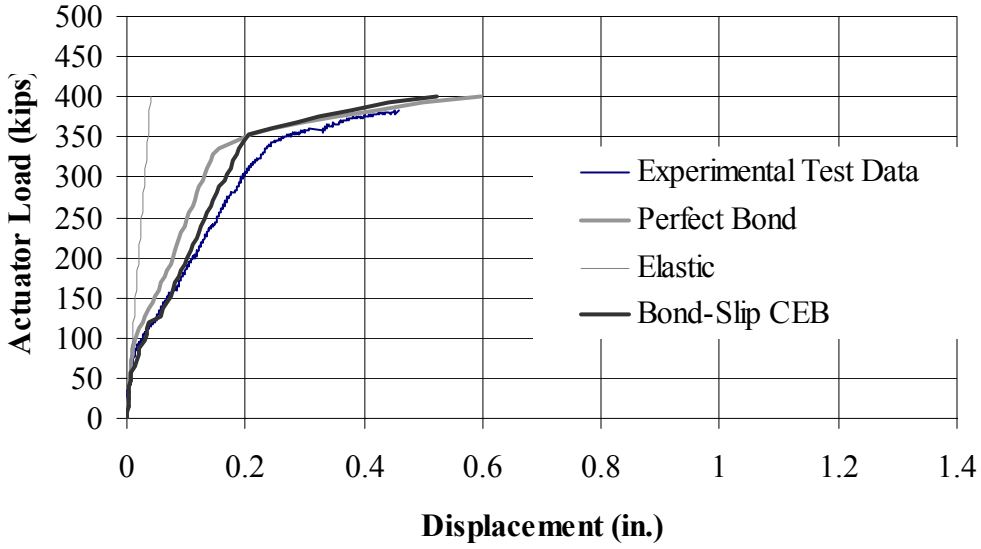

(d) Specimen 2A

Figure 5.12 (Continued)

5.5.2.3 Parametric Studies on the Effect of Bond-Slip Model

Results in Section 5.5.2.2 indicated that the application of the CEB-FIP bond-slip model led to improved predictons of the load-deformation curve for RC bent caps as the simulated load-deformation curves have a better match with the experimental results. The predicted first cracking load and ultimate load of RC bent caps are also in good agreement with the results obtained from the experimental program. In addition, the incorporation of explicit bond-slip model between the concrete and reinforcement led to a similar post-cracking stiffness of the RC bent caps.

In spite of the fact that the use of the CEB-FIP model to simulate interface bond-slip between the concrete and reinforcing steel led to improved correlation with the experimental results, the predicted deformation remains somewhat underestimated, as shown in Fig. 5.12. CEB-FIP model for the concrete and reinforcement interface was derived based on pull-out tests of a single bars in a concrete block. Therefore, the direct application of the model may not be representative of the interfacial slip between the concrete and main reinforcement in RC bent caps where multiple numbers of reinforcing steel are used. In addition, the effect of shear cracking in RC bent caps may somewhat deteriorate the bond-slip stiffness. A parametric study was performed on the effect of the bond-slip model to the simulated response of RC bent caps. It was found that the slope of the post-cracking load-deformation curve of RC bent caps depends upon the initial slope of bond stress-slip model. Based on curve fitting, the following constitutive relationships for bond stress-slip between the concrete and reinforcement interface is proposed:

$$\tau = \tau_{\max}\left(\frac{s}{s_2}\right),\ s < s_2 \qquad (5.2)$$

$$= \tau_{\max} - \frac{(\tau_{\max} - \tau_f)}{(s_3 - s_2)}(s - s_2),\ s_2 < s < s_3$$

$$= \tau_f,\ s > s_3$$

where, $\tau_{max}, \tau_f, s_2, s_3$ are materials constant defined in Eq. 5.1

Fig. 5.13 shows the bond stress-slip curve proposed for the RC bent caps. Essentially, the curve is a modification of the CEB-FIP model by decreasing the initial slope.

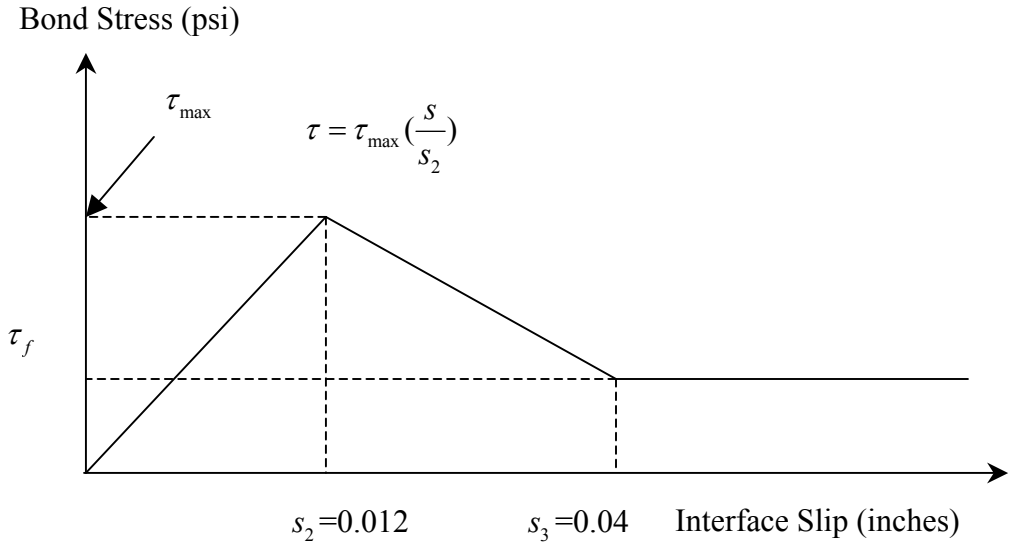

Figure 5.13 Modified Bond-Slip Model

Figs. 5.14 shows the comparison between the experimental results and simulated response of RC bent caps using perfect bond model, CEB-FIP model, and the proposed model. The figure clearly indicates that the proposed model leads to a better improvement in the prediction of the load-deformation of RC bent caps in the first group. From this finding, the proposed bond-slip model is applied to specimens in the second and third groups. Figs. 5.15 and 5.16 show the simulated response of the remaining 10 RC bent caps specimen using the proposed bond-slip model.

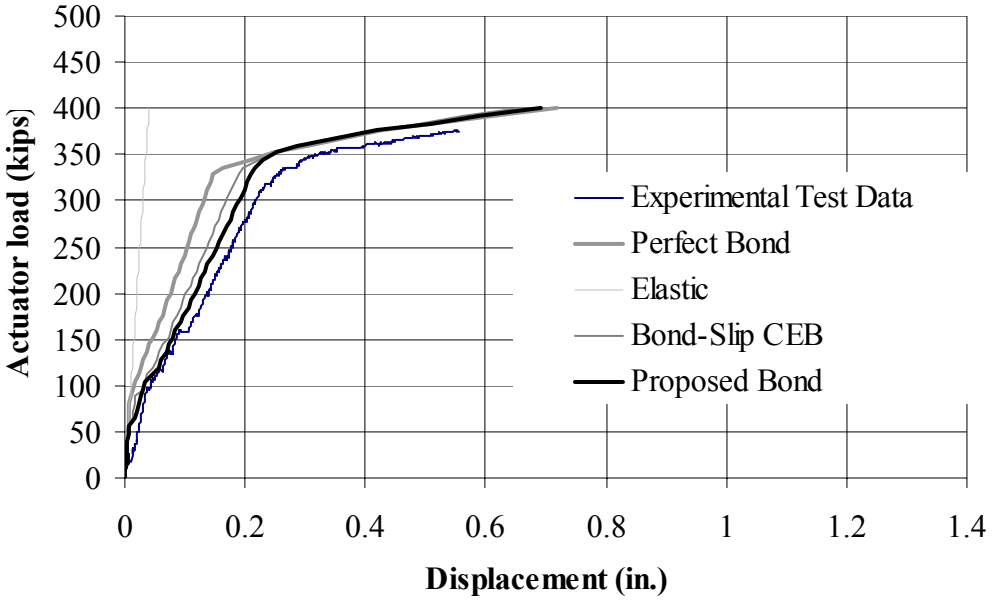

(a) Specimen 1A

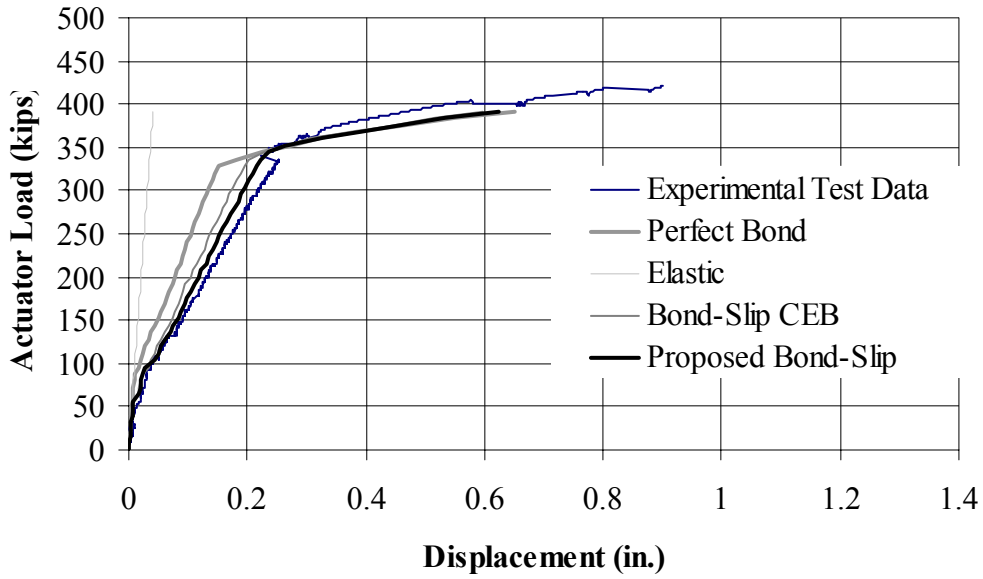

(b) Specimen 1B

Figure 5.14 Parametric Study on the Effect of Bond-Slip Model on Simulated Response of Group 1 Specimens

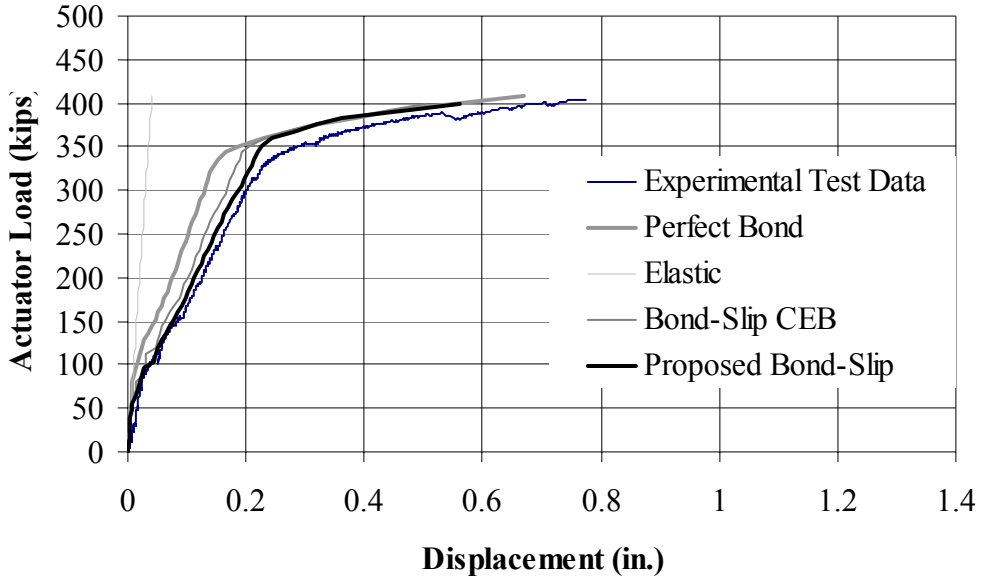

(c) Specimen 2A

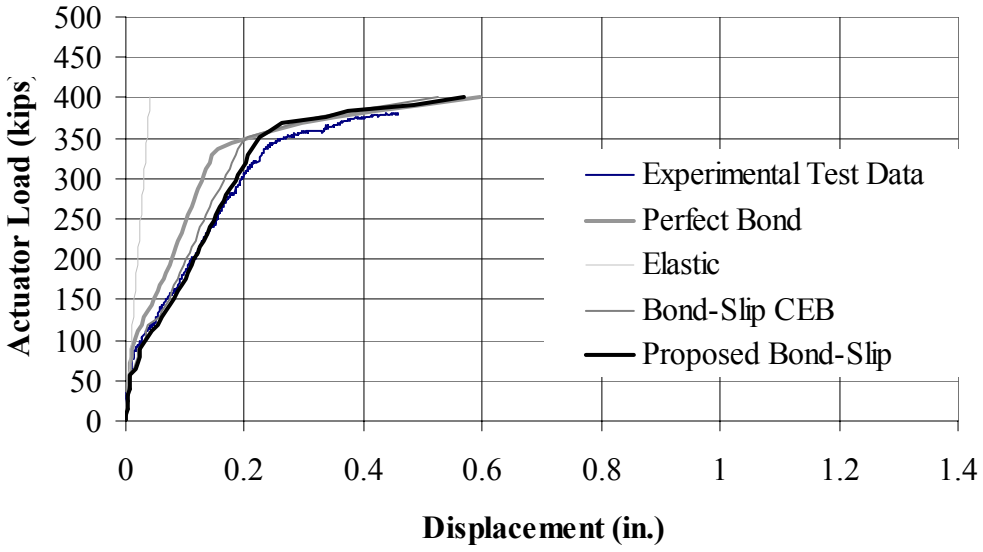

(d) Specimen 2B

Figure 5.14 (Continued)

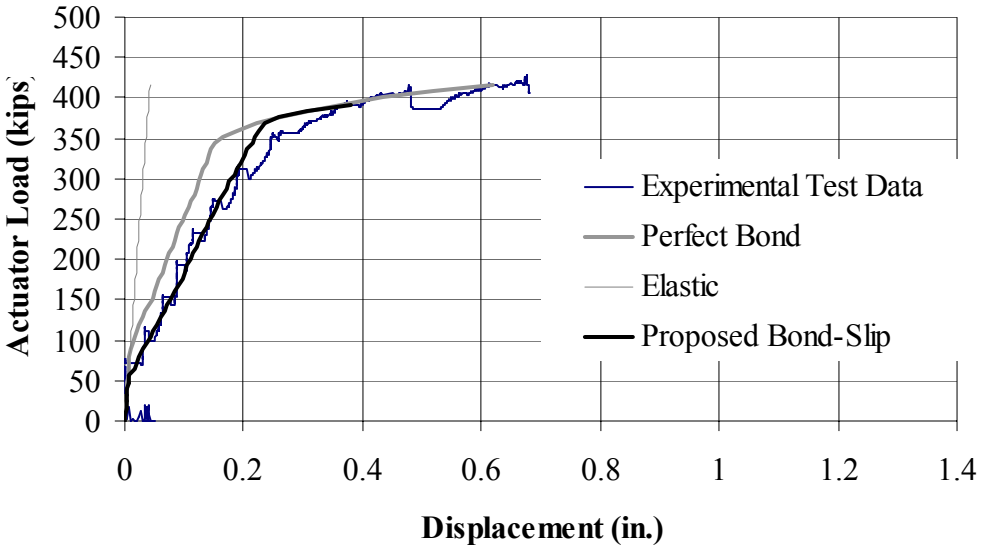

(a) Specimen 3C

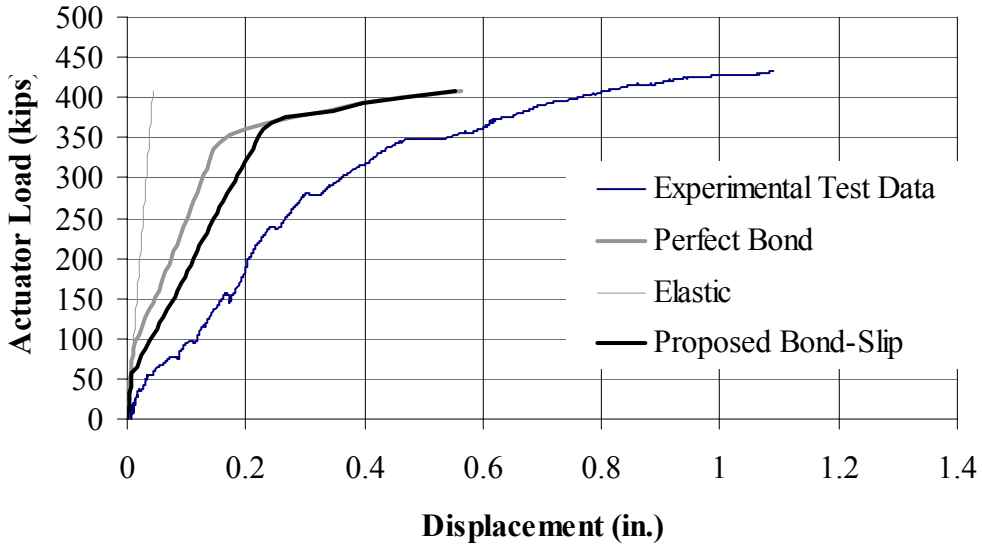

(b) Specimen 3D

Figure 5.15 Simulated Response of Group 2 Specimens Using the Proposed Bond-Slip Model

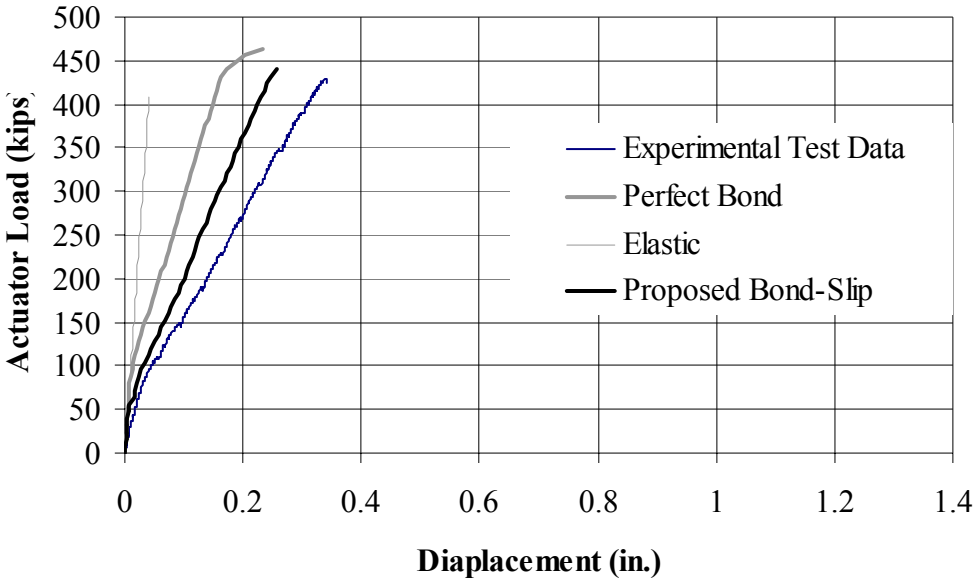

(c) Specimen 4C

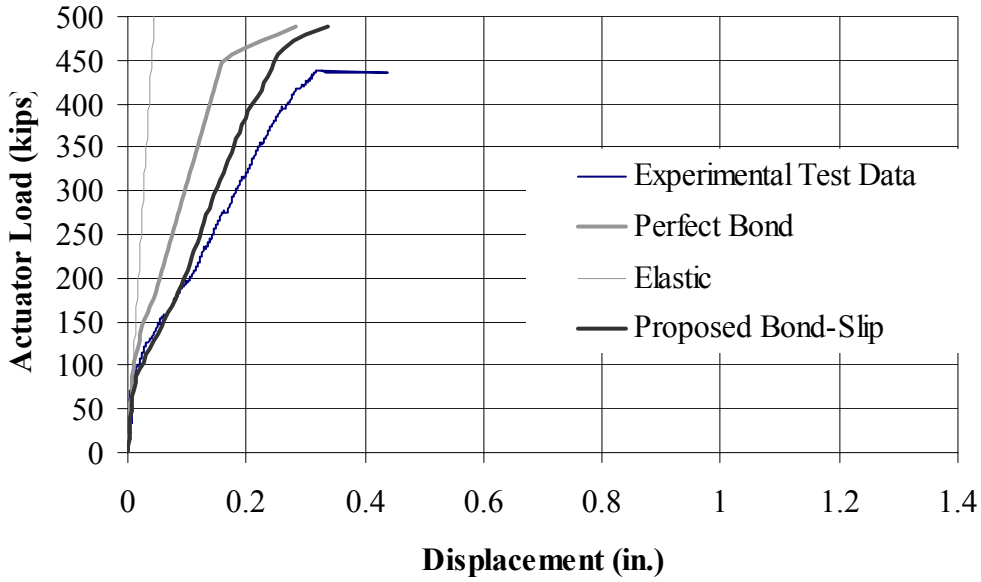

(d) Specimen 4E

Figure 5.15 (Continued)

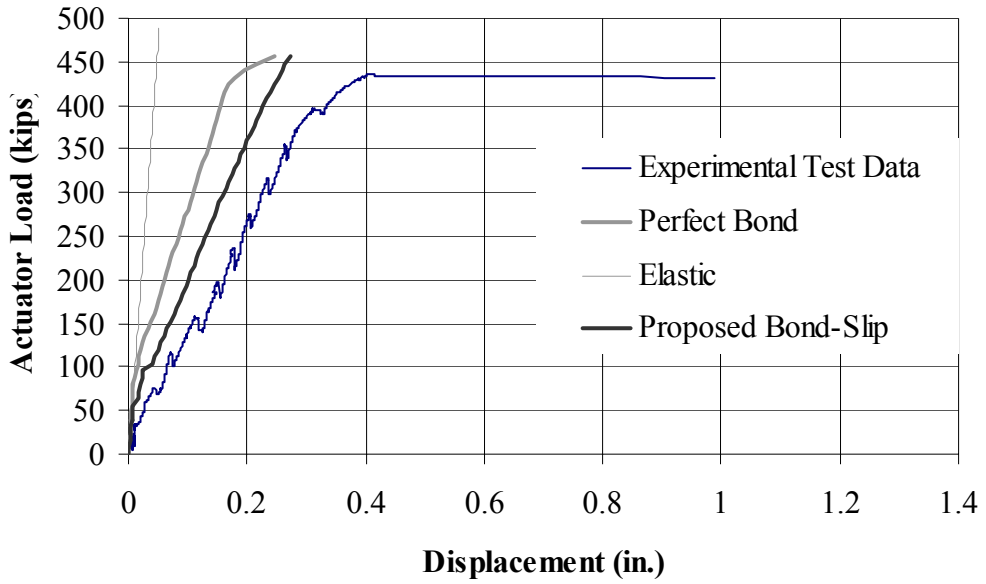

(e) Specimen 5D

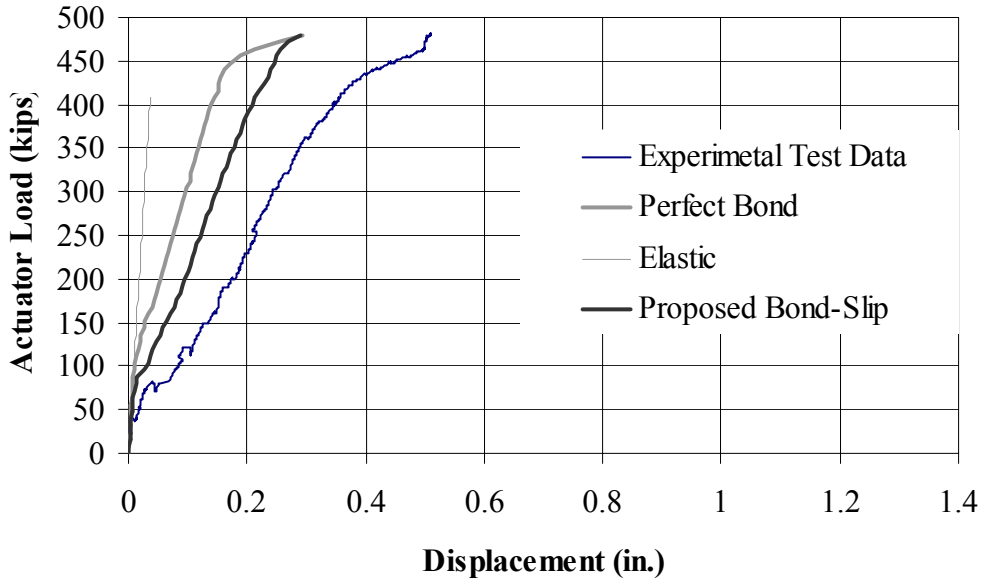

(f) Specimen 5E

Figure 5.15 (Continued)

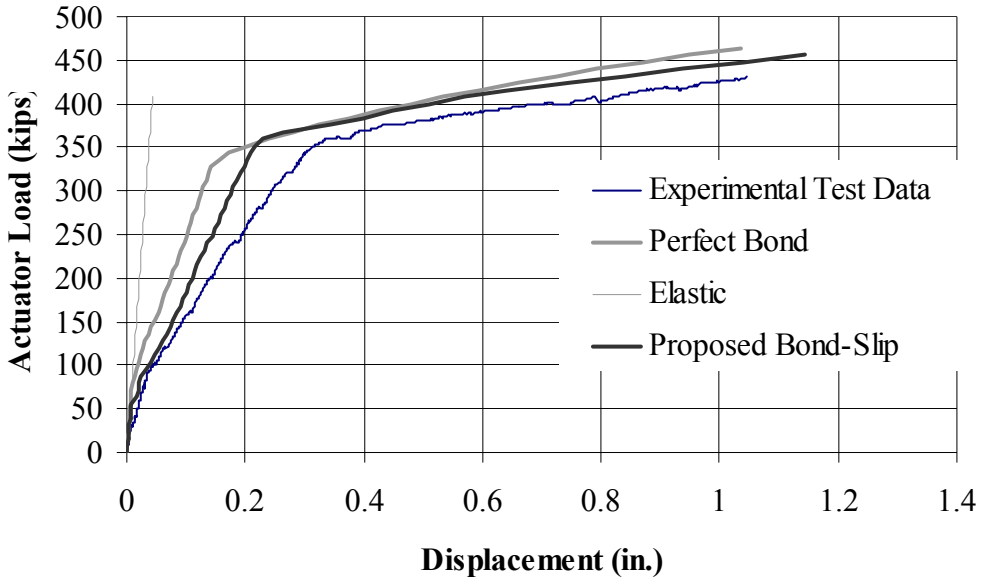

(a) Specimen 6F

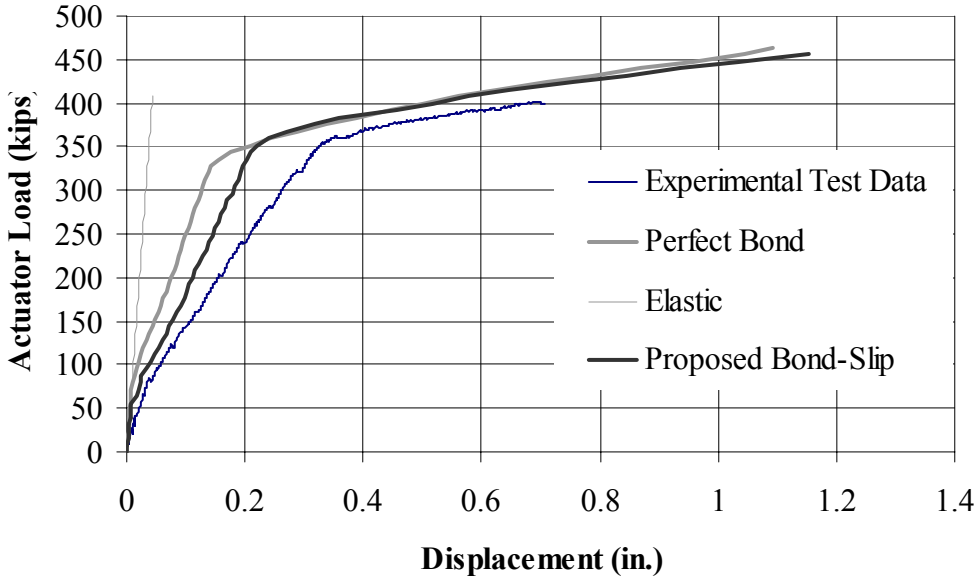

(b) Specimen 6G

Figure 5.16 Simulated Response of Group 3 Specimens Using the Proposed Bond-Slip Model

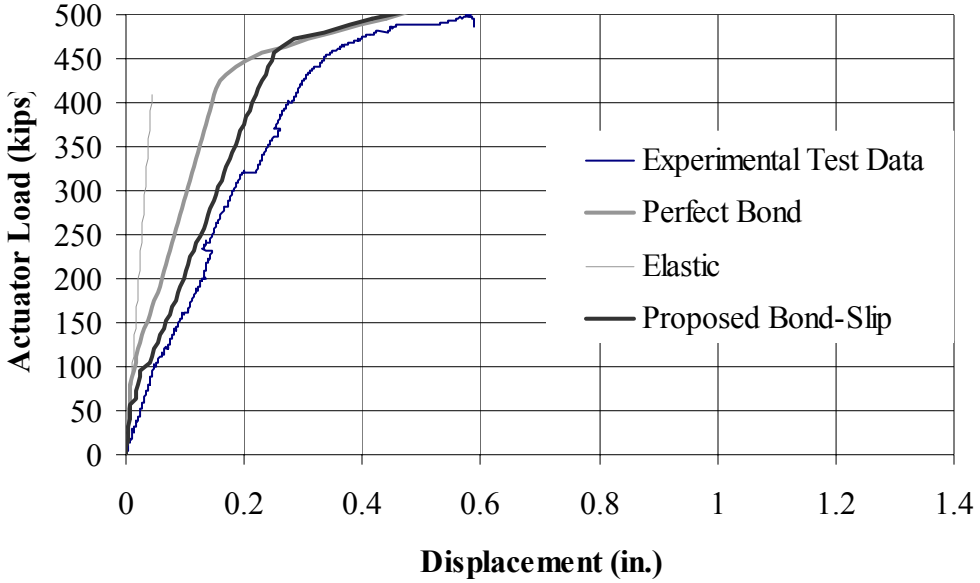

(c) Specimen 7F

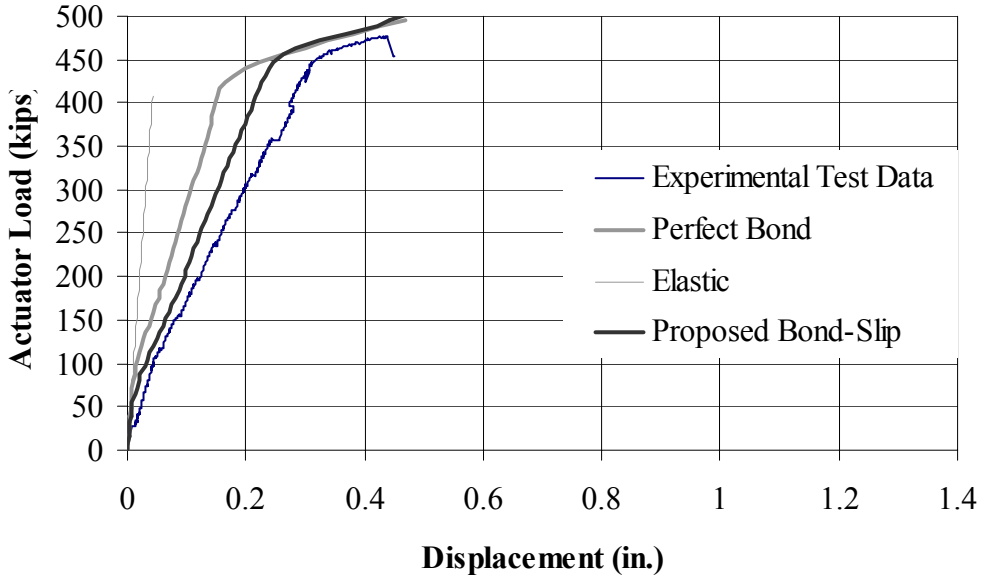

(d) Specimen 7H

Figure 5.16 (Continued)

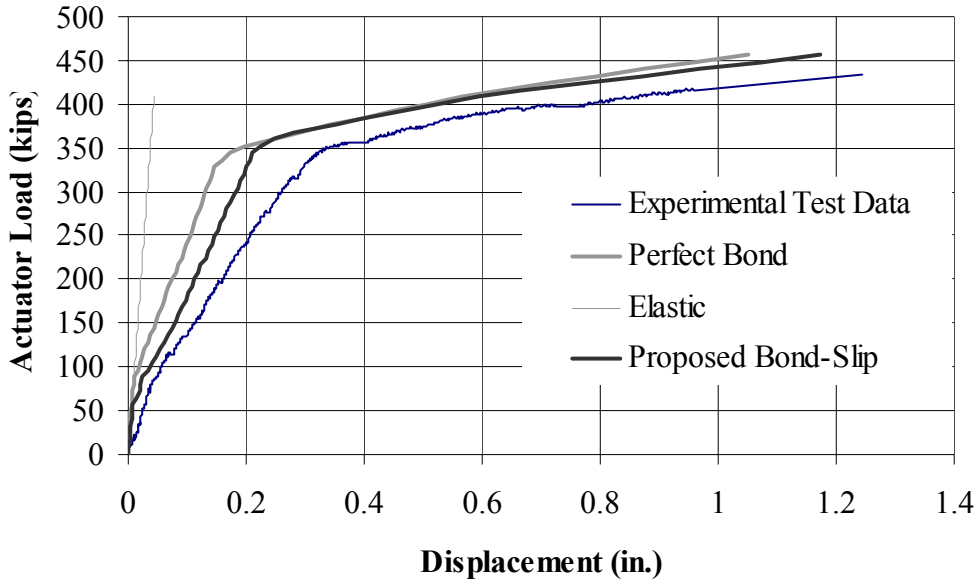

(e) Specimen 8G

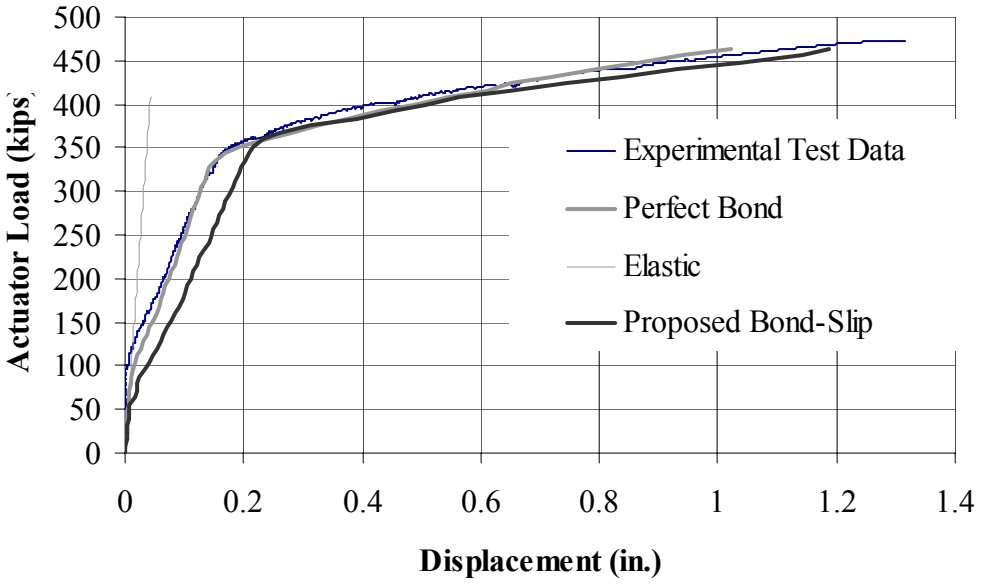

(f) Specimen 8H

Figure 5.16 (Continued)

5.6 SUMMARY

Chapter V verifies the ability of the proposed constitutive relationship in this dissertation to simulate the behavior of a shear-dominated RC member. The proposed constitutive relationship employs the same set of assumptions as the MCFT. However, the effect of confinement is incorporated. The proposed constitutive relationships were used to perform an analytical study on the performance of RC bent caps.

Results in Section 5.3 showed that the effect of confinement due to out-of-plane horizontal leg transverse reinforcement has a significant effect on the strength and deformability of RC bent caps. It shows that the effect of confinement is not mobilized at lower levels of stress as the simulated results for the confined and unconfined models were virtually identical under small stress. Both models also yield an identical result on the prediction of first cracking load. However, at higher levels of stress, the effect of confinement helps increase the deformability of concrete. This, in turn, improves the ductility of the RC bent cap members by delaying the brittle fracture of the concrete in compression. In addition, the effect of confinement also leads to a noticeable increase in the strength of RC members through the post-yield reinforcement strain hardening, which is a consequence of increasing deformability of concrete.

However, the direct application of the proposed constitutive model to RC bent caps leads to an overprediction of the post-cracking stiffness. Parametric studies on two possible causes of the overprediction were performed. The incorporation of shrinkage strains into the constitutive model did not offer any improvement of the predicted slope of post-cracking stiffness of RC members, as shown in Section 5.5.1. Therefore, it was concluded that a too stiff response of the predicted load-deformation relationship of RC bent caps shown in section 5.3 was not caused by shrinkage in the concrete. Section 5.5.2 showed that the use of explicit bond stress-slip models between the concrete and main reinforcement interface could lead to a decrease of the post-cracking stiffness. This results in a closer agreement with the experimental results, in terms of predicting

the deformation of RC bent caps. However, the application of the commonly used constitutive relationships of interfacial slip between the concrete and reinforcement somewhat over-predicted the post-cracking stiffness of RC bent caps. Parametric studies showed that a decreased initial stiffness of the bond stress-slip curve decreased the post-cracking stiffness of an RC bent cap. A modified form of the bond stress-slip model was proposed. Results in Section 5.5.2 showed that through the use the proposed bond-slip model, numerical simulation yielded good results on the prediction of the first cracking load, load at reinforcement yielding, ultimate load, and the load-deformation response of RC bent cap specimens.

CHAPTER VI

CONCLUSIONS

6.1 SUMMARY

The research objective of this dissertation was to evaluate the effect of passive confinement due to out-of-plane horizontal stirrup legs on the overall response of shear-dominated reinforced concrete (RC) members. An experimental program conducted at Texas A&M University on RC bent caps suggested that the use of overlapping stirrups led to noticeable increases in strength and ductility as the load and deformation at failure of test specimens with overlapping stirrups were consistently larger than the same specimen vertically reinforced with a single stirrup. Because double stirrups have twice the reinforcement area as a single stirrup, it is arguable that an increase in strength and ductility is attributed to the stirrups themselves. However, data on strain gauges installed on the stirrups suggested that the stirrups themselves do not significantly contribute to the strength of RC bent caps. This result is in agreement with the conclusions made by Ferguson (1964) on an experimental program of similar bent caps. Therefore, it should be concluded that the overlapping stirrups helped enhance the performance of the RC bent caps through other mechanisms.

The goal of the present study was to discover the mechanism behind the improved performance of RC bent caps caused by the overlapping stirrups. In this dissertation, it was hypothesized that this enhanced performance was attributed to the effect of confinement provided by out-of-plane stirrups legs. The confining stress due to the out-of-plane stirrup legs is a consequence of lateral expansion of concrete when subjected to compressive stress. In order to validate this assumption, an analytical model was proposed under the context of the Modified Compression Field Theory (MCFT). Two dimensional finite element models were used to simulate the behavior of the RC bent caps.

Constitutive relationships of the MCFT were expressed in terms of principal stress and strain in two-dimensional analyses. The confining stress due to out-of-plane stirrups represents stresses in the third direction. In order to incorporate the effect of confinement due to the out-of-plane stirrups, the constitutive relationships of MCFT were modified. This was achieved by modifying the concrete stress-strain relationship in the direction of principal compression. The Hognestad parabola normally used to represent the stress-strain curve of concrete in compression in a principal direction was replaced by the Mander's model where the peak stress and the associated peak strain are adjusted according to the level of confinement provided by the out-of-plane confinement stress due to horizontal legs stirrups and, if applicable, an in-plane compressive stress in cases where both principal stress are compressive. For cases where the principal tensile strain coexists with principal compressive strain, the stress in the principal compressive strain direction is reduced by a softening factor due to perpendicular tensile strains, as originally proposed by the MCFT.

The determination of peak stress and associated peak strain is crucial to the quality of the proposed constitutive relationships of concrete in compression. Following Mander et al. (1988), the five parameters failure surface proposed by Willam and Warnke (1974) was used to calculate the peak stress due to confinement. The associated peak strain must also be adjusted because the confinement not only affects the strength but also the deformability of concrete. An expression proposed by Mander et al. (1988) to determine the associated peak strain was also adopted in the dissertation.

In tension, the principal stress-strain relationship proposed by Collins and Mitchell (1987) was adopted in regions where tension stiffening was expected to mobilize. In unreinforced or relatively low reinforced regions tension-stiffening fields could not be developed. Therefore, the post-peak tensile stress-strain relationship involved only tension softening. An expression proposed by Hordjik (1991) was used to simulate the post-peak stress in tension. In this approach, the post-peak stress of

concrete in tension was expressed as a function of crack width. The concept of strain decomposition, which states that the total strain in tension is the sum of elastic strain in the unloading zone and fracture strain in the localized zone, was used to determine the crack width within an RC element. The crack width is essentially the product between the fracture strain and the length of the localized zone. Under the implementation of two-dimensional finite element modeling, the length of localized zone was determined from the characteristic length of the element.

In the tension-stiffening zone, the crack-check process adopted by Vecchio and Collins (1986) was required. For simplicity in numerical simulations, the decrease the yield strength to an apparent yield stress of reinforcing steel as proposed by Belarbi and Hsu (1994) was adopted. This process was selected to demonstrate that the crack check process, under certain circumstances, yields comparable results to the use of apparent yield stress.

The secant constitutive relationship of concrete was also developed in this dissertation. To take into account the effect of concrete expansion, a non-symmetric stiffness matrix was utilized. Because a commercial finite element package (ABAQUS) capable of handling non-symmetric stiffness matrices was used in the numerical simulations, an explicit form of the stiffness matrix could be used in favor of the pre-strain concept adopted by Vecchio (1991) and Selby (1993), where the convergence of stiffness matrix was used as a convergence criterion of the non-linear solution instead of the residual force used in the current investigation. It was found that the use of the tangential shear stiffness of the rotating crack model developed by Crisfield and Wills (1987) yielded more stable results than the shear stiffness proposed by Vecchio (1986) in the study of the RC bent caps.

Comparisons between the analytical and experimental results showed that the proposed analytical model, which incorporates the confinement effect to the constitutive

relation of the MCFT yielded excellent results on the prediction of strength at first reinforcement yielding and ultimate strength of RC bent caps. Ignoring the effect of confinement led to an underestimation of the RC member strength. However, the deformation was somewhat underestimated throughout the entire load history. In other words, the direct application of the MCFT to the analysis of RC bent caps resulted in a too stiff response. Parametric studies showed that the overestimation was not caused by the change of constitutive relationship of concrete to incorporate the effect of confinement. In fact, the effect of confinement is only mobilized at higher levels of load as the analytical predictions on the load-displacement diagrams are virtually the same before the first reinforcement yielding for models with and without confinement. The effect of the base curves for concrete stress-strain in compression, e.g., Mander's model vs. Hognestad parabola, on the load-deformation was also negligible. Additional parametric studies on the effect of shrinkage through pre-strain concept led to better fit curves. However, it did not provide the correct mechanism as the slope of the load-deformation diagram after initial cracking, which represents the stiffness of the member, remained unchanged.

A remedy to improve the analytical model was proposed in this research by the direct incorporation of an interfacial bond-slip representation between the concrete and main reinforcing steel. It was shown that by using explicit bond-link models to simulate the interface between the concrete and reinforcement, the analytical prediction of the load-deformation relationship can be improved as the stiffness, particularly in the post-cracking range, had a better fit with the experimental results. However, numerical simulations of the explicit bond-link elements using the bond stress-slip relationships normally proposed in the literature did not lead to significant improvements in the analytical prediction of the load-deformation response in the RC bent caps, as opposed to its good performance when flexural deformations are predominant as reported elsewhere. Better results were obtained by decreasing the initial stiffness of the bond stress-slip relationship. In reality, the decrease in bond stress-slip stiffness for the

concrete-reinforcement interface in RC bent caps may be justified because most experiments on interfacial bond-slip between the concrete and reinforcing steel are conducted by the pull-out test of a single bar in a block of concrete. For RC bent caps, multiple reinforcing steel bars of large diameter are arranged into a single layer or possibly multiple layers. The effect of early small splitting cracks between the bars may somewhat alter the bond-slip stiffness. In addition, the effect of inclined cracks due to shear action in RC bent caps could also lead to bond stiffness deterioration. Based on a curve-fit, a new bond-slip relationship was proposed for the current investigation. Results show that improved results of the load-deformation curves for the RC bent caps were obtained while the excellent performance on strength prediction was also maintained.

6.2 RECOMMENDED FUTURE WORK

Based on the findings from this research, the following major research areas are recommended for future works:

(1) Incorporating the behavior under reverse-cyclic loading into the proposed constitutive models

Current seismic design philosophy is shifting towards a performance-based design methodology where both the strength and deformation of structural members and systems under the design earthquake must be correctly identified. Under the current code of practice, the effect of confinement is recognized. To avoid brittle modes of failure, RC members in seismically active zones must have adequate seismic hoop reinforcement in the critical regions such as the locations near the beam-column joints where the external demands for shear are comparable to flexural actions. The purpose of these seismic hoops is not only to provide shear resistance to RC members, but also to provide confinement to concrete core such that imposed seismic energy can be dissipated through inelastic work (hysteretic energy) caused by inelastic member deformations. However, recommendations in the standard code of practice are

qualitative and given as a general case basis. The current investigation showed that a quantitative estimate of the confinement on shear dominated RC members under monotonic loading can be conducted. The quantification of the effectiveness of confining (hoops) reinforcement under reverse-cyclic loading may lead to a better understanding, which might help engineers build better systems and result in a more economical design of RC members. The most crucial part in an extension of the current model to reverse-cyclic loading is the definition of the loading-unloading-reloading path of the concrete stress-strain curve in both tension and compression and the manipulation of cracking or principal tensile direction rotation. In addition, the effect of interfacial slip and bond deterioration under reverse cyclic loading is also a very important factor in the prediction of the overall performance of RC members.

(2) Verification of the proposed bond-slip model with new test data

The current investigation indicated that the use of the perfect bond assumption led to an overestimation of the stiffness of RC members prone to shear deformations (such as bent caps). The overestimation of the stiffness led to the underestimation of deformations, which is a related to the overall cracking and crack width in the member under service load. The direct use of the bond stress-slip relationships proposed in the literature did not significantly improve the prediction of the load-deformation relationship. As suggested previously, there are several factors that could contribute to this problem. For instance, the use of closely spaced flexural reinforcement and the effect of inclined shear cracking can lead to bond stiffness deterioration even under monotonic loading. The proposed bond-slip model used in the current investigation was based on a parametric study by curve-fitting the overall response of a limited number of test specimens, which is, at best, a mere speculation of the real constitutive model of bond stress-slip between reinforcement and concrete interface. Further experimental work is needed for validation of the model.

3) Develop simplified macro-models to account for shear deformations

The current research was conducted under the context of two-dimensional continuum finite element analysis. Despite the simplicity, compared to some other advanced models such as the plasticity theory or damage mechanics, in the manipulation of the material stiffness matrix due to the MCFT assumption, the model remains too complicated to be used by practicing engineers. A simpler model based on structural elements such as the beam-column element should be developed. Under the current constitutive relationships of MCFT, the shear deformation can be taken into account. One possible extension is the development of a Timoshenko beam element, where the shear strain is explicitly included into the model, using the constitutive relationship of the MCFT. The development of analytical macro-models should provide the link between the state-of-the-art research and practicing engineers. This should lead to a wide spread use of a more advanced theory in the design, which, if used appropriately, should lead to the design of safer and more efficient structures.

REFERENCES

Ahn, T.S. (1996). *Tension Stiffening in Reinforced Concrete Membranes.* Ph.D. Dissertation, University of Missouri, Columbia

Bathe, K.J., and Sundberg, J.A. (1986). "A Concrete Material Model." *Computational Modeling of Reinforced Concrete Structures*. Conference on Computer-Aided Analysis and Design of Reinforced Concrete Structures, Split, Yugoslavia, 101-121

Bazant, Z.P. (1983). "Comment of Orthotropic Models for Concrete and Geomaterials." *Journal of Engineering Mechanics*, ASCE, 109(3), 849-865

Bazant, Z.P., and Cedolin, L. (1980). "Fracture Mechanics of Reinforced Concrete." *Journal of Engineering Mechanics*, ASCE, 106(6), 1287-1306

Bazant, Z.P., and Oh, B.H (1985). "Microplane Model for Progressive Fracture of Concrete and Rock." *Journal of Engineering Mechanics*, ASCE, 111(4), 559-581

Bazant, Z.P., and Planas, J. (1998). "Fracture and Size Effect in Concrete and Other Quasibrittle Materials." CRC Press, Boca Raton, FL

Bazant, Z.P., and Prat, P.C. (1988). "Microplane Model for Brittle-Plastic Material: I. Theory, II. Verification." *Journal of Engineering Mechanics*, ASCE, 114(10), 1672-1702

Bazant, Z.P., and Raftshol, W.J. (1982). "Effect of Cracking in Drying and Shrinkage Specimens." *Cement and Concrete Research*, 12(2), 209-226

Belarbi, A. (1991). *Stress-Strain Relationships of Reinforced Concrete in Biaxial Tension-Compression (Steel),* Ph.D. Dissertation, University of Houston, Texas

Belarbi, A., and Hsu, T.T.C. (1994). "Constitutive Laws of Concrete in Tension and Reinforcing Bars Stiffened by Concrete." *ACI Structural Journal*, 91(4), 465-474

Belarbi, A., and Hsu, T.T.C. (1995). "Constitutive Laws of Softened Concrete in Biaxial Tension-Compression." *ACI Structural Journal*, 92(5), 562-573

Bracci, J.M., Keating, P.B., and Hueste, M.B.D. (2000). "Cracking in RC Bent Caps." *Research Report 1851-1*, Texas Transportation Institute, Texas A&M University

Cabot, P,G., and Bazant, Z.P. (1987). "Nonlocal Damage Theory." *Journal of Engineering Mechanics*, ASCE, 113(10), 1512-1533

Carol, I., Prat, P.C., and Bazant, Z.P. (1992). "New Explicit Microplane Model for Concrete: Theoretical Aspects and Numerical Implementation." *International Journal of Solids and Structures*, 29(9), 1173-1191

CEB (Committee Euro-International du Beton) (1990). *CEB-FIP Model Code*, Laussanne, Switzerland

Cedolin, L., Crutzen, Y.R.J., and Del Poli, S. (1977). "Triaxial Stress-Strain Relationships for Concrete." *Journal of Engineering Mechanics*, ASCE, 103(3), 423-439

Chen, A.C.T., and Chen, W.F. (1975). "Constitutive Relations for Concrete." *Journal of Engineering Mechanics*, ASCE, 101(4), 465-481

Chen, W.F., Bazant, Z.P., Chang, T.Y., Buyukozturk, O., Darwin, D., Liu, T.C., and Willam, K.J. (1982). "Constitutive Relations and Failure Theories." *State-of-the-Art Report on Finite Element Analysis of Reinforced Concrete*, Chapter 2, 34-148, ASCE, New York

Chen, W.F., and Han, D.J. (1988). *Plasticity for Structural Engineers*, Springer-Verlag, New York

Chen, W.F., and Saleeb, A.F. (1982), *Constitutive Equations for Engineering Materials*, Vol. 1, "Elasticity and Modeling", John-Wiley & Sons, New York

Chen,W.F., and Suzuki, H. (1980). "Constitutive Models for Concrete." *Computers and Structures*, 12(1), 23-32

Collins, M.P. (1978). "Towards a Rational Theory for RC Members in Shear." *Journal of Structural Engineering*, ASCE, 104(4), 649-666

Collins, M.P., Mitchell, D. (1987). *Prestressed Concrete Basics*, Canadian Prestressed Concrete Institute, Ottawa

Crisfield, M.A., and Wills, J. (1989). "Analysis of R/C Panels Using Different Concrete Models." *Journal of Engineering Mechanics*, ASCE, 115(3), 578-597

Darwin, D., and Pecknold, D.A. (1977). "Nonlinear Biaxial Stress-Strain Law for Concrete." *Journal of Engineering Mechanics*, ASCE, 103(2), 229-241

De Borst, R., Sluys,L.J., Muhlhaus, H.B., and Pamin, J. (1993). "Fundamental Issues in Finite Element Analyses of Localization of Deformation." *Engineering Computations*, 10(2), 99-121

Eligehausen, R., Popov, E., Bertero, V.V. (1983). "Local Bond Stress-Slip Relationships of Deformed Bars under Generalized Excitation." *UCB/EERC Report 83-23*, Earthquake Engineering Research Center, University of California at Berkeley

Eringen, A.C., and Edelen, D.G.B. (1972). "On Nonlocal Elasticity", *International Journal of Engineering Science*s, 10(3), 233-248

Frantz, G.C., and Breen, J.E. (1978). "Control of Cracking on the Side Faces of Large Reinforced Concrete Beams." *Research Report 198-1F*, Center for Highway Research, University of Texas at Austin,

Feenstra, P.H. (1993). *Computational Aspect of Biaxial Stress in Plain and Reinforced Concrete*, Ph.D. Dissertation, Delft University of Technology, Netherlands

Feenstra, P.H. and De Borst, R. (1995). "Constitutive Model for Reinforced Concrete." *Journal of Engineering Mechanics*, 121(5), 1995

Ferguson, P.M. (1964). "Design Criteria for Overhanging Ends of Bent Caps." *Research Report No.52-1F*, Center for Highway Research, University of Texas at Austin,

Gerstle, K.H., Aschl, H., Bellotti, R., Bertachi, P., Kotsovos, M.D., Ko, H.Y., Linse, D., Newman, J.B., Rossi, P., Schickert, G., Taylor, M.A., Traina, L.A., Winkler, H., and Zimmerman, R.M. (1980). "Behavior of Concrete under Multiaxial Stress States." *Journal of Engineering Mechanics*, ASCE, 106(6), 1383-1403

Han, D.J., and Chen, W.F. (1985) "A Non-uniform Hardening Plasticity Model for Concrete Materials." *Mechanics of Materials*, 4(3-4), 282-302

Hordijk, D.A. (1991). *Local Approach to Fatigue of Concrete*, Ph.D. Dissertation, Delft University of Technology, Netherlands

Hseih, S.S., Ting, E.C., and Chen, W.F. (1982). "A Plastic-Fracture Model for Concrete." *International Journal of Solids and Structures*, 18(3), 181-197

Hsu, T.T.C. (1988). "Softened Truss Model Theory for Shear and Torsion." *ACI Structural Journal*, 85(6), 624-635

Hsu, T.T.C., Belarbi, A., Pang, X.B. (1995) "Universal Panel Tester." *Journal of Testing&Evaluation*, ASTM, 23(1), 41-49

Hsu, T.T.C., and Zhang, L.X. (1997). "Nonlinear Analysis of Membrane Elements by Fixed-Angle Softened-Truss Model." *ACI Structural Journal*, 94(5), 483-491

Klisinski, M. (1985). "Degradation and Plastic Deformation of Concrete," *IFTR Report No. 38*, Polish Academy of Science, Warsaw

Kotsovos M.D., and Newman, J.B. (1978). "Generalized Stress-Strain Relations for Concrete." *Journal of Structural Engineering*, ASCE, 104(4), 845-856

Kupfer, H.B., and Gerstle, K.H.(1973). "Behavior of Concrete under Biaxial Stresses." *Journal of Engineering Mechanics*, ASCE, 99(4), 853-866

Kupfer, H.B., Hilsdorf, H.K., and Rusch, H. (1969). "Behavior of Concrete under Biaxial Stresses." *Journal of the American Concrete Institute*, 66(8), 656-666

Lee, J. (1996). *Theory and Implementation of Plastic-Damage Model for Concrete Structures Under Cyclic and Dynamic Loading*, Ph.D. Dissertation, University of California, Berkeley

Maekawa, K., and Okamura, H. (1991). *Nonlinear Analysis and Constitutive Models of Reinforced Concrete*, Gihodo Shuppan Co., Tokyo

Mander, J.B., Priestley, M.J.N., and Park, R. (1988). "Theoretical Stress-Strain Model for Confined Concrete." *Journal of Structural Engineering*, ASCE, 114(8), 1804-1826

Ngo, D., and Scordelis, A.C. (1967). "Finite Element Analysis of Reinforced Concrete Beams." *Journal of the American Concrete Institute*, 64(3), 152-163

Pamin, J. (1994). *Gradient-Dependent Plasticity in Numerical Simulation of Localization Phenomena*, Ph.D. Dissertation, Delft University of Technology, Netherlands

Pang, X.B. (1991). *Constitutive Laws of Reinforced Concrete in Shear (Truss Model Theory)*, Ph.D. Dissertation, University of Houston, Texas

Pang, X.B., and Hsu, T.T.C. (1996). "Fixed Angle Softened Truss Model for Reinforced Concrete." *ACI Structural Journal*, 93(2), 197-207

Popovics, S. (1973). "A Numerical Approach to the Complete Stress-Strain Curve of Concrete." *Cement and Concrete Research*, 3(5), 583-599

Pramono, E. and Willam, K.J. (1989). "Fracture Energy-Based Plasticity Formulation of Plain Concrete." *Journal of Engineering Mechanics*, ASCE, 115(6), 1183-1204

Prevost, J.H., and Hughes, T.J.R. (1981). "Finite-Element Solution of Elastic-Plastic Boundary-Value Problems." *Journal of Applied Mechanics*, ASME, 48(1), 69-74

Pruijssers, A.F. (1988). *Aggregate Interlock and Dowel Action under Monotonic and Cyclic Loading*, Ph.D. Dissertation, Delft University of Technology, Netherlands

Rashid, Y.R. (1968). "Analysis of Prestressed Concrete Pressure Vessels." *Nuclear Engineering and Design*, 7(4), 334-344

Romano, M. (1969). "On Leon's Criterion." *Meccanica*, 4(1), 48-66

Rots,J.G. (1988). *Computational Modeling of Concrete Structures*, Ph.D. Dissertation, Delft University of Technology, Netherlands

Scanlon, A. and Murray, D.W. (1974). "Time Dependent Reinforced Concrete Slab Deflection." *Journal of Structural Engineering*, ASCE, 100(9), 1911-1924

Schickert, G., and Winkler, H. (1977). "Results of Test Concerning Strength and Strain of Concrete Subjected to Multiaxial Compressive Stress." *Deutscher Ausschuss fur Stahlbeton*, 277, Berlin

Solari, M.R., Spacone, E. (2001). "Finite Element Formulations of One-Dimensional Elements with Bond-Slip." *Engineering Structures*, 23(7), 815-826

Tamai, S., Shima, H., Izumo, J., and Okamura, H. (1987). "Average Stress-Strain Relationship in Post-Yield Range of Steel Bar in Concrete", *Concrete Library of JSCE*, Translation of Proceedings of JSCE, 378(6), 117-129

Truesdell, C. (1955) "Hypo-elasticity." *Journal of Rational Mechanics and Analysis*, 4(1), 83-133

Van Mier, J.G.M. (1986). "Multiaxial Strain-Softening of Concrete." *Materials and Structures*, RILEM, 19(111), 179-200

Van Zijl, G.P.A.G. (1999). *Computational Modeling of Masonry Creep and Shrinkage*, Ph.D. Dissertation, Delft University of Technology, Netherlands

Vecchio, F.J. (1989). "Nonlinear Finite Element Analysis of Reinforced Concrete Membranes." *ACI Structural Journal*, 86(10), 26-35

Vecchio, F.J. (1992). "Finite Element Modeling of Concrete Expansion and Confinement." *Journal of Structural Engineering*, ASCE, 118(9), 2390-2406

Vecchio, F.J. (2000). "Disturbed Stress Field Model for Reinforced Concrete: Formulation." *Journal of Structural Engineering*, ASCE, 126(9), 1070-1077

Vecchio, F.J., and Collins, M.P. (1982). "The Response of Reinforced Concrete to In-Plane Shear and Normal Stresses." *Publication No. 82*-03, Department of Civil Engineering, University of Toronto

Vecchio, F. J., and Collins, M.P. (1986). "The Modified Compression Field Theory for Reinforced Concrete Elements Subjected to Shear." *ACI Structural Journal*, 83(2), 219-231

Vecchio, F. J., and Collins, M.P. (1993). "Compression Response of Crack Reinforced Concrete." *Journal of Structural Engineering*, ASCE, 119(12), 3590-3610

Willam, K.J., Hurlbut, B., and Sture, S. (1986). “Experimental and Constitutive Aspects of Concrete Failure.” *Proc. US-Japan Seminar on Finite Element Analysis of Reinforced Concrete Structures*, Tokyo, 1985, ASCE, Special Publication, New York., 226-254

Willam, K.J., Pramono, E., and Sture, S. (1987). “Fundamental Issues of Smeared Crack Models.” *Fracture of Concrete and Rock*, International Conference on Fracture of Concrete and Rock, Houston, SEM-RILEM, 142-153

Willam, K.J., and Warnke, E.P. (1974). “Constitutive Model for the Triaxial Behavior of Concrete.” *Concrete Structures Subjected to Triaxial Stresses*, International Association of Bridge and Structural Engineers Seminar, Paper III-1, Bergamo, Italy,1-30

Young, B.S., Bracci, J.M., Keating, P.B., and Hueste, M.B.D. (2002). “Cracking in Reinforced Concrete Bent Caps.” *ACI Structural Journal*, 99(4), 488-498

Zhang, L.X. (1995). *Constitutive Laws of Reinforced Concrete Membrane Elements with High Strength Concrete*, Ph.D. Dissertation, University of Houston, Texas

Zhu, R.H., Hsu, T.T.C. (2002). “Softened Membrane Model for Reinforced Concrete Elements in Shear.” *ACI Structural Journal*, 99(4), 460-469

VITA

Suraphong Powanusorn was born in Bangkok, Thailand, on October 14, 1972. He graduated from Suankularb Wittayalai School in 1990 and immediately entered Chulalongkorn University where he completed the B.Eng. degree in civil engineering in 1994. He traveled to Sydney, Australia in 1994 and earned the M.Eng.Sc. degree in civil engineering from the University of New South Wales in 1996. Upon graduation with his master's degree, he worked with the Asian Engineering Consultants in Bangkok for three years. He traveled to the United States in August 1999 to begin his doctoral studies.

Suraphong can be contacted at the following address:

Suraphong Powanusorn
3/19 Inthamara 35
Din Dang, Bangkok 10400
THAILAND